Fast Orthogonal Frequency Division Multiplexing (Fast-OFDM) For Wireless Communications

Kai Li

A thesis submitted for the degree of Doctor of Philosophy

Department of Electronic and Electrical Engineering
University College London

August 2008

ProQuest LLC
789 East Eisenhower Parkway
P.O. Box 1346
Ann Arbor, MI 48106-1346

To my parents

Statement of Originality

I declare that the work presented in this thesis and the thesis itself was composed and originated by myself in the Department of Electronic and Electrical Engineering, University College London. The work of other persons is appropriately acknowledged.

Kai Li

Abstract

This thesis presents research that has addressed various design issues related to an adapted orthogonal frequency division multiplexing scheme, namely Fast-OFDM. A comparative study of the system with conventional OFDM in various signal mapping conditions has been investigated. The thesis reports on performance assessment in terms of bit-error-rate (BER), spectral efficiency, peak-to-average-power ratio (PAPR), nonlinear effects and adjacent channel interference (ACI) analysis. The results show that the performance of Fast-OFDM is comparable to OFDM for single dimensional modulation scheme, whereas for complex modulation schemes, the performance of Fast-OFDM degrades severely due to the loss of orthogonality between subcarriers.

Two multi-carrier CDMA schemes, multi-carrier direct sequence CDMA (MC-DS-CDMA) and multi-tone CDMA (MT-CDMA), have been studied in different modulation scenarios. The performance of the overlapping multi-carrier CDMA schemes compared to OFDM and Fast-OFDM has been evaluated in terms of BER, spectral efficiency, PAPR and ACI analysis. The results reveal that the overlapping multi-carrier CDMA systems are comparable to the Fast-OFDM system under single user condition. It is thus feasible to apply multi-carrier CDMA detection techniques in Fast-OFDM systems. Therefore, two different types of linear detectors, zero-forcing (ZF) and minimum mean square error (MMSE) have been employed in complex modulated Fast-OFDM, leading to improvement of system performance.

Overall, the theoretical design and performance assessment issues addressed in this thesis provide an insight into the performance of Fast-OFDM in the presence of additive white Gaussian noise (AWGN). The results obtained can be used by receiver designers for improving signal recovery of complex modulated Fast-OFDM in future wireless communication systems.

Acknowledgement

First, I would like to express my sincere gratitude to my supervisor, Professor Izzat Darwazeh, for his guidance, encouragement, patience and information that he provided me with through the period of the project. Besides learning his engineering techniques and understanding the project, I enjoyed the work that he gave me and I would not hesitate in working again on a similar project under his supervision. Again, I would like to express my deep thanks and gratitude and also his kind understanding of my family affairs.

I also would like to thank Dr. John Mitchell, Dr. Arsenia Chorti and Dr. Miguel Rodrigues, for their valuable advices and helpful discussion about the work. Also I want to thank the present and pass members of the Telecommunication Research Group, especially Bahman Kalantari Sabet, Bo Wen Cao, Ioannis Kanaras, Miguel Pimenta, Dr. Saad Sari, and Dr Darren Shea for their support, friendly guidance and memorable times that we had together.

Last, but certainly not least, I would like to extend special thanks to my wonderful wife, Fei, my parents and my uncle and aunt, Mr. and Mrs. Liu, for their encouragement, unconditional support and understanding throughout these years.

Table of Contents

List of Figures

List of Tables

List of Abbreviations

A/D	Analogue-to-Digital
ACI	Adjacent Channel Inference
ADS	Advanced Design System
ADSL	Asymmetric Digital Subscriber Line
AM/AM	Amplitude Modulation/Amplitude Modulation
AM/PM	Amplitude Modulation/Phase Modulation
AMPS	Advanced Mobile Phone System
ANSI	American National Standards Institute
AWGN	Additive White Gaussian Noise
BER	Bit Error Rate
BFSK	Binary Frequency Shift Keying
BRAN	Broadband Radio Access Networks
BPSK	Binary Phase Shift Keying
CDMA	Code Division Multiple Access
CIR	Channel Impulse Response
CJK	China, Japan and South Korea
CSD	Circuit Switched Data
DAB	Digital Audio Broadcasting
DFT	Discrete Fourier Transform
DS-CDMA	Direct Sequence Code Division Multiple Access
DSL	Digital Subscriber Line

DSP	Digital Signal Processors.
DVB-T	Terrestrial Digital Video Broadcasting
EDGE	Enhanced Data rates for GSM Evolution
EGC	Equal Gain Combining
ETSI	European Telecommunications Standards Institute
FFH	Fast Frequency Hopping
FFT	Fast Fourier Transform
FDM	Frequency Division Multiplexing
FDMA	Frequency Division Medium Access
FH-CDMA	Frequency Hopping CDMA
Fast-OFDM	Fast Orthogonal Frequency Division Multiplexing
GPRS	General Packet Radio Service
GSM	Global System for Mobile communications
HDSL	High-bit-rate Digital Subscriber Lines
HF	High Frequency
HIPERLAN 2	High Performance Radio LAN type 2
HPA	High Power Amplifier
HSCSD	High-Speed Circuit-Switched Data
HSDPA	High-Speed Downlink Packet Access
HSPA	High-Speed Packet Access
IBO	Input Backoff
ICI	Inter-Carrier Interference
IMP	Intermodulation Products
iDEN	Integrated Digital Enhanced Network
IDFT	Inverse Discrete Fourier Transform
IEEE	The Institute of Electrical and Electronics Engineers

IFFT	Inverse Fast Fourier Transform
IMD	Intermodulation distortion
IMT	International Mobile Telecommunications
IS-95	Interim Standard 95
I/Q	In phase and Quadrature
ISI	Inter-Symbol Interference
ITU	International Telecommunication Union
JTACS	Japan Total Access Communications System
MAI	Multiple Access Interference
M-ASK	M-Ary Amplitude Shift Keying
MATLAB	MAThemetical LABoratory
MC	Multi-carrier
MC-CDMA	Multi-carrier Code Division Multiple Access
MC-DS-CDMA	Multi-carrier Direct Sequence Code Division Multiple Access
MFSK	M-ary Frequency Shift Keying
MIMO	Multiple Input Multiple Output
ML	Maximum Likelihood
MMS	Multimedia Messaging Service
MMSE	Minimum Mean Square Error
MRC	Maximum Ration Combining
MT-CDMA	Multi-tone Code Division Multiple Access
NMT	Nordic Mobile Telephone
NTT	Nippon Telegraph and Telephone
OBO	Output Backoff
OFDM	Orthogonal Frequency Division Multiplexing
OFDMA	Orthogonal Frequency Division Multiplexing Access

PAPR	Peak-to-Average Power Ratio
PDC	Personal Digital Cellular
PDF	Probability Density Function
PE	Polynomial Expansion
PHY	Physical Layer
P/S	Parallel-to-Serial
QAM	Quadrature Amplitude Modulation
QPSK	Quadrature Phased Shift Keying
RTMI	Radio Telefono Mobile Integrato
SC	Single-Carrier
SD	Selective Diversity
SER	Symbol Error Rate
SFH	Slow Frequency Hopping
SISO	Single Input Single Output
SMS	Short Message Service
SNR	Signal to Noise Ratio
S/P	Serial-to-Parallel
TACS	Total Access Communications System
TDMA	Time Division Multiplexing Access
TD-SCDMA	Time Division-Synchronous Code Division Multiple Access
TH-CDMA	Time Hopping CDMA
TTA	Telecommunications Technology Association
TWT	Travelling-Wave Tube
UMTS	Universal Mobile Telecommunications System
VHDSL	Very high bit rate DSL
VLSI	Very Large-Scale Integration

WCDMA	Wideband CDMA
WH	Walsh Hadamard
WiMax	Worldwide Interoperability for Microwave Access
WLAN	Wireless Local Area Network
WMAN	Wireless Metropolitan Area Network
WPAN	Wireless Personal Area Network
ZF	Zero-Forcing

List of Symbols

$a_{n,k}$	Transmitting symbol on the n^{th} carrier at k^{th} signalling interval
A	Signal amplitude
A_i	Maximum input saturation power
A_o	Maximum output saturation power
$A(\ )$	Nonlinear amplitude distortion
$b_k(t)$	Information signal of k^{th} user
B	General Transmission bandwidth
BW_{ds}	Bandwidth of each DS-CDMA channel
BW_{MD}	MC-DS-CDMA channel bandwidth
BW_{MT}	MT-CDMA channel bandwidth
BW_{op}	Overlapped bandwidth between channels
BW_{wide}	Overall overlapping DS-CDMA channels
$BW_{\Delta MD}$	MC-DS-CDMA channel separation
$BW_{\Delta MT}$	MT-CDMA channel separation
$c_k[n]$	Single chip of spreading code of k^{th} user
$c_k(t)$	Spreading code of k^{th} user
D_{mv}	Desired signal after multipath fading
E_b/N_o	Energy per bit to noise density ratio
f_c	DS-CDMA carrier frequency
f_{int}	Interleaving space in frequency
f_n	n^{th} subcarrier frequency
f_0	zeroth subcarrier frequency

$G(\ )$	Nonlinear amplifier gain
G_{DS}	Processing gain of DS-CDMA
G_{MC}	Processing gain of MC-CDMA
G_{MD}	Processing gain of MC-DS-CDMA
G_{MT}	Processing gain of MT-CDMA
G_{narrow}	Processing gain of each DS-CDMA channel
G_{wide}	Processing gain of overall overlapped DS-CDMA channels
g_{mv}	Combining scheme coefficient
$g(t)$	OFDM complex subcarriers
$h(t)$	Channel impulse response
k	Index of signalling interval
l	Index of channel impulse response bin
m	Index of IFFT output
n	Index of number of subcarrier
$\mathbf{n_I}$	Noise in matrix form
$n(t)$	Noise signal
$n_d(t)$	Nonlinearly distorted signal
N	OFDM number of subcarriers
N_{code}	Spreading code length
N_e	General processing (spreading) gain
N_{sc}	Number of subcarriers for multi-carrier CDMA systems
$N_{S/P}$	Size of S/P converter
N_0	Noise spectrum density
p	Size of S/P MC-DS-CDMA subcarrier
$p(t)$	Fast-OFDM complex subcarriers
P_a	Signal power of adjacent channel
$P_{average}$	Average signal power

P_{in}	Input signal power
P_{out}	Output signal power
P_{peak}	Peak signal power
P_s	Signal power of transmitting channel
q	Size of S/P converter in S/P MC-DS-CDMA subcarrier
r	Amplitude of input signal
$r(t)$	General received signal
$\mathbf{R}$	Correlation matrix
R_b	Initial bit rate
$R_{Fast-OFDM}$	Fast-OFDM symbol rate
$R_{MC-DS-CDMA}$	MC-DS-CDMA symbol rate
$R_{MT-CDMA}$	MT-CDMA symbol rate
R_{OFDM}	OFDM symbol rate
R_s	Initial symbol rate
$s(t)$	OFDM transmitting signals
$\tilde{s}(t)$	Equivalent baseband signal
$s_d(t)$	Output signal from nonlinear model
$s_u(t)$	Useful signal from nonlinear model
SPG_{MC}	Spectrum gain of MC-CDMA
SPG_{MD}	Spectrum gain of MC-DS-CDMA
SPG_{MD-CO}	Spectrum gain of copier MC-DS-CDMA
$SPG_{MD-S/P}$	Spectrum gain of S/P MC-DS-CDMA
SPG_{MT}	Spectrum gain of MT-CDMA
t	Time interval
T	General symbol duration
T_b	Initial bit duration
T_c	Spreading code duration

T_{c1}	Spreading code duration of DS-CDMA
T_{hop}	Frequency hopping time
T_s	Initial symbol duration
T_{sig}	One signal interval
T_g	Guard interval
T_{info}	Useful part of an OFDM symbol
T_{int}	Interleaving space in time
T_{OFDM}	OFDM symbol duration
v	Integer
W_c	Coherence bandwidth
x_m	IFFT output samples
x_n	Complex symbol
X_n	IFFT input data symbols
$\mathbf{y}$	Matrix form of received signal
z_n	Linear mapping output
Z_m	Decision threshold at the receiver
Z_{mv}	Decision threshold at the receiver for each path
α	Nonlinear attenuation coefficient
$\alpha_{nl}^{(k)}$	Amplitude change due to multipath effects at the k^{th} user, n^{th} subcarrier and l^{th} path
β	Saturation point parameter
γ	Small signal gain
Δf	General subcarrier spacing
$\Delta f_{Fast-OFDM}$	Fast-OFDM subcarrier spacing
Δf_{FOMT}	Further overlapping MT-CDMA subcarrier spacing
Δf_{MC}	MC-CDMA subcarrier spacing
$\Delta f_{MC-S/P}$	S/P MC-CDMA subcarrier spacing
Δf_{MD}	MC-DS-CDMA subcarrier spacing

Δf_{MD-CO}	Copier MC-DS-CDMA subcarrier spacing
$\Delta f_{MD-S/P}$	S/P MC-DS-CDMA subcarrier spacing
Δf_{MT}	MT-CDMA subcarrier spacing
Δf_{MT-CO}	Copier MT-CDMA subcarrier spacing
Δf_{OFDM}	OFDM subcarrier spacing
Δf_{OMD}	Overlapping MC-DS-CDMA subcarrier spacing
Δf_{OMT}	Overlapping MT-CDMA subcarrier spacing
ε	Carrier frequency offset
ε_0	Fine frequency error
η_{FDM}	Spectrum efficiency
η_{mv}	AWGN noise
η_{MC}	Spectrum efficiency of multi-carrier CDMA
λ_{DS}	DS-CDMA overlapping coefficient
λ_{FDM}	FDM overlapping coefficient
λ_{MC}	MC-DS-CDMA overlapping coefficient
λ_{MT}	MT-CDMA overlapping coefficient
ρ	Correlation coefficient
ρ_i	Imaginary component of correlation coefficient
ρ_r	Real component of correlation coefficient
σ^2	Noise variance
τ	Timing offset
τ_c	Coherence time
τ_{kl}	Delay of the k^{th} user on the l^{th} path
φ	Phase offset
$\varphi(\ )$	Nonlinear phase distortion
$\psi_{nl}^{(k)}$	Phase change due to multipath effects at the k^{th} user, n^{th} subcarrier and l^{th} path
ϕ_{kn}	Initial modulation phase of the k^{th} user, n^{th} subcarrier

Chapter 1 Introduction

1.1 Introduction

Due to the preciousness of the usage on the available RF bands, for spectrum conservation the band occupancy of chosen modulation scheme must be as small as possible so as to accommodate more channels in a given band. Orthogonal Frequency Division Multiplexing (OFDM) is such a widely used scheme, which has been rated as one of the most promising solutions for the next generation wireless communications due to its robustness to multipath interference and efficient system implementation using inverse fast Fourier transform (IFFT) and fast Fourier transform (FFT). It has been adopted in a variety of wireless applications including European terrestrial digital video broadcasting (DVB-T), digital audio broadcasting (DAB), indoor wireless local area network (WLAN) IEEE 802.11, high performance radio LAN type 2 (HIPERLAN2) and worldwide interoperability for microwave access (WiMax), IEEE 802.16a. With the increasing demand for bandwidth, improving the bandwidth efficiency is vital in all wireless system designs. Fast-OFDM [1-3] is a system based on OFDM but offering twice the bandwidth efficiency compared to the conventional OFDM. However, its spectral efficiency benefit has not been fully exploited as Fast-OFDM currently only operates with one-dimensional modulation schemes (e.g. BPSK or M-ASK). Therefore, combining the Fast-OFDM system with complex modulation schemes to explore its bandwidth efficiency advantage becomes significantly important.

In order to provide broadband services such as wireless Internet access to users in future wireless communication networks, there are challenges for reliable and high-rate communications over time-dispersive

(frequency selective) channels with limited spectrum and intersymbol interference (ISI) caused by multipath fading. The direct sequence code division multiple access (DS-CDMA) is preferred due to its advantages [4] over conventional time division multiple access (TDMA) and frequency division multiple access (FDMA). However, it suffers from multipath induced multiple access interference (MAI). Multi-carrier code division multiplexing access [5] that combines OFDM and CDMA exploits the advantages of both systems, attracting much attention as an alternative to the conventional DS-CDMA. The concept of overlapping multi-carrier CDMA systems, with varying subcarrier spacing as in Fast-OFDM, has been introduced by Hanzo [6]. Much research has also been carried out into the performance of multi-carrier CDMA systems with advanced detection techniques. It is, therefore, essential to compare the performance of overlapping multi-carrier CDMA systems with OFDM and Fast-OFDM schemes, and adopt system structure and detection mechanisms of the multi-carrier CDMA in Fast-OFDM for system performance improvement.

This thesis is concerned with system modelling and performance assessment of modulation techniques for use in wireless communication systems. A number of topics included are: i) system modelling and performance assessment of OFDM and Fast-OFDM systems, ii) system design and modelling of overlapping multi-carrier schemes and performance comparison of OFDM and Fast-OFDM systems and iii) the implementation of Fast-OFDM with linear detection techniques. The research reported in this thesis is modelling and simulation based. The main simulation tools that have been used for this purpose are Agilent's Advanced Design System (ADS) and MATLAB. The details of the thesis structure are given in the following section.

1.2 Thesis outline

Chapter 2 is concerned with the performance comparison of the Fast-OFDM and conventional OFDM with different mapping schemes. The chapter is divided into six sections. The chapter begins with a general overview of different generations of mobile communications. The following two sections then provide a background and a discussion on the merits and demerits of OFDM. The subsequent section introduces Fast-OFDM, as well as its advantages and drawbacks compared to OFDM. The model implementation and system parameters are described in section 2.6. Finally, the performance of the two systems in terms of bit-error-rate (BER), peak-to-average-power ratio (PAPR), spectral efficiency, nonlinear performance and adjacent channel interference (ACI) analysis are presented and a comparison is made between the two in order to determine the advantages and disadvantages of each in relation to the other.

Chapter 3 investigates the performance comparison of the overlapping multi-carrier CDMA and variable subcarrier spacing FDM systems with different modulation schemes. The chapter begins with a brief overview of CDMA, multi-carrier CDMA and overlapping multi-carrier CDMA schemes. Their advantages and disadvantages in terms of the system structures and the spectral efficiency are addressed. The subsequent section discusses the system modelling and simulation parameters of the two schemes in ADS. Finally the performance assessment of the systems as compared to OFDM and Fast-OFDM in terms of BER performance, PAPR, bandwidth efficiency and ACI analysis are presented.

Chapter 4 explores the performance of Fast-OFDM incorporating equalisation-based detection receivers, zero-forcing (ZF) and minimum mean square error (MMSE), with complex modulation schemes. The chapter is divided into two main sections for ZF and MMSE detectors. Each section focuses on the principles and system implementation of the detector. The performance of each scheme is then assessed and a comparison of the two is made for system evaluation.

The thesis ends with Chapter 5. The chapter describes the main outcomes of the research and presents the concluding remarks. Suggestions for further research of the area are also proposed.

Finally, in the appendices, the simulation models designed in ADS and MATLAB are enclosed. The Appendix A provides the models of the oscillator-based OFDM and Fast-OFDM system and the overlapping multi-carrier CDMA systems developed in ADS.

1.3 Contributions and publications

The work reported in this thesis contains several contributions of the author to the field of wireless communications. A summary of the main contributions in each chapter is listed below:

Chapter 2

- Evaluation of the OFDM and Fast-OFDM systems with BPSK, QPSK and 16-QAM complex modulation schemes. This work is an extension of the work in [3] where only the BPSK scheme was considered. Fast-OFDM is currently limited to one dimensional modulation schemes. In order to fully exploit its benefits in bandwidth efficiency, investigating the performance of the system with complex modulation schemes becomes vital.

- Performance assessment of the FDM system with variable frequency spacing between subcarriers. The simulation results indicated that the BER performance severely degraded as the subcarriers were spaced closer than 50% overlapping (Fast-OFDM). The aim of the work was to study the performance of the FDM systems at other subcarrier spacing and look for the system with an optimum subcarrier spacing that could balance the benefit in spectrum efficiency and system performance.

- Study of the effect of high PAPR and nonlinear effects in OFDM and Fast-OFDM systems. Performance assessment of the two systems in noise limited (additive white Gaussian noise (AWGN)) and interference limited (ACI) environment. OFDM is sensitive to synchronisation errors and nonlinear distortions. In [7], the authors showed that Fast-OFDM systems were sensitive to wireless environments impairments such as frequency offsets and frequency selective fading. The work in this thesis focuses on the performance comparison of OFDM and Fast-OFDM in nonlinear and ACI environment.

Chapter 3

- Evaluation of overlapping multi-carrier CDMA (multi-carrier direct sequence CDMA (MC-DS-CDMA) and multi-tone CDMA (MT-CDMA)) and Fast-OFDM system in AWGN channels with BPSK and QPSK modulation schemes. The results showed comparable performance under such environments. The work was originally inspired by [8] where the performance comparison of MC-CDMA and OFDM systems was investigated. Due to the system similarities between the overlapping multi-carrier CDMA and variable subcarrier spacing FDM, the comparative performance between the two was studied. This led to applying multi-user and multi-carrier detection techniques on Fast-OFDM.

- Study of the effect of high PAPR in multi-carrier CDMA systems. Performance assessment of overlapping multi-carrier CDMA, OFDM and Fast-OFDM in noise limited and interference limited environment.

Chapter 4

- Derivation of analytical expressions of the correlation matrix for Fast-OFDM received signals with ZF and MMSE detectors.

- System implementation and performance assessment of BPSK, QPSK and 8-PSK Fast-OFDM system with ZF and MMSE receivers. The results indicated that MMSE detector exhibited better performance as compared to ZF.

The work in this thesis has led to the following publications:

K. Li and I. Darwazeh, "System performance comparison of Fast-OFDM system and overlapping multi-carrier DS-CDMA scheme," Proceedings of the London Communications Symposium 2006 - UCL, London, UK: 2006, pp. 73-76

K. Li and I. Darwazeh, "System performance comparison of Fast-OFDM system with overlapping MT-CDMA systems," Proceedings of the London Communications Symposium 2007 - UCL, London, UK: 2007. pp. 111-114

K. Li and I. Darwazeh, "Analysis and performance comparison of Fast-OFDM system and overlapping multi-carrier CDMA systems," International Symposium on Communication Theory and Applications ISCTA'07, Ambleside, UK: 2007. pp. 33-36

K. Li and I. Darwazeh, "System performance comparison of Fast-OFDM with overlapping MC-DS-CDMA and MT-CDMA systems," Sixth International Conference on Information, Communication and Signal Processing ICICS 2007, Singapore: 2007. pp. 1-4

K. Li and I. Darwazeh, "System performance analysis of Fast-OFDM system with Zero-forcing equalisation receiver," Multi-Strand Conference at University of Cranfield, UK: 2008. pp. 45-47

Chapter 2 OFDM and Fast OFDM

2.1 Introduction

Orthogonal Frequency Division Multiplexing (OFDM) [9;10] signaling has been made very popular for current and future wireless communications due to its attractive features. It is widely used in both the wired and the wireless industry, such as xDSL families for the wired; DAB, DVB-T, WLAN, HIPERLAN-2 and WiMax in the wireless industry. In combination with wireless multiple input and multiple output (MIMO) systems [11] that involve multiple antennas at the transmitter and the receiver, MIMO-OFDM can offer a much higher capacity compared to a single input single output (SISO) system for multiple user services. Moreover, due to the fact that OFDM has the advantage of mitigating the effects of delay spread in frequency selective channels, it has been proposed as one of the candidate formats to be used in 4^{th} generation (4G) system for high speed, high capacity, low cost and IP based multimedia services.

The chapter starts with a general review of different generations of mobile communications. Subsequently, the fundamentals of multi-carrier transmission techniques are addressed. The principal ideas behind OFDM and Fast-OFDM are presented. The principle concepts such as the oscillator based OFDM system implementation and the FFT based implementation are introduced in section 2.3. The basic elements of OFDM such as the guard time, cyclic prefix, coding and channel estimation are also outlined in section 2.3. Then the drawbacks of OFDM, particularly its vulnerability to synchronization errors and nonlinear distortion are discussed in section 2.4. In section 2.5, a variation of the OFDM scheme with improved bandwidth efficiency, Fast-OFDM, is investigated and compared with the conventional

OFDM. Sections 2.6 and 2.7 present the implementation issues of the systems in ADS and the performance parameters in terms of BER, bandwidth efficiency, PAPR, nonlinear performance and ACI analysis. Finally, a summary of the chapter is included in section 2.7.

2.2 Mobile communication systems overview

The 1st generation (1G) wireless telephone technology is the analogue cellphone standard introduced in the 1980s. The voice signal during a call is modulated to a higher frequency instead of encoding to digital signals in the 2nd generation (2G). Typical systems include the Nordic mobile telephone (NMT), used in Europe and advanced mobile phone system (AMPS), used in the United States [12].

The 2G cellular telecoms networks were fully digital networks, which were launched on the GSM standard in Finland in 1991 [13]. There were a number of advantages of 2G networks compared to 1G; digital encryption of phone conversations to prevent eaves-dropping on calls, efficient spectrum utilization due to digital voice data compression and multiplexing, and finally, introduction of mobile data services (short message service). The main 2G standards are divided into TDMA-based and CDMA-based. GSM is the world most popular TDMA-based 2G standards used in almost all countries on all six inhabited continents (80% world mobile subscription market share [14]). Interim Standard 95 (IS-95) aka cdmaOne, commonly referred as simply CDMA, is a CDMA-based standards used in the Americas and parts of Asia [13].

However, GSM was not able to cope with the increased demand for new users and services. In order to respond to market demand, three systems were proposed, namely the high speed circuit switched data (HSCSD), general packet radio service (GPRS) and enhanced data services for GSM evolution (EDGE), which offered new services and higher data rates. These telecom networks were termed as 2.5G (EDGE was even termed as 2.75G due to the higher data rate compared to GPRS) since they acted as a

bridge between the 2nd and 3rd generation (3G) systems [15]. Circuit switched data (CSD) networks were the systems that were used for data transmission. HSCSD was a system based on the original CSD networks but provided higher data rates by bundling multiple (up to 4) time slots [12]. Due to the high cost of circuit switched networks, GPRS was proposed as its advantages in efficient packet-based data transmission. For the consideration of higher data rate, EDGE was introduced as an initial enhancement of GSM toward UMTS. It provided data rates of up to 384 kb/s for 8 timeslots, while being switchable between EDGE and GSM/GPRS [12]. 2.5G systems were created as enhancement of 2G toward 3G. They were built to introduce the possibilities of wireless application technology to the end consumers, and so increase demand for 3G services.

The two main 3G standards were the Wideband CDMA (WCDMA) (or universal mobile telecommunications systems (UMTS)) and CDMA2000, launched in 2001 in Japan and in South Korea, respectively. In July 2008, 228 3G/WCDMA operators launched in 94 countries, which has 70% share of 328 commercially launched 3G networks [14]. China announced in May 2008, that the telecoms sector was re-organized and three 3G networks would be allocated in China. The largest mobile operator in China, China Mobile, would launch 3G onto the Chinese 3G standard, TD-SCDMA. China Unicom would relinquish its CDMA2000 customer base and launch 3G on the globally leading WCDMA standard. The 3rd 3G standard was the CDMA 1xEV-DO (Ev-DO stands for Evolution Data Optimized) standard launched by China Telecom [14].

The 3G data speed was expected to be minimum of 2 Mb/s and 348 kb/s, whereas in real life, 384 kb/s and 128 kb/s, for stationary or walking users and for a moving vehicle, respectively [16]. In order to have higher speed for 3G data transmission, high-speed downlink packet access (HSDPA) protocol was developed, known as the Super 3G or 3.5G [17]. HSDPA was a 3G protocol in the high-speed packet access (HSPA) family, which allowed networks based on UMTS to support downlink speeds up to 14.4 Mb/s. Further speed increases were available with HSPA+, which provided speeds

of up to 42 Mb/s downlink [18]. By the end of July, 2008, over 90% of commercial WCDMA operators have launched HSPA. Currently, over 200 commercial operators have launched HSDPA in 89 countries [14].

Due to the limitations and issues of itself, 3G is having the problems of delayed deployment and meeting its promised performance and throughput. Therefore, the next generation of mobile network, 4G, has already been considered [19-21]. A 4G system will be able to provide a comprehensive IP solution where voice, data and streamed multimedia can be delivered to users on an "Anytime, Anywhere" basis with higher data rates and an affordable cost. 4G will be a fully IP-based integrated system and will be capable of providing between 100 Mb/s and 1 Gb/s speeds both indoors and outdoors, with premium quality and high security [20]. Applications (Figure 2.1) such as, wireless broadband access, multimedia messaging service (MMS), video chat, mobile TV, high definition television (HDTV) content, digital video broadcasting (DVB), voice and data, and other streaming services will be provided in a 4G system [20]. There are three modulation schemes that could be used in 4G networks: CDMA, TDMA and OFDMA, where OFDMA is the strongest candidate that will be considered [10].

Figure 2.1. Applications driving wireless technologies [17]

2.3 Principles of OFDM

Multi-carrier systems are advantageous in immunity to impulse noise and fast fades due to the extended symbol duration compared to conventional single-carrier systems. OFDM and multi-carrier CDMA are the two most popular schemes and have been widely utilized and studied. OFDM offers numerous advantages over the conventional serial modem schemes, although it is only natural that it also imposes a number of disadvantages [22]. It has been used in a wide range of applications and is considered to be the most likely format to be adopted in 4G systems [10;19;20]. In order to support multi-user transmissions at the same time, spreading codes are applied in conjunction with OFDM, which leads to the concept of multi-carrier CDMA. The OFDM and multi-carrier CDMA are further detailed in this chapter and the following chapter, respectively.

An OFDM system is a multi-carrier modulation scheme that simultaneously transmits a number of narrow-band carriers (subcarriers), each modulated at a low data rate. It is different from a single-carrier modulation scheme which transmits data sequentially on a single carrier in that the signaling interval of a multi-carrier system is much larger than that of an equivalent single-carrier system. Therefore, the time dispersive effects of a multi-path fading channel can be efficiently combated without complex time-domain equalization at the receiver.

OFDM scheme initially originated from conventional frequency division multiplexing (FDM) technology to transmit information on multiple carriers. The orthogonality was later proposed where the spectra of different subcarriers were assigned to overlapping frequency slots, to ensure that there was no loss of information even when the subcarriers were overlapped. Reducing the frequency separation between subcarriers, results in a more efficient utilization of the available bandwidth when compared to the conventional FDM. OFDM had been the subject of important work in the mid-1960s at Bell Laboratories, and was termed as OFDM by R.W. Chang in 1970 [23;24]. In the 1980s, OFDM was studied for

high-speed modems, digital mobile communications and high density recording. In the 1990s and early 2000s, OFDM was adopted in many applications such as high-bit-rate digital subscriber lines (HDSL), ADSL, very high-speed digital subscriber line (VHDSL), DAB [25], DVB-T [26], new WLAN such as IEEE 802.11a, HiperLAN2 [27] and WiMax, IEEE 802.16a [28]. OFDM is almost certainly going to be used in future wireless multimedia applications and 4G wireless networks [29;30]. Table 2.1 and Table 2.2 show a summary of wired and wireless OFDM applications and milestones in the history of OFDM. In the following sections the principles of OFDM are described.

Table 2.1. OFDM applications [8]

Table 2.2. Milestones in the history of OFDM [8]

2.3.1. Oscillator-based and FFT-based OFDM

OFDM is a multi-carrier transmission technique, which divides the available spectrum into subcarriers, each being modulated by a low data rate stream (Figure 2.2). The simultaneous transmission of these sub-carriers increases the symbol duration, which combats multi-path delay spread over the wireless channel and results in high data rate transmission. By making the subcarriers orthogonal to one another, the channels can be placed closer together, resulting in a more efficient use of the allocated bandwidth. The original method of generating OFDM signals is oscillator-based which requires N oscillators to generate N subcarriers for each low data rate stream. Such implementation suffers from mutual interference between the subcarriers, leading to the distortion of the signal. It has been shown in [31] that an OFDM system can be implemented efficiently using an inverse discrete Fourier transform (IDFT) instead of a bank of oscillators. At the receiver a forward discrete Fourier transform (DFT) is used to recover the transmitted data bits. The implementation of an oscillator-based OFDM and FFT-based OFDM systems are reviewed in the following paragraphs.

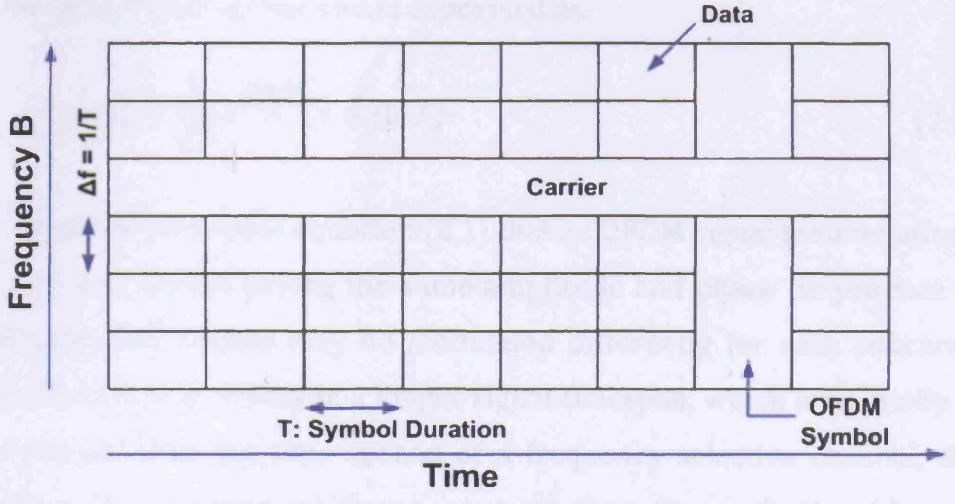

Figure 2.2. OFDM Time-Frequency grid

An oscillator-based OFDM signal can be implemented by modulating a low rate data stream of symbol duration, T, with a number of orthogonal overlapping oscillator-generated subcarriers, each separated by a frequency spacing of $1/T$ Hz. A frequency separation of $1/T$ is the minimum separation to achieve orthogonality. Consequently, the correlation between adjacent subcarriers is zero at the sampling instants. Hence, the subcarriers may overlap with no loss of information. The OFDM signal is generated by adding up all the individual modulated subcarriers. The resulting data rate is N/T b/s, where N is the total number of the subcarriers used. In other words, the total data rate to be sent on the channel is divided between the subcarriers.

The Complex envelope representation of an OFDM signal, ignoring the cyclic prefix, is shown in [32] as:

$$S_{Tx,OFDM}(t) = \sum_{k=-\infty}^{\infty} \sum_{n=0}^{N-1} a_{n,k} g_n(t - kT) \tag{2.1}$$

where $a_{n,k}$ is the complex symbol transmitted on the n^{th} subcarrier at the k^{th} signalling interval, N is the number of OFDM subcarriers, $g_n(t - kT)$ is the OFDM complex subcarrier and is expressed as:

$$g_n(t) = \frac{1}{\sqrt{T}} e^{j\frac{2\pi nt}{T}}, t \in [0, T] \tag{2.2}$$

It can be seen from equation (2.1) that an OFDM signal is summation of low rate subcarriers having the same amplitude and phase (in practice the amplitudes and phases may be modulated differently for each subcarrier [33]). Therefore, it results in a longer signal timespan, which is normally set to be longer than the time spread of a frequency selective channel, thus resulting in improved performance over frequency selective channels compared to a high data rate single carrier system occupying the same bandwidth. The block diagram of an oscillator based OFDM baseband system is shown in Figure 2.3.

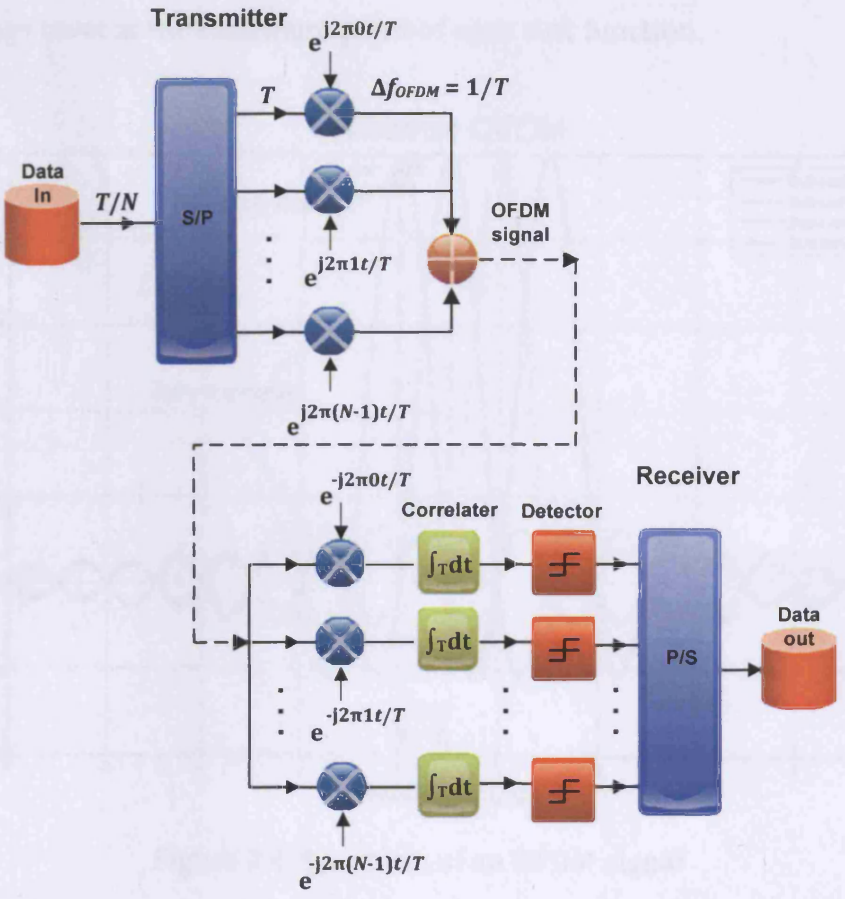

Figure 2.3. Oscillator based OFDM system

At the receiver, the complex symbol is recovered by multiplying the OFDM symbol with the complex conjugate of the sub-carriers and integrating over the signaling interval. The n^{th} recovered symbol at the k^{th} signaling interval is then given by:

$$\hat{a}_{n,k} = \frac{1}{\sqrt{T}} \int_0^T S_{Rx,OFDM}(t) \cdot g_n^*(t - kT)dt \tag{2.3}$$

Figure 2.4 shows the spectrum overlap of a 4-subcarrier OFDM signal. It is found that the frequency response of an OFDM signal is comprised of a number of overlapping sinc[1] functions. No mutual interference (inter-carrier

[1] sinc function is defined as sin(πx)/ πx, in order to have integer intervals instead of π, 2π,...

interference) is found between the subcarriers due to the fact that the zero-crossings meet at the maximum point of each sinc function.

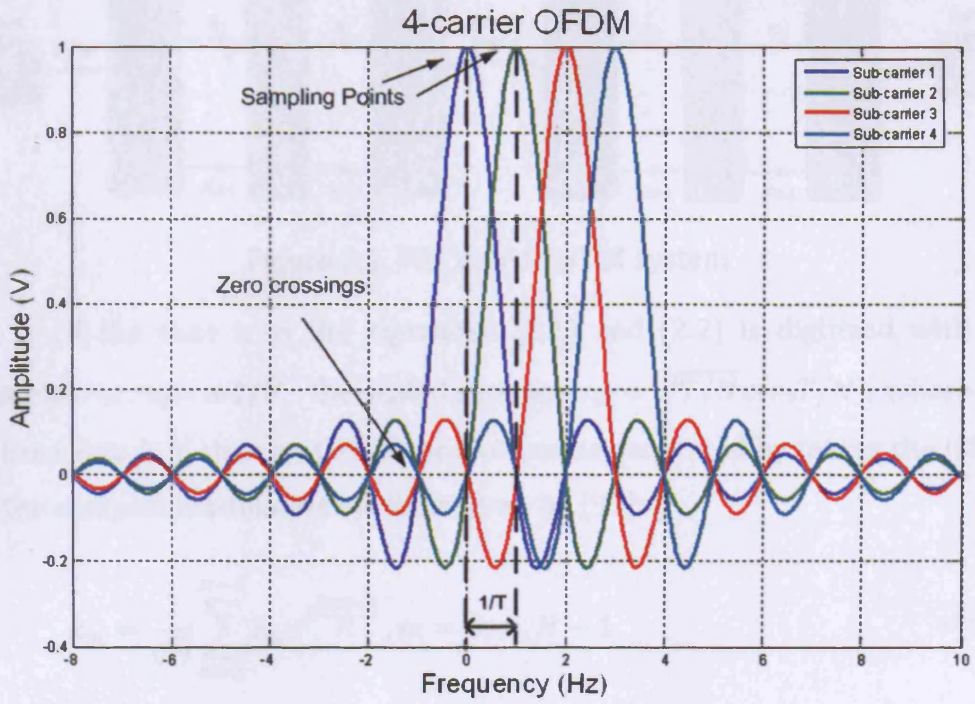

Figure 2.4. Spectrum of an OFDM signal

One disadvantage of the oscillator-base OFDM implementation is that it results in high complexity due to the utilization of N oscillators especially when N is large. The novel solution to this problem is to use IFFT and FFT to generate a discrete version of OFDM signals. It was first proposed by Weinstein and Ebert in [31] that OFDM generation and detection could be achieved by using an IDFT and a DFT at the transmitter and receiver, respectively. In practice, a combination of IFFT and FFT, which are mathematically equivalent versions of IDFT and DFT but more efficient to implement using modern DSP and VLSI technology, is used for OFDM signal generation and recovery. The block diagram of a FFT-based OFDM system is shown in Figure 2.5.

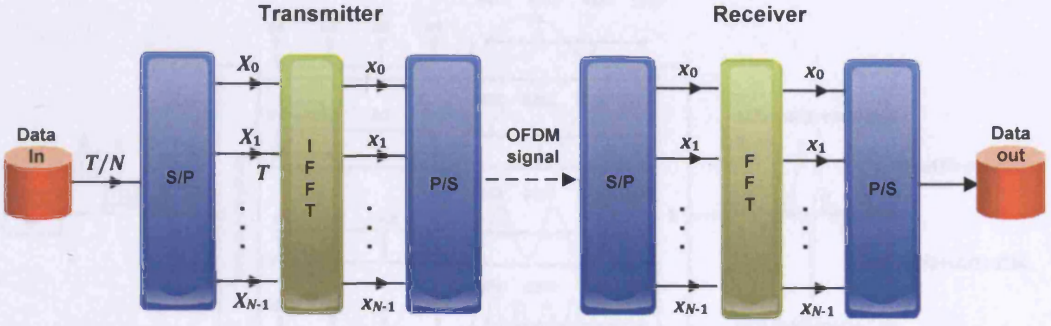

Figure 2.5. FFT based OFDM system

If the time t, in the equations (2.1) and (2.2) is digitized with N samples, i.e. $t_m = mT/N$, the scaled samples $x_m = \sqrt{T/N}x(mT/N)$, where m is from 0 to N-1, then an OFDM symbol can be generated by taking the IFFT of the complex modulation symbols given by [31]:

$$x_m = \frac{1}{\sqrt{N}} \sum_{n=0}^{N-1} X_n e^{j\frac{2\pi mn}{N}}, m = 0, \dots, N-1 \tag{2.4}$$

where X_n are the modulated data symbols, N is the number of the IFFT samples, n = 0,...,N-1 are the position of the subcarriers and x_m, m = 0,...,N-1 are the output IFFT samples. Therefore, it can be noticed that for each sample x_m, it is a summation of all the data symbols multiplied with the corresponding discrete version of the subcarriers. This is different from the oscillator-based OFDM where for each output OFDM sample, it corresponds to one complex symbol modulated by one subcarrier. However, the principle is still the same since in both methods a low rate data is modulated by orthogonal subcarriers. A comparison of the implementation of both OFDM systems is shown in Figure 2.6. Assuming the input data is represented in a digital way, after serial-to-parallel (S/P) conversion, the reduced bit rate samples are fed into the multiple oscillators and IFFT respectively, whereas the output from both of the systems reveal the same results.

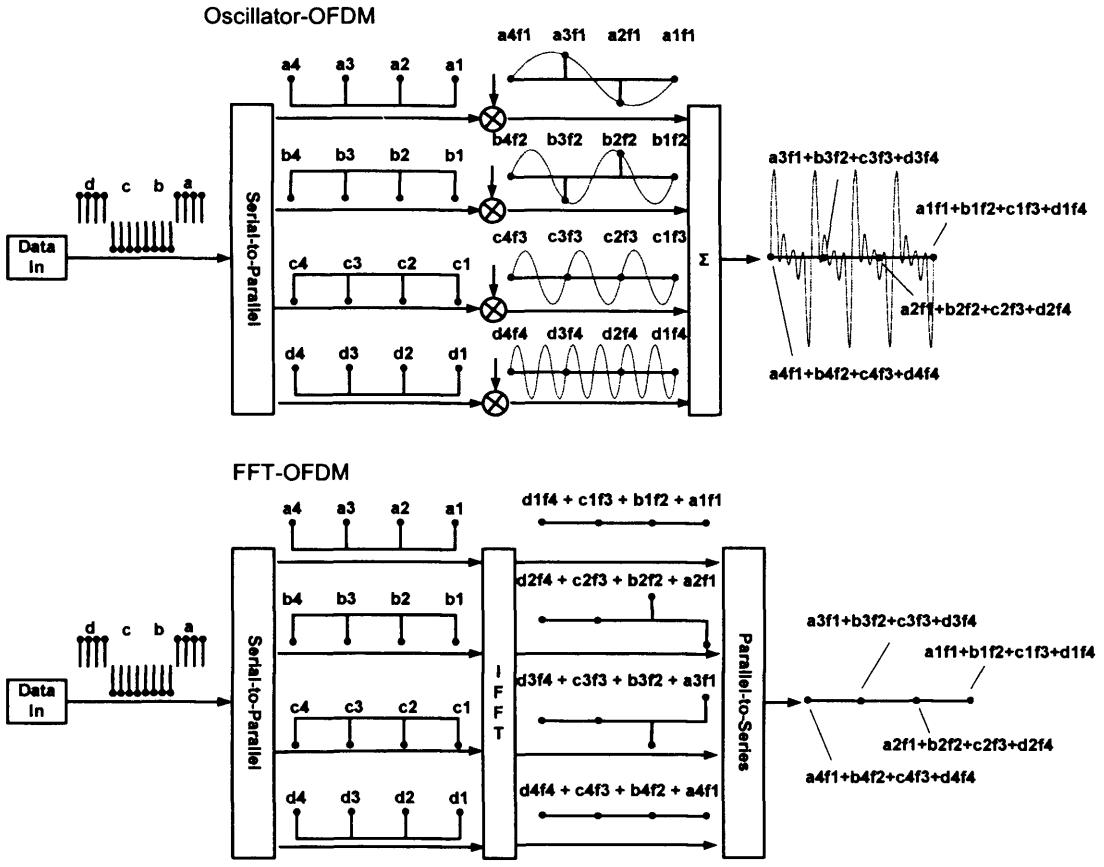

Figure 2.6. Oscillator-OFDM and FFT-OFDM sample generation

At the receiver, the OFDM signal is recovered using a forward FFT, thus:

$$X_n = \frac{1}{\sqrt{N}} \sum_{n=0}^{N-1} x_m e^{-j\frac{2\pi mn}{N}}, n = 0, \ldots, N-1 \tag{2.5}$$

2.3.2. Guard interval and cyclic prefix

Due to the effects in multipath transmissions, an OFDM frame is distorted by its previous OFDM frames, which causes inter-symbol interference (ISI). In addition, interference occurs amongst the OFDM symbol's own subcarriers, which in turn causes inter-carrier interference (ICI). To eliminate the effects of ISI, a guard interval (Figure 2.7) which has a duration longer than the duration of the impulse response of the channel, can be added by inserting zeros at the end of each OFDM frame. Moreover,

by making the guard interval cyclically extended, it can also eliminate the effects of ICI [34].

Cyclic extension on each OFDM frame is shown in Figure 2.8. A number of IFFT output samples with duration of T_g are inserted at the start of the OFDM symbol at the transmitter, while at the receiver, the first T_g samples of the symbol are removed. Therefore, if the total system duration is T, the duration of the useful part of an OFDM symbol is $T_{info}=T-T_g$. Hence, the frequency separation between subcarriers equals $1/(T-T_g)$. The reason for applying the cyclic extension can be interpreted as follows. Due to the multipath effects, an OFDM signal is attenuated and delayed during transmission; a number of replicas of the transmitted OFDM signal are received at the receiver. With an ordinary guard interval, whose duration is longer than the channel relative delay, the sum of those replicas does not yield a continuous wave, in other words, the number of cycles within the FFT interval is not an integer. As a result, there is no integer number of cycles difference between adjacent subcarriers, or the subcarriers are no longer orthogonal, hence, causes ICI at the receiver. However, with the presence of cyclic extended guard interval, the repeated extension of the OFDM frame ensures that the OFDM signal and its replicas are all continuous, and the summation of these components yields an attenuated or phase rotated version of the same sub-carrier (Figure 2.9). Therefore, the OFDM signals can be made periodic so that cyclic convolution can be performed. Subcarriers remain orthogonal as integer number of cycles is retained within the FFT interval. Hence, no ICI occurs among subcarriers and each data symbol is received only with a random amplitude or phase rotation.

One disadvantage of this scheme is the reduction of bandwidth efficiency since some of the bandwidth is used for the guard interval without carrying information. Moreover, insertion of the cyclic prefix also causes loss in the signal-to-noise ratio (SNR) since the power of the guard interval samples are discarded at the receiver.

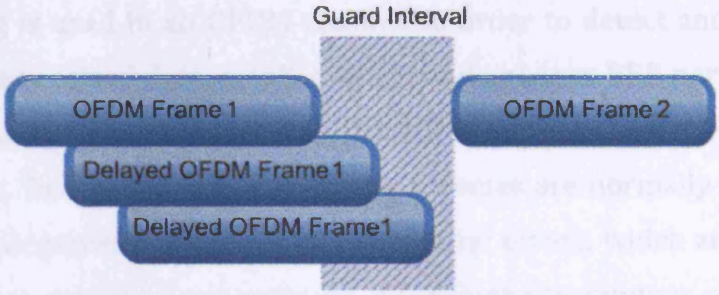

Figure 2.7. Guard interval on OFDM signal

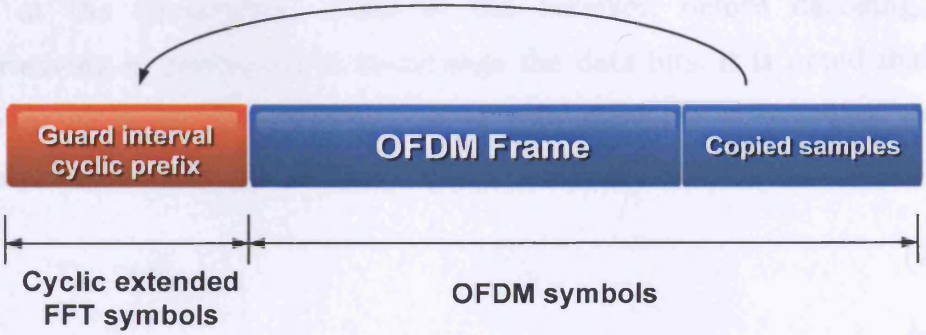

Figure 2.8. Cyclic extended OFDM frame

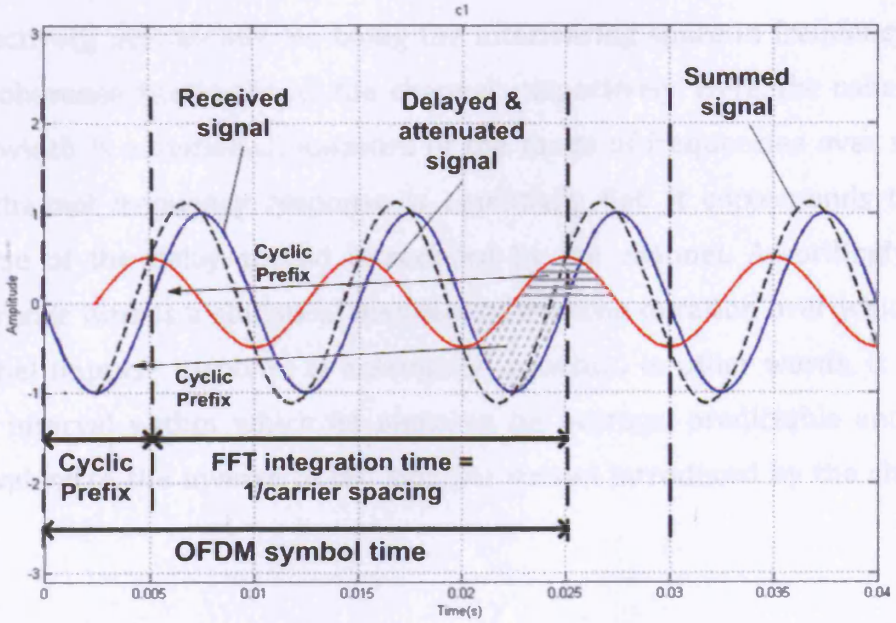

Figure 2.9. Cyclic extended OFDM frame viewed in time domain

2.3.3. Coding and interleaving

Coding is used in an OFDM channel in order to detect and/or correct errors in the received data, combat fading and enhance BER performance. A number of channel coding schemes [32;35] have been proposed for OFDM applications. Due to the fact that coding schemes are normally designed to deal with independent errors rather than burst errors, which are caused by deep fades on groups of sub-carriers, interleaving techniques are therefore introduced to deal with the effects of randomly scattered errors. Interleaving is a process where adjacent data bits are separated by several bits at the transmitter, while at the receiver, before decoding, de-interleaving is performed to re-arrange the data bits. It is noted that the amount of separation in time and in frequency for interleaving should satisfy the following conditions [35]:

$$T_{int} > \tau_c \tag{2.6}$$

$$f_{int} > W_c \tag{2.7}$$

with T_{int}, τ_c being the interleaving space in time and the coherence time, respectively, and f_{int} and W_c being the interleaving space in frequency and the coherence bandwidth of the channel, respectively. Here, the coherence bandwidth is a statistical measure of the range of frequencies over which the channel frequency response is essentially flat. It corresponds to the inverse of the delay spread introduced by the channel. Accordingly, the coherence time is a statistical measure of the time duration over which the channel impulse response is essentially invariant. In other words, it is the time interval within which its phase is, on average, predictable and it is equivalent to the inverse of the Doppler spread introduced by the channel [36].

2.3.4. Channel estimation and pilot symbols

For an OFDM system with coherent detection at the receiver, channel estimation is necessary to provide an estimate of the amplitude and phase

references of the constellation in each sub-carrier for correct data symbol demodulation. It is a process of inserting some known symbols or pilot carriers into the OFDM signal and obtaining estimates of the frequency response of the channel using interpolation. Subsequently, the knowledge of the channel impulse response will help to correct the effects of the channel on the transmitted symbols. Different arrangements of the pilot symbols result in different performance in the estimators. Here the pilots are redundant symbols with specific pattern arrangement but carry no useful information. The pilot symbols are used to mitigate the effects of fading and to estimate the channel impulse response. A typical pilot pattern is shown in Figure 2.10. This is determined by the nature of the system. For example, in a fast fading channel more scattered pilot patterns are necessary so that the channel impulse response can be tracked more precisely. However, in a slow fading environment with constant channel impulse response, fewer pilot symbols can be used. Moreover, the minimum separation between pilots in time and in frequency depends on the coherence time and coherence bandwidth of the channel, respectively. The higher density of pilot symbols the better the accuracy, but the lower the bandwidth efficiency and data rate [35]. Therefore, a trade-off exists between data rate and good channel estimation performance.

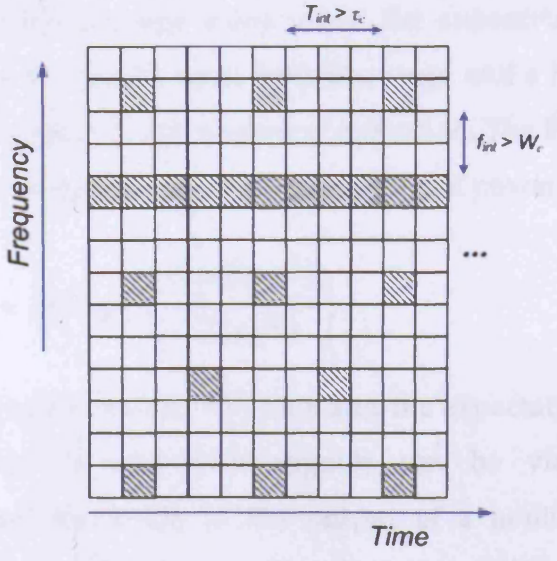

Figure 2.10. Typical pilot structure viewed in time and frequency

2.4 Drawbacks of OFDM System

OFDM exhibits a number of advantages, such as high data rate transmission due to its parallel data transmissions and robustness in multi-path fading environment due to its multi-carrier data delivery. Long symbol durations allow for relatively long cyclic prefix durations to eliminate ICI and ISI with minimal SNR loss. A Simple system implementation is also feasible when IFFT/FFT is used instead of a bank of oscillators and lower complexity in equalization at the receiver is achieved when compared to an equivalent single-carrier system. However, OFDM also has some drawbacks. Due to the fact that OFDM signals have a large signal dynamic range and thus a high PAPR, it is therefore sensitive to the nonlinear distortion caused from the nonlinear devices in the system. Moreover, OFDM is also vulnerable to synchronization errors mainly from symbol timing offsets and carrier frequency offsets. Both of the above are discussed in the following two sub-sections.

2.4.1. OFDM nonlinearities

An OFDM signal consists of a large number of carriers that are added together. This causes a time varying envelope. The signal peak power is much higher than the average value when the subcarriers are added in phase. This results in a large signal dynamic range and a high PAPR, which makes OFDM highly sensitive to nonlinear distortion. The PAPR is defined as the ratio of the peak signal power to the mean signal power,

$$PAPR = 10\log_{10}\left(\frac{\max_{n}\{|x_n|^2\}}{E\{|x_n|^2\}}\right) \tag{2.8}$$

where x_n is the complex symbol, E{.} indicates the expectation operator. The effects of nonlinearity on OFDM signals can be viewed from two perspectives; signal distortion at the output of a nonlinear device and harmonic distortion and intermodulation distortion (IMD) due to the multi-carrier nature of an OFDM signal.

When an OFDM signal passes through a nonlinear device, such as a high power amplifier (HPA), the signal peaks may occasionally thrust into the saturation region of the power amplifier. As a result, the output suffers from nonlinear distortion (Figure 2.11). Therefore, highly linear amplifiers with a wide dynamic range are required to reduce the effects on nonlinear distortion, however, such kind of devices are expensive.

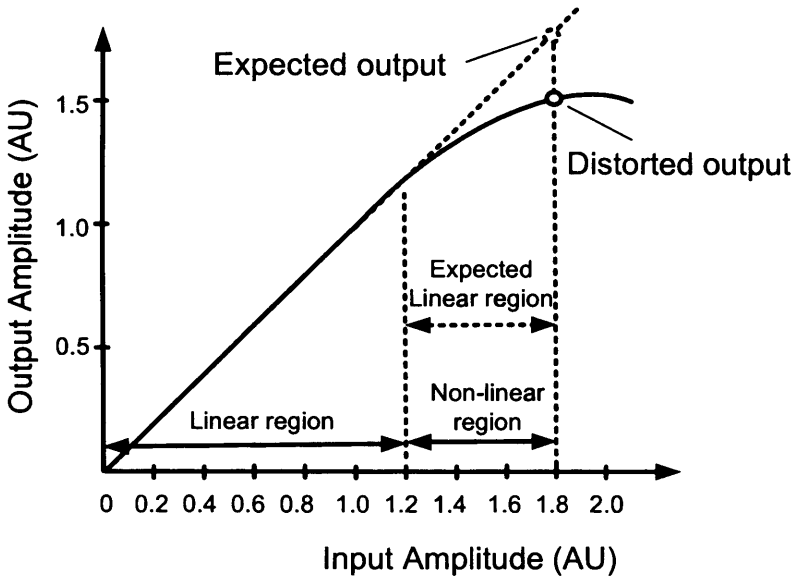

Figure 2.11. Nonlinear signal distortion of a HPA

Nonlinearity in OFDM system also results in introduction of harmonic distortion and IMD by the nonlinear elements in the systems. For example, the nonlinear distortion performance of an amplifier is often expressed in terms of intercept points or intermodulation points. The intercept points are found by extrapolating fundamental and harmonic input-output amplitude curves from the signal range where little distortion occurs [37]. It is also important to note that even-order distortion is mapped to bands that are far from the original OFDM signal passband. It is assumed that these are filtered out and do not influence the symbol-error-rate (SER). Therefore, only odd-order distortion is of importance. Furthermore, the 3rd order distortion is often dominant and will give a good estimate of the SER to be expected. Therefore, if the 3rd order harmonics are considered, the distorted signal will contain three parts: the original signal with frequency f_1, f_2 and f_3; the harmonics $3f_1$, $3f_2$ and $3f_3$; and IMD products of the form $f_i+f_j+f_v$, $f_i+f_j-f_v$, $2f_i+f_j$

and $2f_i$-f_j where i, j and v are integers of different harmonics. These newly generated frequency terms cause in-band and out-of-band distortion, which leads to error performance degradation and signal spectral spreading, respectively.

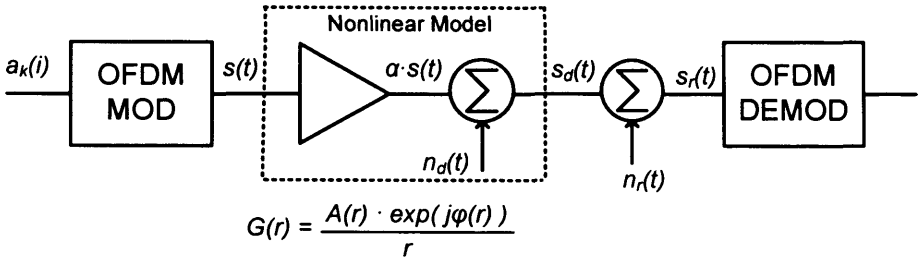

Figure 2.12. Nonlinear OFDM system model in non-fading AWGN channel

Figure 2.12 shows an equivalent OFDM system with nonlinear effects (nonlinear amplifier) in non-fading AWGN channel. Different types of nonlinear models can be applied. Here the Saleh model [38], which is a widely accepted travelling-wave tube (TWT) model, is described. According to the central limit theorem, the complex baseband OFDM signal can be modelled as a complex Gaussian process when the number of subcarriers is large. This allows the analytical treatment of nonlinear OFDM systems making use of the more general results for nonlinear distortions of Gaussian signals. Therefore the Bussgang theorem [39] can be applied in the TWT model, which indicates that a nonlinear output is the sum of a useful attenuated input replica and an uncorrelated nonlinear distortion. This can be expressed by:

$$s_d(t) = s_u(t) + n_d(t) = \alpha \cdot s(t) + n_d(t) \tag{2.9}$$

When additive white Gaussian noise is considered, the final output signal $s_r(t)$ is given by:

$$s_r(t) = s_d(t) + n(t) = \alpha \cdot s(t) + n_d(t) + n(t) \tag{2.10}$$

where $s(t)$ is the input OFDM signal, $s_u(t)$ and $n_d(t)$ are the useful and distorted signal, $s_d(t)$ is the output signal from nonlinear model, $n(t)$ is the Gaussian noise signal, α is the attenuation coefficient of the useful

component, and finally $G(r)$ is the gain of the amplifier with amplitude and phase distortions. For a Saleh model, the gain $G(.)$ is given by:

$$G(|s(t)|) = \frac{A(|s(t)|) \cdot e^{\{j\varphi(|s(t)|)\}}}{|s(t)|} \tag{2.11}$$

where $|s(t)|$ denotes the amplitude of $s(t)$, function $A(.)$ and $\varphi(.)$ represent an AM/AM (amplitude) and AM/PM (phase) distortions, respectively. For a TWT model, both functions are given by:

$$A(r) = \frac{\gamma r}{1 + \beta \cdot r^2} \tag{2.12}$$

$$\varphi(r) = \frac{\alpha_\varphi \cdot r^2}{1 + \beta_\varphi \cdot r^2} \tag{2.13}$$

Here r represents the amplitude of the input signal $r = |s(t)|$, γ is a small signal gain. β is a parameter defining the saturation point of the input and output signal of the Saleh model. The maximum input saturation voltage A_i can be found by partial derivative of the function $A(.)$. Therefore, it is found that when $A_i = 1/\sqrt{(\beta)}$, the maximum output amplitude A_o equals half of the input amplitude, $A_o = A_i/2$. Note that A_i and A_o are the maximum saturation input and output amplitude, respectively. They can be used to define two common parameters that quantify the nonlinear distortion: input backoff (IBO) and output backoff (OBO) [40], which are defined as:

$$IBO = 10 \log \frac{A_i^2}{P_{in}} \tag{2.14}$$

$$OBO = 10 \log \frac{A_o^2}{P_{out}} \tag{2.15}$$

Where A_i^2 and A_o^2 are the maximum input and output power, P_{in} and P_{out} are the average input and output power, respectively. It should be noted that higher IBO gives less distortion due to the nonlinearity.

In recent years, considerable attention has been drawn in the field of performance assessment and performance improvement of nonlinear OFDM systems [40-44]. A number of PAPR reduction techniques have been

proposed to reduce the signal dynamic range and improve the performance of OFDM systems in nonlinearities. Techniques such as clipping and filtering [45] and peak cancelling [46], have been proposed that based on the principles of reducing the PAPR by distorting the signal with high peaks. There are also other techniques [47-49] that have been proposed for OFDM nonlinearity system performance improvement. The study of these techniques is beyond the scope of this thesis.

2.4.2. OFDM synchronization

Synchronization errors are mainly caused by symbol timing offsets and carrier frequency offsets in OFDM systems [50-52]. The carrier frequency offsets originate from frequency inaccuracy in the local oscillator at the transmitter and receiver. The symbol timing offset error occurs when an OFDM signal is delayed and/or the symbol is not sampled at the correct intervals.

Carrier frequency offsets introduce a shift in the spectrum of the received OFDM signal. It comprises of two parts as shown below:

$$\varepsilon = \varepsilon_0 + 2\pi \cdot nf_s \tag{2.16}$$

where ε represents the carrier frequency offsets, ε_0 is the fine frequency error which represents the frequency error that is less than half of the subcarrier spacing, and nf_s is the coarse frequency that indicates the integer number of carrier spacing. These errors are illustrated in Figure 2.13.

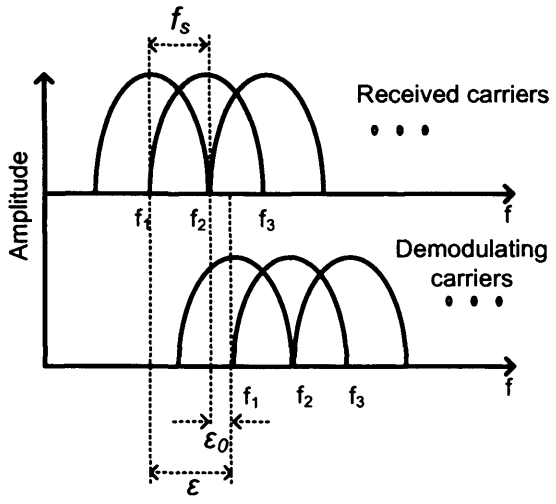

Figure 2.13. Frequency offset errors

If the frequency error is an integer number of the subcarrier spacing, i.e. fine frequency error is zero, orthogonality still holds between subcarriers. However, when the demodulated data at the output of FFT do not correspond to the correct transmitted symbols, a very high BER occurs. Similarly, if the frequency offset is not an integer number of the subcarrier spacing, the orthogonality is lost between subcarriers, which in turn introduces ICI and distorts the demodulated signal. It is also noted that the effect of frequency offset becomes severer as the number of subcarriers increases within a given bandwidth, since the frequency separation between the subcarriers is reduced. It is shown in [51] that the subcarriers at the centre of the frequency band suffer nearly twice the ICI than the subcarriers at the edge of the band. This is because interference affects the subcarriers in the centre more than at the edge of the OFDM band. Frequency offsets therefore induce degradation in the BER.

OFDM is relatively robust to timing offsets, due to the use of cyclically extended guard time without causing any ISI and ICI. Timing offset occurs when the received symbol is delayed and/or is not sampled at the correct intervals. When the timing offset extends over the OFDM symbol boundaries, then ISI and ICI occur. However, when the timing offset does not extend over the symbol interval, each subcarrier only suffers from a phase offset. The

relationship between the phase offset φ at the n^{th} subcarrier and the timing offset τ is given by:

$$\varphi_n = 2\pi \cdot nf_s \cdot \tau \tag{2.17}$$

Therefore, for an OFDM system with N subcarriers and a frequency spacing of $1/T$, a timing delay of one sampling interval of T/N causes a phase shift of $2\pi(1\text{-}1/N)$ rad between the first and last subcarriers.

There are also other problems which cause synchronisation errors. For example, phase noise, which is caused by the random perturbation of the phase of the local oscillator frequency [50;51]. Sampling frequency errors also occur when the clock at the receiver is not aligned with that of the transmitter. Hence, the received OFDM symbol has a different sampling rate from the transmitted symbols and thus results in timing jitter [52].

2.5 Fast-OFDM System

Fast-OFDM is an adaptation of OFDM, which was developed by Rodrigues and Darwazeh at University College London in 2002 and by Xiong at Cleveland State University [1;2]. The basic feature of Fast-OFDM is its bandwidth efficiency when compared to OFDM, as it requires only half the bandwidth of an OFDM system using the same modulation system to transmit the same data rate. This feature currently applies only for single dimensional modulation schemes like binary phase shift keying (BPSK) or M-ary amplitude shift keying (M-ASK) [3]. In this thesis we consider Fast-OFDM for user with complex modulation schemes such as quadrature phase shift keying (QPSK) and 16-quadrature amplitude modulation (16-QAM).

2.5.1. Definition of Fast-OFDM system

Fast-OFDM is based on the OFDM principle with the advantage of having twice the bandwidth efficiency of OFDM, where the frequency separation of the sub-carriers is $(1/2T)$ Hz with T being the duration of the

signalling interval. In other words, a Fast-OFDM system will achieve the same data rate as OFDM, while using only half of the bandwidth.

The complex envelope of a Fast-OFDM signal is shown as follows:

$$S_{Tx,Fast-OFDM}(t) = \sum_{k=-\infty}^{\infty} \sum_{n=0}^{N-1} a_{n,k} p_n(t - kT) \tag{2.18}$$

where each Fast-OFDM complex carrier is

$$p_n(t) = \frac{1}{\sqrt{T}} e^{j\frac{\pi n t}{T}}, t \in [0, T]$$

For FFT-based Fast-OFDM, the mathematical expression is written as follows:

$$x_{m,Fast-OFDM} = \frac{1}{\sqrt{N}} \sum_{n=0}^{N-1} X_n e^{j\frac{\pi m n}{N}}, m = 0, \ldots, N-1 \tag{2.19}$$

where the scaled sample are $x_m = \sqrt{T/N} x(mT/N)$. These two equations may be compared to the OFDM equations (2.1) and (2.4), respectively.

The block diagrams for an oscillator-based and FFT-based OFDM system are shown in Figure 2.14 and Figure 2.15, respectively. A comparison of OFDM and Fast-OFDM is given in Table 2.3. It is important to note that one way of producing a Fast-OFDM symbol is based on the partial symmetry in the IFFT samples, as it is observed that a partial symmetry in the IFFT samples exists when real symbols are applied to an IFFT [53]. Such symbols can be obtained when data has only real values, as in one dimensional modulation schemes such as BPSK or M-ASK.

For partial symmetry, it is observed that the output IFFT samples are such that $x_{N-m} = x_m^*$ for m=0,...,N-1. Therefore, by transmitting the first (N/2)+1 IFFT samples and discarding the rest, a Fast-OFDM signal is effectively generated using the IFFT, whereby at the receiver the discarded samples are recovered by taking the complex conjugates of the received values.

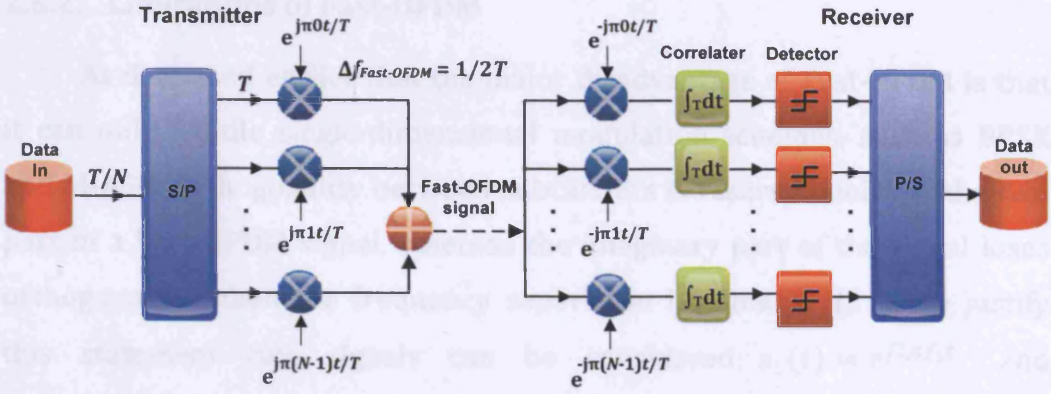

Figure 2.14. Oscillator based Fast OFDM system

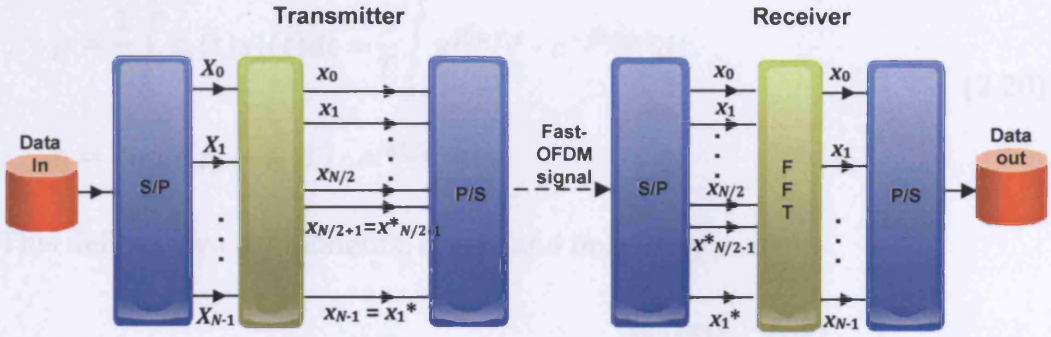

Figure 2.15. FFT based Fast OFDM system

Table 2.3. Comparison of OFDM and Fast-OFDM systems

	OFDM	Fast-OFDM
Principle	**OFDM** is a transmission scheme that distributes the high-rate data stream into many low-rate data streams that are transmitted in a parallel way over many orthogonal sub channels separated with $(1/T)$ Hz	**Fast-OFDM** is based on the OFDM principle, with the advantage of having twice the bandwidth efficiency of OFDM, where the frequency separation of the sub-carriers is $(1/2T)$ Hz
Complex envelope	$S_{Tx,OFDM}(t) = \sum_{k=-\infty}^{\infty} \sum_{n=0}^{N-1} a_{n,k} g_n(t - kT)$ $g_n(t-kT)$ are the OFDM complex subcarriers $g_n(t) = \frac{1}{\sqrt{T}} e^{j\frac{2\pi nt}{T}}, t \in [0, T]$	$S_{Tx,Fast-OFDM}(t) = \sum_{k=-\infty}^{\infty} \sum_{n=0}^{N-1} a_{n,k} p_n(t - kT)$ $p_n(t-kT)$ are the Fast-OFDM complex subcarriers $p_n(t) = \frac{1}{\sqrt{T}} e^{j\frac{\pi nt}{T}}, t \in [0, T]$
Discrete time	$x_{m,OFDM} = \frac{1}{N} \sum_{n=0}^{N-1} X_n e^{j\frac{2\pi mn}{N}}, m = 0, \dots, N-1$	$x_{m,Fast-OFDM} = \frac{1}{\sqrt{N}} \sum_{n=0}^{N-1} X_n e^{j\frac{\pi mn}{N}}, m = 0, \dots, N-1$

2.5.2. Limitations of Fast-OFDM

As discussed earlier that the major disadvantage of Fast-OFDM is that it can only handle single-dimensional modulation schemes, such as BPSK and M-ASK. Orthogonality between subcarriers is reserved only for the real part of a Fast-OFDM signal, whereas the imaginary part of the signal loses orthogonality when the frequency separation becomes $1/(2T)$. To justify this statement two signals can be considered: $s_1(t) = e^{j2\pi f_1 t}$ and $s_2(t) = e^{j2\pi f_2 t}$. Both of the signals have duration T and their correlation coefficient ρ is given as:

$$\rho = \frac{1}{T}\int_0^T s_1(t)s_2^*(t)dt = \frac{1}{T}\int_0^T e^{j2\pi f_1 t} \cdot e^{-j2\pi f_2 t}dt$$
$$\rho = sinc[(f_1 - f_2)T] \cdot e^{j\pi(f_1 - f_2)T} \tag{2.20}$$

This defines two components, real ρ_r and imaginary ρ_i as:

$$\rho_r = Re(\rho) = sinc[(f_1 - f_2)T] \cdot \cos\pi(f_1 - f_2)T = \frac{\sin(2\pi(f_1 - f_2)T)}{2\pi(f_1 - f_2)T}$$
$$\rho_i = Im(\rho) = sinc[(f_1 - f_2)T] \cdot \sin\pi(f_1 - f_2)T = \frac{\sin^2(\pi(f_1 - f_2)T)}{\pi(f_1 - f_2)T} \tag{2.21}$$

Figure 2.16 shows plots of the real and imaginary part of the correlation coefficient versus normalised frequency difference $(f_1 - f_2)T$. It can be observed from the figure that ρ_r is zero when the frequency difference between he two signals is an integer multiple of $1/2T$. Therefore, the real parts of the two signals are orthogonal when their frequency separation is $1/2T$. On the other hand, ρ_i is zero when the frequency difference between the two signals is an integer multiple of $1/T$. In the OFDM case, where the separation of the subcarriers is $1/T$, orthogonality is preserved in both the real and the imaginary part of the OFDM signal. Whereas, in the Fast-OFDM case, where the subcarrier separation is $1/2T$, orthogonality between the subcarriers is preserved only for the real part of the signal, thereby limiting the use of Fast-OFDM to real signals.

Figure 2.16. Plots of ρ versus normalised frequency difference: a) Real and b) imaginary part [3]

Hence, for a received signal *r(t)* over an ideal noiseless channel, assuming time interval *k* starts from 0, (′) indicating received signal,

$$r(t) = S_{Rx,Fast-OFDM}(t) = \sum_{k'=0}^{\infty} \sum_{n'=0}^{N-1} a'_{n,k} \cdot p'_{n',Fast-OFDM}(t - k'T) \tag{2.22}$$

The recovered symbol $y_{n,k}$ is found as:

$$y_{n,k} = \int_{kT}^{(k+1)T} r(t) \cdot p^*_{n,Fast-OFDM}(t - kT)dt$$

$$= \int_{kT}^{(k+1)T} \sum_{k'=0}^{\infty} \sum_{n'=0}^{N-1} a'_{n,k} \cdot p'_{n',Fast-OFDM}(t - k'T) \cdot p^*_{n,Fast-OFDM}(t - kT)dt$$

$$= \frac{1}{T} \int_0^T \sum_{n'=0}^{N-1} a_{n'} \cdot e^{j\frac{\pi \cdot n' \cdot t}{T}} \cdot e^{j\frac{-\pi \cdot n \cdot t}{T}} dt$$

$$= \frac{1}{T} \int_0^T \sum_{n'=0}^{N-1} a_{n'} \cdot e^{j\frac{\pi \cdot (n' - n) \cdot t}{T}} dt$$

$$= \sum_{n'=0}^{N-1} a_{n'} sinc\left(\frac{n' - n}{2}\right) \cdot e^{j\frac{\pi \cdot (n' - n)}{2}} \tag{2.23}$$

For real received signals (with BPSK or M-ASK), which are multiplied by the complex sinc term in equation (2.23), only the imaginary part of the recovered symbol will be distorted. The symbol can be recovered with no ICI by decoding its real part, as information is carried only in the real part of the symbol. However, for complex modulation scheme, like QPSK or 16-QAM, multiplication with the complex sinc term will distort both the real and imaginary parts of the symbol, and hence makes the recovery of the symbol difficult.

2.6 System modeling in ADS

In order to assess the capabilities and limitation of the Fast-OFDM technique, a system model was designed and studied. The performance metrics of the Fast-OFDM system are compared to OFDM. This section describes the proposed system models of OFDM and Fast-OFDM schemes implemented in ADS. The system assumptions and configurations are also detailed.

2.6.1. System implementation of OFDM and Fast-OFDM

Figure 2.17 shows a block diagram of the proposed OFDM system transmitter implemented in ADS. A screenshot of the ADS model is also shown in the Appendix A.1.

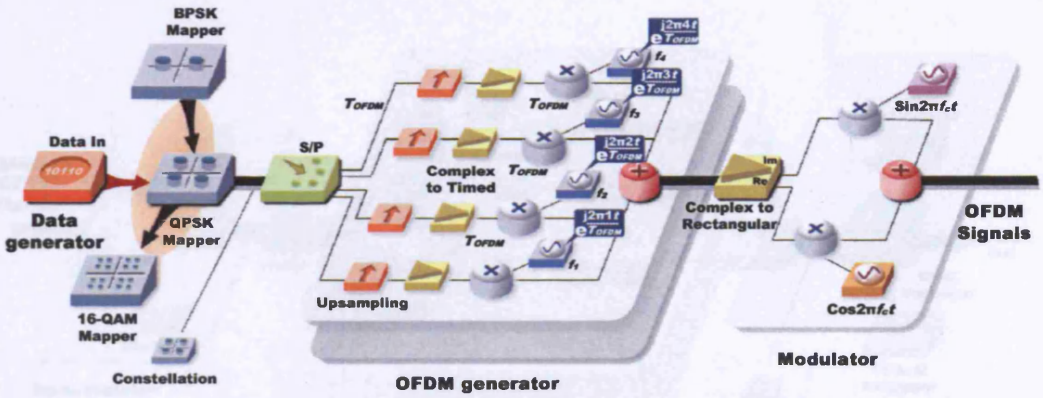

Figure 2.17. Oscillator based OFDM/Fast-OFDM system model - transmitter

The system is a 4-subcarrier oscillator-based passband OFDM system in a time-invariant AWGN channel. In this work the guard interval is excluded. The data generator ("Date In") generates random binary bits with an initial bit rate R_b of 1 Mb/s or bit period T_b of 1 μs, which are then mapped into complex symbols using different mapping schemes with the symbol rate of R_s or the symbol duration of T_s. The mapped complex symbols are then serial-to-parallel (S/P) converted into four lower rate sub-data streams, which has a symbol rate of R_{OFDM} ($R_s/4$) or symbol period of T_{OFDM} ($4T_s$) on each data stream. Upsampling and numeric to timed conversion are

the two techniques applied for timing information insertion. The sub-data streams are modulated by four complex sub-carriers with a frequency spacing of $1/T_{OFDM}$ and summed for OFDM signal generation. The signal is then split into its real and imaginary parts and fed into an IQ modulator for RF signal transmission.

During transmission, the complex AWGN is added to the arriving signal. The elements of the noise signal are independent Gaussian random variables with zero mean and variance $N_0/2$. The received signals are de-modulated using an IQ demodulator. The demodulated signal is then multiplied with the complex conjugate of each subcarrier, integrated over the signaling interval T_{OFDM}, and sampled at time T_{OFDM} for signal detection. The detected signals are parallel-to-serial (P/S) converted and, finally, demapped into the original date bits. Figure 2.18 shows the block diagram of the OFDM receiver.

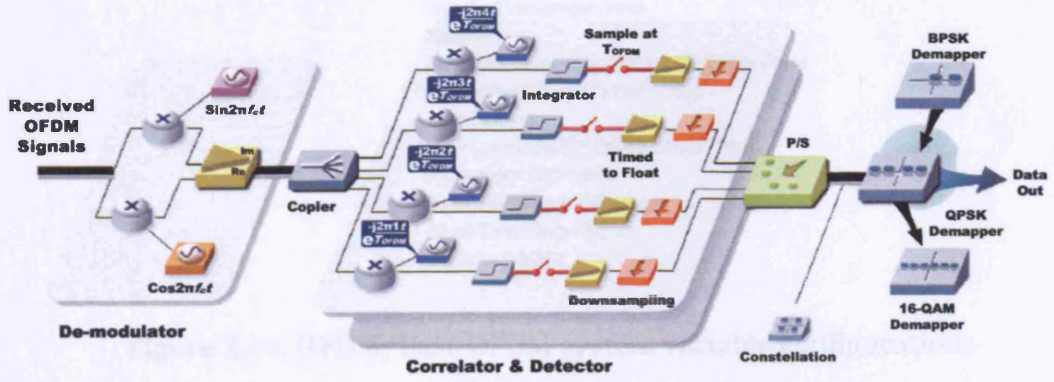

Figure 2.18. Oscillator based OFDM/Fast-OFDM system model - receiver

For the Fast-OFDM system, the transceiver is similar to OFDM except that the frequency separation between subcarriers is adjusted to $1/(2T_{OFDM})$.

2.6.2. System implementation in ADS

2.6.2.1 OFDM system implementation

In order to implement the system in ADS, designs discussed in the previous section need to be translated into the discrete sampled world of the ADS simulation platform. As an illustration, we take both systems to have the same data rate, the simulation time step (i.e. "TStep") must be set in such a way so that both systems have 1 μs bit duration. Figure 2.19 shows the variable configurations defined for the BPSK OFDM/Fast-OFDM system. The simulation time step is set to a hundred times smaller than the initial bit period. The frequency spacing (i.e. "DF") is the inverse of OFDM symbol duration, which is controlled by an overlapping coefficient λ_{FDM} (i.e. "Lambda"), with λ_{FDM} = 1 and 0.5 for OFDM and Fast-OFDM, respectively.

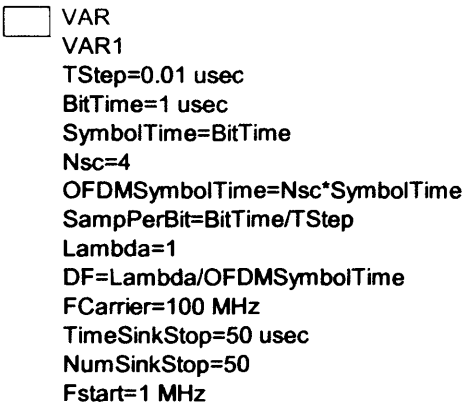

Figure 2.19. OFDM/Fast-OFDM system variable configurations

In ADS there are two types of simulation methods, "numeric" and "timed". The difference between the two is that in "timed" simulation the duration of each pulse and consequently the period and frequency of the signal are known. "Numeric" simulation is usually used to model baseband system, whereas, "timed" simulation is more suitable for RF systems. Both of the simulation can be performed at the same time in ADS.

Taking the BPSK OFDM/Fast-OFDM system as an example, the source information of the system is initially generated using a single numeric "Bits" component and then mapped into complex symbols using a "Mapper" component with different mapping schemes (Figure 2.20). The "Bits"

component is configured to generate equiprobable random binary bit sequences. Figure 2.21 shows the first 11 bits of the data and the mapping. The mapped bits are then S/P converted using a "Distributor" followed by a "BusSplit" component (Figure 2.22). The "Distributor" component synchronously splits one input stream into N output streams. With "BlockSize" = 1, it sends the first bit to the first output, the second bit to the next output, until the N^{th} output. Then the $(N+1)^{th}$ bit to the first output, $(N+2)^{th}$ bit to the next output, and so on.

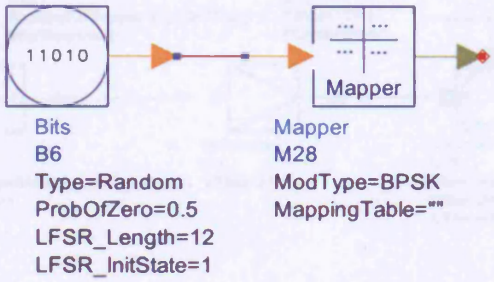

Figure 2.20. Data generation and mapping

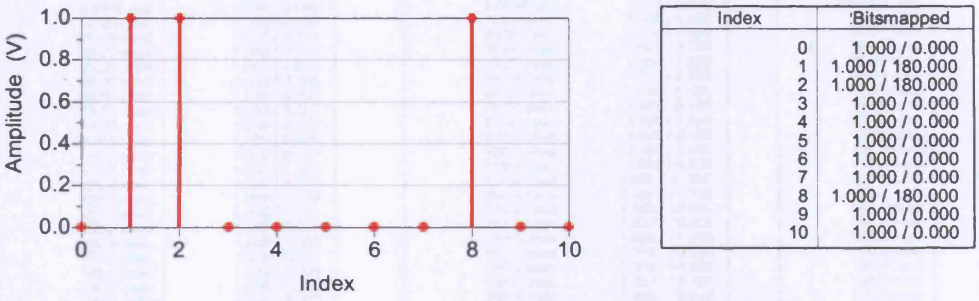

Figure 2.21. First eleven bits generation and mapping

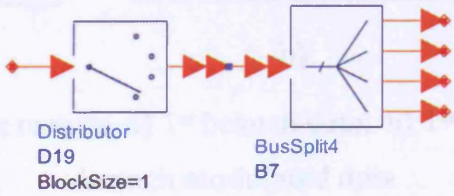

Figure 2.22. Serial to parallel converter

After S/P conversion, each branch of binary bit sequence is upsampled and assigned with timing information using a "Repeat" component and a "IntToTimed" component, respectively. The timed data is then modulated

with an exponential subcarrier generated using a "ComplexExp" and a "CxToTimed" component (Figure 2.23). The subcarrier frequency is set to $2\pi\Delta ft \times N$ with N being the N^{th} subcarrier. The first subcarrier is centred around 2.25 MHz during baseband modulation. Figure 2.24 and Figure 2.25 show the numeric results and signal shape in time domain of the 1st branch of data stream modulated with the 1st subcarrier, respectively.

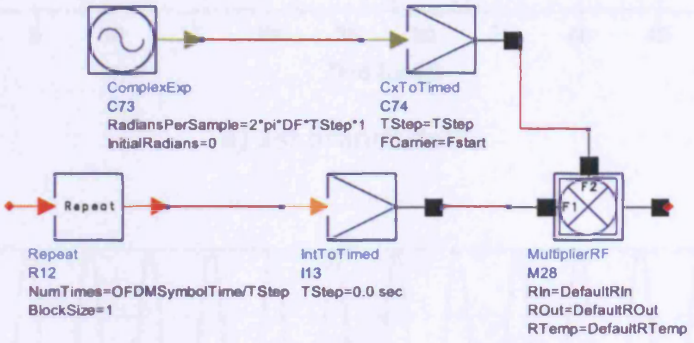

Figure 2.23. 1st OFDM subcarrier modulation [2]

time	var("014datacarrier1")
0.0000 sec	1.000 / 0.000
10.00 nsec	1.000 / 0.000
20.00 nsec	1.000 / 0.000
30.00 nsec	1.000 / 0.000
40.00 nsec	1.000 / 0.000
50.00 nsec	1.000 / 0.000
60.00 nsec	1.000 / 0.000
70.00 nsec	1.000 / 0.000
80.00 nsec	1.000 / 0.000
90.00 nsec	1.000 / 0.000
100.0 nsec	1.000 / 0.000
110.0 nsec	1.000 / 0.000
120.0 nsec	1.000 / 0.000
130.0 nsec	1.000 / 0.000
140.0 nsec	1.000 / 0.000
150.0 nsec	1.000 / 0.000
160.0 nsec	1.000 / 0.000
170.0 nsec	1.000 / 0.000
180.0 nsec	1.000 / 0.000
190.0 nsec	1.000 / 0.000
200.0 nsec	1.000 / 0.000
210.0 nsec	1.000 / 0.000
220.0 nsec	1.000 / 0.000
230.0 nsec	1.000 / 0.000
240.0 nsec	1.000 / 0.000
250.0 nsec	1.000 / 0.000
260.0 nsec	1.000 / 0.000
270.0 nsec	1.000 / 0.000
280.0 nsec	1.000 / 0.000
290.0 nsec	1.000 / 0.000

a)

time	var("013subcarrier1")
0.0000 sec	1.000 / 0.000
10.00 nsec	1.000 / 0.900
20.00 nsec	1.000 / 1.800
30.00 nsec	1.000 / 2.700
40.00 nsec	1.000 / 3.600
50.00 nsec	1.000 / 4.500
60.00 nsec	1.000 / 5.400
70.00 nsec	1.000 / 6.300
80.00 nsec	1.000 / 7.200
90.00 nsec	1.000 / 8.100
100.0 nsec	1.000 / 9.000
110.0 nsec	1.000 / 9.900
120.0 nsec	1.000 / 10.800
130.0 nsec	1.000 / 11.700
140.0 nsec	1.000 / 12.600
150.0 nsec	1.000 / 13.500
160.0 nsec	1.000 / 14.400
170.0 nsec	1.000 / 15.300
180.0 nsec	1.000 / 16.200
190.0 nsec	1.000 / 17.100
200.0 nsec	1.000 / 18.000
210.0 nsec	1.000 / 18.900
220.0 nsec	1.000 / 19.800
230.0 nsec	1.000 / 20.700
240.0 nsec	1.000 / 21.600
250.0 nsec	1.000 / 22.500
260.0 nsec	1.000 / 23.400
270.0 nsec	1.000 / 24.300
280.0 nsec	1.000 / 25.200
290.0 nsec	1.000 / 26.100

b)

time	...r("02carrier1mod")
0.0000 sec	0.500 / 0.000
10.00 nsec	0.500 / 0.900
20.00 nsec	0.500 / 1.800
30.00 nsec	0.500 / 2.700
40.00 nsec	0.500 / 3.600
50.00 nsec	0.500 / 4.500
60.00 nsec	0.500 / 5.400
70.00 nsec	0.500 / 6.300
80.00 nsec	0.500 / 7.200
90.00 nsec	0.500 / 8.100
100.0 nsec	0.500 / 9.000
110.0 nsec	0.500 / 9.900
120.0 nsec	0.500 / 10.800
130.0 nsec	0.500 / 11.700
140.0 nsec	0.500 / 12.600
150.0 nsec	0.500 / 13.500
160.0 nsec	0.500 / 14.400
170.0 nsec	0.500 / 15.300
180.0 nsec	0.500 / 16.200
190.0 nsec	0.500 / 17.100
200.0 nsec	0.500 / 18.000
210.0 nsec	0.500 / 18.900
220.0 nsec	0.500 / 19.800
230.0 nsec	0.500 / 20.700
240.0 nsec	0.500 / 21.600
250.0 nsec	0.500 / 22.500
260.0 nsec	0.500 / 23.400
270.0 nsec	0.500 / 24.300
280.0 nsec	0.500 / 25.200
290.0 nsec	0.500 / 26.100

c)

Figure 2.24.Numeric results a) 1st branch data, b) 1st subcarrier and c) 1st branch modulated data

[2] In ADS, different types of blocks are distinguished using different color coding schemes. A "timed" block has a black arrow, whereas a "numeric" block has a yellow arrow. A blue arrow represents floating point input/output number (real), whereas a green arrow indicates complex input/output number. Finally, a red arrow indicates any input/output.

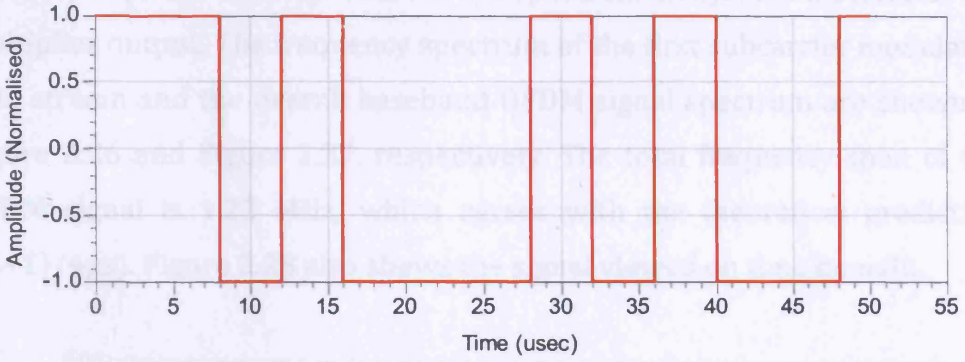

a) 1st branch data

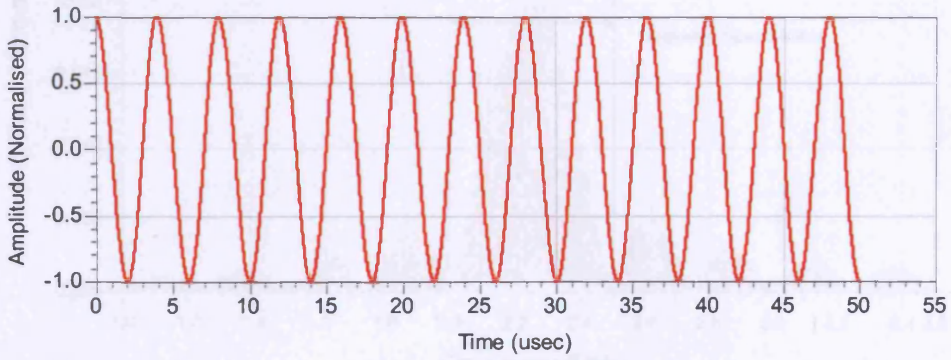

b) 1st subcarrier (Real part)

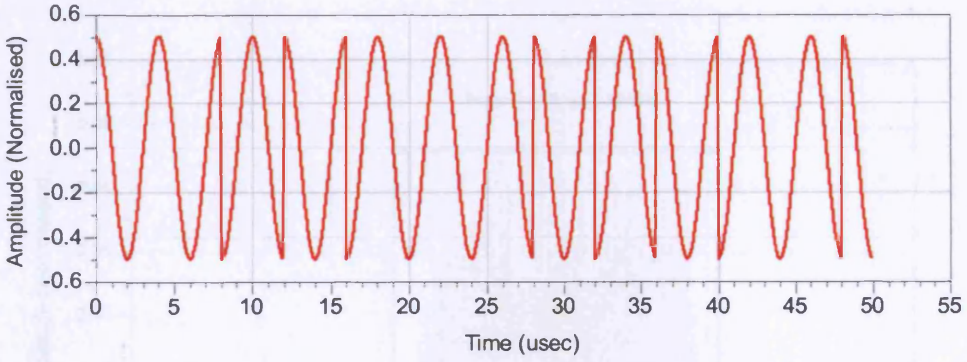

c) 1st branch modulated data (Real part)

Figure 2.25.Time domain representation

The block "MultiplierRF" in Figure 2.23 requires both "timed" input and output (black arrows). Therefore, a spectrum analyzer is inserted at the multiplier output. The frequency spectrum of the first subcarrier modulated data stream and the overall baseband OFDM signal spectrum are shown in Figure 2.26 and Figure 2.27, respectively. The total frequency span of the OFDM signal is 1.25 MHz, which agrees with the theoretical prediction ((4+1)/4μs). Figure 2.28 also shows the signal viewed on time domain.

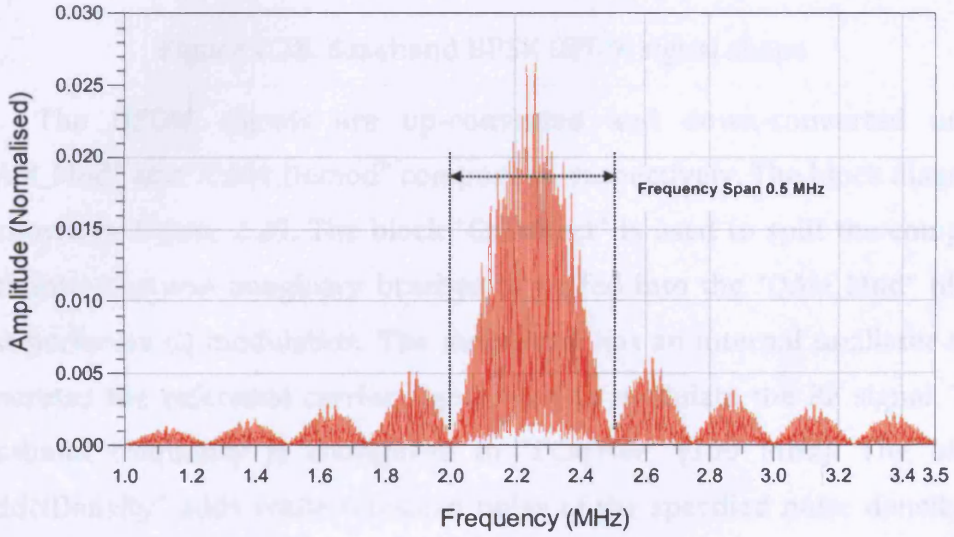

Figure 2.26. Signal spectrum of 1st subcarrier modulated data stream for OFDM

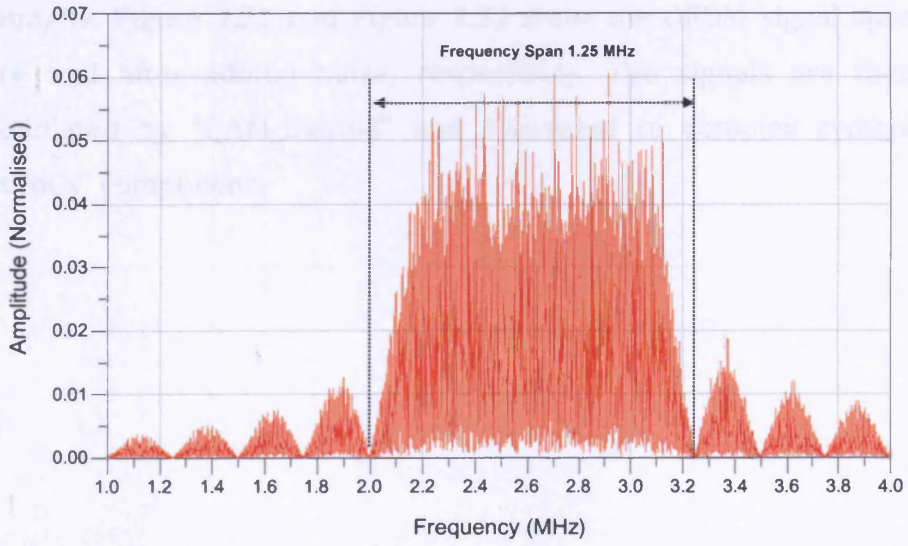

Figure 2.27. Baseband BPSK OFDM signal spectrum

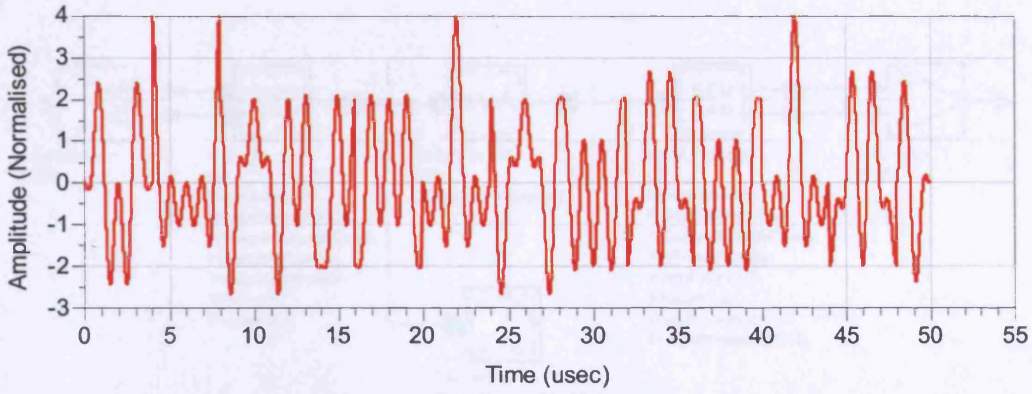

Figure 2.28. Baseband BPSK OFDM signal shape

The OFDM signals are up-converted and down-converted using "QAM_Mod" and "QAM_Demod" component, respectively. The block diagram is shown in Figure 2.29. The block "CxToRect" is used to split the complex data into real and imaginary braches to be fed into the "QAM_Mod" block that performs IQ modulation. The modulator has an internal oscillator that generates the reference carrier signal used to modulate the RF signal. The passband frequency is configured to "FCarrier" (100 MHz). The block "AddNDensity" adds white Gaussian noise of the specified noise density to the input signal. Figure 2.30 shows the AWGN channel configurations. "ModOutPower" is the signal power measured at the input of "AddNDensity". "NDensity" is the noise power spectrum density determined in dBm/Hz. Figure 2.31 and Figure 2.32 show the OFDM signal spectrum before and after adding noise, respectively. The signals are then I/Q demodulated by "QAM_Demod" and converted to complex symbols by "RectToCx" component.

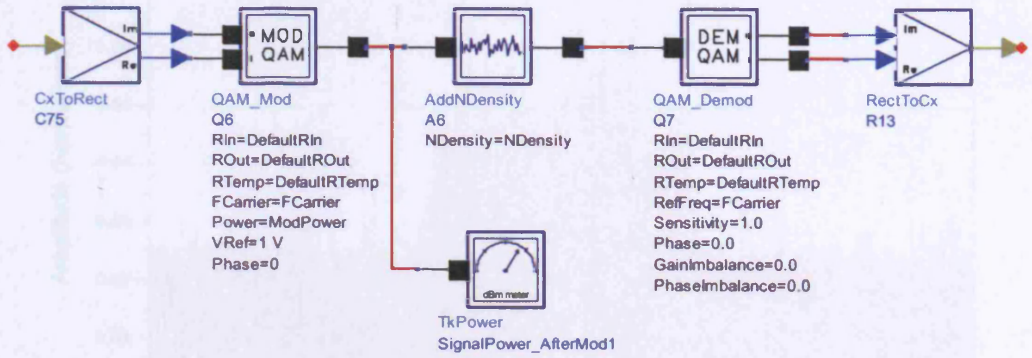

Figure 2.29. Up-conversion and down-conversion

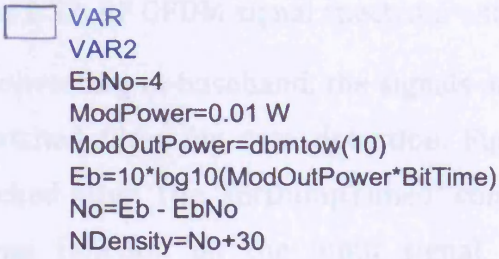

Figure 2.30. AWGN channel configuration

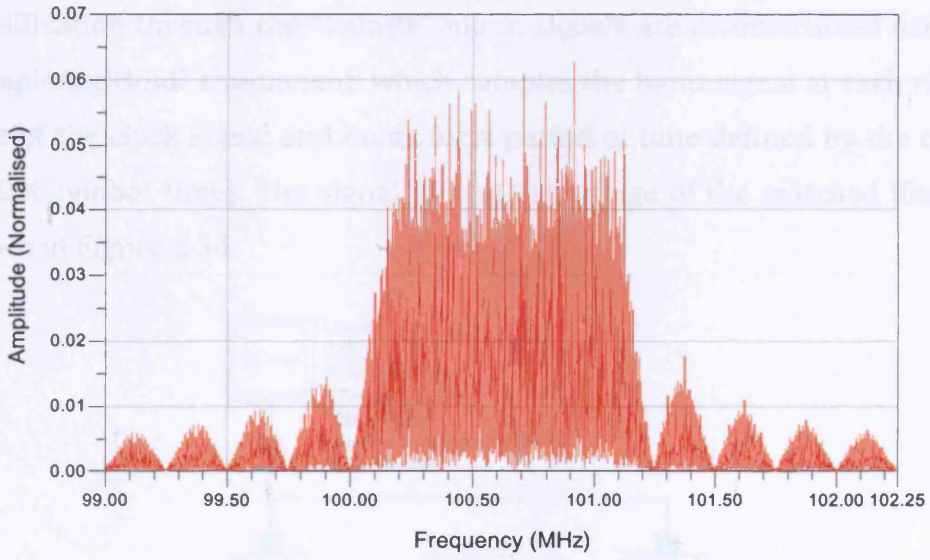

Figure 2.31. RF OFDM signal spectrum without noise

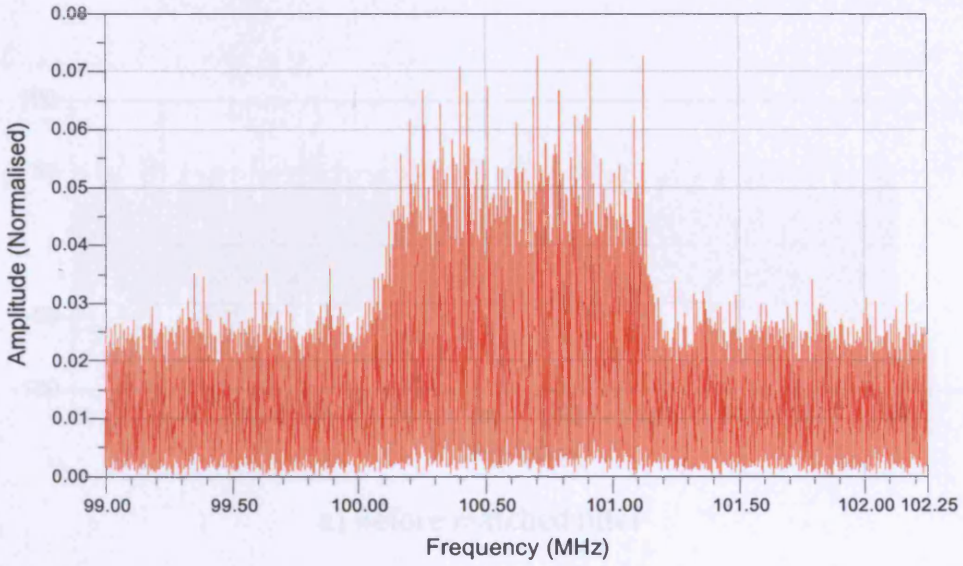

Figure 2.32. RF OFDM signal spectrum with noise

After down-converting to baseband, the signals are then demodulated and fed into a matched filter for data detection. Figure 2.33 shows the content of the matched filter. The "IntDumpTimed" component performs an integrate and dump function on the input signal, where the time of integration is determined by the clock signal generated from the "Clock" component. The period of the clock is the OFDM symbol duration. After amplification through the "GainRF" block, signals are reconstructed using a "SampleAndHold" component, which samples the input signal at each rising edge of the clock signal and holds for a period of time defined by the clock (OFDM symbol time). The signal plot at each stage of the matched filter is shown in Figure 2.34.

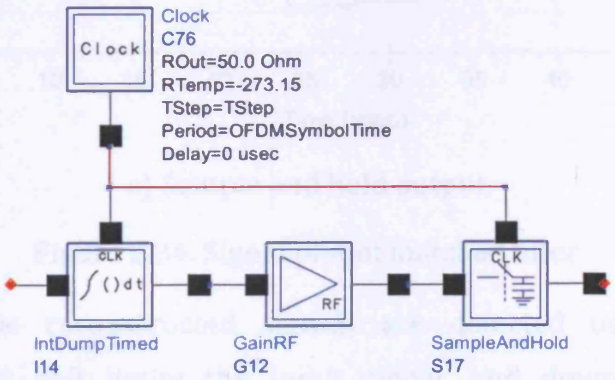

Figure 2.33. Block diagram of matched filter

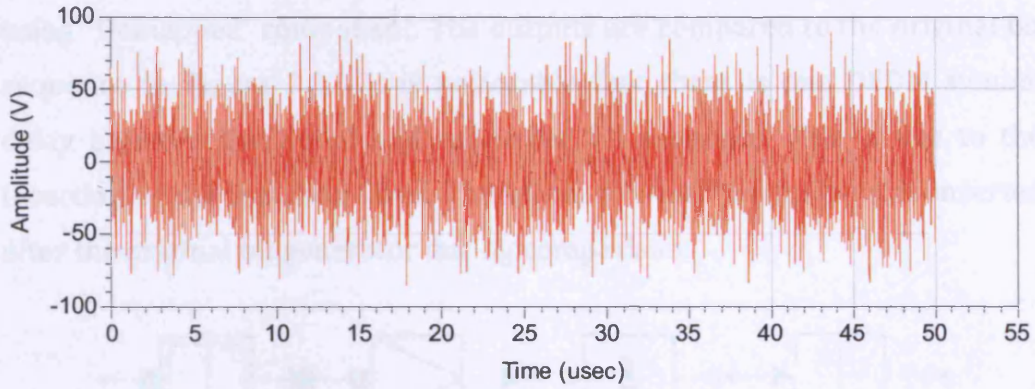

a) Before matched filter

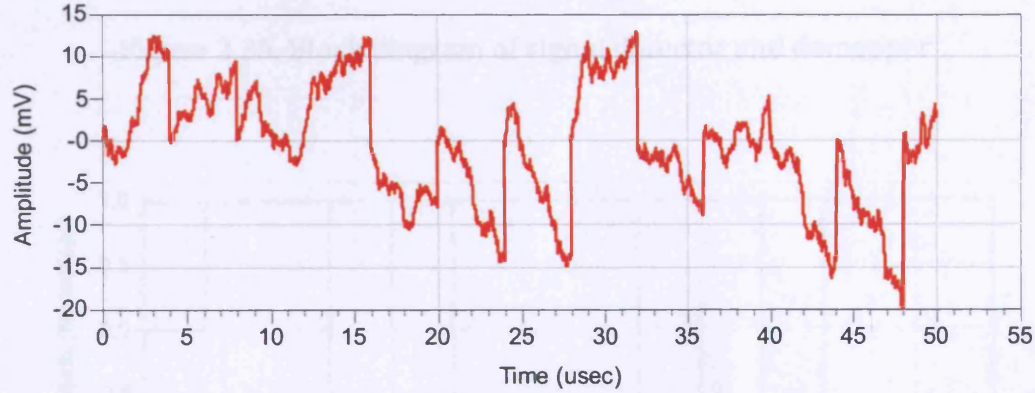

b) After integration and amplification

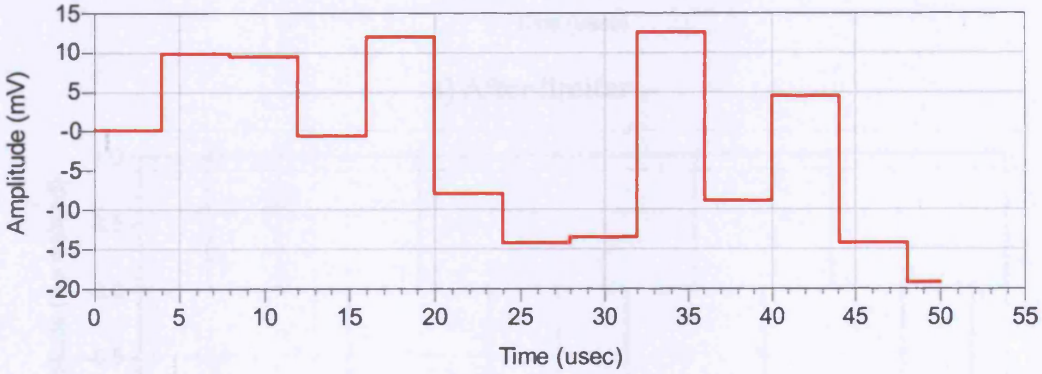

c) Sample and hold output

Figure 2.34. Signal plot of matched filter

Finally the reconstructed signals are detected using a Limiter component that soft limits the input signal, and downsampled using "TimedToFloat" and "DownSample" component for symbol regeneration

(Figure 2.35). The shape of the signal at the detector is shown in Figure 2.36. The regenerated complex symbols are demapped into binary bit sequences using "Demapper" component. The outputs are compared to the original bit sequence in Figure 2.37. It is noticeable that there is one OFDM symbol delay between the initial and recovered bit sequence. This is due to the insertion of the matched filter. Therefore, a "Delay" component is inserted after the original bit generator during comparison.

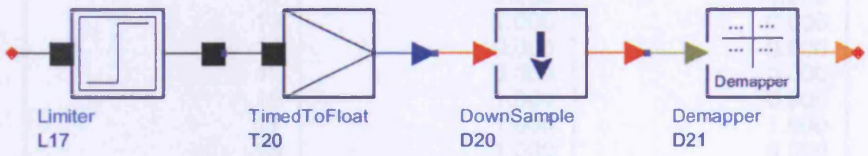

Figure 2.35. Block diagram of signal detector and demapper

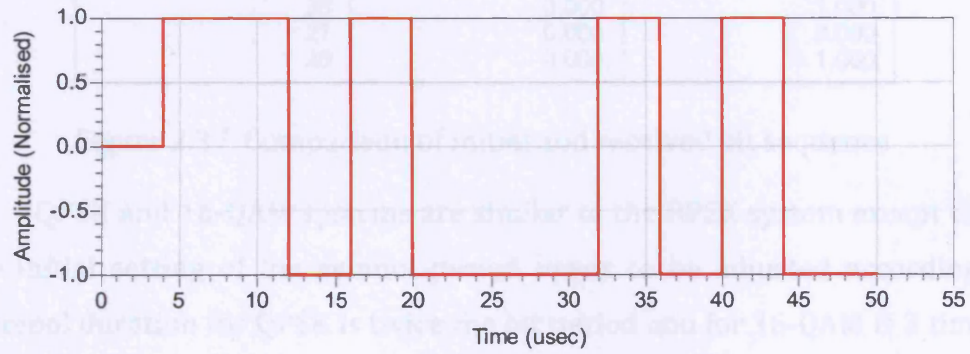

a) After limiter

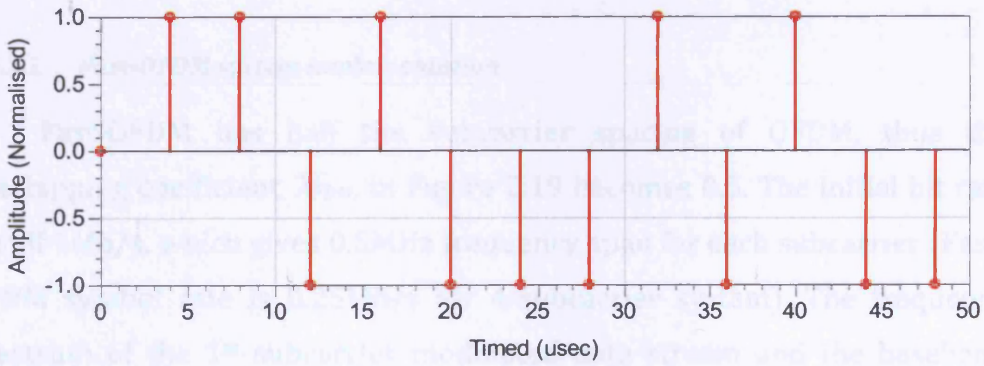

b) Downsamppling

Figure 2.36. Signal plot at the detector

Index	var("01Bits")	var("17demapped")
0	0.000	0.000
1	1.000	0.000
2	1.000	0.000
3	0.000	0.000
4	0.000	0.000
5	0.000	1.000
6	0.000	1.000
7	0.000	0.000
8	1.000	0.000
9	0.000	0.000
10	0.000	0.000
11	0.000	0.000
12	0.000	1.000
13	1.000	0.000
14	0.000	0.000
15	0.000	0.000
16	1.000	0.000
17	1.000	1.000
18	1.000	0.000
19	0.000	0.000
20	1.000	1.000
21	0.000	1.000
22	1.000	1.000
23	0.000	0.000
24	1.000	1.000
25	0.000	0.000
26	0.000	1.000
27	0.000	0.000
28	0.000	1.000

Delay

Figure 2.37. Comparison of initial and received bit sequence

QPSK and 16-QAM systems are similar to the BPSK system except that the initial setting of the symbol period needs to be adjusted accordingly (symbol duration for QPSK is twice the bit period and for 16-QAM is 3 times of the bit period).

2.6.2.2 Fast-OFDM system implementation

Fast-OFDM has half the subcarrier spacing of OFDM, thus the overlapping coefficient, λ_{FDM}, in Figure 2.19 becomes 0.5. The initial bit rate is still 1Mb/s, which gives 0.5MHz frequency span for each subcarrier (Fast-OFDM symbol rate is 0.25Mb/s for 4-subcarrier system). The frequency spectrum of the 1st subcarrier modulated data stream and the baseband Fast-OFDM signal are shown in Figure 2.38 and Figure 2.39 , respectively.

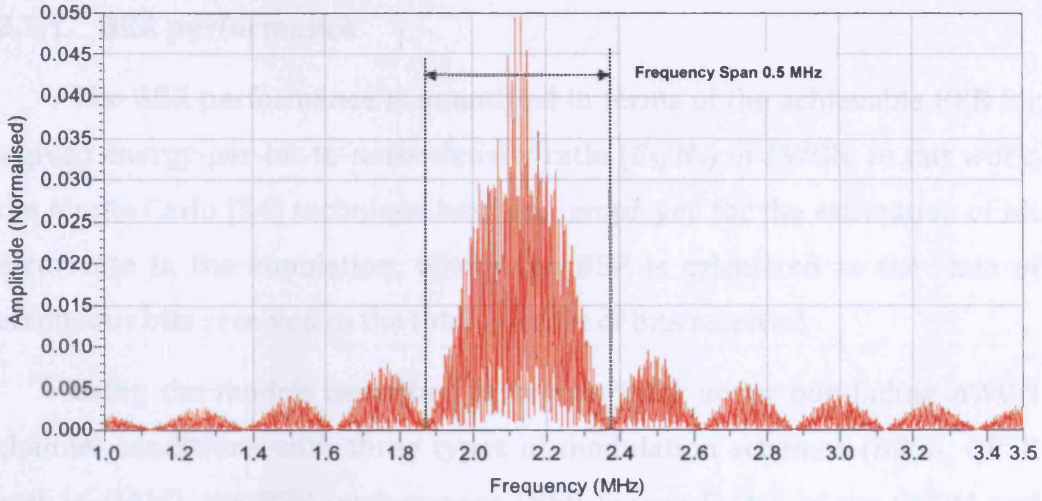

Figure 2.38. Spectrum of the 1st subcarrier modulated data stream of Fast-OFDM

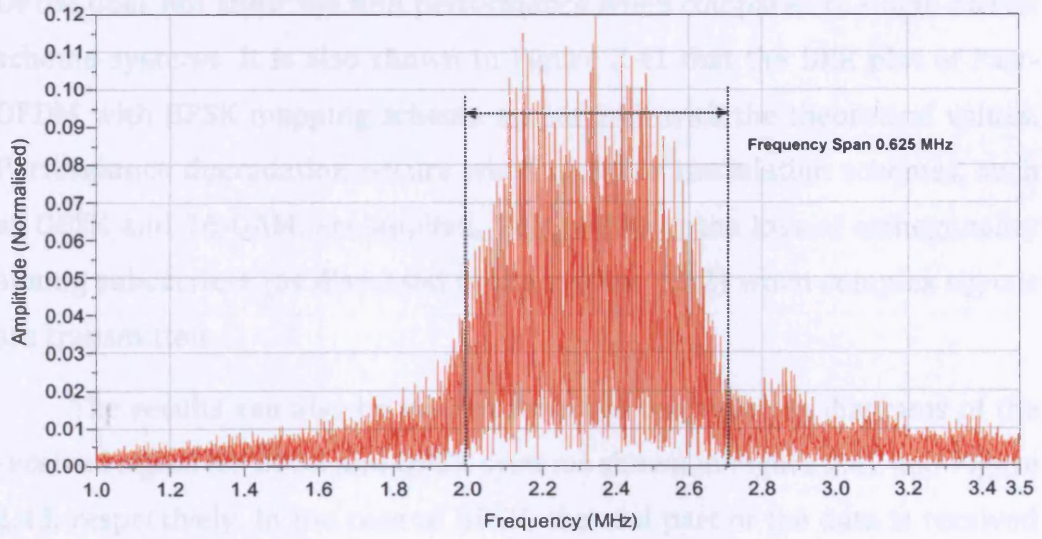

Figure 2.39. Spectrum of the baseband Fast-OFDM signal

2.7 Performance comparison of OFDM and Fast-OFDM

2.7.1. BER performance

The BER performance is quantified in terms of the achievable BER for a given energy-per-bit-to-noise-density ratio (E_b/N_o) in AWGN. In this work, the Monte Carlo [54] technique has been employed for the estimation of bit error rate in the simulation, where the BER is calculated as the ratio of erroneous bits received to the total number of bits received.

Using the models described in section 2.6.1 under non-fading AWGN channel conditions with three types of modulation schemes (BPSK, QPSK and 16-QAM), the BER performance (BER versus E_b/N_o) of the OFDM and the Fast-OFDM systems are shown in Figure 2.40 and Figure 2.41, respectively.

From Figure 2.40, it can be observed that, as expected, the insertion of OFDM does not affect the BER performance when compared to single carrier scheme systems. It is also shown in Figure 2.41 that the BER plot of Fast-OFDM with BPSK mapping scheme agrees well with the theoretical values. Performance degradation occurs when complex modulation schemes, such as QPSK and 16-QAM, are applied. This is due to the loss of orthogonality among subcarriers (as discussed in the section 2.5.2) when complex signals are transmitted.

The results can also be viewed from the constellation diagrams of the received signal for BPSK and QPSK systems shown in Figure 2.42 and Figure 2.43, respectively. In the case of BPSK, the real part of the data is received without ICI whereas the imaginary part of the data is not. A series of vertically aligned demodulated points are received, indicating the additional imaginary components (Figure 2.42 b)). Thus, the transmitted data can be recovered by taking the real part of the received signal. On the other hand, when complex mapping is applied, for example QPSK, both of the real and imaginary part of the data are affected by ICI, which makes the data recovery difficult. This explains the severe degradation in the BER performance for Fast-OFDM with complex modulations in Figure 2.41

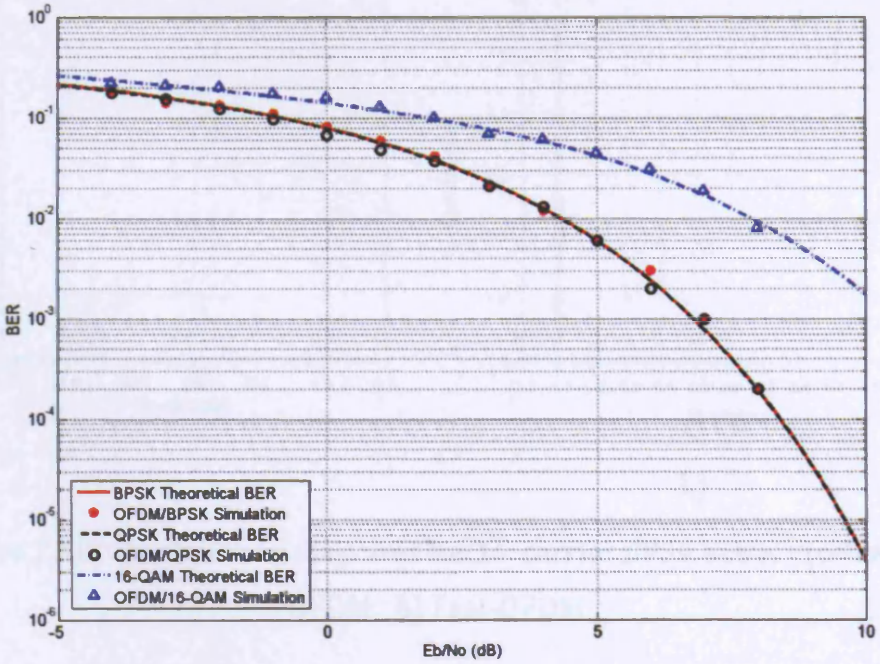

Figure 2.40. BER plot for OFDM in AWGN channel for BPSK, QPSK and 16-QAM modulations. The number of bits is 10^4; $N = 4$.

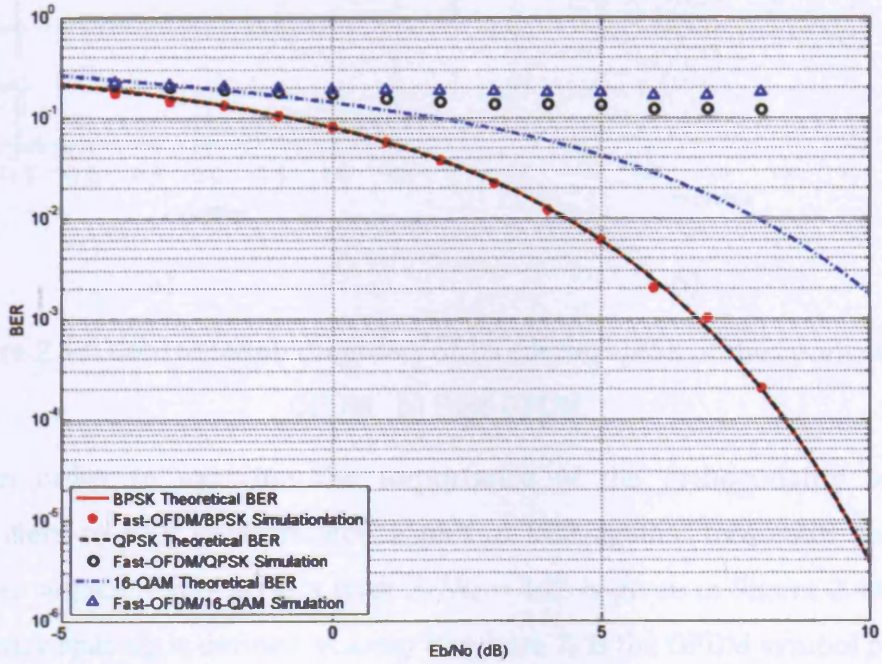

Figure 2.41. BER plot for Fast-OFDM in AWGN channel for BPSK, QPSK and 16-QAM modulations. The number of bits is 10^4; $N = 4$.

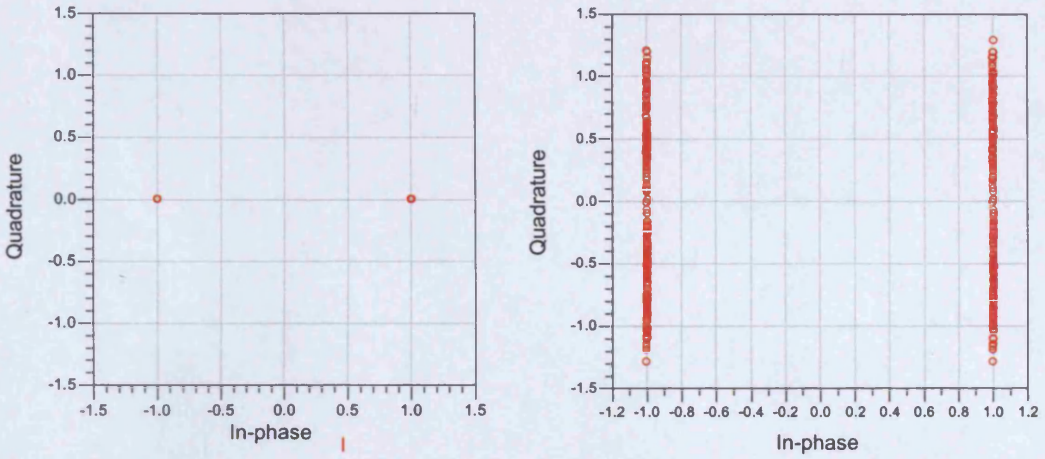

a) b)

Figure 2.42. Constellation diagrams for 16-carrier BPSK at the receiver a) OFDM b) Fast-OFDM

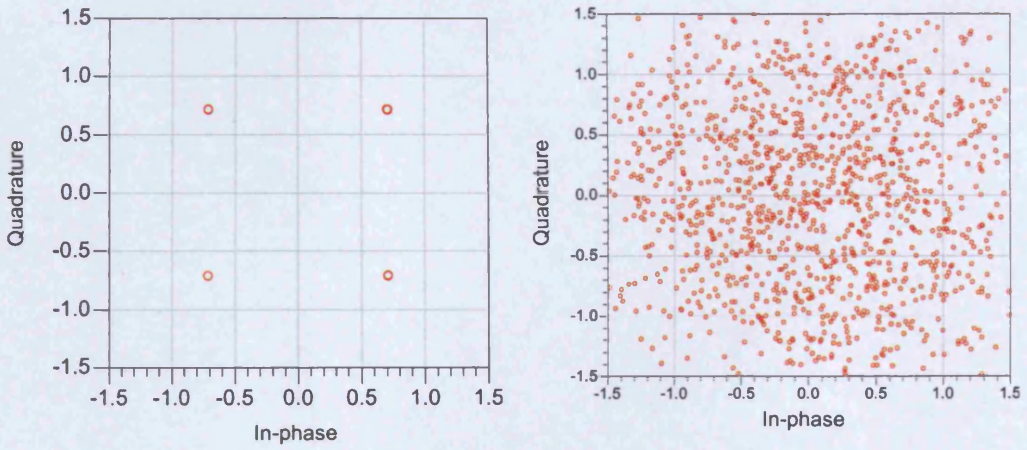

a) b)

Figure 2.43. Constellation diagrams of 16-carrier QPSK at the receiver a) OFDM b) Fast-OFDM

In order to examine the importance of the orthogonality of the subcarriers to BER performance, a plot of BER against frequency spacing between adjacent subcarriers with E_b/N_0 = 4dB is given in Figure 2.44. The frequency spacing is defined as λ_{FDM}/T_s, where T_s is the OFDM symbol period and λ_{FDM} is the overlapping coefficient for frequency spacing varying FDM systems. The overlapping coefficient varies from 0 to 2. The values of λ_{FDM} are chosen to be 0, 0.5, 1 and 2 to represent full overlapping, Fast-OFDM,

OFDM and FDM, respectively. It can be observed from the figure that, for the BPSK systems, the BER performances are close to the theoretical BPSK BER value at the points of 0.5, 1, 1.5 and 2, where the orthogonality remains between subcarriers. However, in the case of QPSK, BER performance degrades when λ_{FDM} equals 0.5 (and 1.5). This is due to the loss of orthogonality in the imaginary part of the complex Fast-OFDM signals.

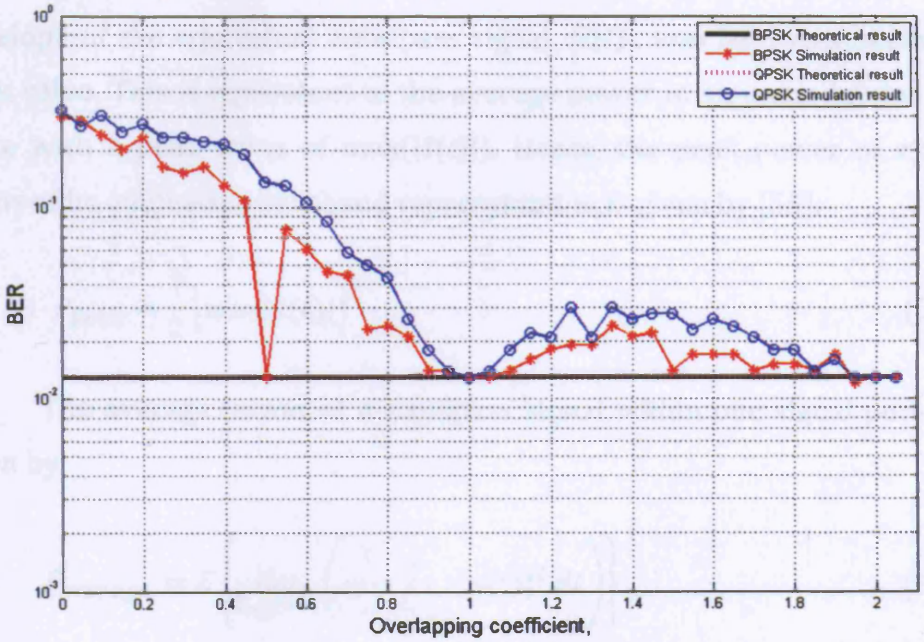

Figure 2.44. BER vs λ_{FDM} plot for variable subcarrier spacing FDM schemes. The number of bits is 10^4; $N = 4$; $E_b/N_o = 4$dB.

2.7.2. Peak to average power ratio (PAPR)

In a multi-carrier system, employing non-linear elements, the BER performance of the system is influenced by the envelope fluctuations of the transmitted signal, which are measured in terms of the PAPR of the signal. As described in section 2.4.1, the PAPR is the ratio of the peak power of the transmitted signal over the average power. The peak power of a baseband signal, $s(t)$, is given as the average power that would be obtained if the envelope of the equivalent bandpass signal, $|\tilde{s}(t)|$, was held constant at its peak value. This is equivalent to the average power in an unmodulated sine wave with a peak value of $\max(|\tilde{s}(t)|)$. Hence, the peak power of $s(t)$, in terms of its equivalent baseband representation is given by [55]:

$$P_{peak} = \frac{1}{2}\left[\max|\tilde{s}(t)|\right]^2 \tag{2.24}$$

The average power of a bandpass signal within one signal period is given by:

$$P_{average} = E\left\{\lim_{T_{sig}\to\infty}\left(\frac{1}{T_{sig}}\int_{T_{sig}}[s(t)]^2\,dt\right)\right\} \tag{2.25}$$

where T_{sig} is the duration of $s(t)$ and E{.} is the expectation operator.

The average power of $s(t)$ in terms of its equivalent baseband representation is given by [36]:

$$P_{average} = E\left\{\lim_{T_{sig}\to\infty}\left(\frac{1}{T_{sig}}\int_{T_{sig}}\frac{1}{2}|\tilde{s}(t)|^2\,dt\right)\right\} \tag{2.26}$$

From equations (2.24) and (2.26),

$$PAPR = \frac{\frac{1}{2}\left[\max|\tilde{s}(t)|\right]^2}{E\left\{\lim_{T_{sig}\to\infty}\left(\frac{1}{T_{sig}}\int_{T_{sig}}\frac{1}{2}|\tilde{s}(t)|^2\,dt\right)\right\}} \tag{2.27}$$

In this work, the PAPR is calculated over a duration of 10^4 OFDM symbols. As the main aim of the work is not to obtain the precise value of the PAPR but to present a comparison between the different implementations, 10^4 symbols is taken to be a sufficient duration for the simulation.

The PAPR of the OFDM and Fast-OFDM signals at the output of the transmitter BPSK and QPSK mapping schemes are shown in Figure 2.45. From this figure, it can be observed that the PAPR increases with the number of subcarriers N, for both mapping schemes. This is because as N increases, the peak power of the signal increases while the average power is kept constant. Theoretically, the PAPR of an OFDM signal is expressed as $10\log_{10}N$ [45]. In other words, doubling the number of subcarriers leads to a 3 dB increase in PAPR. It also can be noticed that the PAPR value of the Fast-OFDM signals are comparable to OFDM. This is due to the fact that reducing the subcarrier spacing does not affect the peak amplitude of the signals. Figure 2.46 shows the envelope of a 16-subcarrier OFDM and Fast-OFDM signal within 5-symbol periods. It can be seen from the figure that both the OFDM and Fast-OFDM signals have the same peak signal amplitudes. However, with less peaks as compared to OFDM, the Fast-OFDM signal may have lower percentage of achieving high peak amplitudes. This can be observed from the complementary cumulative distribution function (CCDF) of OFDM and Fast-OFDM in Figure 2.47. The signal range in the figure is the transient absolute signal power minus the average signal power. It can be observed that for a specific value of signal range, e.g. -20 dB, OFDM has higher possibility of achieving this value than Fast-OFDM.

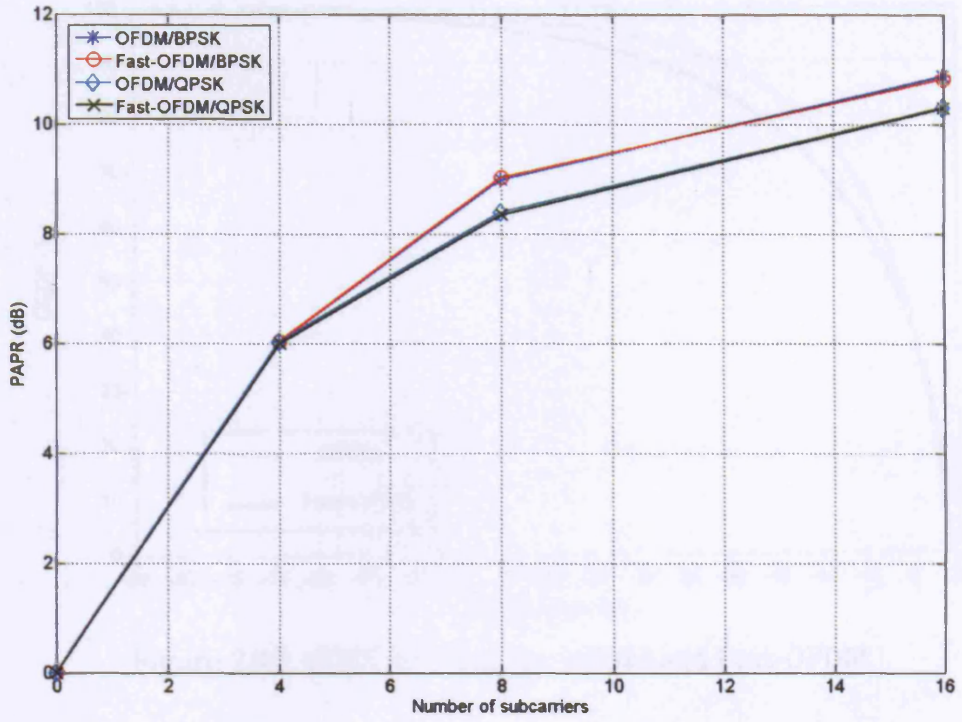

Figure 2.45. PAPR comparison of Fast-OFDM and OFDM

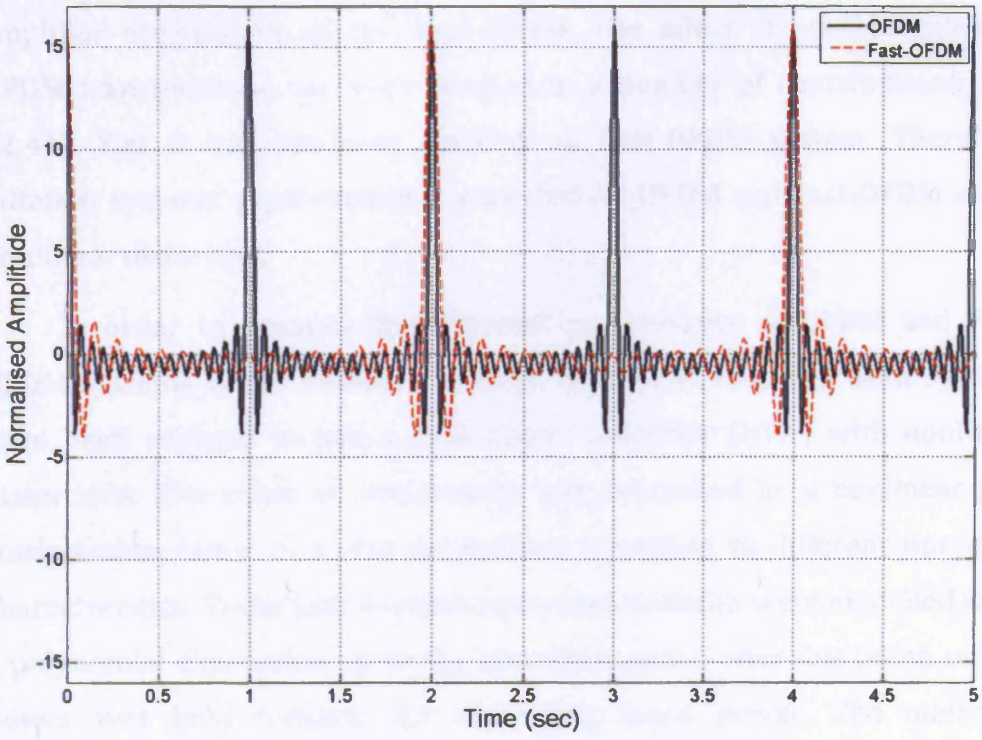

Figure 2.46. Signal envelope of 16-subcarrier OFDM and Fast-OFDM

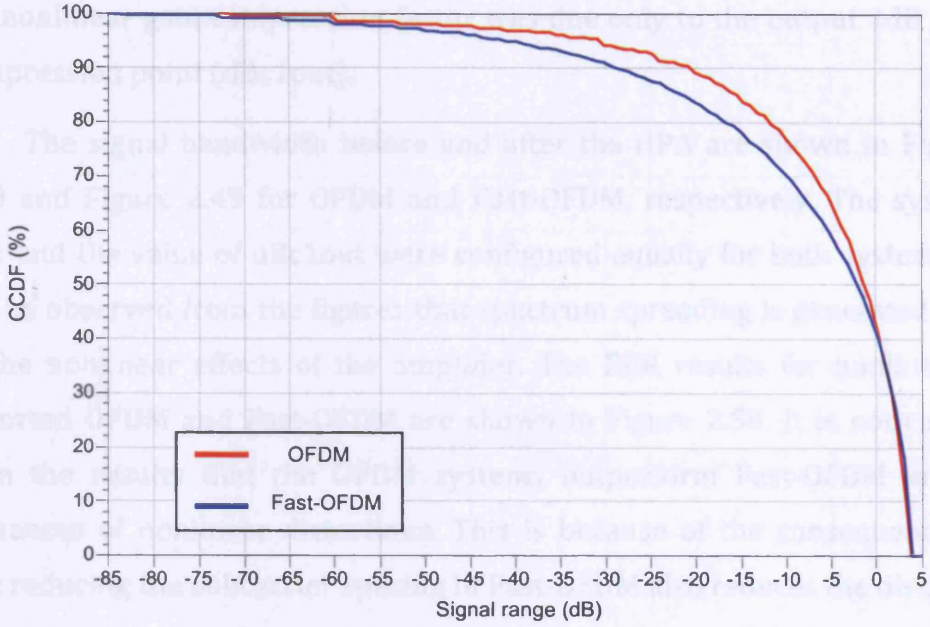

Figure 2.47. CCDF for 4-carrier OFDM and Fast-OFDM

For high power efficiency attaining, a Fast-OFDM system needs to operate near saturation regions of the transmitter power amplifier, which may result in nonlinear distortion. It is thus important to assess the effect of amplifier nonlinearity of the Fast-OFDM. The effect of nonlinearities on OFDM transmissions has been studied in a number of contributions [40-42;44]. Yet, it has not been applied on Fast-OFDM system. Therefore, different systems' performance is expected for OFDM and Fast-OFDM under nonlinear distortion.

In order to examine the different performance of OFDM and Fast-OFDM systems under nonlinear effects, the BPSK models of both systems have been adapted to add a high power amplifier (HPA) with nonlinear distortions. The effect of nonlinearity was controlled by a nonlinear gain compression factor that was determined according to different nonlinear characteristics. Those gain compression characteristics were modelled using a polynomial expression up to the saturation point; after this point, output power was held constant for increasing input power. The nonlinear characteristic of the model was the 1dB gain compression. In other words,

the nonlinear gain compression factor was due only to the output 1dB gain compression point (dBc1out).

The signal bandwidth before and after the HPA are shown in Figure 2.48 and Figure 2.49 for OFDM and Fast-OFDM, respectively. The system gain and the value of dBc1out were configured equally for both systems. It can be observed from the figures that spectrum spreading is generated due to the nonlinear effects of the amplifier. The BER results for nonlinearly distorted OFDM and Fast-OFDM are shown in Figure 2.50. It is noticeable from the results that the OFDM systems outperform Fast-OFDM in the presences of nonlinear distortions. This is because of the consequence of that reducing the subcarrier spacing in Fast-OFDM also reduces the distance between the wanted carriers and the nearby intermodulation products (IMP) generated due to nonlinear effects. Therefore, it is more difficult to filter out the IMP that may fall in-band to recover the signals. Therefore, the determining factor of BER degradation is effectively the spectral spreading.

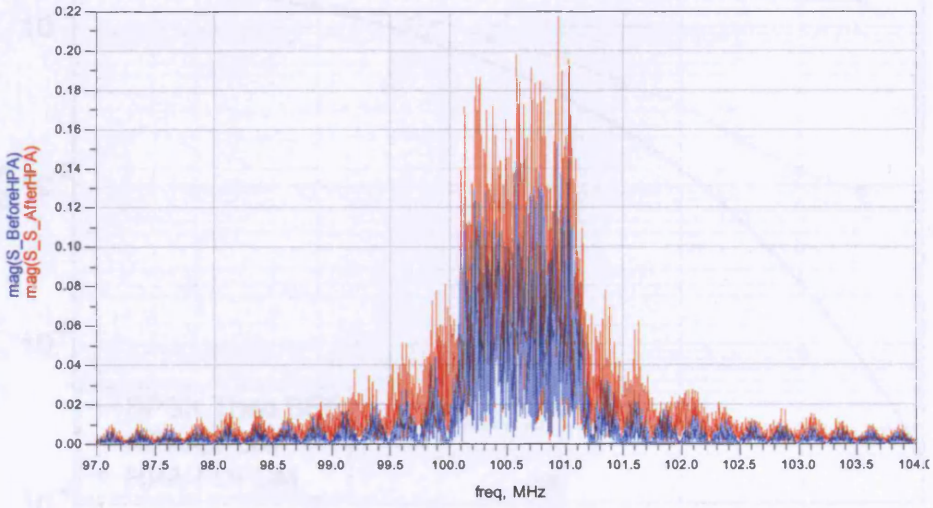

Figure 2.48. Frequency spectrum of nonlinear distorted 4-carrier OFDM system

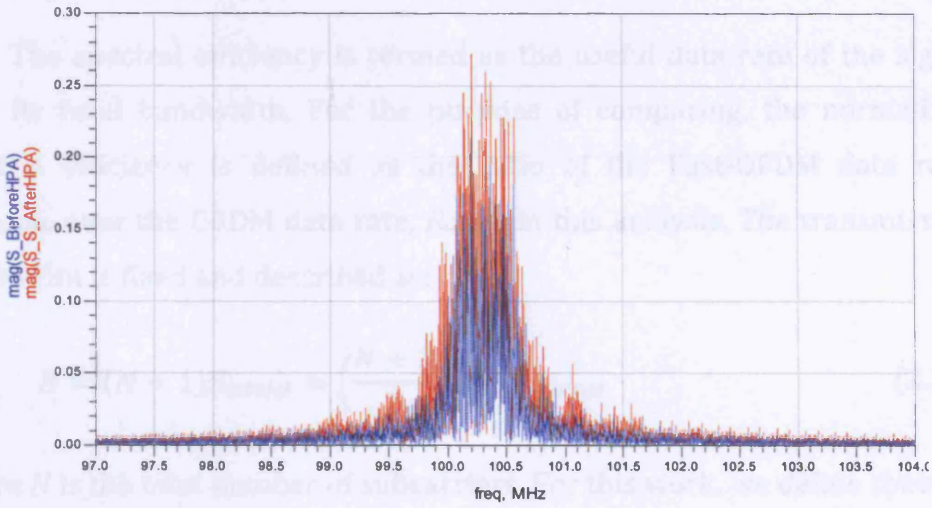

Figure 2.49. Frequency spectrum of nonlinear distorted 4-carrier Fast-OFDM

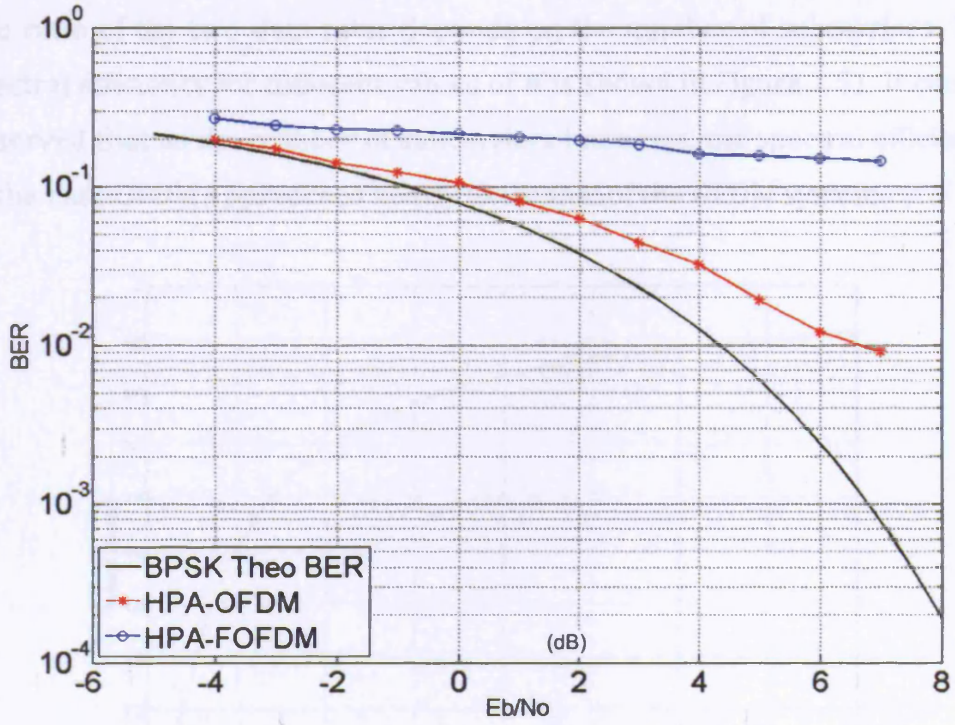

Figure 2.50. BER performance of nonlinearly distorted OFDM and Fast-OFDM

2.7.3. Spectral efficiency

The spectral efficiency is termed as the useful data rate of the signal over its total bandwidth. For the purpose of comparing, the normalized spectral efficiency is defined as the ratio of the Fast-OFDM data rate, $R_{FastOFDM}$, over the OFDM data rate, R_{OFDM}, in this analysis. The transmission bandwidth is fixed and described as:

$$B = (N+1)R_{OFDM} = \left(\frac{N+3}{2}\right)R_{Fast-OFDM} \tag{2.28}$$

where N is the total number of subcarriers. For this work, we define spectral efficiency as:

$$\eta_{FDM} = \frac{R_{Fast-OFDM}}{R_{OFDM}} = \frac{(N+1)}{\left(\frac{N+3}{2}\right)} \tag{2.29}$$

The ratio of the two data rates depends on the number of subcarriers. The spectral efficiency for different values of N is shown in Figure 2.51. It can be observed that as the number of subcarriers increases, the spectral efficiency of the Fast-OFDM approaches nearly twice that of the OFDM system.

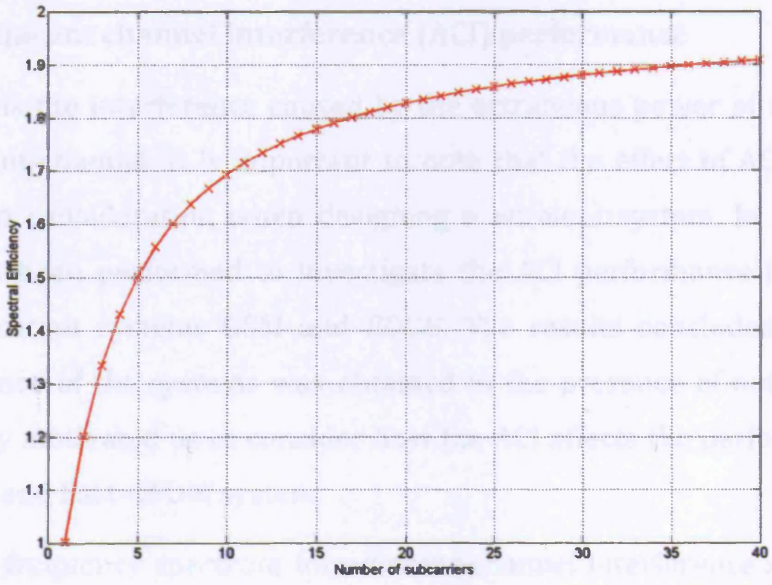

Figure 2.51. Spectral efficiency of Fast-OFDM compared to OFDM

An alternative way of comparing the two systems is to keep the data rate constant in both cases and compare the occupied bandwidth. The plot (Figure 2.52) in this case is an inverted plot of Figure 2.51. This is because, for a constant data rate, the Fast-OFDM will occupy nearly half of the bandwidth of the conventional OFDM when the number of subcarriers is large.

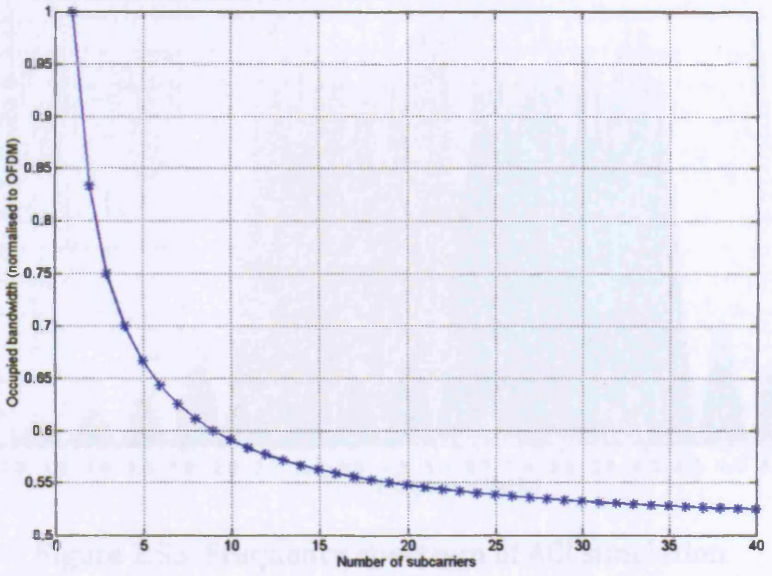

Figure 2.52. Occupied bandwidth comparison of OFDM and Fast-OFDM

2.7.4. Adjacent channel interference (ACI) performance

ACI is the interference caused by the extraneous power of a signal in an adjacent channel. It is important to note that the effect of ACI must be taken into consideration when designing a wireless system. In [56;57], a study has been performed to investigate the ACI performance for mobile communication systems GSM and EDGE. The results concluded different performance of the systems was obtained in the presence of noise or ACI. This study motivated us to consider how the ACI affects the performance of an OFDM and Fast-OFDM system.

The frequency spectrum for adjacent channel interference simulation is given in Figure 2.53. A 20% (one symbol period) spectrum overlapping is placed between the transmitting channel and the adjacent channel. Figure

2.54 shows a simplified plot of two overlapping channels for the 4 subcarrier OFDM scenario. P_s and P_a represent the power of the wanted signal and adjacent channel signal, respectively. A screenshot of the ADS model is also shown in the Appendix A.1.

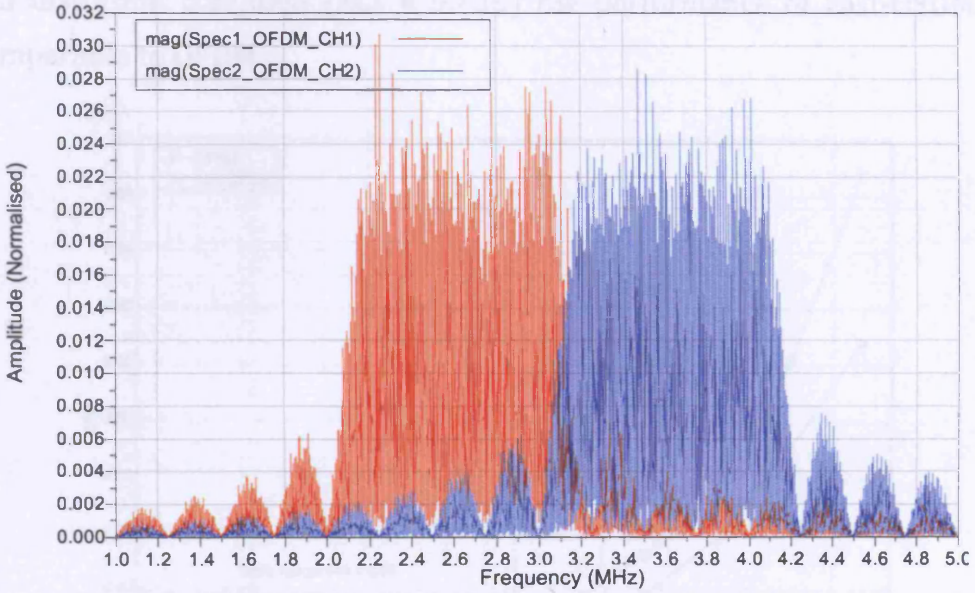

Figure 2.53. Frequency spectrum of ACI simulation

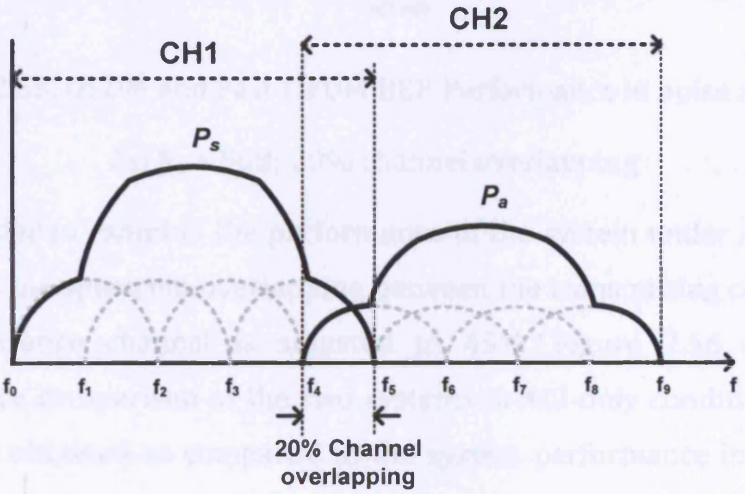

Figure 2.54. 4-carrier OFDM ACI spectrum

The performance of the systems in noise and ACI is shown in Figure 2.55 with the input E_b/N_o at 5 dB. The x-axis represents the ACI signal power normalised to the transmitting signal power. In other words, the ACI is defined as:

$$ACI = 10\log_{10}\frac{P_a}{P_s} \tag{2.30}$$

The results show that OFDM performs better than Fast-OFDM as the interfering signal power increases. It also may be observed that for small ACI distortion condition (ACI < 0.7dB) the performance of Fast-OFDM is comparable to OFDM.

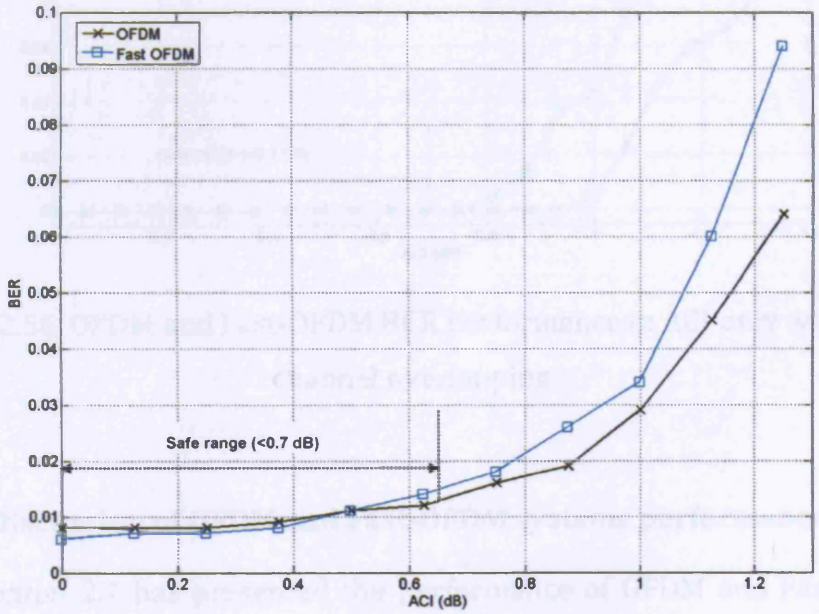

Figure 2.55. OFDM and Fast-OFDM BER Performance in noise and ACI;

E_b/N_o = 5dB; 20% channel overlapping

In order to examine the performance of the system under ACI-limited conditions, the spectrum overlapping between the transmitting channel and the interference channel is adjusted to 45%. Figure 2.56 shows the performance comparison of the two systems in ACI-only condition. Similar results are obtained as compared to the system performance in noise and ACI.

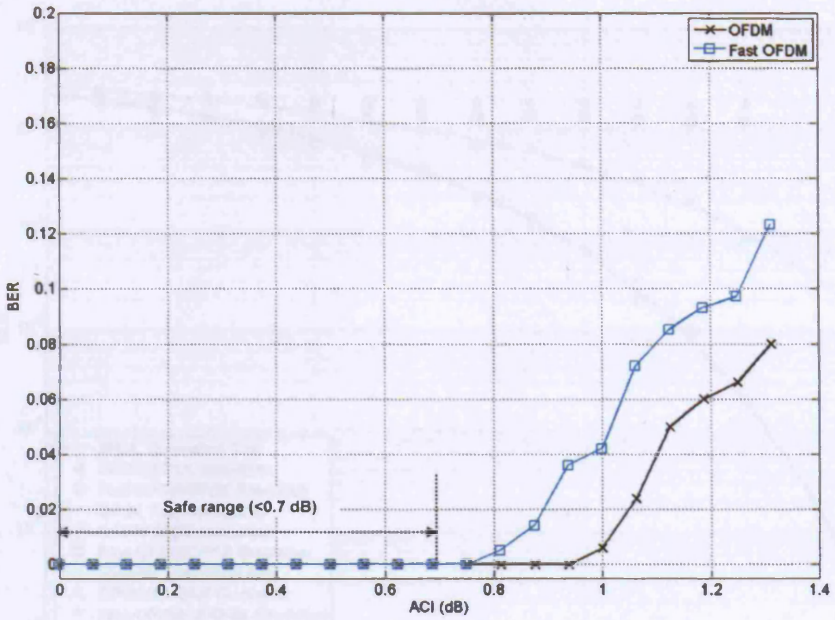

Figure 2.56. OFDM and Fast-OFDM BER Performance in ACI-only with 45% channel overlapping

2.7.5. Discussion of OFDM and Fast-OFDM systems performance

Section 2.7 has presented the performance of OFDM and Fast-OFDM for different mapping schemes. In both cases, the initial data rate was made constant. Comparing the two schemes for the same input data rate shows that as the number of subcarriers increases, the spectral efficiency of the Fast-OFDM approaches nearly twice of the OFDM system.

Comparing the BER performance of the two systems in the presence of AWGN for different mapping schemes (Figure 2.57) shows that the BER performance of Fast-OFDM is comparable to OFDM in the case of BPSK and deteriorates severely when complex modulation schemes (QPSK and 16-QAM) are applied. It is also interesting to note that further decreasing the subcarrier spacing (as compared to Fast-OFDM) results in exponential BER performance degradation due to ICI (Figure 2.44).

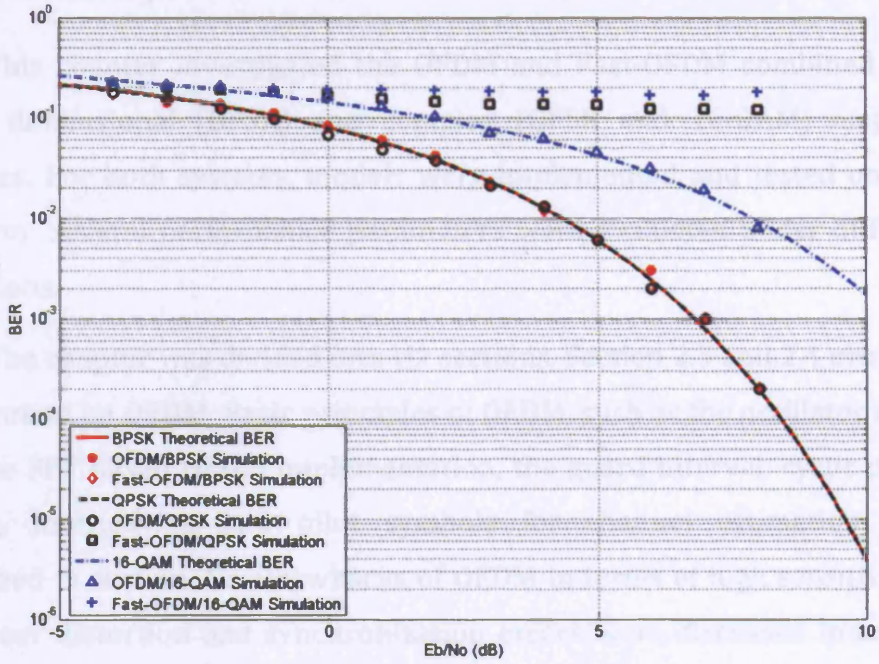

Figure 2.57. BER plots for OFDM and Fast-OFDM for BPSK, QPSK and 16-QAM modulations. The number of testing bits is 10^4, $N = 4$.

Figure 2.45 presents the PAPR variations of the two implementations for different mapping schemes. Comparison of the results reveals that the PAPR of Fast-OFDM is comparable to that of OFDM for both BPSK and QPSK mapping schemes. In both cases, the PAPR increases with the number of subcarriers. It is also interesting to note that OFDM systems outperforms Fast-OFDM in the presences of nonlinear distortions, though Fast-OFDM has better CCDF due to the fact that less peaks happen in Fast-OFDM compared to OFDM.

Comparing the performances of the two systems with BPSK mapping scheme in ACI-limited and ACI plus noise scenarios shows that OFDM performs better than Fast-OFDM. This is a consequence of the fact that in the case of Fast-OFDM, reducing the subcarrier spacing in half generates larger ICI between subcarriers and ACI from adjacent Fast-OFDM channels as compared to OFDM.

2.8 Summary

This chapter investigated the OFDM and Fast-OFDM combined with single dimensional (BPSK) and complex (QPSK and 16-QAM) mapping schemes. For both systems, models were implemented and tested on ADS platform. Several performance parameters were evaluated under different conditions.

The chapter was divided into six sections. Section 2.3 and 2.4 provided background on OFDM. Basic principles of OFDM, such as the oscillator based and the FFT based OFDM implementation, the guard interval, cyclic prefix, coding, interleaving and pilot symbols for channel estimation were described in section 2.3. Drawbacks of OFDM in terms of high sensitivity to nonlinear distortion and synchronization errors were discussed in section 2.4. Section 2.5 introduced the Fast-OFDM and also included a discussion on the relative merits and demerits of the scheme compared to conventional OFDM. Section 2.6 presented the two implementations in ADS. The system models for both implementations were described together with system features and key parameters. Finally, the system performance parameters of the two schemes are investigated in section 2.7 in terms of BER, bandwidth efficiency, PAPR, nonlinear performance and ACI analysis.

The performance comparison of the two systems showed that Fast-OFDM had an advantage in bandwidth efficiency over conventional OFDM for large number of subcarriers. Yet Fast-OFDM suffered the limitation of supporting only single dimensional modulation schemes. Furthermore, it exhibits worse nonlinear performance and resistance to ACI as compared to OFDM. Therefore, finding the possibilities of combining Fast-OFDM with complex modulation schemes to take full advantage of the bandwidth efficiency benefits becomes vitally important. This is the subject of the Chapter 4, whilst, the following chapter explores the similarities and differences between Fast-OFDM and other newly emerging multi-carrier systems.

Chapter 3 Multi-carrier CDMA

3.1 Introduction

Over the past few years, the combination of OFDM and CDMA schemes has generated great interest in the field of wireless communications, providing high data rate and robustness to multipath effects. This combination is referred to multi-carrier CDMA or OFDM/CDMA [22;58-63]. Among different classes of multi-carrier CDMA schemes, multi-carrier direct sequence CDMA (MC-DS-CDMA) systems have the advantage of higher frequency diversity and improved overall system performance when compared to other multi-carrier schemes. Multi-tone CDMA (MT-CDMA) is appealing due to the usage of longer spreading code sequences and strong spectral overlapping, as this allows improved user accommodation when compared to DS schemes and as it provides higher bandwidth efficiency. On the other hand, The concept of overlapping multi-carrier CDMA systems was introduced by Hanzo [6], in which the overlapping was modelled by varying the frequency spacing between subcarriers for MC-DS-CDMA and MT-CDMA systems. Extensive research has been carried out on the performance analysis among different multi-carrier CDMA schemes [4;5;64;65] and between multi-carrier CDMA and OFDM [6;8]. However, there are no studies of system performance comparison between overlapping multi-carrier CDMA systems and variable subcarrier spacing FDM systems (including OFDM and Fast-OFDM). Such studies are the subject of this chapter.

In this chapter the basic concepts of CDMA and multi-carrier CDMA are discussed. The first section starts with a general introduction to CDMA. The section 3.3 will then concentrate on the three main classes of multi-carrier CDMA systems and the various variations of these systems. The principles of

overlapping multi-carrier CDMA system are presented in the section 3.4. Finally, the system implementation and performance assessment of the overlapping multi-carrier CDMA and its comparison to OFDM and Fast-OFDM are discussed in section 3.5 and section 3.6, respectively.

3.2 CDMA

Traditionally, TDMA and FDMA techniques have been employed for multiple access. In TDMA, the time-domain transition frame is periodically divided into time slots, while in FDMA the allocated spectrum is divided into frequency slots. Users are separated either in time domain or in frequency domain by accessing different time/frequency slots.

CDMA is a multiple access technique which allows multiple users to transmit independent information within the same bandwidth simultaneously. It is a strong candidate for future generation wireless systems as it provides the transmission of high data rates over "hostile" wireless channel. The basic idea of CDMA is to transmit independent information within the same frequency band at the same time, where users' separation is done by assigning a pseudo-random code to each user. It was first introduced by Claude Shannon and Robert Pierce in 1949 [66]. In 1978, CDMA was then proposed for cellular applications by Cooper and Nettleton [67]. During the 1980s, CDMA was investigated for cellular system, which led to the standardization of CDMA in 1993. The first CDMA system, IS-95 [68] started operation in 1995. In the late 20th century and at the beginning of 21st century, wideband CDMA systems [69] with a bandwidth of 5 MHz or over have been studied for 3rd generation mobile communication systems. Such systems include Wideband CDMA (W-CDMA) in Europe/Japan, cdma2000 [70] in the US, TTA-I and TTA-II in Korea and TDS-CDMA in China [14]. During recent years, multi-carrier CDMA systems which combine the multi-carrier techniques and CDMA schemes have attracted more attention and become the key candidate in 4G mobile network physical layer (PHY) implementations [19].

3.2.1. CDMA fundamentals

In a CDMA multiple access system, users are separated by pseudo-random code sequences, which are then "modulated" with the user data. The receiver, knowing the code sequence of the individual user, decodes the received signal after reception and recovers the original data. This then allows the sharing of the same spectrum by multiple users without causing excessive multiple access interference. The bandwidth of the code signal is much greater than the bandwidth of the information bearing signal. Hence, the spectrum is enlarged (or spread) during the encoding process. The resulting signal is called spread spectrum signal and CDMA is referred as spreading spectrum multiple access scheme. The codes are known as spreading codes.

One of the most important concepts of CDMA is the processing gain, which is defined as the ratio of the information signal period, T_s, to the transmitted signal period, T_c, i.e. $N_e = T_s/T_c$. One criteria that must be fulfilled is that the processing gain must be greater than one, in other words, $T_s > T_c$. For WCDMA, the bandwidth of the transmitted signal must be independent of the bandwidth of the information signal.

CDMA systems can be mainly divided into two groups, averaging systems and avoidance systems (Figure 3.1). Averaging systems reduce the interference in the system by averaging it over a wide time interval, such as direct sequence CDMA (DS-CDMA) schemes. Avoidance system reduces the interference by avoiding it for a large part of time, for example, frequency hopping CDMA (FH-CDMA) and time hopping CDMA (TH-CDMA) schemes. There is also a combined CDMA system, hybrid CDMA, which applies for both.

Figure 3.1. CDMA Classification by modulation method [69]

3.2.2. Various CDMA systems

3.2.2.1 DS-CDMA

In a DS-CDMA system (Figure 3.2), the information bearing signal is first multiplied by a spreading code signal that has good orthogonal properties. The spreading code signal consists of a number of code bits called "chips". The rate of the spreading code signal is much higher than the rate of the input data signal (Figure 3.3). The spread data is then modulated onto a carrier for transmission. Mathematically, the complex envelope of the transmitted signal for k^{th} user is given by:

$$s_k(t) = A \cdot b_k(t) \cdot c_k(t) \cdot e^{j2\pi f_c t} \tag{3.1}$$

Where A is the amplitude of the carrier signal, f_c is the carrier frequency, $b_k(t)$ is the information signal and $c_k(t)$ is the spreading code.

At the receiver, the received data is despread by multiplying the down-converted received signal with a locally generated copy of the user specific spreading code signal, which needs to be synchronized with the received signal.

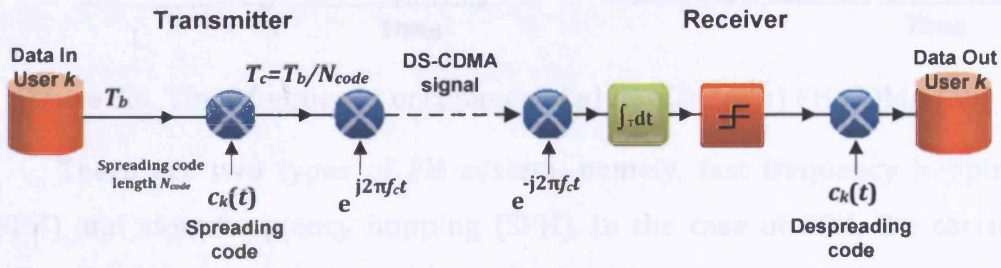

Figure 3.2. Single user DS-CDMA System

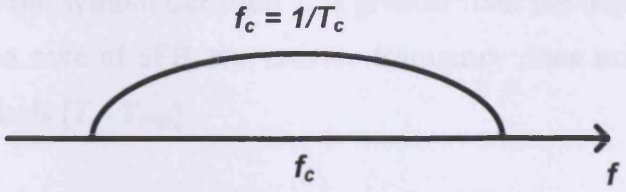

Figure 3.3. Power spectrum of the DS-CDMA signal

3.2.2.2 FH-CDMA

In FH-CDMA, the available frequency band and time axis are divided into multiple slots. The carrier frequency of the modulated information signal changes according to the user specific spreading code sequence. The carrier frequency remains the same during a given time interval, it then hops to another frequency (or stays the same if it hops on the same frequency). The hopping pattern is determined by the user specific spreading code. The processing gain is equal to the number of hopping frequencies. Unlike the DS-CDMA that occupies the whole frequency band, a FH system uses only a small frequency slot during transmission. The location of the frequency slots differs with time. Figure 3.4 compares the time-frequency occupancy of DS-CDMA and FH-CDMA.

Figure 3.4. Time-frequency occupancy of a) DS-CDMA; b) FH-CDMA [69]

There are two types of FH system, namely, fast frequency hopping (FFH) and slow frequency hopping (SFH). In the case of FFH, the carrier frequency changes a number of times during the transmission of one symbol,

in other words, the symbol duration T, is greater than the hopping time T_{hop}. However, in the case of SFH, the carrier frequency does not change for a number of symbols ($T < T_{hop}$).

3.2.2.3 TH-CDMA

In TH-CDMA systems, the time axis is divided into frames and each frame is divided into N timeslots. The user transmits in one of N timeslots during each frame. Which of the N timeslots is transmitted depends on the code signal assigned to the user. The processing gain in this case is same as the number of timeslots in each frame. Figure 3.5 shows the time-frequency occupancy of TH-CDMA.

Figure 3.5. Time-frequency occupancy of TH-CDMA [69]

3.2.2.4 Hybrid CDMA systems

Hybrid CDMA systems is a combination of the above CDMA schemes with some other multiple access techniques (such as TDMA). Mixing two or more CDMA systems combines the advantages of the individual techniques. Combining with multi-carrier modulation schemes produces multi-carrier CDMA systems that provide higher data rate transmission.

3.3 Multi-carrier CDMA

Instead of using a single carrier for serial data transmission, the CDMA schemes can be applied to use multiple subcarriers with parallel data transmission. Due to the fact that OFDM has the advantages of high data rate, low complexity of the system and good performance in a multipath channel, the combination of OFDM and CDMA schemes has generated great interests in the field of wireless communications. The main attractions are the high data rate in wireless transmissions and low complexity of the receiver with FFT-OFDM implementations. This combination is referred as multi-carrier CDMA or OFDM/CDMA.

Multi-carrier CDMA schemes were first introduced in 1993 [59;61;62]. Depending on different activation of the subcarriers, the schemes can be classified as the non-frequency hopping multi-carrier CDMA and the frequency-hopping assisted multi-carrier CDMA [6]. The non-frequency hopping multi-carrier CDMA schemes can be further divided into four classes: Frequency-domain spreading multi-carrier CDMA (or MC-CDMA) proposed by N. Yee, J-P Linnartz and G Fettweis [63], K. Fazel and L. Papke [59], and A. Chouly, A. Brajal and S. Jourdan [62]; Subchannel band-limited multi-carrier direct-sequence proposed by S. Kondo and L. Milstein [63]; Orthogonal multi-carrier DS-CDMA (or MC-DS-CDMA) proposed by V. DaSilva and E. S. Sousa [58]; Multi-tone DS-CDMA (MT-CDMA) by L. Vandendorpe [60]. There are also several frequency-hopping assisted multi-carrier CDMA schemes proposed in [71-73].

The basic principle of a multi-carrier CDMA system is that each user data is spread using a user specific spreading code and then modulated onto a set of subcarriers using OFDM. The main difference between these types of multi-carrier CDMA schemes is the way in which the data is spread and modulated on to different subcarriers. One major advantage of this system is that by transmitting a data stream in parallel, it lowers the symbol rate in each subcarrier, in other words, it extends the symbol duration and makes it easier to quasi-synchronize the transmission.

3.3.1. MC-CDMA

In the MC-CDMA scheme, the data stream is spread over N_{sc} subcarriers using a given spreading code of $\{c_n[0], c_n[1],...,c_n[N_{sc}-1]\}$ with processing gain G_{MC} (assuming $G_{MC} = N_{sc}$) in the frequency domain. The basic structure of MC-CDMA scheme is similar to an OFDM scheme except for that MC-CDMA scheme transmits the same symbol in parallel through a set of orthogonal subcarriers whereas the OFDM scheme transmits different symbols. Figure 3.6 shows the diagram of a single user MC-CDMA system. The input user data stream is first copied into N_{sc} parallel data streams. Each stream is then multiplied by a single chip of the given spreading code. As the serial data stream is not serial-to-parallel converted, there is no spreading modulation on each subcarrier. The data rate on each of the branch is the same as the input data rate. After multiplication with the spreading code, the data branches are modulated onto a set of orthogonal subcarriers separated by Δf_{MC}, where the frequency spacing Δf_{MC} is set to the inverse of the bit duration T_b. Therefore, the frequency spectrum is 50% overlapped (Figure 3.7) and the bandwidth required by the MC-CDMA system is $(N_{sc}+1)/T_b$. The spectrum gain SPG_{MC}, which is defined as the ratio between the bandwidth required with no overlapping and the actual bandwidth of a specific scheme, is given by:

$$SPG_{MC} = \frac{N_{sc}(2/T_b)}{(N_{sc}+1)(1/T_b)} = \frac{2N_{sc}}{N_{sc}+1} \tag{3.2}$$

The spectrum gain approaches two when N_{sc} is a large number. With the reference to Figure 3.6 the k^{th} MC-CDMA user's complex envelope of the transmitted signal can be expressed as [6]:

$$s_k(t) = \sqrt{\frac{2P_s}{N_{sc}}} \sum_{n=0}^{N_{sc}-1} b_k(t) \cdot c_k[n] \cdot e^{j2\pi f_n t} \tag{3.3}$$

where P_s is the transmitted power of the MC-CDMA signal, $b_k(t)$ represents the binary data sequence, N_{sc} is the number of subcarriers as well as the spreading gain, $\{c_k[0], c_k[1], \ldots c_k[N_{sc}- 1]\}$ is the spreading code, $\{f_n, n = 0,$

1, … , N_{sc} – 1} are the subcarrier frequencies, taking the values $f_0 + n/T_b$ for n = 0, 1, … , N_{sc} – 1 and f_0 is the zeroth carrier frequency.

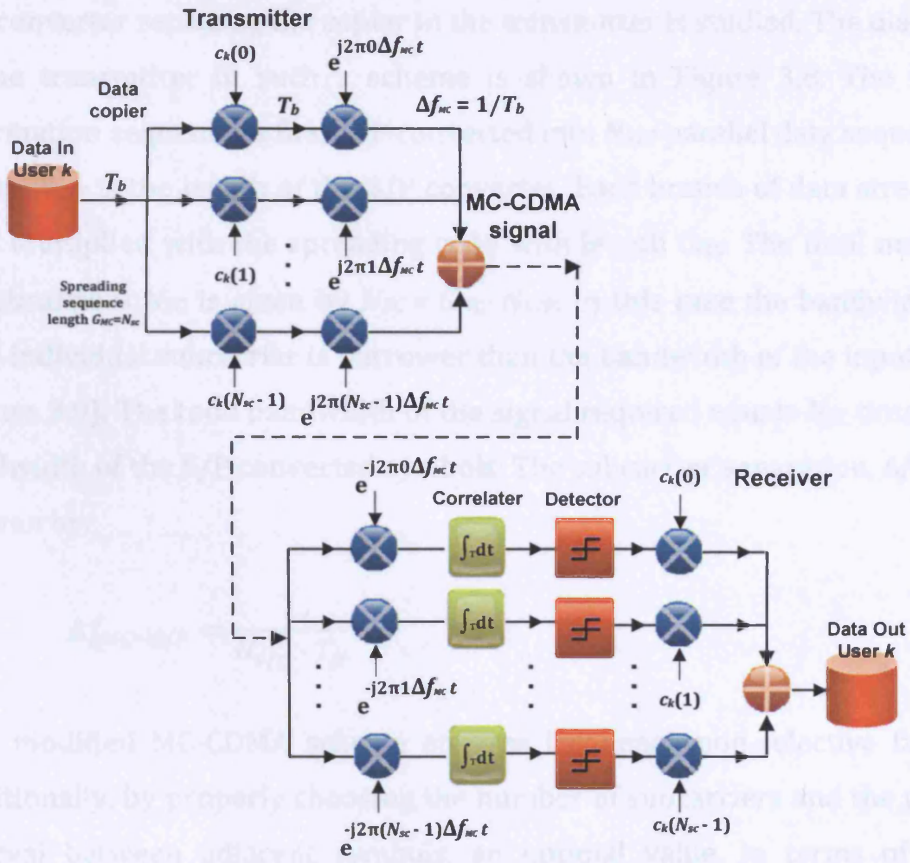

Figure 3.6. Single user MC-CDMA System

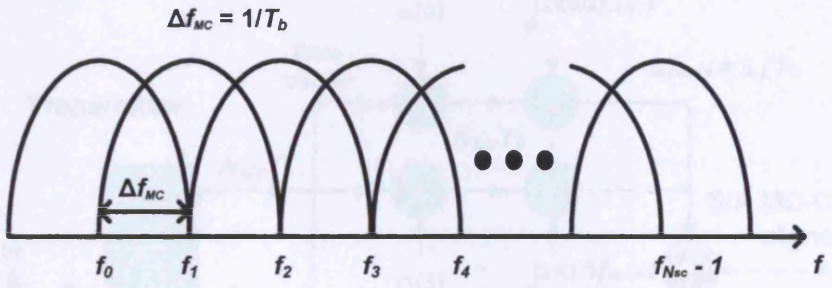

Figure 3.7. Spectrum of the MC-CDMA signal

The MC-CDMA scheme in Figure 3.6 assumes that the number of subcarriers is same as the code length (processing gain). In other words, the duration of the symbol at the output of the transmitter is same as the duration of the symbol at the input. However, in order to have flat frequency fading over each subcarrier in multi-carrier transmission, the original

symbol rate needs to be lowered by serial-to-parallel (S/P) conversion of the input signals. The total number of subcarriers does not have to be the same as the processing gain. In [74] an adaptive MC-CDMA scheme with a S/P converter replacing the copier in the transmitter is studied. The diagram of the transmitter in such a scheme is shown in Figure 3.8. The input information sequence is first S/P converted into $N_{S/P}$ parallel data sequences, where $N_{S/P}$ is the length of the S/P converter. Each branch of data stream is then multiplied with the spreading code with length G_{MC}. The total number of subcarriers N_{SC} is given by $N_{SC} = G_{MC} \cdot N_{S/P}$. In this case the bandwidth of each individual subcarrier is narrower than the bandwidth of the input data (Figure 3.9). The total bandwidth of the signal required equals N_{SC} times the bandwidth of the S/P converted symbols. The subcarrier separation, $\Delta f_{MC\text{-}S/P}$, is given by:

$$\Delta f_{MC-S/P} = \frac{1}{N_{s/p} \cdot T_b} \tag{3.4}$$

This modified MC-CDMA scheme ensures frequency non-selective fading. Additionally, by properly choosing the number of subcarriers and the guard interval between adjacent symbols, an optimal value, in terms of BER performance, may be obtained [74].

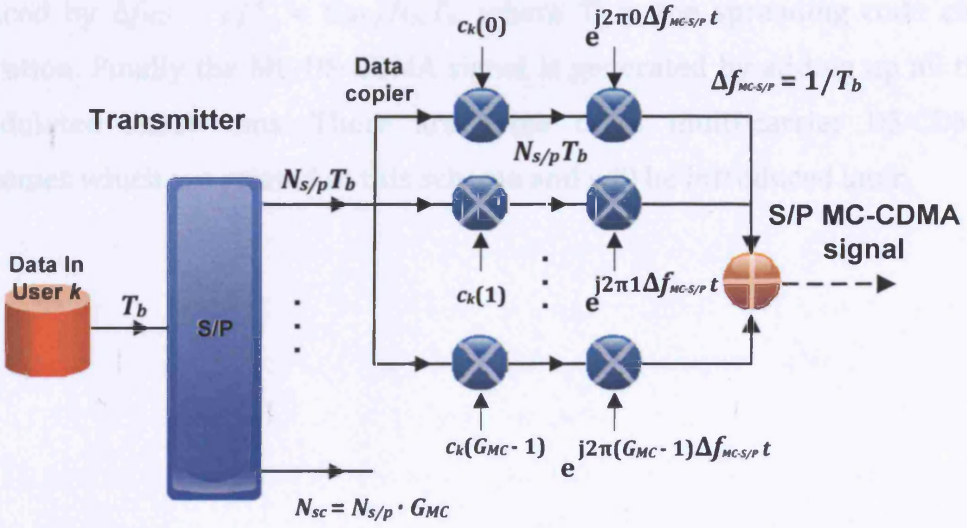

Figure 3.8. Modified single-user S/P MC-CDMA system - transmitter

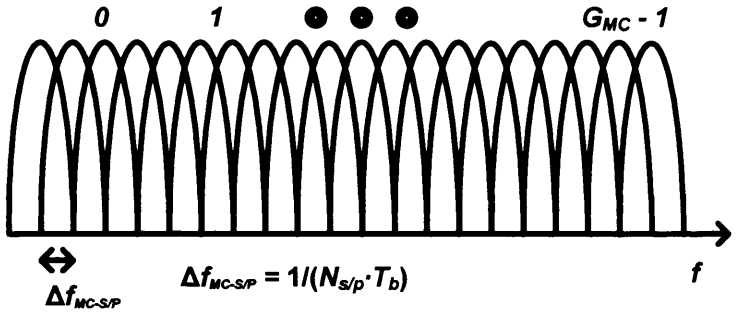

Figure 3.9. Power spectrum of the modified MC-CDMA signal

3.3.2. MC-DS-CDMA

Instead of spreading the data stream in frequency domain, the multi-carrier CDMA transmitter can spread a set of S/P converted data streams using a given spreading code and then modulates a different subcarrier with each of the data stream, in other words, the spreading operation is done in time domain. This category of multi-carrier CDMA schemes is referred as MC-DS-CDMA [5]. Figure 3.10 and Figure 3.11 show the single-user MC-DS-CDMA system and its output power spectrum, respectively. The transmitter first converts the original data stream into N_{sc} parallel substreams, which are then multiplied with a spreading code of processing gain, G_{MD}. The spread substreams are then modulated with N_{sc} subcarriers frequency spaced by $\Delta f_{MD} = 1/T_c = G_{MD}/N_{sc}T_b$, where T_c is the spreading code chip duration. Finally the MC-DS-CDMA signal is generated by adding up all the modulated substreams. There are some other multi-carrier DS-CDMA schemes which are related to this scheme and will be introduced later.

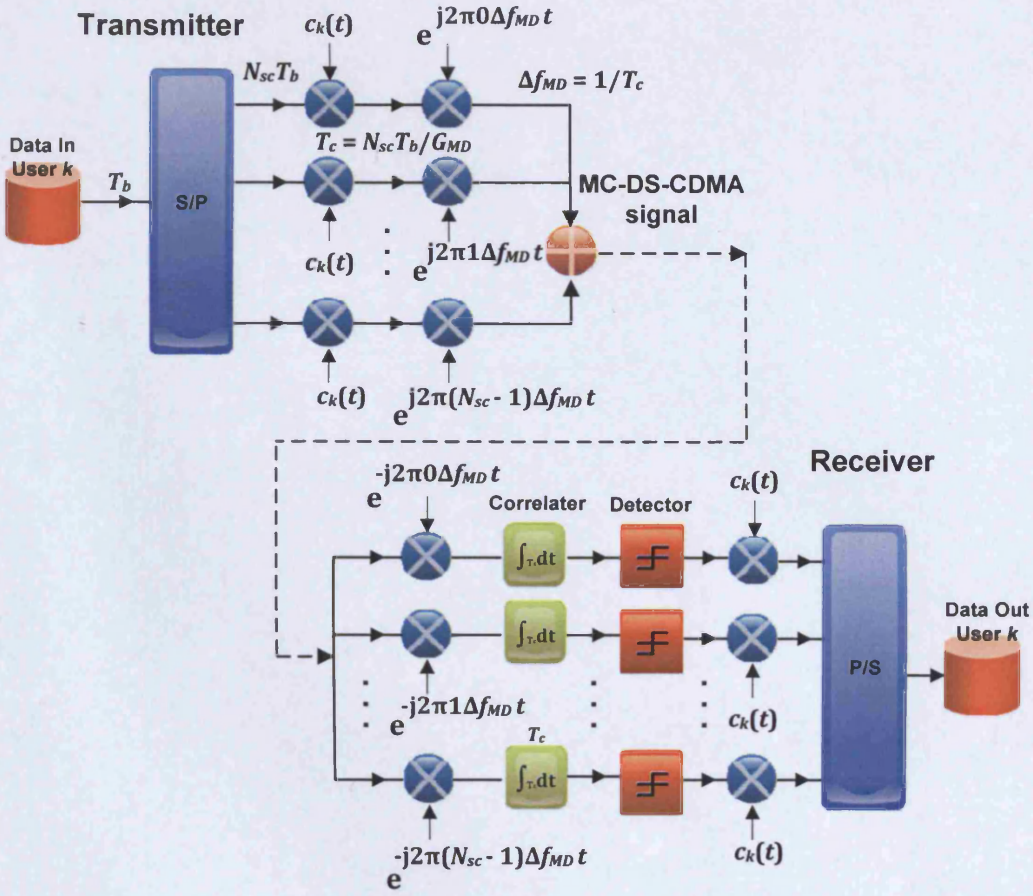

Figure 3.10. Single-user MC-DS-CDMA System

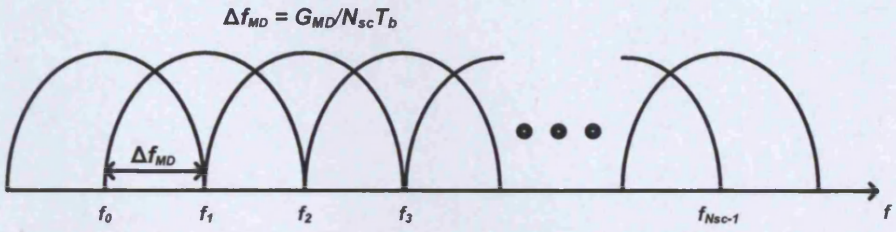

Figure 3.11. Power spectrum of MC-DS-CDMA signal

One type of MC-DS-CDMA scheme proposed by S. Kondo and L. Milstein [63] is similar to MC-CDMA in a way that a data copier is used instead of a S/P converter in the transmitter. However, the difference is that in MC-DS-CDMA scheme, each subcarrier signal is direct sequence spread using a common spreading sequence $c_k(t)$, instead of a single chip in the case of MC-CDMA. Figure 3.12 shows the structure of this type of MC-DS-CDMA system. This scheme does not include S/P data conversion. Therefore, the symbol duration of the multi-carrier DS-CDMA signal is the same as that of

the input data bit duration. The complex envelope of the transmitted signal of the k^{th} user can be formulated as [6]:

$$s_k(t) = \sqrt{\frac{2P_s}{N_{sc}}} \sum_{n=0}^{N_{sc}-1} b_k(t) \cdot c_k(t) \cdot e^{j2\pi f_n t} \tag{3.5}$$

The spectrum of this MC-DS-CDMA scheme is shown in Figure 3.13. To achieve orthogonality between subcarriers in the copier MC-DS-CDMA, the minimum spacing $\Delta f_{MD\text{-}CO}$ between adjacent subcarriers should also be the inverse of the chip duration, i.e. $\Delta f_{MD\text{-}CO} = 1/T_c$. The spectral gain $SPG_{MD\text{-}CO}$ is thus given by

$$SPG_{MD-CO} = \frac{N_{sc}(2/T_c)}{(N_{sc}+1)(1/T_c)} = \frac{2N_{sc}}{N_{sc}+1} \tag{3.6}$$

The spectrum gain approaches two when N_{sc} is a large number with 50% overlap of the main lobes of the adjacent subcarrier spectra. At the receiver the frequency diversity is achieved by combining all the N_{sc} correlator's outputs associated with the N_{sc} subcarriers. There are number of advantages of this multi-carrier DS-CDMA system compared with single carrier DS-CDMA scheme. Firstly, it provides good performance in multipath fading channels due to the frequency diversity achieved over the subcarriers. Secondly, it also suppresses the effects of narrowband interference in the system due to the DS spreading. Thirdly, the multi-carrier DS-CDMA system provides a lower speed, parallel-type of signal processing, instead of a fast serial-type of signal processing in a signal carrier system [6]. By having a lower chip rate of the spreading code, it has the advantages of reduced-complexity parallel implementation in the system.

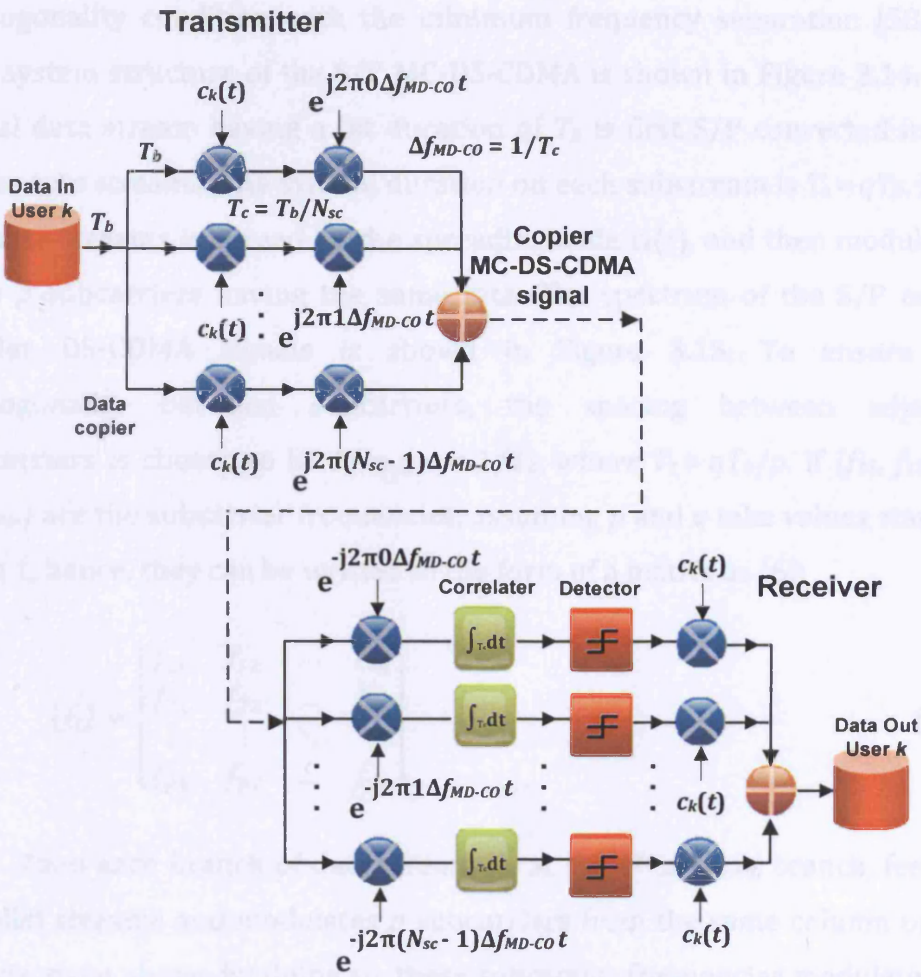

Figure 3.12. Single-user Copier Orthogonal MC-DS-CDMA System

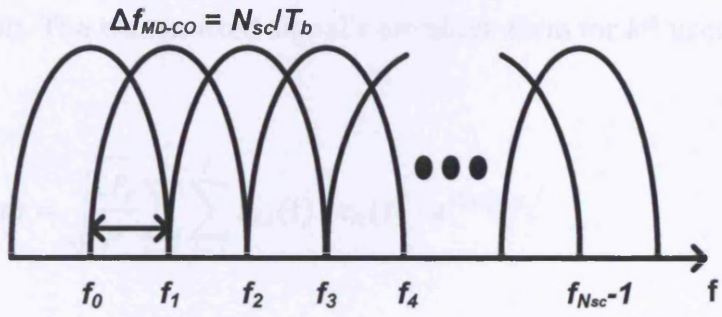

Figure 3.13. Spectrum of the Copier Orthogonal MC-DS-CDMA System

As an extension of the copier MC-DS-CDMA scheme, there is another MC-DS-CDMA system which applies a serial-to-parallel converter instead of the copier of the first type. This orthogonal MC-DS-CDMA scheme spreads the S/P converted data streams using a given spreading code in the time domain so that the resulting spectrum of each subcarrier can satisfy the

orthogonality condition with the minimum frequency separation [58;75]. The system structure of the S/P MC-DS-CDMA is shown in Figure 3.14. The initial data stream having a bit duration of T_b is first S/P converted into q lower-rate streams. The symbol duration on each substream is $T_s = qT_b$. Each of these streams is spread by the spreading code $c_k(t)$, and then modulated with p subcarriers having the same rate. The spectrum of the S/P multi-carrier DS-CDMA signals is shown in Figure 3.15. To ensure the orthogonality between subcarriers, the spacing between adjacent subcarriers is chosen to be $\Delta f_{MD\text{-}S/P} = 1/T_c$, where $T_c = qT_b/p$. If $\{f_{11}, f_{12}, \dots, f_{Nsc=pq},\}$ are the subcarrier frequencies, assuming p and q take values starting from 1, hence, they can be written in the form of a matrix as [6]:

$$\{f_i\} = \begin{bmatrix} f_{11} & f_{12} & \cdots & f_{1q} \\ f_{21} & f_{22} & \cdots & f_{2q} \\ \vdots & \vdots & \ddots & \vdots \\ f_{p1} & f_{p2} & \cdots & f_{pq} \end{bmatrix} \tag{3.7}$$

Then each branch of data stream b_{ki} at the k^{th} user, i_{th} branch, feeds p parallel streams and modulates p subcarriers from the same column of the matrix given above. By doing so, these subcarrier frequencies modulated by the same data bit have maximum frequency separation, which ensures the independence of the fading endured by the subcarriers modulated by the same data bit. The transmitted signal's envelope form for k^{th} user is given by [6]:

$$s_k(t) = \sqrt{\frac{2P_s}{p}} \sum_{i=1}^{q} \sum_{j=1}^{p} b_{ki}(t) \cdot c_k(t) \cdot e^{j2\pi f_{ji} t} \tag{3.8}$$

where $b_{ki}(t)$ represents the binary data sequence of k^{th} user at i_{th} branch of data stream, q is number of S/P data streams, p is the number of subcarriers for each substreams. The spectral gain $SPG_{MD\text{-}S/P}$ is thus given by

$$SPG_{MD-S/P} = \frac{pq(2/T_c)}{(pq+1)(1/T_c)} = \frac{2N_{sc}}{N_{sc}+1} \tag{3.9}$$

which approaches two as the total number of subcarriers $N_{sc} = pq$ increases. Similarly to the copier MC-DS-CDMA scheme, this scheme mitigates the effect of multipath interference due to DS spreading and frequency/time diversity. Adding an S/P converter extends the chip duration, which may lead to more relaxed synchronization schemes. However, the drawback is the high complexity in system implementation due to the further employment of RAKE combiners for suppression of frequency selective fading effects at the receiver.

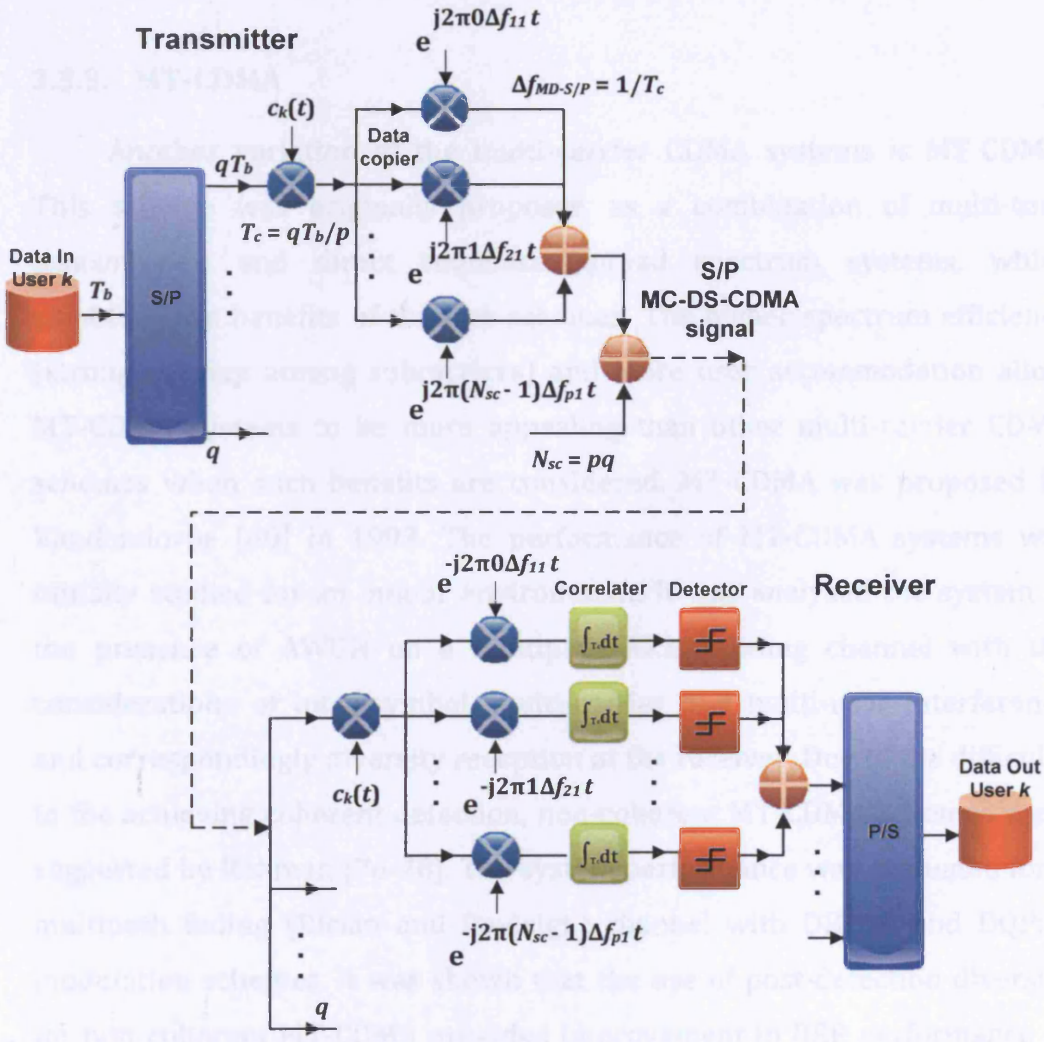

Figure 3.14. Single-user S/P Orthogonal MC-DS-CDMA System

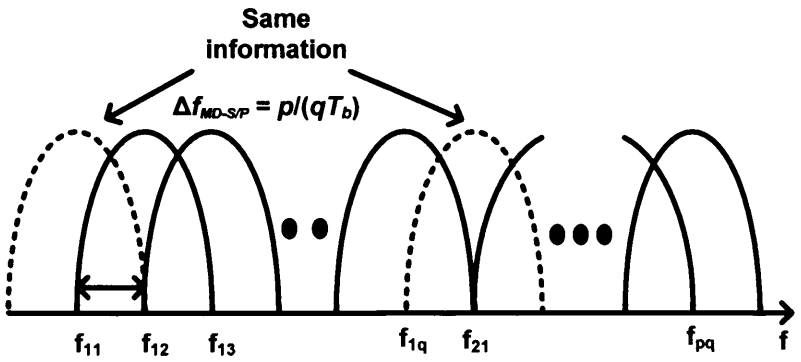

Figure 3.15. Spectrum of the S/P Orthogonal MC-DS-CDMA System

3.3.3. MT-CDMA

Another variation of the multi-carrier CDMA systems is MT-CDMA. This scheme was originally proposed as a combination of multi-tone transmission and direct sequence spread spectrum systems, which combines the benefits of the two schemes. The higher spectrum efficiency (strong overlap among subcarriers) and more user accommodation allow MT-CDMA systems to be more appealing than other multi-carrier CDMA schemes when such benefits are considered. MT-CDMA was proposed by Vandendorpe [60] in 1993. The performance of MT-CDMA systems was initially studied for an indoor environment. It was analyzed the system in the presence of AWGN on a multipath Rician fading channel with the considerations of inter-symbol, multi-carrier and multi-user interference and correspondingly diversity reception at the receiver. Due to the difficulty in the achieving coherent detection, non-coherent MT-CDMA schemes were suggested by Rahman [76-78]. The system performance was evaluated for a multipath fading (Rician and Rayleigh) channel with DBPSK and DQPSK modulation schemes. It was shown that the use of post-detection diversity for non-coherent MT-CDMA provided improvement in BER performance as compared to its non-diversity counterpart. In addition, a higher number of tones and a higher diversity order could reduce the system BER, whereas these two parameters are limited by the transmission rate and permissible channel resources.

On the other hand, being an OFDM based multi-carrier system, MT-CDMA experiences similar impairments as discussed in section 2.4, namely nonlinear effects and vulnerability to synchronization errors. In [79], a system performance comparison for conventional single-carrier (SC) DS, MC-CDMA and MT-CDMA systems in the presence of imperfect phase synchronization was provided. The results showed that, for a fixed data rate and fixed bandwidth with conventional correlator based receivers, the MT systems were not as robust as the SC and MC systems with frequency errors and phase noise due to the larger spectral overlap. In [64], a system performance comparison for MC-CDMA and MC-DS-CDMA systems in the presence of nonlinear effects was given by Hathi. Therefore, a gap must be filled by providing a study of MT-CDMA systems. Moreover, a further study on overlapping MT-CDMA system which is based on varying the frequency spacing between subcarriers can also be considered in a nonlinear transmission environment, due to its attractive effective bandwidth usage. The principles of the overlapping MT-CDMA systems will be discussed in more details in the section 3.4.

The basic principle of MT-CDMA system is similar to MC-DS-CDMA. A MT-CDMA transmitter, applying an S/P converter, spreads the S/P converted data streams using a given spreading code in time domain. The spreading is processed after the combination of all the substreams modulated with a set of orthogonal subcarriers separated at the symbol rate. Therefore, strong spectral overlap among the different subcarriers after data spreading exists in the MT-CDMA scheme. The scheme structure and signal output spectrum are shown in Figure 3.16 and Figure 3.17, respectively. The original data stream is first S/P converted into N_{sc} substreams. The extended symbol duration is $T_s = N_{sc}T_b$. The n^{th} substream modulates the subcarrier frequency f_n, $n \in \{1,2,\ldots,N_{sc}\}$ $n \in \{1,2,\ldots,N_{sc}\}$, where the frequency separation among subcarriers is $\Delta f_{MT} = 1/T_s = 1/(N_{sc}T_b)$. The modulated substreams are then added and multiplied with a spreading code to obtain the MT-CDMA signals. The complex envelope of the transmitted signal of the k^{th} user can be written as [6]:

$$s_k(t) = \sqrt{2P_s} \sum_{n=0}^{N_{sc}-1} b_{kn}(t) \cdot c_k(t) \cdot e^{j2\pi f_n t} \tag{3.10}$$

where $b_{kn}(t)$ represents the binary data sequence of the k^{th} user at the n^{th} branch of data stream. Therefore, the spectral gain (SPG_{MT}) of the multi-tone DS-CDMA system is given by:

$$SPG_{MT} = \frac{N_{sc}(2/T_c)}{(2/T_c) + (N_{sc} - 1)/T_s} = \frac{2N_e N_{sc}}{2N_e + N_{sc} - 1} \tag{3.11}$$

Where N_e is defined as the spreading gain of the subcarrier signal (i.e. $N_e = T_s/T_c$). The spectrum gain for MT-CDMA scheme approaches N_{sc}, when N_e is a large number, which is the highest spectrum gain compared with other multicarrier schemes, whose spectrum gain ≈ 2.

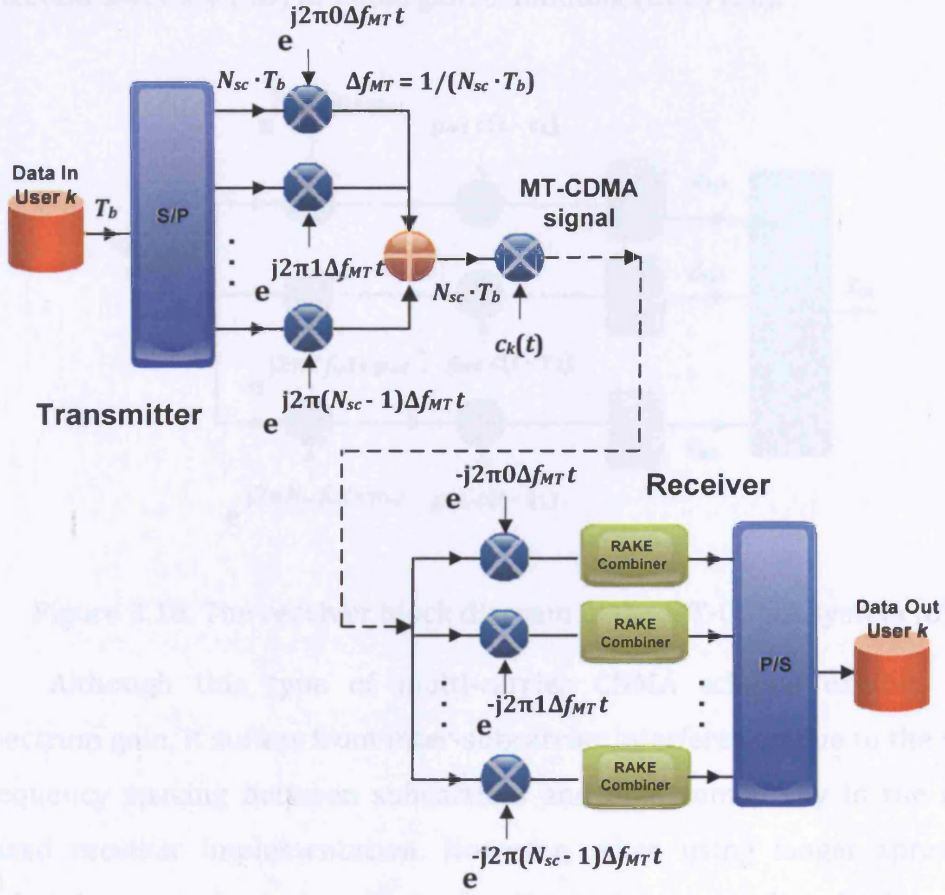

Figure 3.16. Single-user MT-CDMA System

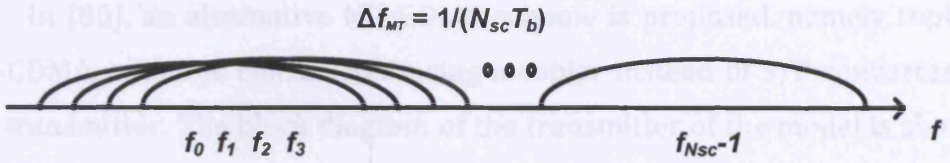

Figure 3.17. Spectrum of the MT-CDMA System

At the receiver, N_{sc} rake combiners are used for MT-CDMA signal recovery. Each rake combiner contains multiple correlators, each synchronized to a different resolvable path in the received composite signal [5]. A block diagram of the receiver at subcarrier frequency of f_m, for $1<m<N_{sc}$, is shown in Figure 3.18. Here φ_{ml} for l=1,2,...L, are the phase rotation introduced in the multipath transmission and L is the number of channel paths. g_{ml} for l=1,2,...L, are the coefficients that indicate which combining scheme is used, such as maximum ratio combining (MRC), selection diversity (SD) or equal gain combining (EGC) [22].

Figure 3.18. The receiver block diagram of the MT-CDMA system [6]

Although this type of multi-carrier CDMA scheme exhibits high spectrum gain, it suffers from inter-subcarrier interference, due to the short frequency spacing between subcarriers and high complexity in the rake-based receiver implementation. However, when using longer spreading codes, it can reduce the effect of self-interference and multiple access interference, as compared to single-carrier DS-CDMA scheme.

In [80], an alternative MT-CDMA scheme is proposed, namely replica MT-CDMA, which is constructed using a copier instead of S/P converter at the transmitter. The block diagram of the transmitter of the model is shown in Figure 3.19. This replica MT-CDMA is different from the MC-CDMA in a way that a spreading code is multiplied with data instead of single chip in the MC-CDMA. It is different to the copier MC-DS-CDMA in that the spacing between subcarriers is $1/T_b$ rather than $1/T_c$ in the MC-DS-CDMA. It is also shown in [80] that with the same bandwidth, the replica MT-CDMA system outperforms the conventional MT-CDMA system in Rayleigh distributed multipath fading channel. However, using a copier at the transmitter does not extend the symbol period and thus renders the system vulnerable to timing errors and sensitive to large delay spreads.

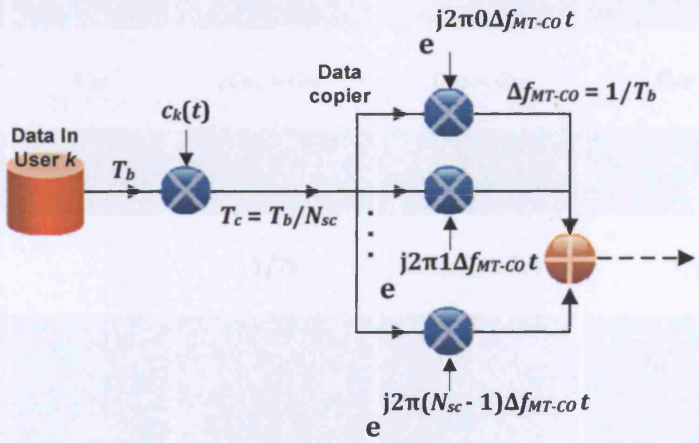

Figure 3.19. Single-user Replica MT-CDMA System - Transmitter

3.3.4. Comparison of multi-carrier CDMA schemes and DS-CDMA

As a summary, a comparison among the schemes (DS-CDMA, the first type of MC-CDMA, MC-DS-CDMA and MT-CDMA) described previously is outlined in Table 3.1. It can be observed that when a Nyquist filter with roll-off factor = 0 is used, the required bandwidths of MC-CDMA and MC-DS-CDMA are almost half as wide as that of DS-CDMA scheme, while the MT-CDMA scheme has the same bandwidth as the DS-CDMA scheme. However,

when a small roll-off factor is used in the Nyquist filter in the DS-CDMA scheme, the required bandwidths of MC-CDMA and MC-DS-CDMA schemes become comparable with that of DS-CDMA scheme [65].

Table 3.1. System features comparison

	DS-CDMA	MC-CDMA	MC-DS-CDMA	MT-CDMA
Original bit duration	T_b	T_b	T_b	T_b
Use S/P converter or copier in Tx	-	Copier	S/P converter	S/P converter
Number of subcarriers	1	$N_{sc} = G_{MC}$	N_{sc}	N_{sc}
Symbol duration at subcarrier	$T_s = T_b$	$T_s = T_b$	$T_s = N_{sc}T_b$	$T_s = N_{sc}T_b$
Processing gain	G_{DS}	$G_{MC} \approx G_{DS}$	$G_{MD} = G_{DS}$	$G_{MT} = N_{sc}G_{DS}$
Chip duration	$T_c = T_b / G_{DS}$	-	$T_c = N_{sc}T_b / G_{MD}$	$T_c = N_{sc}T_b / G_{MT}$
Subcarrier separation	-	$1/T_b$	$G_{MD} / (N_{sc}T_b)$	$1/(N_{sc}T_b)$
Required bandwidth	$\frac{G_{DS}}{T_b}$	$\frac{(N_{sc}+1)\cdot G_{MC}}{N_{sc}\cdot T_b}$	$\frac{(N_{sc}+1)\cdot G_{MD}}{N_{sc}\cdot T_b}$	$\frac{(N_{sc}-1)+2G_{MT}}{N_{sc}\cdot T_b} = \frac{N_{sc}-1}{N_{sc}\cdot T_b} + \frac{2}{T_c}$
Spectrum gain (SPG)	1	$\frac{2N_{sc}}{N_{sc}+1} \approx 2$ when N_{sc} is large	$\frac{2N_{sc}}{N_{sc}+1} \approx 2$ when N_{sc} is large	$\frac{2N_eN_{sc}}{2N_e+N_{sc}-1} \approx N_{sc}$ When spreading gain of each carrier $N_e = T_s/T_c = N_{sc}T_b/T_c$ is large

For the MC-DS-CDMA and MT-CDMA schemes introduced in sections 3.2.2 and 3.2.3, respectively. The different systems' features may be compared by reference to the summary Table 3.2. In order to quantify the processing gain of each subcarrier signal, N_e, (the ratio of subcarrier bandwidth, $1/T_c$, to the bandwidth of the symbol at the subcarrier, $1/T_s$) for

a multi-carrier CDMA system, an equivalent single-carrier DS-CDMA system having identical data rate and identical system bandwidth is considered (Figure 3.20). The G_{DS} in the following table is the processing gain of the single-carrier DS-CDMA system, which is defined as the ratio of the original bit duration, T_b, to the chip duration of the spreading code in the single-carrier DS-CDMA system, T_{c1}. T_s is the symbol duration of the signals before data spreading and modulating to subcarriers. It can be seen from Table 3.2 that the MT-CDMA schemes have the advantage of the highest overall system processing gain among the multi-carrier schemes considered.

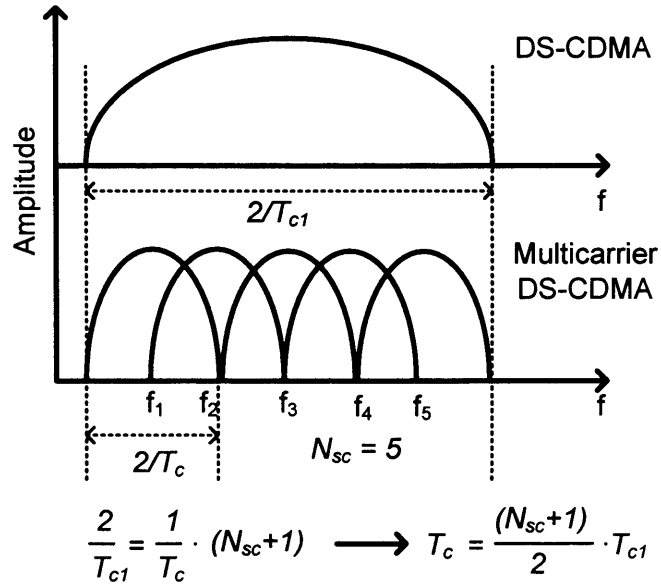

Figure 3.20. Spectrum comparison of an equivalent DS-CDMA system spectrum to a 5-carrier multi-carrier DS-CDMA system

Table 3.2. MC-DS-CDMA and MT-CDMA system features comparison

	MC-DS-CDMA	Copier MC-DS-CDMA	S/P MC-DS-CDMA	MT-CDMA
Original bit duration	T_b	T_b	T_b	T_b
Use S/P converter or copier in Tx	S/P converter	Copier	S/P converter	S/P converter
Number of subcarriers	N_{sc}	N_{sc}	$N_{sc} = pq$	N_{sc}
Symbol duration at subcarrier	$T_s = N_{sc}T_b$	$T_s = T_b$	$T_s = qT_b$	$T_s = N_{sc}T_b$
Chip duration	$T_c = \frac{N_{sc} \cdot T_b}{G_{DS}}$	$T_c = \frac{T_b}{G_{DS}}$	$T_c = \frac{N_{sc} \cdot T_b}{G_{DS}}$	$T_c = \frac{N_{sc} \cdot T_b}{G_{DS}}$
Chip duration compared to DS-CDMA with 50% overlapping	$T_c = \frac{N_{sc}+1}{2} \cdot T_{c1}$	$T_c = \frac{N_{sc}+1}{2} \cdot T_{c1}$	$T_c = \frac{pq+1}{2} \cdot T_{c1}$	$T_c = \frac{2N_{sc}G_{DS}}{2N_{sc}G_{DS} - N_{sc} + 1} \cdot T_{c1}$
Spreading gain at each subcarrier, N_e	$N_e = T_s/T_c$ $= \frac{2N_{sc}}{N_{sc}+1} \cdot \frac{T_b}{T_{c1}}$ $= \frac{2N_{sc}G_{DS}}{N_{sc}+1}$	$N_e = T_s/T_c$ $= \frac{2}{N_{sc}+1} \cdot \frac{T_b}{T_{c1}}$ $= \frac{2G_{DS}}{N_{sc}+1}$	$N_e = T_s/T_c$ $= \frac{2q}{pq+1} \cdot \frac{T_b}{T_{c1}}$ $= \frac{2qG_{DS}}{N_{sc}+1}$	$N_e = T_s/T_c$ $= \frac{N_{sc}T_b}{T_{c1}} \cdot \frac{2N_{sc}G_{DS} - N_{sc} + 1}{2N_{sc}G_{DS}}$ $= N_{sc}G_{DS} - \frac{N_{sc}-1}{2}$
Overall spreading gain	$G_{MD} = N_e \cdot N_{sc}$ $= \frac{2N_{sc}^2 G_{DS}}{N_{sc}+1} \approx 2$ When N_{sc} is large	$G_{MD-CO} = N_e \cdot N_{sc}$ $= \frac{2N_{sc}G_{DS}}{N_{sc}+1} \approx 2$ When N_{sc} is large	$G_{MD-S/P} = N_e \cdot p$ $= \frac{2pqG_{DS}}{pq+1} \approx 2$ When pq is large	$G_{MT} = \frac{N_{sc}(2/T_c)}{(2/T_c) + (N_{sc}-1)/T_s}$ $= \frac{2N_eN_{sc}}{2N_e + N_{sc} - 1} \approx N_{sc}$ When N_e is large, since different data bits transmitted on different subcarriers

3.4 Overlapping CDMA systems

In the previous section, the comparison among the multi-carrier CDMA schemes reveals that a high spectrum overlapping is achieved in MT-CDMA systems and thus improved bandwidth efficiency is gained. This makes the scheme more appealing than other multi-carrier systems. Additionally, longer spreading code sequences are used due to the short carrier spacing used between subcarriers in MT-CDMA based systems. Therefore, it provides the benefits of better correlation properties for CDMA applications and thus can accommodate more users than other multi-carrier CDMA schemes. On the other hand, MC-DS-CDMA systems have the advantage of higher frequency diversity and improved overall system performance compared to other multi-carrier schemes. Therefore, both systems are worthy of further studies for use in overlapping multi-carrier CDMA systems. In this section, two types of overlapping CDMA systems are introduced, namely, single-carrier overlapping DS-CDMA systems and multi-carrier overlapping CDMA schemes based on MT-CDMA or MC-DS-CDMA.

3.4.1. Overlapping DS-CDMA schemes

Spectrum overlapping CDMA system was originally proposed by Schilling and Pickholtz in 1992 [81], in which a wideband CDMA system was partitioned into several narrow band systems. It was shown as one of the possible schemes that could improve the bandwidth efficiency and increase the channel capacity, i.e. the max number of users for a certain average bit error rate requirement. When multiple DS-CDMA systems are overlapped in frequency with a fixed overall bandwidth [82], as shown in Figure 3.21, an increase in the bandwidth of each channel is achieved, along with an increase in the adjacent channel interference due to the reduced spacing between carriers. However, the increased processing gain leads to a decrease in interference, hence, an increase in capacity. The total number of narrowband CDMA systems is assumed to be N and an overlapping coefficient is defined as:

$$\lambda_{DS} = \frac{BW_{op}}{BW_{ds}} \tag{3.12}$$

where BW_{op} is the overlapped bandwidth between channels and BW_{ds} is the bandwidth of each channel, the overall bandwidth BW_{wide} is fixed, then the following equation is obtained:

$$BW_{wide} = BW_{ds} \cdot N + BW_{op} \cdot (N - 1) \tag{3.13}$$

Substituting $BW_{wide} = 2/T_{c1}$, where T_{c1} is the chip duration of the spreading code in the signal-carrier DS-CDMA system, $BW_{ds} = 2/T_c$, and $BW_{op} = \lambda_{DS} BW_{ds}$ into equation (3.13), the spreading gain of each narrow band, G_{narrow}, is then derived as [83],

$$G_{narrow} = \frac{G_{wide}}{\lambda_{DS} + N - \lambda_{DS} \cdot N} \tag{3.14}$$

where G_{wide} is the spreading gain of the wideband system, i.e. T_s/T_{c1}.

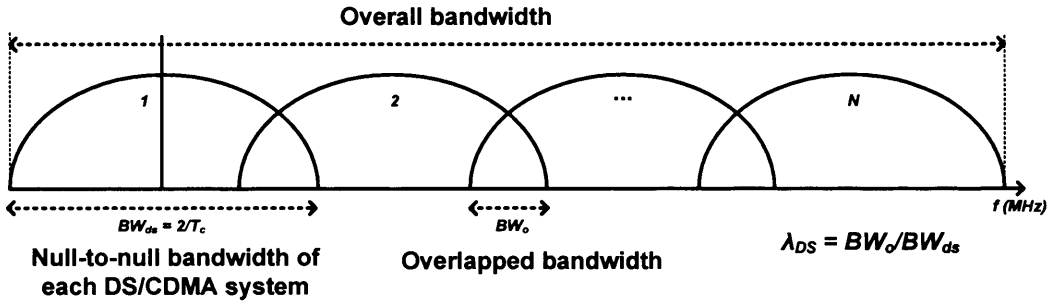

Figure 3.21. Spectrum of multiple overlapping DS-CDMA systems [84]

The coefficient λ_{DS} is varied from 0 (non-overlapping) to 1 (full overlapping). Hence, the configuration of an overlay system is determined by the two parameters, N and λ_{DS}. For a fixed overall bandwidth, if N increases the processing gain of each channel, G_{narrow}, decreases with fixed λ_{DS}. On the other hand, when N is fixed, G_{narrow} increases as λ_{DS} increases. It has been shown in [82] that an optimum portion of overlapping exists in order to achieve the maximum capacity of channels for ideal rectangular-shaped time domain pulses. When λ_{DS} equals 0.75 (corresponding to 25% overlapping), a 16% increase in channel capacity is achievable. It is also

suggested in [83] that when both the overlapping coefficient, λ_{DS}, and the number of narrow band channels, N, are considered, 5% and 20% of capacity improvement is achieved with optimised λ_{DS}=0.5 (corresponding to 50% overlapping) and N = 2 in both non-fading and multipath Rayleigh fading channels. The optimal λ_{DS} that maximises the capacity also increases with the number of overlapped systems N [84]. A maximum of 50% of increase in capacity is feasible with increased N, when λ_{DS} = 0.5 for non-fading channels. For a multipath Rayleigh fading channel, an optimised value of N can be chosen according to the signal to noise ratio and the required bit error rate of the system. It is also found in [83] that N decreases as the required bit error rate is reduced, this is because the multipath immunity characteristic becomes more important as the required BER decreases. Furthermore, multiple direct-sequence CDMA systems using different modulation schemes such as binary frequency shift keying (BFSK) and M-ary frequency shift keying (MFSK) are considered in [85]. It has been shown that in both cases, there exists an optimum overlapping portion of subcarrier spacing which provides improved BER performance when compared to the non-overlapping systems. It is also suggested by the author that the results obtained can also be extended to the analysis of multi-carrier CDMA systems when overlapping subcarrier frequency bands are used.

3.4.2. Overlapping multi-carrier CDMA

In sections 3.3.2 and 3.3.3, MC-DS-CDMA and MT-CDMA systems were introduced, respectively. The differences between these two systems are the place where data spreading is applied at the transmitter and the frequency spacing introduced between adjacent subcarriers. In MC-DS-CDMA systems, adjacent subcarriers are separated by $1/T_c$, whereas in the MT-CDMA systems, subcarriers are spaced at $1/T_s$. A comparison of transmitter block diagram and power spectrum of the output signals is shown in Table 3.3. The initial bit duration, the number of subcarriers and the spreading gain

are assumed to be T_b = 1μs, N_{sc} = 4 and G_{DS} = 8, respectively. The symbol duration after S/P transmission, T_s, is 4μs. The chip duration, T_c, in both systems is given by:

—— ——— (3.15)

Substituting the values given above, the equation gives T_c = 0.5 μs which yields a frequency spacing between the subcarriers of 2 MHz and 0.25 MHz for MC-DS-CDMA system and MT-CDMA system, respectively.

Table 3.3. Overlapping CDMA system

	MC-DS-CDMA [5]	MT-CDMA [60]
Transmitter model	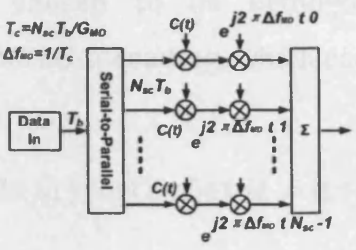	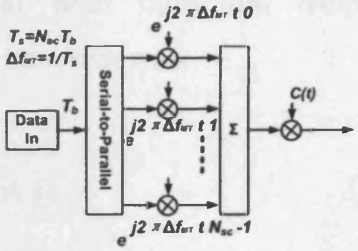
T_b	1 μs	1 μs
T_s	4 μs	4 μs
N_{sc}	4	4
G_{DS}	8	8
T_c	$T_c = T_s/G_{DS}$ = 0.5 μs	$T_c = T_s/G_{DS}$ = 0.5 μs
Δf	Δf_{MD} = 1/ T_c = 2 MHz	Δf_{MT} = 1/ T_s = 0.25 MHz
Power Spectrum	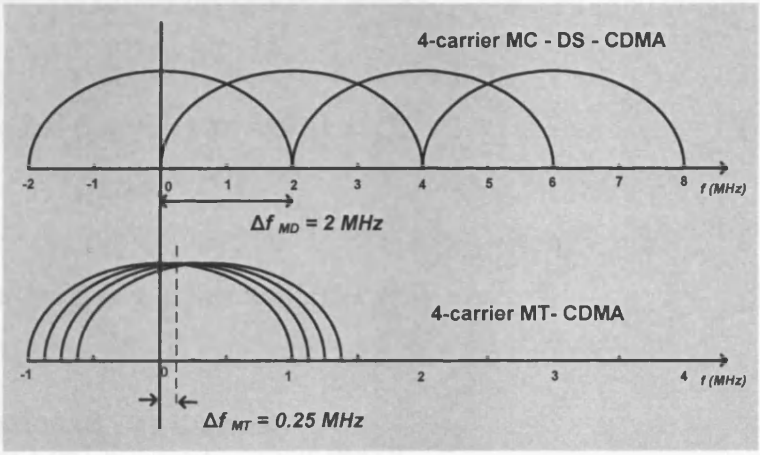	

It is shown in [6] that, if $G_{DS} = T_s/T_c$, where G_{DS} is the spreading gain of the DS spread subcarrier signal, each subcarrier signal has the same null-to-null bandwidth of $2/T_c$, the MT-CDMA scheme remains the orthogonality between subcarriers when the frequency spacing varies from $1/T_s$ to $1/T_c$. To verify this, two subcarriers at frequencies f_i and f_j are chosen to be orthogonal in MT-CDMA system which should satisfy the following condition:

$$\int_0^{T_s} \cos(2\pi f_i t)\cos(2\pi f_j t)\,dt = 0, (i \neq j) \tag{3.16}$$

The frequency spacing is $1/T_s$, and the subcarrier frequencies take the values f_0+i/T_s for i=0,1,..., N_{sc}-1. Similarly, in MC-DS-CDMA systems, the subcarriers are chosen to be orthogonal with minimum frequency separation after the DS spreading, which can be written as:

$$\int_0^{T_c} \cos(2\pi f_i t)\cos(2\pi f_j t)\,dt = 0, (i \neq j) \tag{3.17}$$

The frequency separation is $1/T_c$, and the subcarrier frequencies take the values f_0+i/T_c for i=0,1,..., N_{sc}-1. As $G_{DS} = T_s/T_c$ and also each subcarrier signal has the same null-to-null bandwidth of $2/T_c$, the subcarrier frequency f_i of the MC-DS-CDMA signal is written as:

$$f_i = f_j + 1/T_c = f_i + G_{DS}/T_s \tag{3.18}$$

Substituting equations (3.18) into (3.16), yields:

$$\frac{1}{2}\int_0^{T_s} \cos(2\pi(f_i + f_j)t)\,dt = 0, (i \neq j) \tag{3.19}$$

$$\frac{1}{2}\int_0^{T_s} \cos(2\pi(f_i - f_j)t)\,dt = 0, (i \neq j) \tag{3.20}$$

Focusing on equation (3.20), it gives:

$$\int_0^{T_s} \cos(2\pi(f_j + 1/T_c - f_j)t)\, dt = 0, (i \neq j) \tag{3.21}$$

Finally,

$$\int_0^{T_s} \cos\left(\frac{2\pi t}{T_c}\right) dt = 0 \tag{3.22}$$

Replacing T_s with $T_c \cdot G_{DS}$, equation (3.22) can be further written as

$$\sum_{l=0}^{G_{DS}-1} \int_{lT_c}^{(l+1)T_c} \cos\left(\frac{2\pi t}{T_c}\right) dt = 0 \tag{3.23}$$

It can be observed from the equation (3.23) that each term of the sum is zero and hence it gives:

$$\int_0^{T_c} \cos\left(\frac{2\pi t}{T_c}\right) dt = 0 \tag{3.24}$$

which reflects the orthogonality between subcarrier frequencies having minimum frequency separation after spreading in equation (3.17). In other words, the orthogonality property of the multi-tone system is not altered by direct sequence spectrum spreading.

Therefore, an overlapping multi-carrier CDMA system can be constructed based on the multi-tone CDMA scheme, denoted as overlapping MT-CDMA, in which the overlapping frequency spacing between subcarriers is λ_{MT}/T_s (λ_{MT} = 1, 2,..., G_{DS}), where here λ_{MT} is an overlapping coefficient that is different from the one in single-carrier overlapping DS-CDMA schemes in section 3.4.1. It is the overlapped bandwidth normalised to symbol rate ($1/T_s$), i.e.

$$\lambda_{MT} = \frac{BW_{\Delta MT}}{BW_{MT}} \tag{3.25}$$

where $BW_{\Delta MT}$ is the MT-CDMA channel separation and BW_{MT} is the bandwidth of each MT-CDMA channel before spreading. When $\lambda_{MT} = 1$, the system belongs to the class of MT-CDMA, while $\lambda_{MT} = G_{DS}$ is the case of MC-DS-CDMA. Furthermore, when $\lambda_{MT} = 2G_{DS}$, the frequency spacing is $2/T_c$, and there exists no overlap between the mainlobes of the modulated subcarrier signals after DS spreading. Varying the overlapping coefficient, λ_{MT}, results in different type of multi-carrier CDMA systems and different effects in terms of multi-user and multi-carrier interference. For example, if λ_{MT} is low, there is a strong overlapping between subcarriers. If the total bandwidth is given, then a low value of λ_{MT} leads to a high spreading gain, hence, reduction of multi-user interference. Conversely, if λ_{MT} is high – for example $\lambda_{MT} = 2G_{DS}$ – for a given total bandwidth, there is no overlap between subcarriers. Therefore, there is reduced multi-carrier interference, but with an increase in multi-user interference due to the reduced processing gain on each subcarrier signal. Hence, a trade-off exists between the overlapping bandwidth and the processing gain and there exists an optimum value of λ_{MT} that provides good performance in the system in terms of minimal multi-user and multi-carrier interference, improved bandwidth efficiency and BER performance. It has been shown in [6] that normalised value of λ_{MT} (normalised to G_{DS}) approximately equal to 0.8 provides better BER performance compared to MT-CDMA and MC-DS-CDMA schemes. The system is considered to experience frequency selective fading and the receiver is assumed to have the ability of combining a limited number of the resolvable paths. In [86;87], a further reduced frequency spacing overlapping MT-CDMA scheme combined with BPSK modulation scheme is investigated, i.e. the overlapping coefficient, λ_{MT}, is less than 1. For example, $\lambda_{MT} = 0.5$ is the case of fast MT-CDMA that provides further improvement in bandwidth efficiency. However, training symbols and multi-stage inter-carrier interference cancellation need to be considered at the receiver in order to obtain satisfactory system performance. As a result, the data rate is

reduced due to the transmission of dummy training sequences and the system complexity increases because of the insertion of ICI cancellation mechanisms.

On the other hand, if the same idea of Fast-OFDM is applied in MC-DS-CDMA, then the overlapping multi-carrier CDMA system can be generated based on a MC-DS-CDMA scheme (Figure 3.10) with the frequency separation between sub-carriers set to λ_{MC}/T_c, where T_c is the code duration and λ_{MC} is the overlapping coefficient of the MC-DS-CDMA system. In this thesis this scheme is called overlapping MC-DS-CDMA. λ_{MC} is defined as the ratio of overlapping bandwidth between subcarriers to the bandwidth of each channel after spreading:

$$\lambda_{MC} = \frac{BW_{\Delta MD}}{BW_{MD}} \tag{3.26}$$

where $BW_{\Delta MD}$ is the MC-DS-CDMA channel separation and BW_{MD} is the bandwidth of each MC-DS-CDMA channel after spreading. λ_{MC} varies from 0 to 2 corresponding to an overlapping percentage of 100% to 0%. λ_{MC} = 1 corresponds to 50% overlapping which is the case similar to OFDM. λ_{MC} = 0.5 corresponds to 75% overlapping is the case similar to Fast-OFDM. It should be noted that the λ_{MC} is related to λ_{MT} as the ratio of T_s/T_c, i.e. $\lambda_{MT} = \lambda_{MC} \cdot T_s/T_c = \lambda_{MC} \cdot G_{DS}$. The power spectrum of the overlapping MC-DS-CDMA system is shown in Figure 3.22.

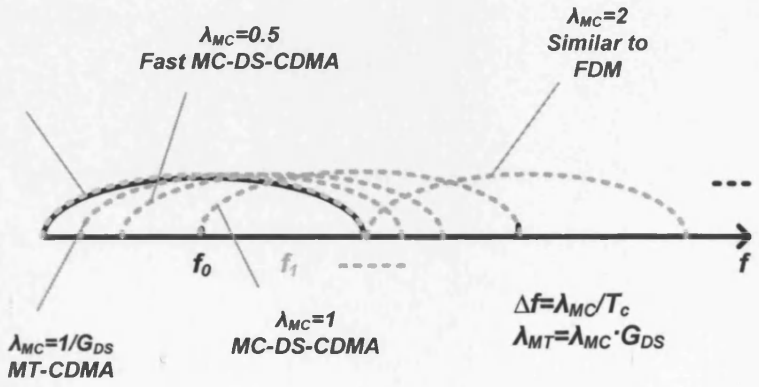

Figure 3.22. Power spectrum of the overlapping MC-DS-CDMA systems

As a summary, the overlapping multi-carrier CDMA systems can be illustrated as in Figure 3.23. Different types of overlapping systems are obtained with variable value of λ (Table 3.4).

Table 3.4. Overlapping multi-carrier CDMA with various λ

λ	Systems
$0 < \lambda < 1$	Further overlapping MT-CDMA
0.5	Fast MT-CDMA
1	MT-CDMA
$1 < \lambda < G_{DS}$	Overlapping MT-CDMA
$G_{DS}/2$	Fast MC-DS-CDMA
G_{DS}	MC-DS-CDMA
$G_{DS} < \lambda < 2G_{DS}$	Overlapping MC-DS-CDMA

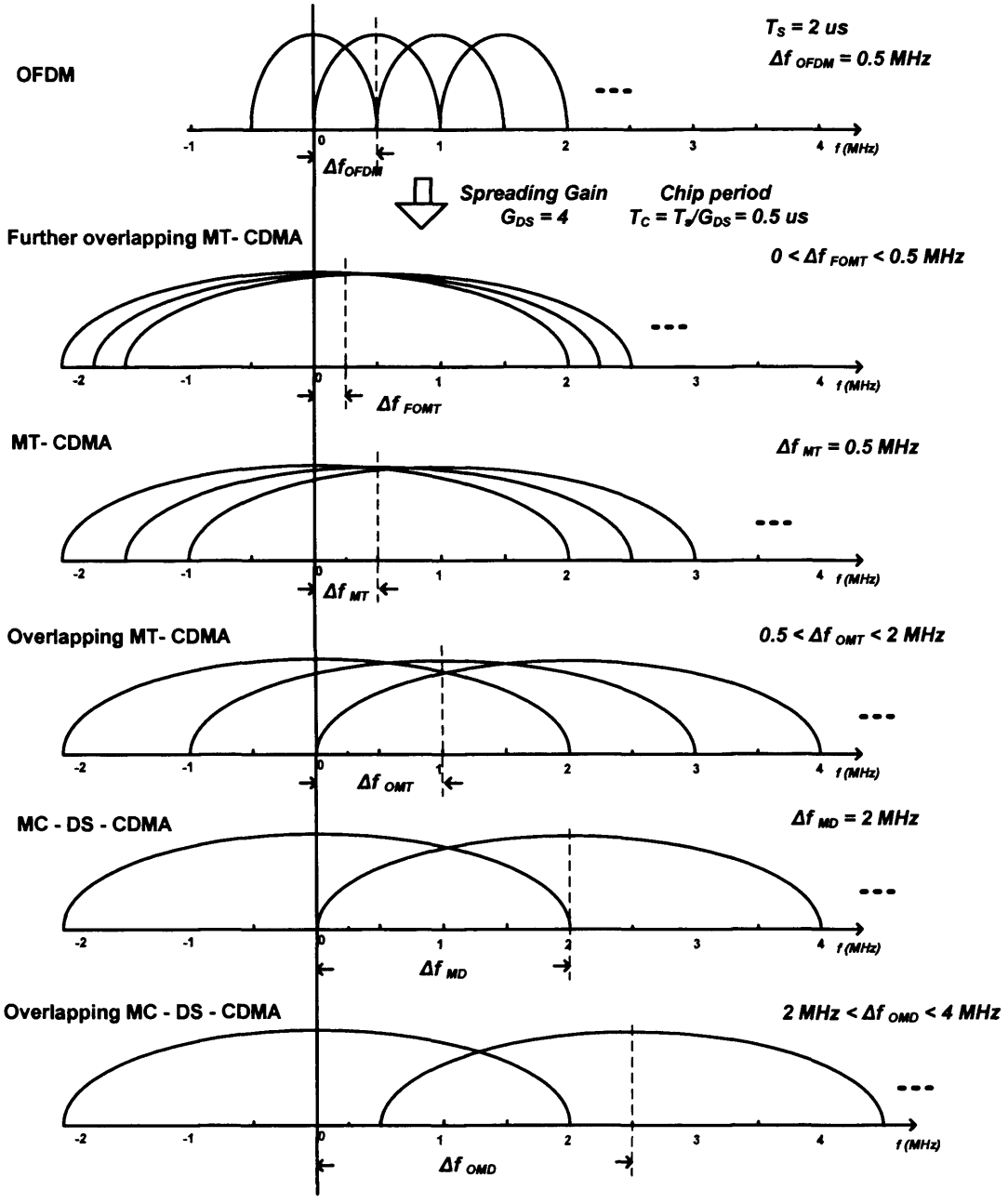

Figure 3.23. Overlapping multicarrier CDMA systems

3.4.3. Multi-user multi-carrier CDMA

A block diagram of the system model of the overlapping MT-CDMA scheme using rake combiners receiver is shown in Figure 3.24.

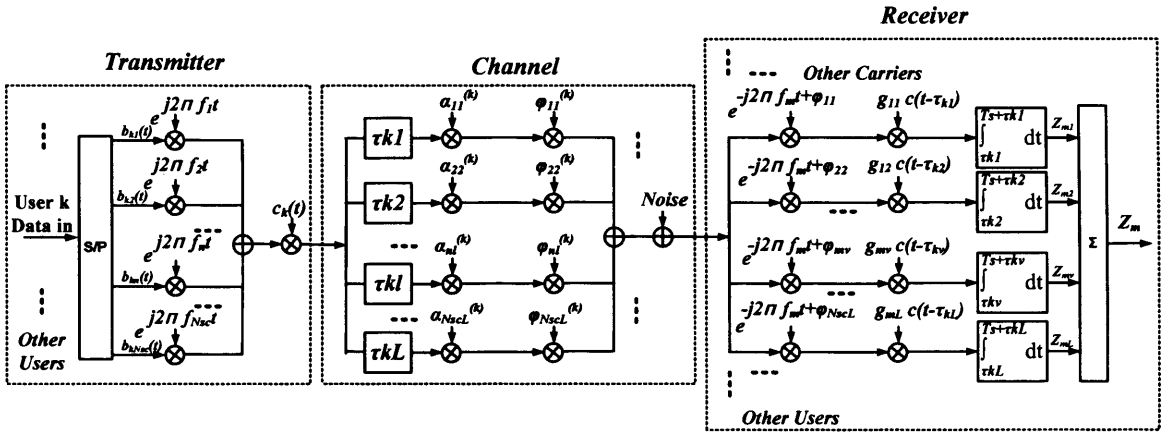

Figure 3.24. Block diagram of overlapping MT-CDMA system

Hence, the transmitted signal of the k^{th} user can be written as:

$$s_k(t) = \sqrt{2P_s} \sum_{n=1}^{N_{sc}} b_{kn}(t) \cdot c_k(t) \cdot e^{j(2\pi f_n t + \phi_{kn})} \tag{3.27}$$

where ϕ_{kn}, n = 1,2,...N_{sc}, are the modulation phases, {f_n, n = 1, 2, ...N_{sc}} are the subcarrier frequencies expressed as:

$$f_n = f_0 + \frac{\lambda_{MT}(n-1)}{T_s}, n = 1,2,\dots,N_{sc} \tag{3.28}$$

λ_{MT} = 1, 2,...,2G_{DS}, corresponding to Δf = 1/T_s, 2/T_s,...,2G_{DS}/T_s, when the maximum spacing between two adjacent subcarriers is assumed to be 2G_{DS}.

Assuming the signals are fed to a frequency selective fading channel, where the total number of independent path is L, the complex envelope of the channel impulse response of k^{th} user is given by [22]:

$$h_{kn}(t) = \sum_{l=1}^{L} \alpha_{nl}^{(k)} \delta(t - \tau_{kl}) e^{j(\Psi_{nl}^{(k)})} \tag{3.29}$$

where l is the index of the channel impulse response (CIR) bin, δ(.) is the Dirac function, $\alpha_{nl}^{(k)}$, $\psi_{nl}^{(k)}$ and τ_{kl} are the amplitude, phase and delay

introduced at l^{th} path, assumed mutually independent. The delay τ_{kl} is assumed to be:

$$\tau_{kl} = (l-1)T_c + \tau_k \tag{3.30}$$

In other words, the delays are assumed equally spaced in the spreading code duration, T_c in [0, T_s). The amplitudes $\alpha_{nl}^{(k)}$ for l=1,2,...,L are Rayleigh distributed independent random variables, which satisfy the probability density function (PDF) that is given by [22]:

$$f(\alpha_{nl}^{(k)}) = \frac{2\alpha_{nl}^{(k)}}{E\left[\left(\alpha_{nl}^{(k)}\right)^2\right]} \cdot e^{\left(\frac{-\left(\alpha_{nl}^{(k)}\right)^2}{E\left[\left(\alpha_{nl}^{(k)}\right)^2\right]}\right)} \tag{3.31}$$

$E[(\alpha_{nl}^{(k)})^2]$ is the average amplitude of each path, while it is assumed that the sum of the amplitude of each path is unit, leading to $E[(\alpha_{nl}^{(k)})^2]=1/L$. The phases $\psi_{nl}^{(k)}$, l=1,2,...,L are uniformly distributed random variables in [0, 2π).

Figure 3.24 shows the receiver structure for signal recovery of the *mth* branch of data. Combining equations (3.27) and (3.29), the received signal $r(t)$ without noise, is given by:

$$r(t) = \sqrt{2P_s}\sum_{k=1}^{K}\sum_{n=1}^{N_{sc}}\sum_{l=1}^{L}\alpha_{nl}^{(k)}b_{kn}(t-\tau_{kl})\cdot c_k(t-\tau_{kl})\cdot e^{j\left(2\pi f_n t+\varphi_{nl}^{(k)}\right)} \tag{3.32}$$

where $\varphi_{nl}^{(k)} = \phi_{kn} + \Psi_{nl}^{(k)} - 2\pi f_n \tau_{kl}$ is contributed by the channel. The decision threshold Z_m at the receiver can be written as:

$$Z_m = \sum_{v=1}^{L} Z_{mv}, m = 1,2,\dots,N_{sc} \tag{3.33}$$

$$Z_{mv} = \int_{\tau_v}^{T_s+\tau_v} r(t)\cdot g_{mv}\cdot c(t-\tau_v)\cdot e^{-j(2\pi f_m t+\varphi_{mv})} \tag{3.34}$$

where g_{mv} is the coefficient that decides which combining schemes is used. In the case of MRC, $g_{mv} = \alpha_{mv}$. If τ_v is assumed to be 0, substituting equations (3.32) into (3.34), Z_{mv} can be further written as:

$$Z_{mv} = \sqrt{2P_s}\sum_{k=1}^{K}\sum_{n=1}^{N_{sc}}\sum_{l=1}^{L}\int_{0}^{T_s} \alpha_{nl}^{(k)} b_{kn}(t-\tau_{kl}) \cdot c_k(t-\tau_{kl}) \cdot e^{j(2\pi(f_n-f_m)t+\varphi_{nl}^{(k)}-\varphi_{mv}^{(k)})} \cdot g_{mv} \cdot c(t)\, dt \tag{3.35}$$

It can be further derived as:

$$Z_{mv} = \sqrt{2P_s}\left\{ D_{mv} + \eta_{mv} + \sum_{\substack{l=1 \\ l\neq v}}^{L} I_1^{(s)} + \sum_{\substack{n=1 \\ n\neq m}}^{N_{sc}}\sum_{\substack{l=1 \\ l\neq v}}^{L} I_2^{(s)} + \sum_{k=2}^{K}\sum_{\substack{l=1 \\ l\neq v}}^{L} I_1^{(k)} + \sum_{\substack{n=1 \\ n\neq m}}^{N_{sc}}\sum_{k=2}^{K}\sum_{\substack{l=1 \\ l\neq v}}^{L} I_2^{(k)} \right\} \tag{3.36}$$

where η_{mv} represents the AWGN noise component with zero mean and variance $g^2_{mv}\, N_0/2E_b$, where $E_b=PT_s$ is the bit energy. D_{mv} represents the desired signal which is given by setting k=1, l=v and n=m in equation (3.35) as:

$$D_{mv} = \alpha_{mv} b_m[0] g_{mv} \tag{3.37}$$

The last four terms in equation (3.36) are the different types of interference: $I_1^{(s)}$ denotes the interference generated from different paths to the same subcarrier. It can be evaluated by setting k=1, $l\neq v$ and n=m in the equation (3.35) as

$$I_1^{(s)} = \sqrt{2P_s} \cdot \alpha_{ml} \cdot g_{mv} \cdot e^{j(\varphi_{ml}-\varphi_{mv})} \int_{0}^{T_s} b_m(t-\tau_l)c(t-\tau_l)c(t)\, dt \tag{3.38}$$

The term $I_2^{(s)}$ is the interference from different paths of other subcarriers and is determined by letting k=1, $l\neq v$ and $n\neq m$ in equation (3.35) as:

$$I_2^{(s)} = \sqrt{2P_s} \cdot \alpha_{nl} \cdot g_{mv} \cdot e^{j(\varphi_{nl}-\varphi_{mv})} \int_0^{T_s} b_n(t-\tau_l)c(t-\tau_l)c(t)e^{j2\pi(f_n-f_m)t}\,dt \tag{3.39}$$

Similarly, $I_1^{(k)}$ is the interference from different paths of different users at the same subcarrier and is determined by letting $k\neq1$, $l\neq v$ and $n=m$ in equation (3.35) as:

$$I_1^{(k)} = \sqrt{2P_s} \cdot \alpha_{ml} \cdot g_{mv} \cdot e^{j(\varphi_{ml}-\varphi_{mv})} \int_0^{T_s} b_m(t-\tau_l)c(t-\tau_l)c(t)\,dt \tag{3.40}$$

Finally, $I_2^{(k)}$ is the interference from different paths of different users at other subcarriers and is determined by letting $k\neq1$, $l\neq v$ and $n\neq m$ in equation (3.35) as:

$$I_2^{(k)} = \sqrt{2P_s} \cdot \alpha_{nl}^{(k)} \cdot g_{mv} \cdot e^{j(\varphi_{nl}-\varphi_{mv})} \cdot \int_0^{T_s} b_{nk}(t-\tau_{kl}) \cdot c(t-\tau_{kl}) \cdot c(t) \cdot e^{j2\pi(f_n-f_m)t}\,dt \tag{3.41}$$

One thing to be noted is that if the multipath and multiuser effects are not considered, i.e. K=1 and L=1, then there will still be intercarrier interference which however can be eliminated by making the subcarriers orthogonal, i.e. f_n-f_m is an integer.

3.5 System modeling

3.5.1. System implementation of overlapping multi-carrier systems

3.5.1.1 Overlapping MC-DS-CDMA

Figure 3.25 illustrates the transmitter model of an overlapping MC-DS-CDMA system for a single user scenario. The practical ADS block diagram is also shown in the Appendix A.2.

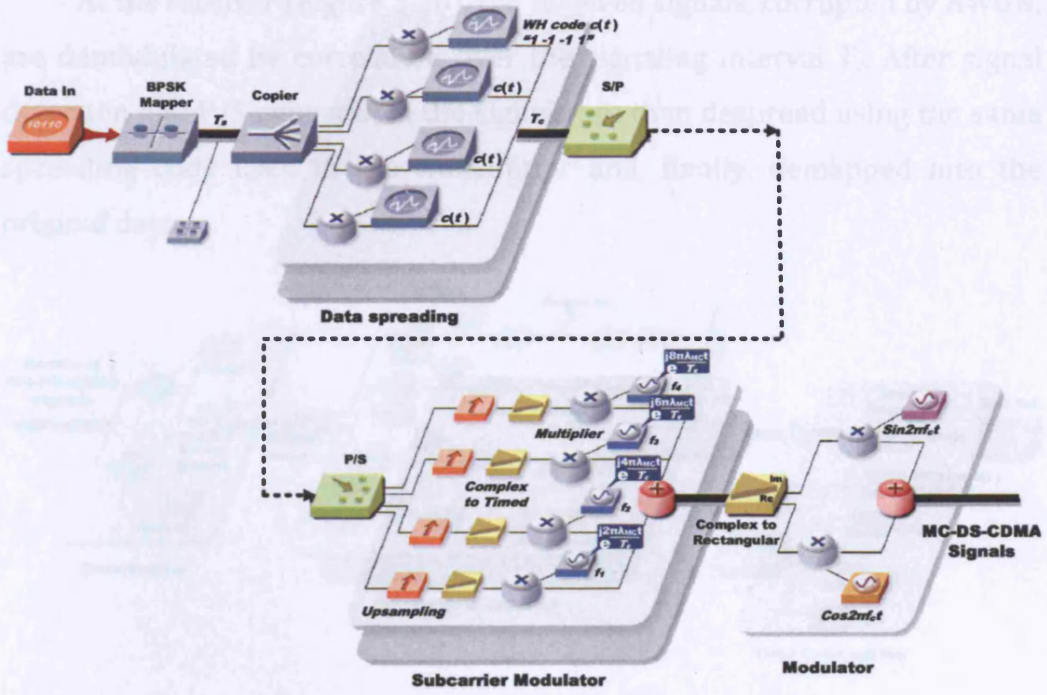

Figure 3.25. Single-user overlapping MC-DS-CDMA transmitter

The original data bits are first BPSK mapped into data symbols, and then S/P converted into N_{sc} parallel data streams. The symbol duration of each sub-data stream extends to $N_{sc}T_s$. T_s is equivalent to the bit duration T_b, and $2T_b$, for BPSK and QPSK signal mapping schemes, respectively. Subsequently, the S/P converted data streams are spread using a given spreading code with variable coding length (processing gain), G_{MD}. The spread substreams are then modulated with N_{sc} subcarriers with overlapping subcarrier spacing of Δf_{OMD} that can be expressed as:

$$\Delta f_{OMD} = \frac{\lambda_{MC}}{T_c} = \frac{\lambda_{MC} \cdot G_{MD}}{T_s \cdot N_{sc}} \tag{3.42}$$

The overlapping coefficient λ_{MC} can vary between 0 to 2, which results in overlapping percentage of 100% to 0%. For the case similar to OFDM, λ_{MC} = 1 (corresponds to 50% overlapping) while λ_{MC} = 0.5 (corresponds to 75% overlapping) is the case similar to Fast-OFDM. Finally the MC-DS-CDMA signal is generated by adding up all the modulated substreams and passes through the IQ modulator to shift the signals to passband.

At the receiver (Figure 3.26), the received signals, corrupted by AWGN, are demodulated by correlation over the signaling interval T_c. After signal detection and P/S conversion, the signals are then despread using the same spreading code used in the transmitter and, finally, demapped into the original data.

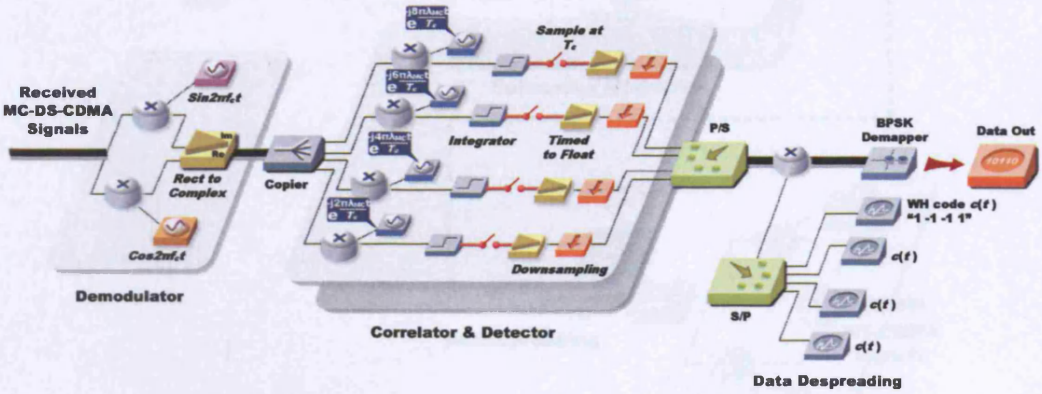

Figure 3.26. Single-user overlapping MC-DS-CDMA receiver system model

3.5.1.2 Overlapping MT-CDMA

Figure 3.27 and Figure 3.28 illustrate the transmitter and receiver model of the overlapping MT-CDMA system, respectively. The practical ADS block diagram is also shown in the Appendix A.3. The description of the system is discussed in section 3.4.2. This system differs from the overlapping MC-DS-CDMA system in that the data spreading is performed after the modulation of each subcarrier. The overlapping frequency spacing (Δf_{OMT}) is λ_{MT}/T_s (λ_{MT} = 1, 2,..., G_{DS}), where G_{DS} is the spreading gain and λ_{MT} is the overlapping coefficient, whereby taking integer values of λ_{MT} maintains the orthogonality among subcarriers. The special case of λ_{MT} = 1 belongs to the class of MT-CDMA system, while $\lambda_{MT} = G_{DS}$ is the case similar to MC-DS-CDMA scheme.

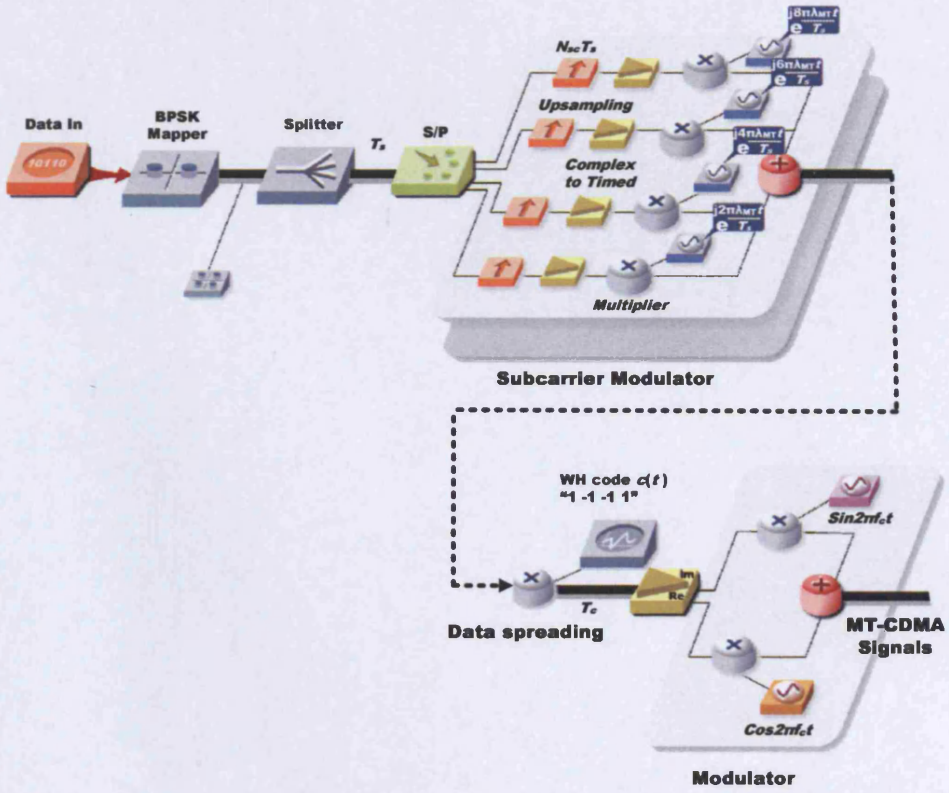

Figure 3.27. Single-user overlapping MT-CDMA transmitter system model

At the receiver, multiple correlators are used for signal recovery instead of multiple rake combiners (Figure 3.18). This is due to the fact that multi-path and multi-user effects are not considered here. The system can be implemented with rake combiners when multi-path fading effects and multi-user interference are considered.

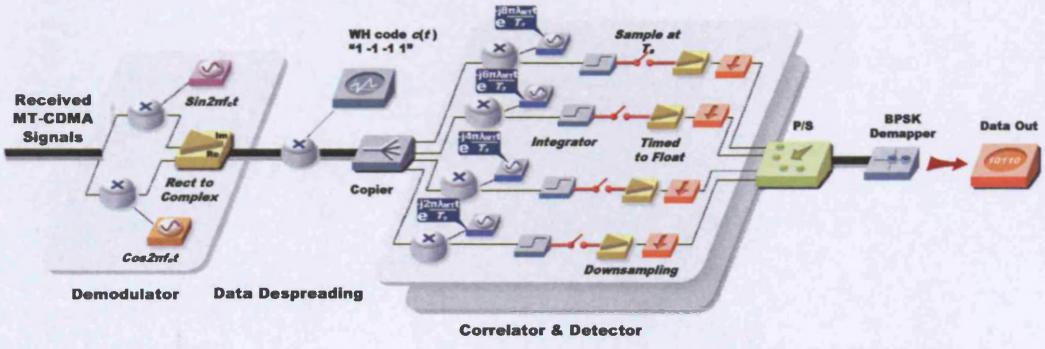

Figure 3.28. Single-user overlapping MT-CDMA receiver system model

3.5.2. System implementations in ADS

The overlapping MC-DS-CDMA system discussed in the previous section is implemented in ADS. Figure 3.29 shows the variable configurations defined for the BPSK overlapping MC-DS-CDMA system. The simulation time step (i.e. "TStep") is set to 1% of the bit period. The variable "CodeLength" defines the length of the spreading code. The frequency spacing (i.e. "DeltaF") is the inverse of spreading code chipping duration, which is also controlled by an overlapping coefficient.

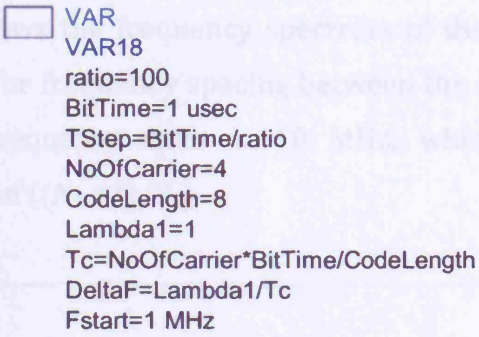

Figure 3.29. BPSK overlapping MC-DS-CDMA system configurations

The implementation of an overlapping MC-DS-CDMA system is similar to OFDM except for the insertion of code spreading during parallel data stream modulation on each subcarrier. Taking the BPSK system as an example, the initial bit generation, mapping and S/P conversion are same as the OFDM implementation described in section 2.6.2.1. The output of the S/P converter is then spread by multiplying each stream with the same copy of the user specific spreading code generated by the "WaveForm" component before modulating with each subcarrier (Figure 3.30). Similarly at the receiver, the recovered data are despread by multiplying the same spreading code as in the transmitter.

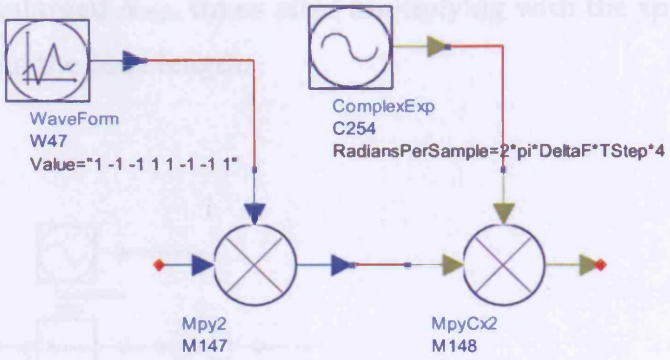

Figure 3.30. MC-DS-CDMA data spreading

Figure 3.31 shows the frequency spectrum of the modulated MC-DS-CDMA subcarriers. The frequency spacing between the subcarriers is 2 MHz ($1/T_c$). The total frequency span is 10 MHz, which agrees with the theoretical calculation ($(N_{sc}+1)/T_c$).

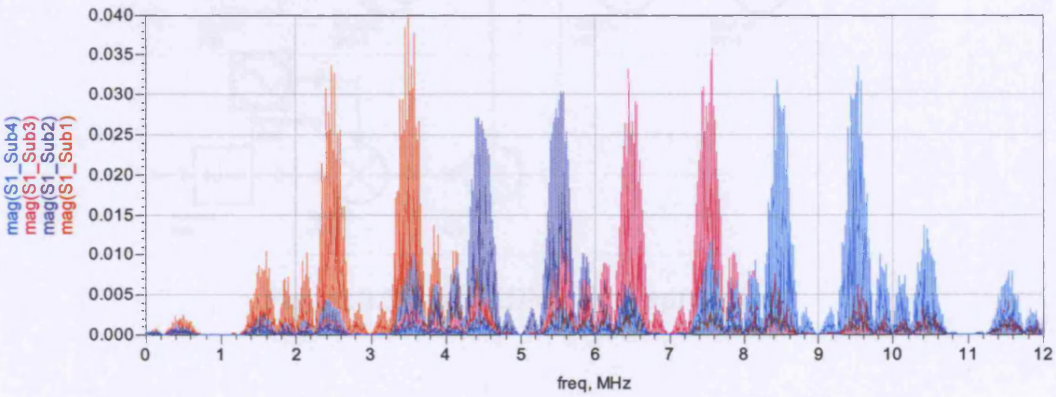

Figure 3.31. Frequency spectrum of MC-DS-CDMA (4 subcarriers)

Overlapping MT-CDMA system differs from MC-DS-CDMA in the insertion of data spreading and frequency spacing between subcarriers (Figure 3.32). In the case of MT-CDMA, the data spreading is performed after the OFDM signal is generated and the frequency spacing between MT-CDMA subcarriers is the inverse of the OFDM symbol duration. Figure 3.33 shows the spectrum of the MT-CDMA subcarriers. It is observed that the frequency spacing is shortened to $1/T_s$. Strong overlapping exists between subcarriers. Figure 3.34 and Figure 3.35 reveal the frequency spectrum of the first subcarrier modulated data stream before and after code spreading, respectively. It can be noticed from the figures that the frequency span of

the signal is enlarged N_{code} times after multiplying with the spreading code, with N_{code} being the code length.

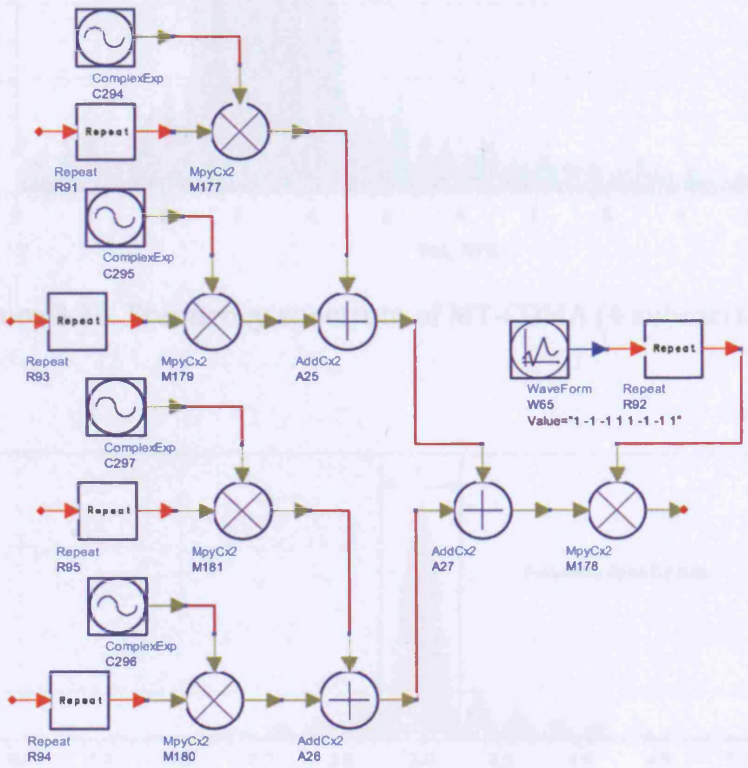

Figure 3.32. MT-CDMA data spreading

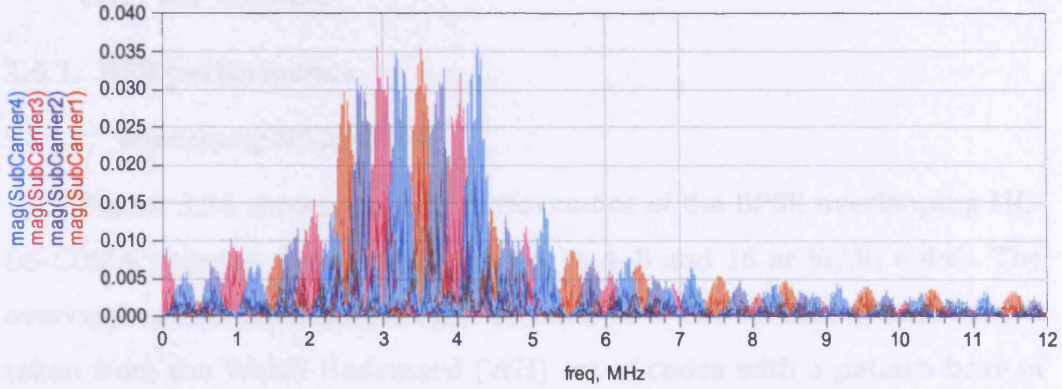

Figure 3.33. Frequency spectrum of MT-CDMA (4 subcarriers)

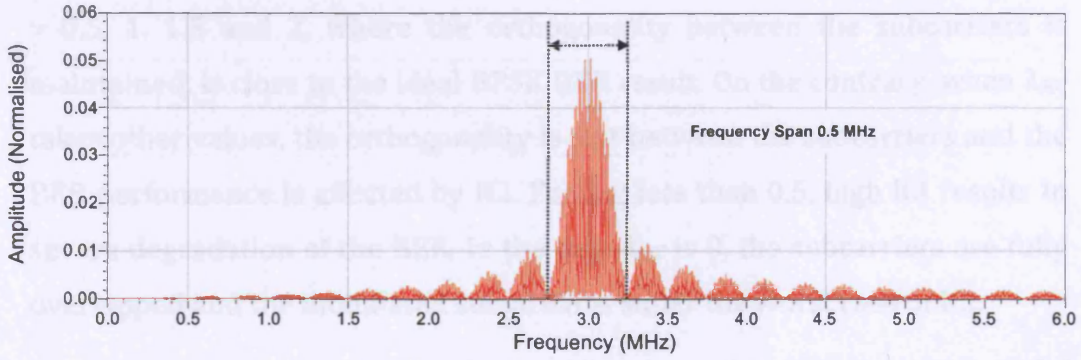

Figure 3.34. MT-CDMA before data spreading (single subcarrier)

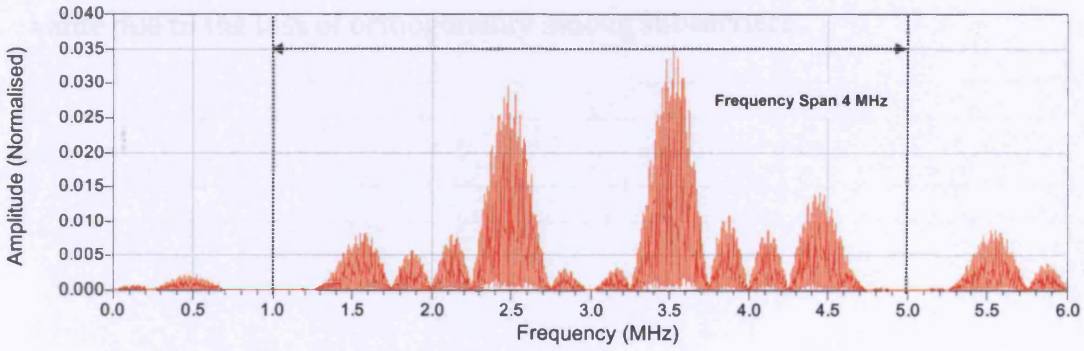

Figure 3.35. MT-CDMA after data spreading (single subcarrier)

3.6 System performance of the overlapping multi-carrier CDMA

3.6.1. BER performance

3.6.1.1 Overlapping MC-DS-CDMA

Figure 3.36 shows the BER performance of the BPSK overlapping MC-DS-CDMA systems with code length set to 4, 8 and 16 at E_b/N_o = 4dB. The overlapping coefficient λ_{MC}, is varied from 0 to 2. The spreading code used is taken from the Walsh Hadamard (WH) set of codes with a pattern base of (1,-1,-1, 1). It can be observed from the figure that different code lengths produce similar BER performance. This indicates that the BER performance is not affected by the code length. Furthermore, the BER performance at λ_{MC} = 0.5, 1, 1.5 and 2, where the orthogonality between the subcarriers is maintained, is close to the ideal BPSK BER result. On the contrary, when λ_{MC} takes other values, the orthogonality is lost between the subcarriers and the BER performance is affected by ICI. For λ_{MC} less than 0.5, high ICI results in severe degradation of the BER. In the case λ_{MC} is 0, the subcarriers are fully overlapped and the modulated substreams suffer the worst case of ICI.

Figure 3.37 shows the BER performance of the system with QPSK modulation. Similar results are gained except that at the points of λ_{MC} = 0.5 and λ_{MC} = 1.5, where the BER results are away from the theoretical BPSK value due to the loss of orthogonality among subcarriers.

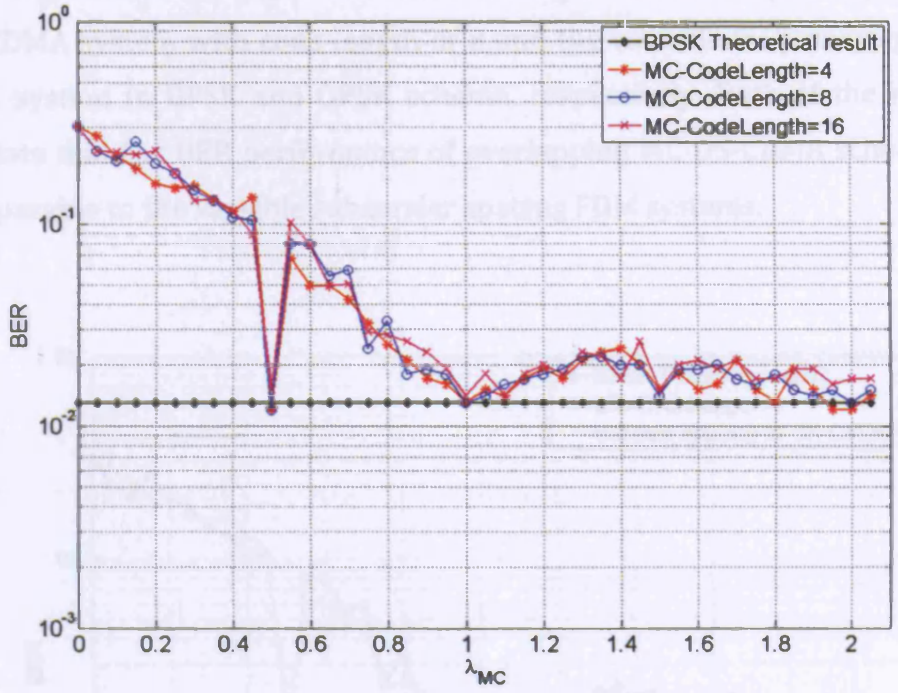

Figure 3.36. BPSK BER plot with varied λ_{MC} at E_b/N_o=4dB

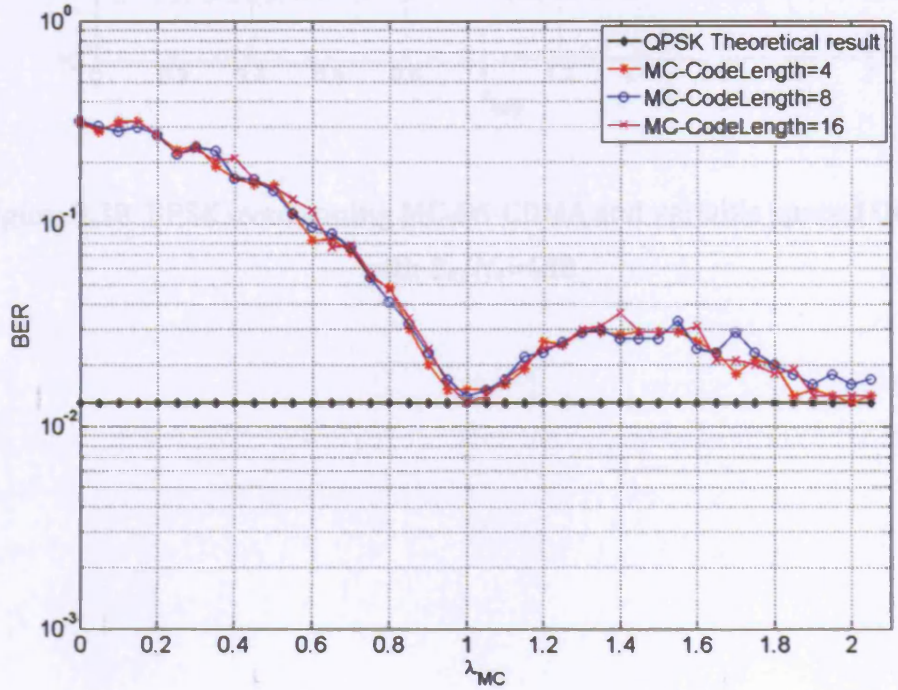

Figure 3.37. QPSK BER plot with varied λ_{MC} at E_b/N_o=4dB

Figure 3.38 and Figure 3.39 show a comparison of the overlapping MC-DS-CDMA system with code length of 8 and the variable frequency spacing FDM system in BPSK and QPSK scheme, respectively. Both of the results indicate that the BER performance of overlapping MC-DS-CDMA schemes is comparable to the variable subcarrier spacing FDM systems.

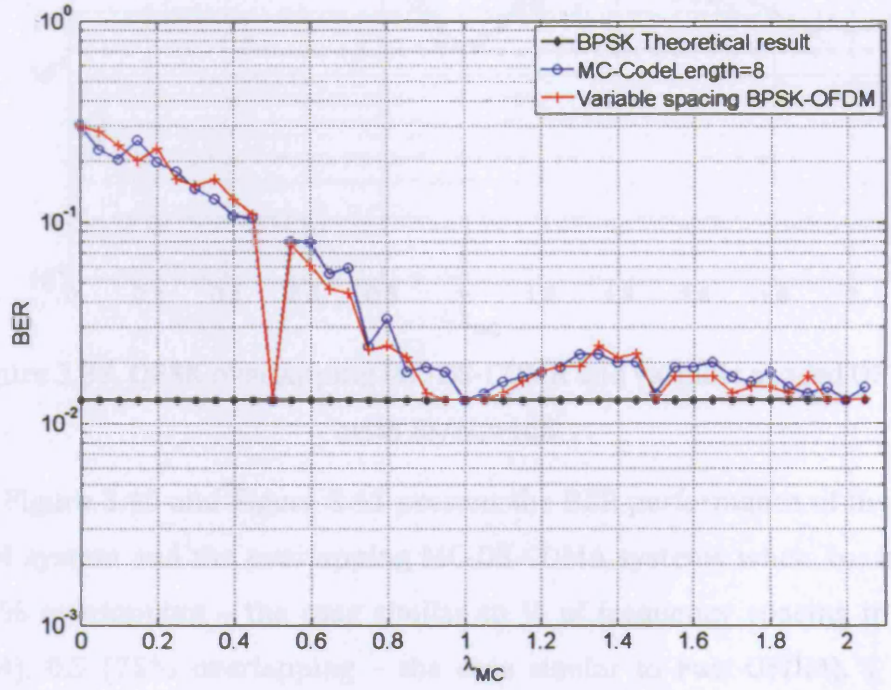

Figure 3.38. BPSK overlapping MC-DS-CDMA and variable spaced OFDM with E_b/N_o=4dB

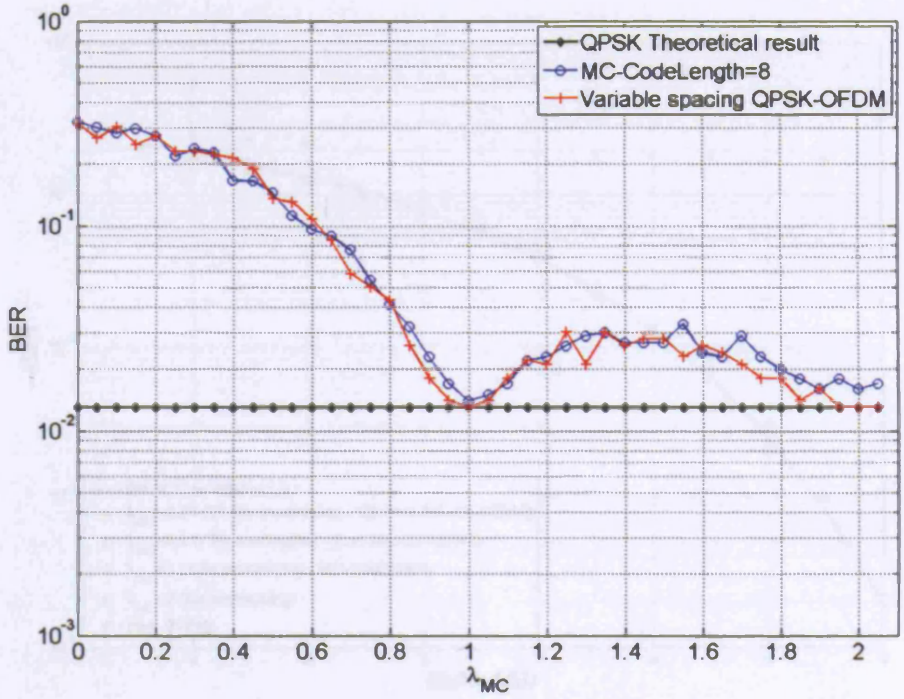

Figure 3.39. QPSK overlapping MC-DS-CDMA and variable spaced OFDM with E_b/N_o=4dB

Figure 3.40 and Figure 3.41 present the BER performance of the Fast-OFDM system and the overlapping MC-DS-CDMA systems when λ_{MC} is 0.25 (87.5% overlapping – the case similar to ½ of frequency spacing in Fast-OFDM), 0.5 (75% overlapping – the case similar to Fast-OFDM), 1 (50% overlapping – the case similar to OFDM) and 2 (0% overlapping – the case similar to FDM) in BPSK and QPSK system, respectively. In the BPSK system, the orthogonality among subcarriers is lost when λ_{MC} = 0.25, leading to degraded BER performance when compared to the theoretical BPSK BER result. For λ_{MC} = 0.5, λ_{MC} = 1 and λ_{MC} = 2, the orthogonality is maintained. The BER performances are close to the ideal result. As expected for the QPSK system, the overlapping MC-DS-CDMA system (λ_{MC} = 0.5) exhibits similar properties when compared to the Fast-OFDM system that shows BER degradation due to the loss of orthogonality.

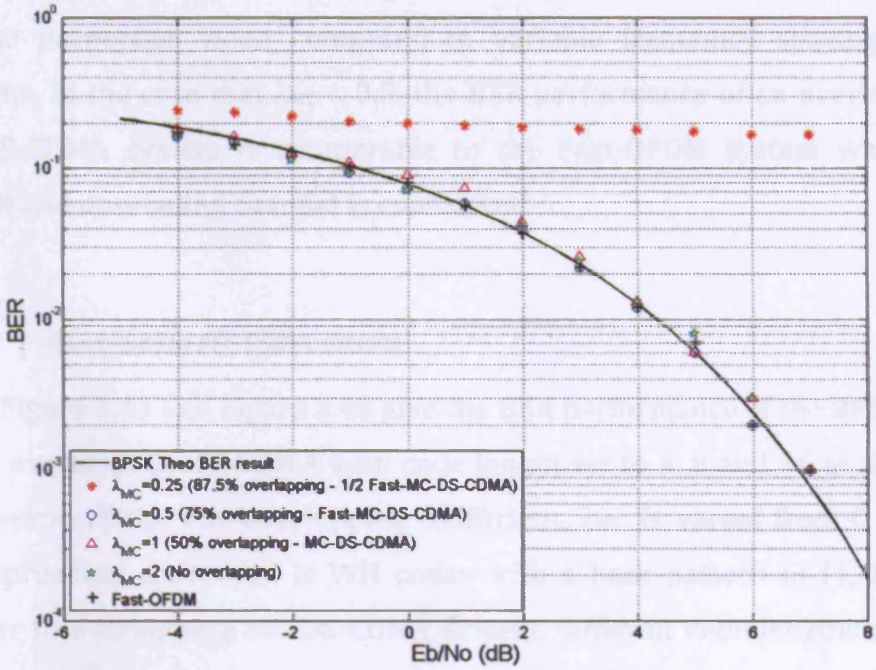

Figure 3.40. BPSK overlapping MC-DS-CDMA BER performance

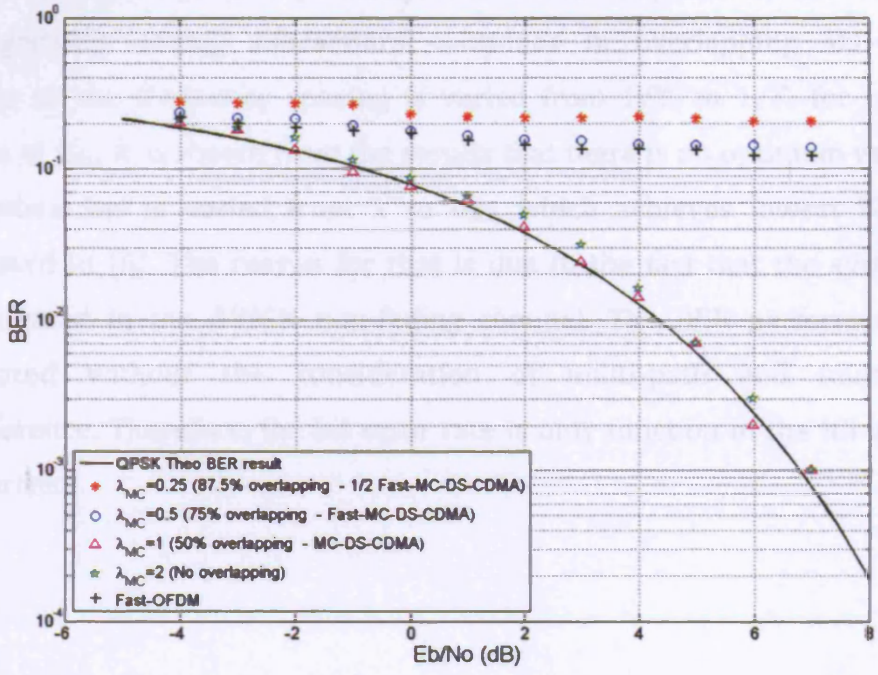

Figure 3.41. QPSK overlapping MC-DS-CDMA BER performance

In summary, the overlapping MC-DS-CDMA system is shown to exhibit similar properties when compared to variable frequency spacing FDM systems. In the case that λ_{MC} = 0.5, the BER performance of an overlapping MC-DS-CDMA system is comparable to the Fast-OFDM system when an AWGN and non-fading channel is considered.

3.6.1.2 Overlapping MT-CDMA system

Figure 3.42 and Figure 3.43 give the BER performance of the BPSK and QPSK overlapping MT-CDMA with code length set to 4, 8 and 16 at E_b/N_o = 4dB, respectively. The overlapping coefficient, λ_{MT}, is varied from 0 to 16. The spreading code used is WH codes with a base pattern of (1,-1,-1,1). Similar to overlapping MC-DS-CDMA system, different code lengths do not affect the BER performance. Furthermore, the BER performance is close to the theoretical BPSK and QPSK systems in AWGN when λ_{MT} equals $0.5i$ (i = 1,2,...) and i (i = 1,2,...), respectively. This further explains the fact that the orthogonality among subcarriers continues in overlapping MT-CDMA system as the frequency spacing is varied from $1/T_s$ to $1/T_c$ for integer values of λ_{MT}. It is shown from the results that there is no optimum value of λ_{MT}, when λ_{MT} is varied from 1 to G_{DS}, which achieves lowest BER as discussed in [6]. The reason for that is due to the fact that the system is investigated in the AWGN non-fading channel. The BER performance is evaluated without the consideration of multi-path and multi-user interference. Therefore, the bit error rate is only function of the ICI among subcarriers.

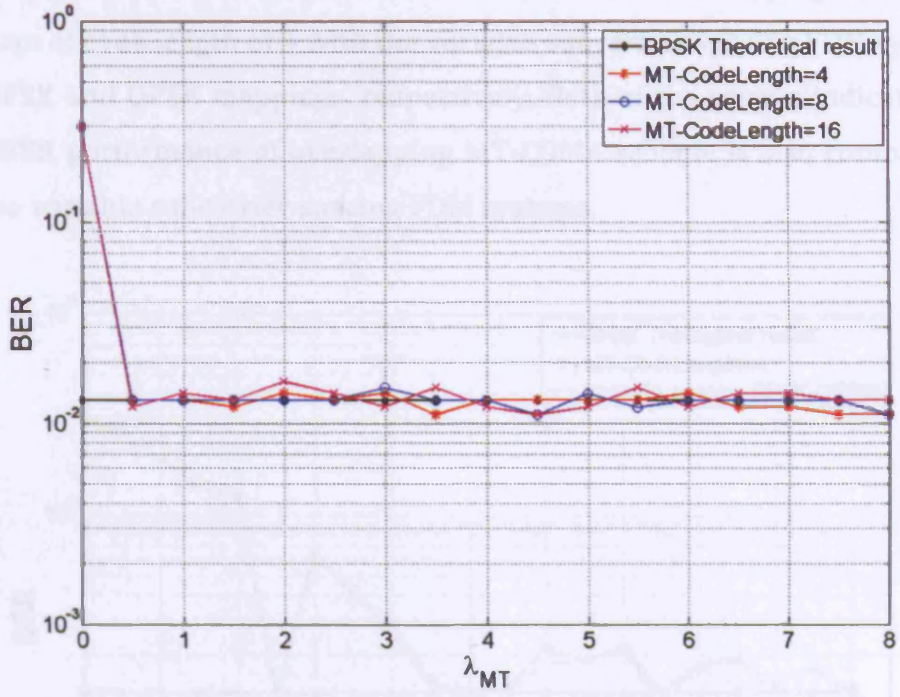

Figure 3.42. BPSK overlapping MT-CDMA BER performance at E_b/N_o = 4dB

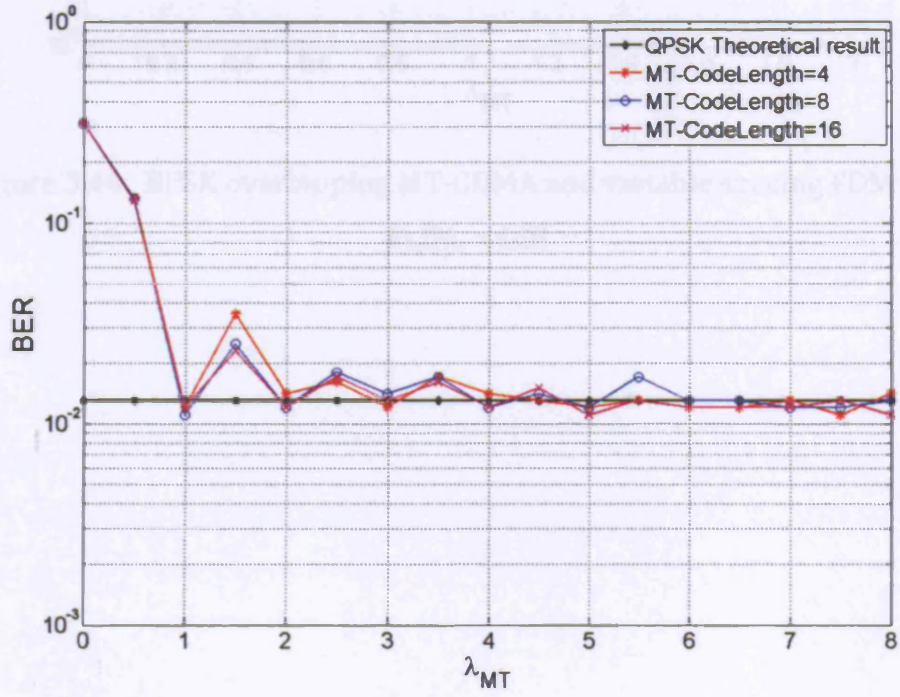

Figure 3.43. QPSK overlapping MT-CDMA BER performance at E_b/N_o = 4dB

Figure 3.44 and Figure 3.45 compare the overlapping MT-CDMA system of code length of 4 with the variable subcarrier spacing FDM systems in BPSK and QPSK mappings, respectively. Both of the results indicate that the BER performance of overlapping MT-CDMA scheme is also comparable to the variable subcarrier spacing FDM systems.

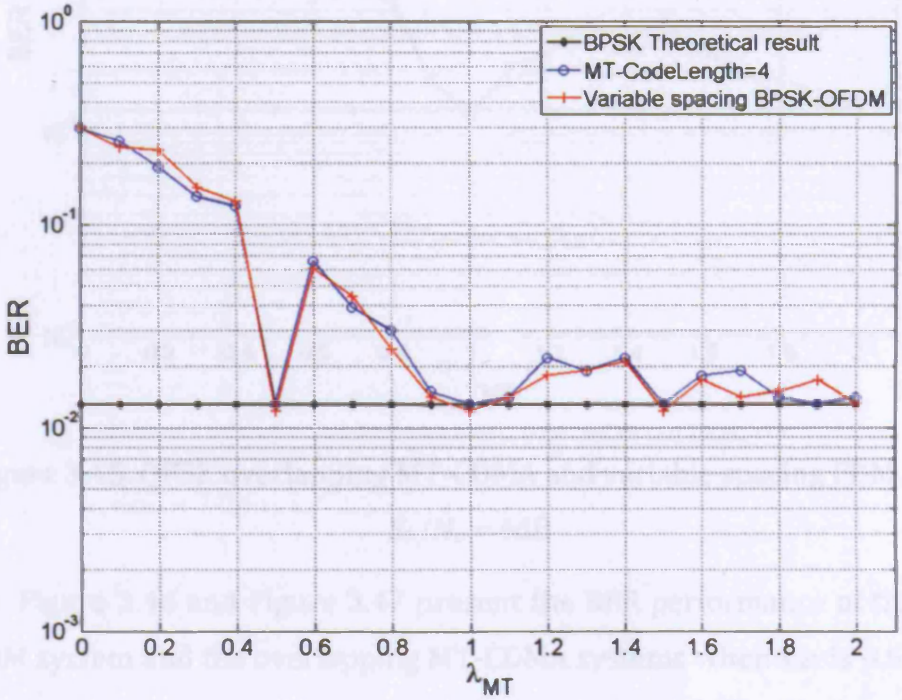

Figure 3.44. BPSK overlapping MT-CDMA and variable spacing FDM with E_b/N_o = 4dB

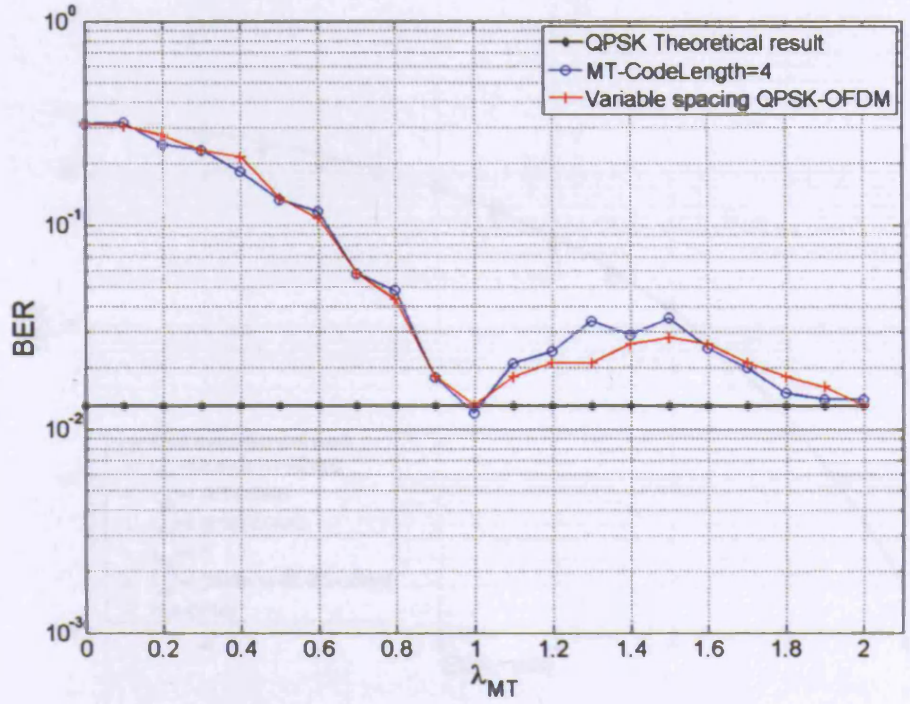

Figure 3.45. QPSK overlapping MT-CDMA and variable spacing FDM with E_b/N_o = 4dB

Figure 3.46 and Figure 3.47 present the BER performance of the Fast-OFDM system and the overlapping MT-CDMA systems when λ_{MT} is 0.5 ($\Delta f_{OMT} = 1/(2T_s)$ – the case similar to Fast-OFDM), 1 ($\Delta f_{OMT} = 1/T_s$ – the case of MT-CDMA), 2 ($\Delta f_{OMT} = 2/T_s$), 2.5 and 4 ($\Delta f_{OMT} = G_{DS}/T_s = 1/T_c$ – the case similar to MC-DS-CDMA) with BPSK and QPSK modulations, respectively. In the BPSK system, as the orthogonality remains for $\lambda_{MT} = 0.5i$ (i=1,2,3,...,$2G_{DS}$), the BER performance of the overlapping MT-CDMA system is close to the ideal BPSK system. While, as expected for QPSK system, the overlapping MT-CDMA exhibits similar properties as compared to the Fast-OFDM system when λ_{MT} = 0.5, which leads to a degradation in BER performance due to the loss of orthogonality among subcarriers.

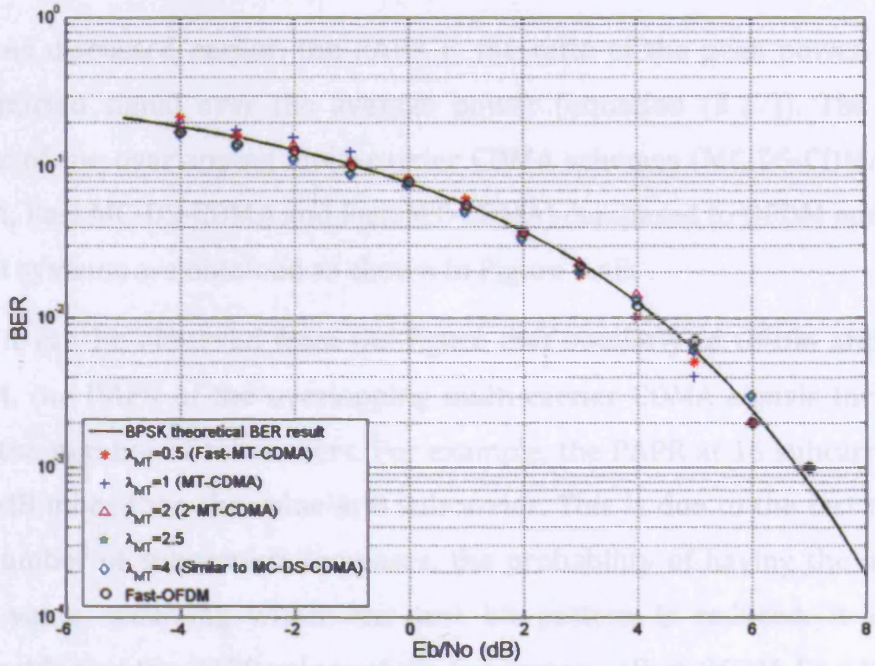

Figure 3.46. BPSK BER plot with varied overlapping coefficients

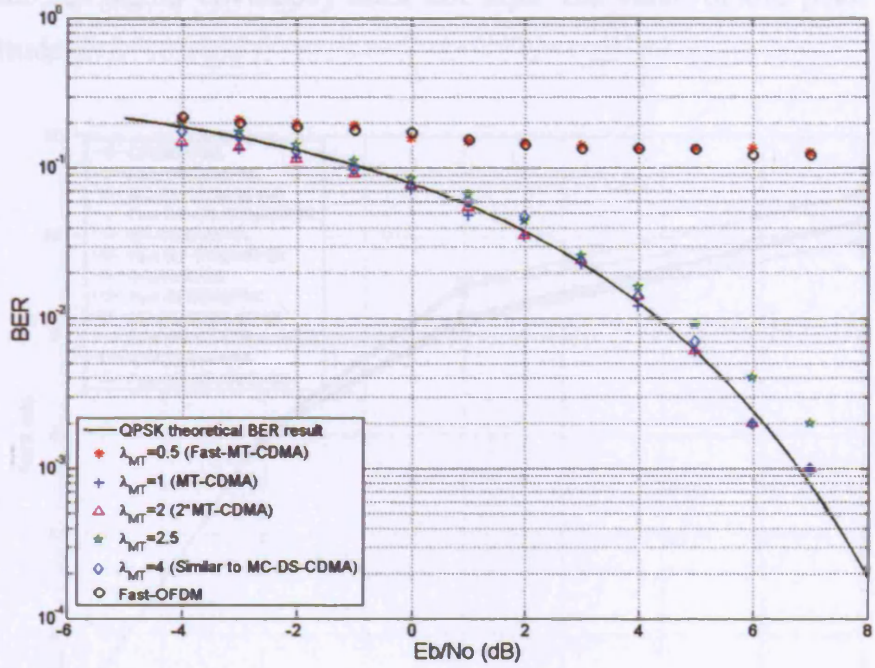

Figure 3.47. QPSK BER plot with varied overlapping coefficients

3.6.2. Peak to average power ratio (PAPR)

As discussed earlier, the PAPR is the ratio of the peak power of the transmitted signal over the average power (equation (2.27)). The PAPR values of the overlapping multi-carrier CDMA schemes (MC-DS-CDMA, MT-CDMA, Fast MC-DS-CDMA and Fast MT-CDMA) compared to OFDM and Fast-OFDM systems are obtained as shown in Figure 3.48.

It can be observed from the figure that similarly to OFDM and Fast-OFDM, the PAPR of the overlapping multi-carrier CDMA signals increases with the number of subcarriers. For example, the PAPR at 16 subcarriers is not 3dB more than the value at 8 subcarrier. This is due to the fact that as the number of subcarriers increases, the probability of having the highest peak value occurring within the test bit pattern is reduced. It is also noticeable that the PAPR values of the fast systems (Fast-OFDM, Fast MC-DS-CDMA and Fast MT-CDMA) are comparable to the conventional schemes. This may be attributed to the fact that reducing the subcarrier spacing (extend the signal envelope) does not alter the value of the peak signal amplitude.

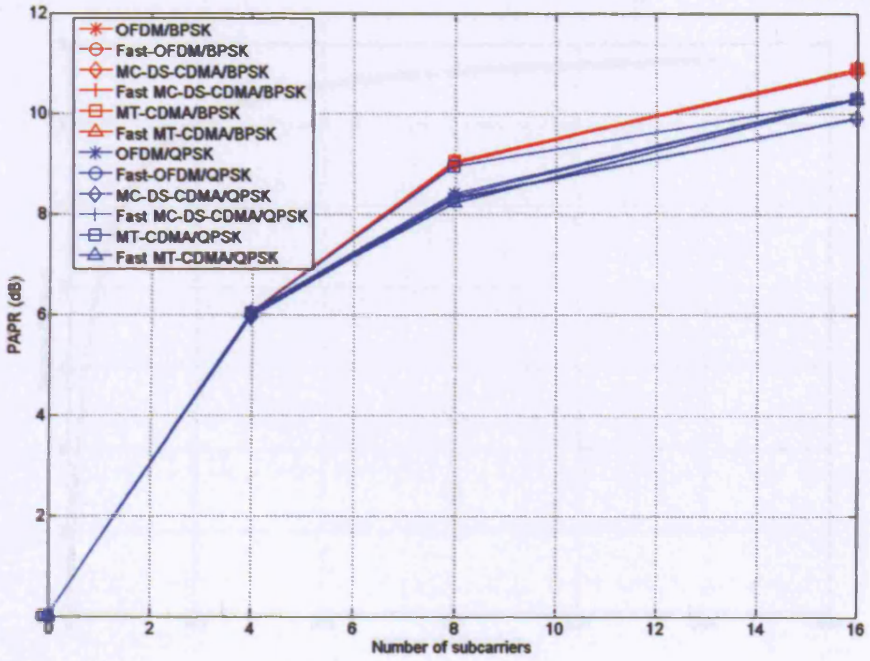

Figure 3.48. PAPR of overlapping multi-carrier CDMAs

3.6.3. Spectral efficiency

In order to compare the spectral efficiency between MC-DS-CDMA and MT-CDMA, a normalized spectral efficiency is defined as the ratio of the MT-CDMA data rate, $R_{MT\text{-}CDMA}$, over the MC-DS-CDMA data rate, $R_{MC\text{-}DS\text{-}CDMA}$, in this analysis. The transmission bandwidth has been fixed and is described as:

$$B = (N-1)\frac{R_{MT-CDMA}}{N_{code}} + 2R_{MT-CDMA} = (N+1)R_{MC-DS-CDMA} \tag{3.43}$$

The spectral efficiency is obtained as:

$$\eta_{MC} = \frac{R_{MT-CDMA}}{R_{MC-DS-CDMA}} = \frac{(N+1)}{\left(\frac{N-1}{N_{code}}\right)+2} \tag{3.44}$$

The ratio of the two data rates depends on the number of subcarriers and the code length. The spectral efficiency for different values of N is shown in Figure 3.49. It can be observed that as the number of subcarriers increases, the spectral efficiency of the MT-CDMA approaches nearly N_{code} times (in this case, N_{code} = 8) of the MC-DS-CDMA system, where in this case the code length is 8.

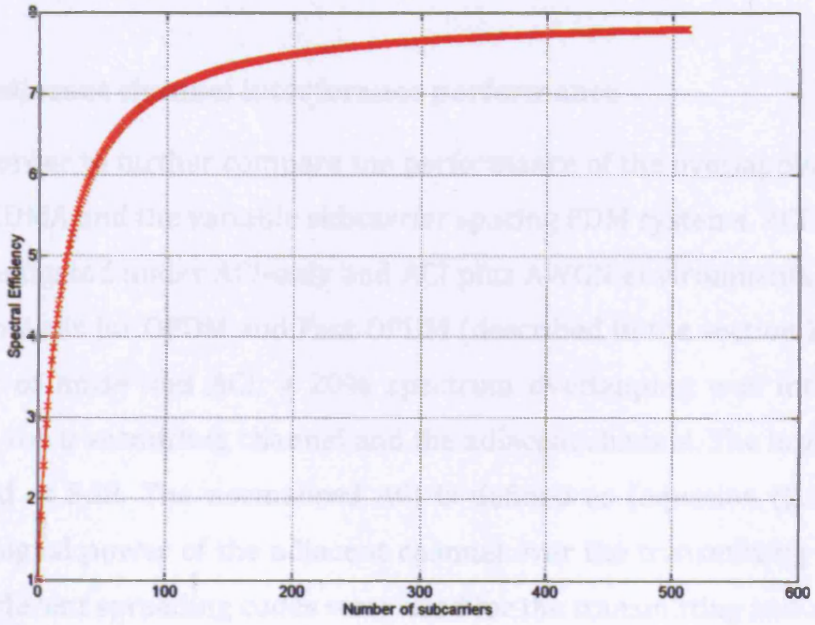

Figure 3.49. Spectral efficiency of MT-CDMA compared to MC-DS-CDMA

Alternatively, in order to compare the two systems, the data rate is kept constant in both cases to compare the occupied bandwidth. The occupied bandwidth comparison plot (Figure 3.50) in this case is an inverted plot of Figure 3.49. This is because, for a constant data rate, the MT-CDMA will occupy nearly one $N_{code}{}^{th}$ (i.e. 1/8) bandwidth of MC-DS-CDMA for large subcarriers.

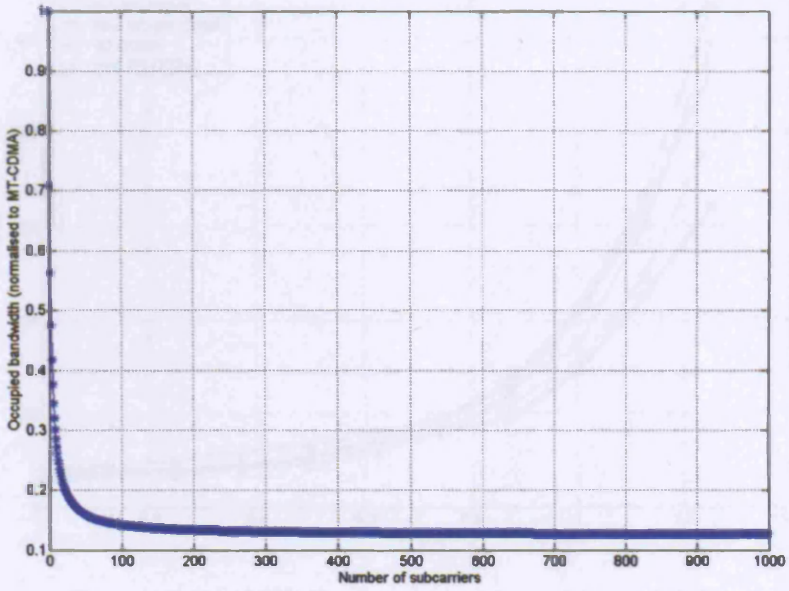

Figure 3.50. Occupied bandwidth comparison of MC-DS-CDMA & MT-CDMA

3.6.4. Adjacent channel interference performance

In order to further compare the performance of the overlapping multi-carrier CDMA and the variable subcarrier spacing FDM systems, ACI analysis was investigated under ACI-only and ACI plus AWGN environments. Similar to ACI analysis for OFDM and Fast-OFDM (described in the section 2.7.4), in the case of noise and ACI, a 20% spectrum overlapping was introduced between the transmitting channel and the adjacent channel. The input E_b/N_o was fixed at 5dB. The normalised ACI is defined as (equation (2.30)) the ratio of signal power of the adjacent channel over the transmitting channel in dB. Different spreading codes were used for the transmitting and adjacent multi-carrier CDMA channels. The performance of the systems in noise and ACI is shown in Figure 3.51. The Fast-OFDM, Fast MC-DS-CDMA and Fast

MT-CDMA are the systems with the subcarrier spacing reduced by half as compared to the conventional ones. It can be observed from the results that generally the conventional systems perform better than the fast ones, whereas, for small ACI distortion conditions the performance of the fast schemes are comparable to the conventional systems.

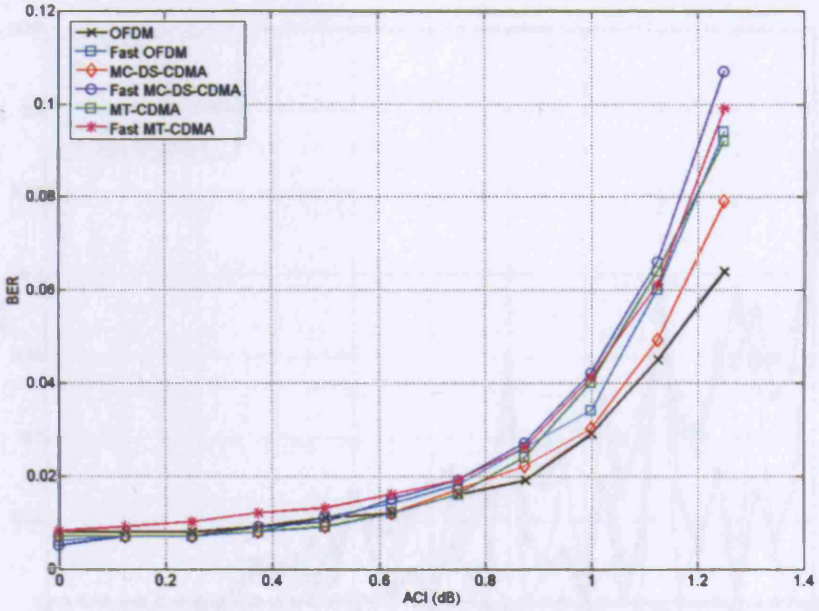

Figure 3.51. BER Performance in noise and ACI

Similarly to the ACI-limited performance assessment for OFDM and Fast-OFDM in section 2.7.4, the spectrum overlapping between the transmitting channel and the adjacent channel was set to 45%. The overlapping percentage was chosen according to the results obtained in Figure 3.52. This is a plot of BER performance at input E_b/N_o of 5dB versus channel overlapping in the case where the signal power of the wanted channel is same as the adjacent channel. It is observed from the result that in the high overlapping regions (>40%), especially when complete sub-channel superposition occurs, the OFDM performance degrades severely.

Figure 3.53 presents the BER performance of the systems under ACI-only condition. The results show that the MT-CDMA and MC-DS-CDMA perform better than OFDM. This is a consequence of the fact that the insertion of the spreading code in the multi-carrier CDMA schemes provides better resistance to ACI. This trend can also be recognized in the comparison

of Fast-OFDM and fast multi-carrier CDMA schemes for small ACI distortions. As ACI keeps increasing and becomes larger than the wanted signal, Fast-OFDM performs better. It is also noticeable that when the ACI is greater than 1, the performance of the fast systems degrade severely due to the higher ICI and increased ACI as compared to conventional schemes.

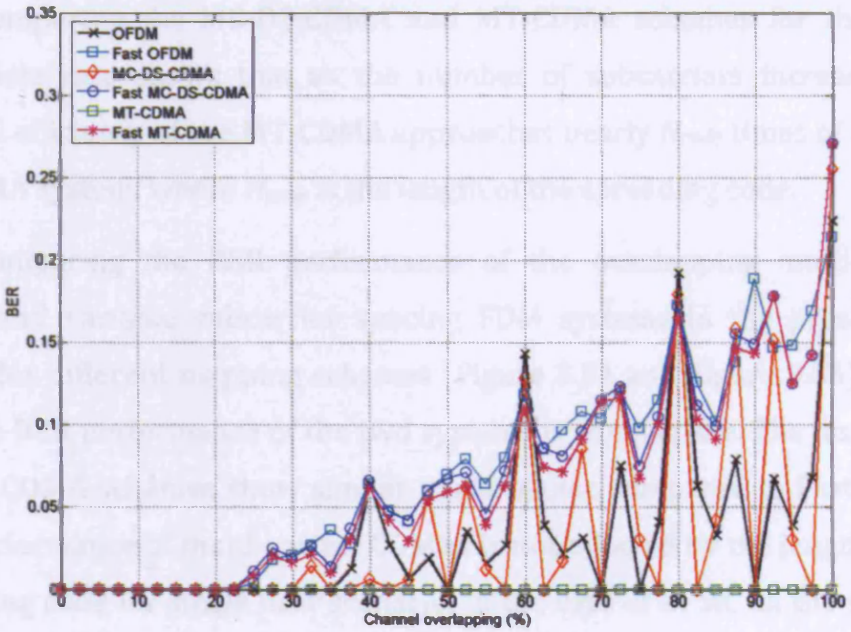

Figure 3.52. BER Performance for variable channel separations

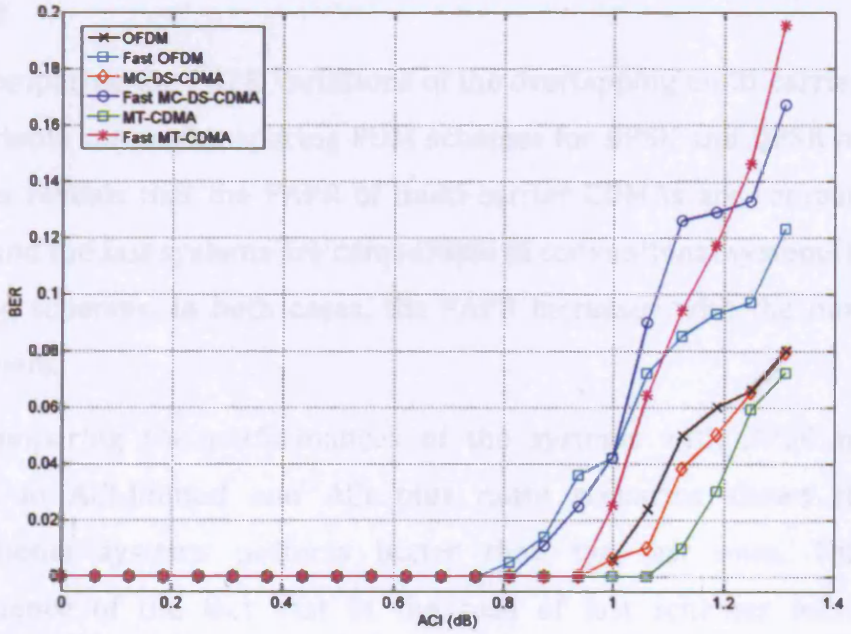

Figure 3.53. BER Performance in ACI-only

3.6.5. Results discussion

Section 3.6 presented the performance of multi-carrier CDMA (MC-DS-CDMA and MT-CDMA) as compared to OFDM and Fast-OFDM for different mapping schemes. In all the cases, the initial data rate has been made constant.

Comparing the MC-DS-CDMA and MT-CDMA schemes for the same input data rate shows that as the number of subcarriers increases, the spectral efficiency of the MT-CDMA approaches nearly N_{code} times of the MC-DS-CDMA system, where N_{code} is the length of the spreading code.

Comparing the BER performance of the overlapping multi-carrier CDMA and variable subcarrier spacing FDM systems in the presence of AWGN for different mapping schemes (Figure 3.54 and Figure 3.55) shows that the BER performance of the two systems is comparable. The fast multi-carrier CDMA schemes show similar performance compared to Fast-OFDM. The performance of multi-carrier CDMAs is not affected by the length of the spreading code for single user scenario. In the case of BPSK, all the systems are close to the ideal BPSK BER results. Yet, as expected, when QPSK mapping is applied, the BER performance of the fast systems deteriorates severely.

Comparing the PAPR variations of the overlapping multi-carrier CDMA and variable subcarrier spacing FDM schemes for BPSK and QPSK mapping schemes reveals that the PAPR of multi-carrier CDMAs are comparable to OFDM and the fast systems are comparable to conventional systems for both mapping schemes. In both cases, the PAPR increases with the number of subcarriers.

Comparing the performances of the systems with BPSK mapping scheme in ACI-limited and ACI plus noise scenarios shows that the conventional systems perform better than the fast ones. This is a consequence of the fact that in the case of fast schemes halving the subcarrier spacing generates larger ICI between subcarriers and ACI from adjacent channels. Moreover, multi-carrier CDMA provides better resistance

to ACI when compared to OFDM due to the insertion of the spreading code for user separation.

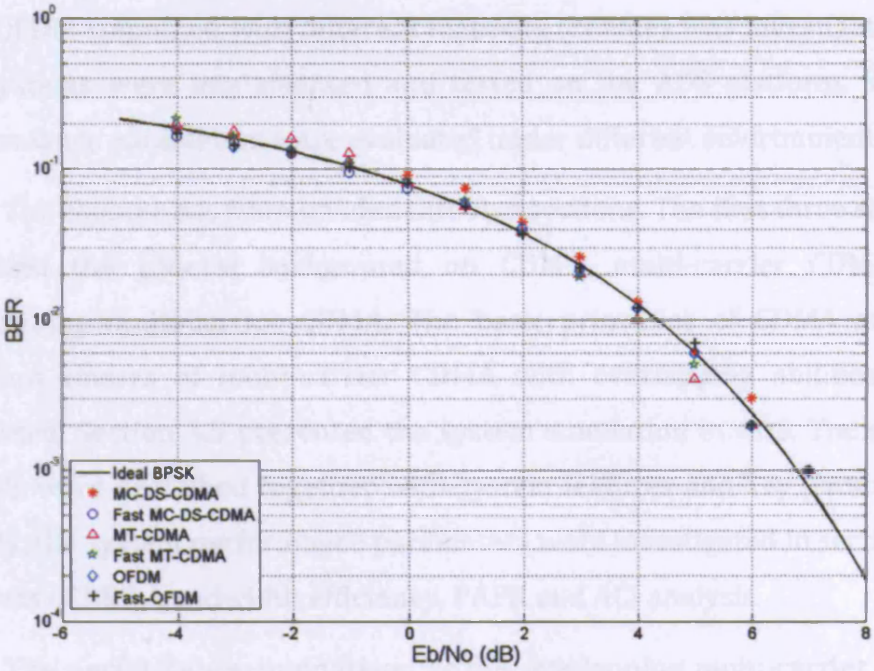

Figure 3.54. BER for BPSK overlapping multi-carrier CDMAs, OFDM and Fast-OFDM

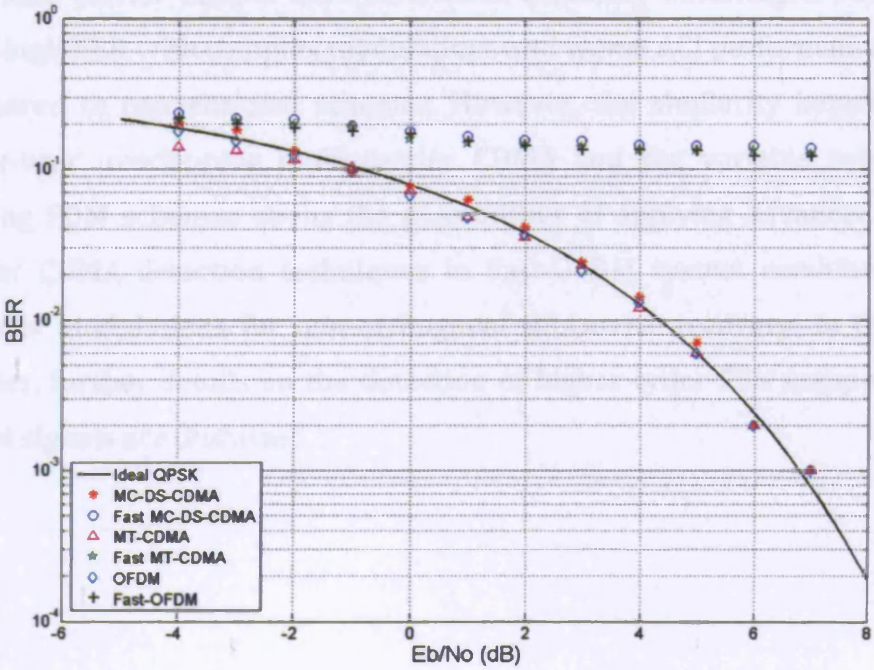

Figure 3.55. BER for QPSK overlapping multi-carrier CDMAs, OFDM and Fast-OFDM

3.7 Summary

In this chapter, the overlapping multi-carrier CDMA and OFDM and Fast-OFDM combined with different mapping schemes was investigated. All the systems were implemented and tested on the ADS platform. Several performance parameters were evaluated under different environments.

The chapter has been divided into five sections. The first three sections provided the general background on CDMA, multi-carrier CDMA and overlapping multi-carrier CDMA. The basic principles of CDMA and the different classes of multi-carrier CDMA with overlapping abilities were discussed. Section 3.5 presented the system simulation in ADS. The system models were described together with system features and key parameters. Finally, the system performance parameters were investigated in section 3.6 in terms of BER, bandwidth efficiency, PAPR and ACI analysis.

The performance comparison of the overlapping multi-carrier CDMA and variable subcarrier spacing FDM systems, showed that both systems are comparable under different modulation scenarios. Similar to Fast-OFDM, the fast multi-carrier CDMAs have bandwidth efficiency advantages, but suffer from high BER with complex modulations and worse ACI performance when compared to conventional schemes. However, the similarity between the single-user overlapping multi-carrier CDMA and the variable subcarrier spacing FDM schemes opens the possibilities of applying advanced multi-carrier CDMA detection techniques in Fast-OFDM system combined with complex modulations for non-orthogonal subcarrier recovery. In the next chapter, further details on the detection of higher order PSK mapped Fast-OFDM signals are discussed.

Chapter 4 Linear detection techniques for Fast-OFDM systems

4.1 Introduction

Linear multi-user detection is originally designed for multi-user and multi-carrier transmission, such as DS-CDMA and multi-carrier CDMA, where detectors apply a linear mapping to the output of the conventional detector to reduce the multiple access interference (MAI). A linear detector has computational complexity significantly lower than that of the maximum likelihood sequence detector which increases its complexity exponentially with the number of users [36]. As discussed in the previous chapter, the overlapping multi-carrier CDMA is comparable to the variable subcarrier spacing FDM systems in a single user scenario. It is therefore reasonable to apply linear detection techniques in Fast-OFDM when complex modulation schemes are employed. In [86;87], the authors investigated linear detectors applied in MT-CDMA with BPSK. However, the method is limited to a small number of subcarriers and has not yet been tested with complex mapping schemes. Therefore, the study can be extended for the implementation of Fast-OFDM with higher order PSK modulations and a large number of subcarrier.

This chapter begins with a general overview of the common multi-user detection techniques. It then investigates the application of zero-forcing (ZF) and minimum mean square error (MMSE) detectors in Fast-OFDM with various signal mapping schemes. The performance of the two detectors is then presented and a critical comparison is made between the two in order to determine the merits and demerits of each implementation.

4.2 Common detection techniques overview

In order to recover the received signals in a multi-user and multi-carrier system, the correlation within the user itself (autocorrelation) and with all the other users (cross-correlation) need to be considered at the receiver. The conventional detector is the matched filter (correlator) detector, which samples the soft correlator outputs at the bit times and makes hard detection decisions to regenerate the data. There are many other detection techniques proposed for improving multi-user and multi-carrier system performance. Most of the proposed detectors can be classified in one of the two categories: linear multi-user and subtractive interference cancellation detectors [88]. In this section, some common linear detection techniques which are applied in the work are discussed.

4.2.1. Maximum likelihood (ML) detection

The detector which yields the most likely transmitted sequence, d, chooses d to maximize the probability that d was transmitted given that $r(t)$ was received, where $r(t)$ extends over the whole message. Under the assumption that all possible transmitted sequences are equally probable, this detector is known as the ML detector [36].

The problem of ML approach is that it needs to compare the outputs with all the possible inputs, which leads to an exhaustive search for large message sizes and number of users. The complexity of a ML system increases exponentially with the number of users and the modulation cardinality, making the implementation impractical. In many practical systems, suboptimal detector may be considered due to the fact that they are simpler to implement.

4.2.2. Zero-forcing (ZF) detectors

An important group of multi-user detectors are linear detectors. These detectors apply a linear mapping to the soft output of the conventional detector

to reduce the MAI seen by each user. Assuming the received signal, **y**, is represented using matrix expression, then it can be written as:

$$\mathbf{y} = \mathbf{R}\cdot\mathbf{A}\cdot\mathbf{a} + \mathbf{n}_i \qquad (4.1)$$

where **R**, **A**, **a** and $\mathbf{n}_i$ are the correlation matrix, received amplitude, transmitted data bits and noise component, respectively. ZF detector applies the inverse of the correlation matrix, $\mathbf{R}^{-1}$, to the conventional detector output in order to decode the data. ZF detector has computational complexity significantly lower than that of the ML detector. One disadvantage of this method is that it causes noise enhancement by multiplying $\mathbf{R}^{-1}$ with the noise component. (The topic is further discussed in section 4.3).

4.2.3. Minimum mean square error (MMSE) detectors

Unlike ZF, the MMSE detector [89] is a linear detector which takes into account the background noise and utilizes knowledge of the received signal power. It implements the linear mapping that can minimise the mean-squared error between the received data and the output of the conventional detector. As it takes the background noise into account, the MMSE detector generally provides better probability of error performance than the ZF detector. An important disadvantage of this detector is that it requires estimation of the received amplitudes. Further, the performance of the MMSE detector depends on the power of the interfering users. (MMSE detection is further discussed in section 0)

4.3 Fast-OFDM system with ZF detectors

4.3.1. Principles of ZF detection

ZF is one of the most popular interference cancellation based linear detection techniques. The ZF detector (also referred as decorrelating detector) applies the inverse of the correlation matrix to the conventional detector output in order to decouple the data. The complex envelope of an OFDM signal is expressed as:

$$s(t) = \frac{1}{\sqrt{T_s}} \sum_{n=0}^{N_{sc}-1} a_n \cdot e^{\frac{j2\pi nt}{T_s}}, 0 \le t \le T_s \tag{4.2}$$

where a_n is the data at n^{th} subcarrier; N is the total number of subcarriers, T_s is the symbol duration. At the receiver, the transmitted signal is added AWGN noise, $n(t)$, with zero mean and spectrum density of $N_o/2$ W/Hz. The received waveform $r(t)$ can be expressed as

$$r(t) = s(t) + n(t) \tag{4.3}$$

With conventional optimal detection, the recovered signal, $y_{n'}$, is given by:

$$y_{n'} = \frac{1}{\sqrt{T_s}} \int_0^{T_s} r(t) e^{\frac{-j2\pi n't}{T_s}} dt \tag{4.4}$$

where the mark (') indicates the signal at the receiver side. The above equation can be extended to:

$$y_{n'} = \frac{1}{\sqrt{T_s}} \left(\frac{1}{\sqrt{T_s}} \int_0^{T_s} \sum_{n=0}^{N_{sc}-1} a_n \cdot e^{\frac{j2\pi nt}{T_s}} e^{\frac{-j2\pi n't}{T_s}} dt + \int_0^{T_s} n(t) \cdot e^{\frac{-j2\pi n't}{T_s}} dt \right) \tag{4.5}$$

The above equation can be reduced to:

$$y_{n'} = \frac{1}{T_s} \sum_{n=0}^{N_{sc}-1} \int_0^{T_s} a_n \cdot e^{\frac{j2\pi(n-n')t}{T_s}} dt + \frac{1}{\sqrt{T_s}} \int_0^{T_s} n(t) \cdot e^{\frac{-j2\pi n't}{T_s}} dt \tag{4.6}$$

This can further be expressed as:

$$y_{n'} = \frac{1}{T_s} \sum_{n=0}^{N_{sc}-1} a_n \cdot \frac{e^{\frac{j2\pi(n-n')T_s}{T_s}} - 1}{\frac{j2\pi(n-n')}{T_s}} + \frac{1}{\sqrt{T_s}} \int_0^{T_s} n(t) \cdot e^{\frac{-j2\pi n't}{T_s}} dt$$

$$y_{n'} = \sum_{n=0}^{N_{sc}-1} a_n \cdot \frac{e^{j\pi(n-n')} e^{j\pi(n-n')} - e^{j\pi(n-n')} e^{-j\pi(n-n')}}{j2 \cdot \pi(n-n')} + \frac{1}{\sqrt{T_s}} \int_0^{T_s} n(t) \cdot e^{\frac{-j2\pi n't}{T_s}} dt \tag{4.7}$$

$$y_{n'} = \sum_{n=0}^{N_{sc}-1} a_n \cdot \frac{\left(e^{j\pi(n-n')} - e^{-j\pi(n-n')}\right) \cdot e^{j\pi(n-n')}}{j2 \cdot \pi(n-n')} + \frac{1}{\sqrt{T_s}} \int_0^{T_s} n(t) \cdot e^{\frac{-j2\pi n' t}{T_s}} dt$$

$$y_{n'} = \sum_{n=0}^{N_{sc}-1} a_n \cdot \frac{\sin \pi(n-n') \cdot e^{j\pi(n-n')}}{\pi(n-n')} + \frac{1}{\sqrt{T_s}} \int_0^{T_s} n(t) \cdot e^{\frac{-j2\pi n' t}{T_s}} dt$$

$$y_{n'} = \sum_{n=0}^{N_{sc}-1} a_n \cdot sinc(n-n') \cdot e^{j\pi(n-n')} + \frac{1}{\sqrt{T_s}} \int_0^{T_s} n(t) \cdot e^{\frac{-j2\pi n' t}{T_s}} dt$$

The recovered signal can be represented as a matrix **y**, whose dimensions are $N_{sc} \times k$ with k being different time intervals. This can be given by:

$$\mathbf{y} = \mathbf{R} \cdot \mathbf{A} \cdot \mathbf{a} + \mathbf{n_i} \tag{4.8}$$

Taken the example of 0^{th} bit of all the subcarriers, with **R**, **A**, **a** and $\mathbf{n_i}$ being the correlation matrix, received amplitude, transmitting data bits and noise component, respectively. Therefore,

$$\mathbf{a} = [a_{0,0} \quad a_{1,0} \quad a_{2,0} \quad \ldots \quad a_{N-1,0}]^T \tag{4.9}$$

The term $a_{n,0}$ is the 0^{th} bit of the n^{th} subcarrier; superscript T denotes transpose.

$$\mathbf{n_i} = [n_{0,0} \quad n_{1,0} \quad n_{2,0} \quad \ldots \quad n_{N-1,0}]^T \tag{4.10}$$

The term $n_{n,0}$ is the noise component of the 0^{th} bit.

$$\mathbf{A} = \text{diag}\{A_0 \quad A_1 \quad A_2 \quad \ldots \quad A_{N-1}\} \tag{4.11}$$

where $A_n = 1$ is the received amplitude of the n^{th} subcarrier bits, and the **R** matrix is given by:

$$\mathbf{R} = \begin{bmatrix} \rho_{0,0} & \rho_{0,1} & \rho_{0,2} & \rho_{0,N_{sc}-1} \\ \rho_{1,0} & \rho_{1,1} & \rho_{1,2} & \rho_{1,N_{sc}-1} \\ \rho_{2,0} & \rho_{2,1} & \rho_{2,2} & \rho_{2,N_{sc}-1} \\ \rho_{N_{sc}-1,0} & \rho_{N_{sc}-1,1} & \rho_{N_{sc}-1,2} & \rho_{N_{sc}-1,N_{sc}-1} \end{bmatrix} \tag{4.12}$$

Where $\rho_{n,n'} = sinc(n - n') \cdot e^{j\pi(n-n')}$

From equations (4.8) and (4.12), it can be deduced that the BER performance of the receiver depends on the noise variance and the non-diagonal elements of the **R** matrix, which correspond to AWGN and inter-carrier interference (ICI). The non-diagonal elements of the **R** matrix account for the ICI influence on the individual correlator outputs. According to equation (4.7), the ICI can be derived as:

$$I_{n'} = \sum_{\substack{n=0 \\ n \neq n'}}^{N_{sc}-1} a_n \cdot sinc(n - n') \cdot e^{j\pi(n-n')} \tag{4.13}$$

In the case of orthogonal subcarrier recovery, the **R** matrix is an identity matrix, i.e. the non-diagonal elements of the **R** matrix are zero, which indicates zero ICI. The noise component is:

$$n_i = \frac{1}{\sqrt{T_s}} \int_0^{T_s} n(t) \cdot e^{\frac{-j2\pi n' t}{T_s}} dt \tag{4.14}$$

where $n(t)$ is zero mean and the variance of n_i is σ^2 when an integer number of symbol rate is selected.

For example, assuming the number of subcarrier N = 3 and the subcarrier spacing (Δf) is $1/T_s$. The transmitting subcarrier frequencies are described as

$$[f_c + 1/T_s \quad f_c + 2/T_s \quad f_c + 3/T_s] \tag{4.15}$$

and likewise at the receiver,

$$[f_c + 1/T_s \quad f_c + 2/T_s \quad f_c + 3/T_s] \tag{4.16}$$

where f_c is the carrier frequency. From equation (4.12), the **R** matrix can be expressed as

$$\mathbf{R} = \begin{bmatrix} 1 & 0 & 0 \\ 0 & 1 & 0 \\ 0 & 0 & 1 \end{bmatrix} \tag{4.17}$$

In the case of a reduced subcarrier spacing, e.g. $\Delta f = 0.5/T_s$ or $0.25/T_s$, the **R** matrics are calculated as follows:

$$[f_c + 0.5/T_s \quad f_c + 1/T_s \quad f_c + 1.5/T_s] \tag{4.18}$$

$$\mathbf{R_{0.5}} = \begin{bmatrix} 1 & 0 + 0.6366j & 0 \\ 0 + 0.6366j & 1 & 0 + 0.6366j \\ 0 & 0 + 0.6366j & 1 \end{bmatrix} \tag{4.19}$$

$$[f_c + 0.25/T_s \quad f_c + 0.5/T_s \quad f_c + 0.75/T_s] \tag{4.20}$$

$$\mathbf{R_{0.5}} = \begin{bmatrix} 1 & 0.6366 + 0.6366j & 0 + 0.6366 \\ 0.6366 + 0.6366j & 1 & 0.6366 + 0.6366j \\ 0 + 0.6366 & 0.6366 + 0.6366j & 1 \end{bmatrix} \tag{4.21}$$

The BER performance with subcarrier spacing of $0.25/T_s$ is worse than $0.5/T_s$, due to the non-diagonal elements of the **R** matrix.

This detection technique is based on ZF receiver. It is very similar to the zero-forcing equalizer used for mitigation of intersymbol interference [36]. Using ZF receiver aims at reducing the loss in performance due to ICI. Since the **R** matrix is known at the transmitter, then pre-computation of the inverse **R** matrix can be applied at the receiver to cancel ICI.

$$\begin{aligned} \mathbf{y_{n',k'}} &= \mathbf{R^{-1}\,(R \cdot A \cdot a + n_i)} \\ \mathbf{y_{n',k'}} &= \mathbf{A \cdot a + R^{-1}\,n_i} \end{aligned} \tag{4.22}$$

Figure 4.1 shows the block diagram of the ZF receiver for the case of 3 subcarriers. The ZF detector has several advantages as listed in [88]. One disadvantage of this method is that it causes noise enhancement. The soft-decision is free of ICI, but the noise-part is coloured and potentially amplified. Therefore, the use of this detector acts as a trade-off between lowering the ICI and increasing Gaussian noise.

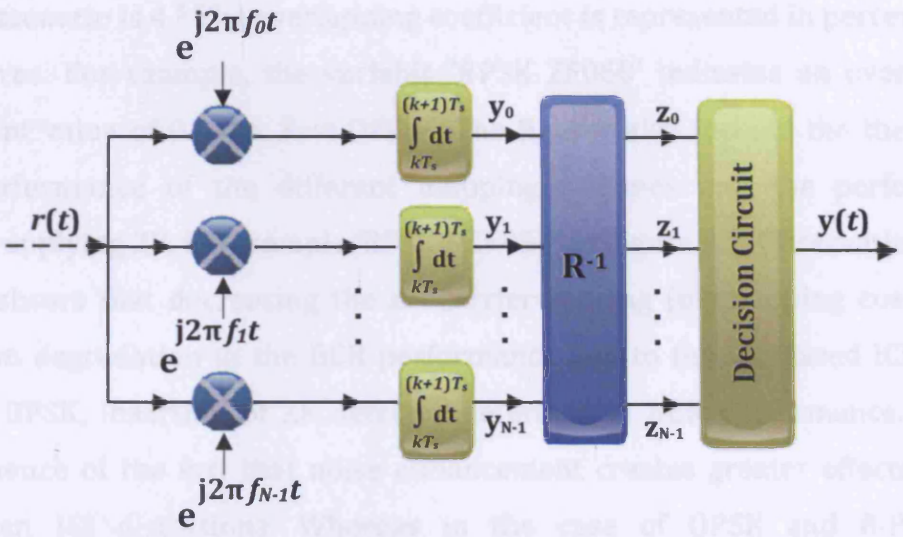

Figure 4.1. ZF receiver for reduced subcarrier spacing FDM signals

4.3.2. System implementation of Fast-OFDM with ZF detector

In order to study the Fast-OFDM system and evaluate its performance under different modulation conditions with a ZF detector, a Fast-OFDM model was developed. The model simulations were performed in MATLAB due to the involvement of matrix manipulation. The simulation parameters and block diagram of the system were similar to the Fast-OFDM model developed in Chapter 3, except that at the receiver, the outputs of the integrator were multiplied with the inverse of the correlation matrix, $\mathbf{R^{-1}}$. The results were then fed to a detector with predefined threshold decisions for data recovery.

4.3.3. Simulation results and discussion of Fast-OFDM with ZF detector

In order to view the BER performance of variable subcarrier spacing FDM, different overlapping coefficients are considered in the simulation. Figure 4.2, Figure 4.3 and Figure 4.4 show the BER performance of varying subcarrier spacing FDM schemes with ZF detector under BPSK, QPSK and 8-PSK modulation conditions, respectively. The number of subcarriers of the systems considered

for this scenario is 4.[3] The overlapping coefficient is represented in percentage in the figures. For example, the variable 'BPSK ZF050' indicates an overlapping coefficient value of 0.5, i.e. Fast-OFDM. The figures also include the theoretical BER performance of the different mapping schemes and the performance without applying ZF, for example 'BPSK NZF050' in Figure 4.2. Observation of the figures shows that decreasing the subcarrier spacing (overlapping coefficient) results in degradation in the BER performance due to the increased ICI. In the case of BPSK, insertion of ZF detector deteriorates BER performance. This is consequence of the fact that noise enhancement creates greater effects on the BER than ICI distortions. Whereas in the case of QPSK and 8-PSK, the improvement of BER performance is noticeable as compared to conventional Fast-OFDM, as the ICI distortion becomes the main impairment.

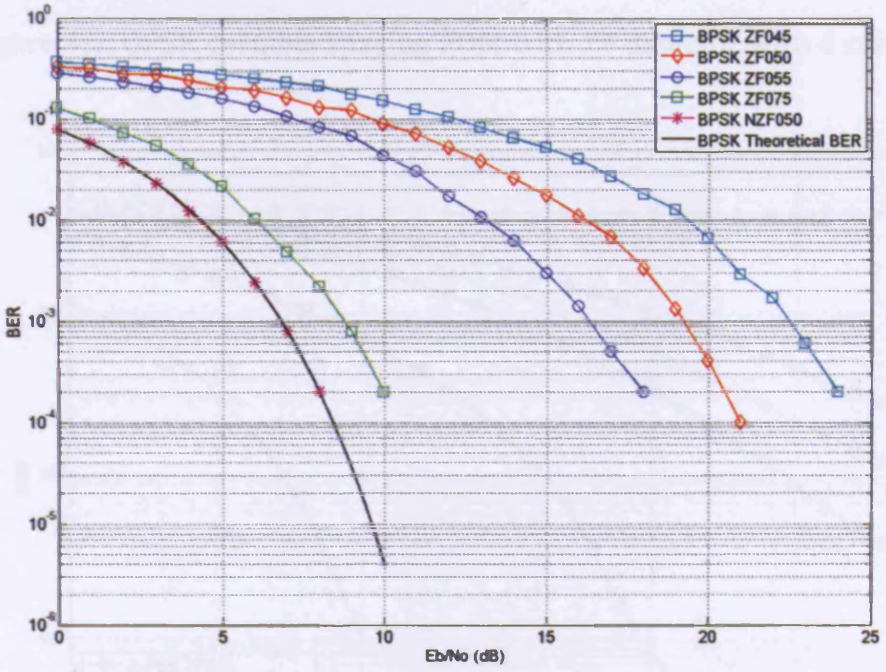

Figure 4.2. BPSK variable spacing FDM with ZF detector with 4 subcarriers

[3] A small number of subcarriers was used throughout the simulations. This is to have reasonable simulation time and to allow the assessment of the concepts proposed by careful study of the signal parameters.

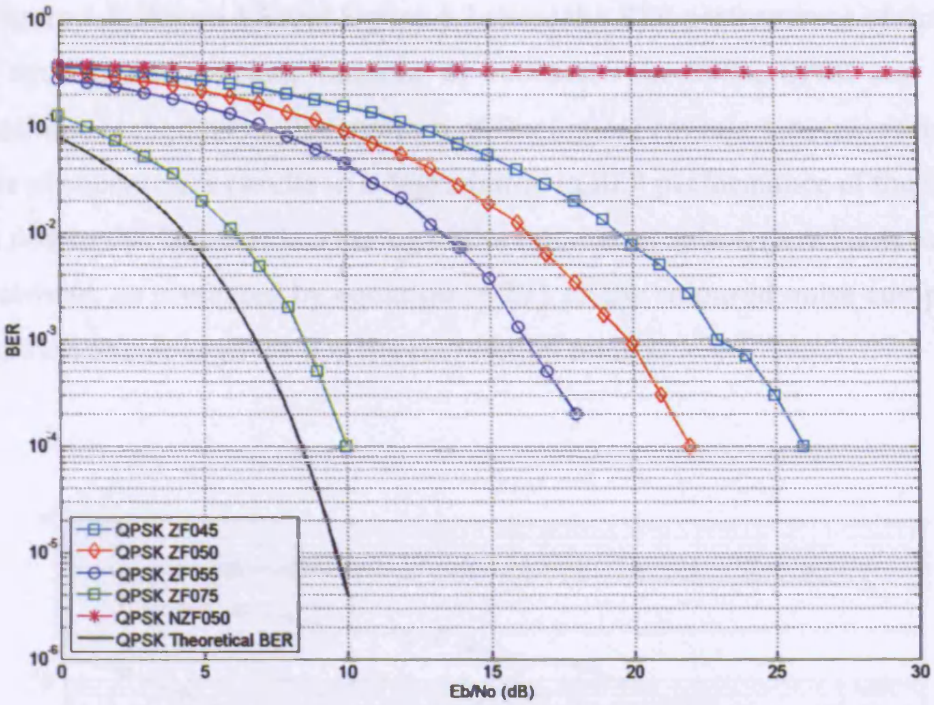

Figure 4.3. QPSK variable spacing FDM with ZF detector with 4 subcarriers

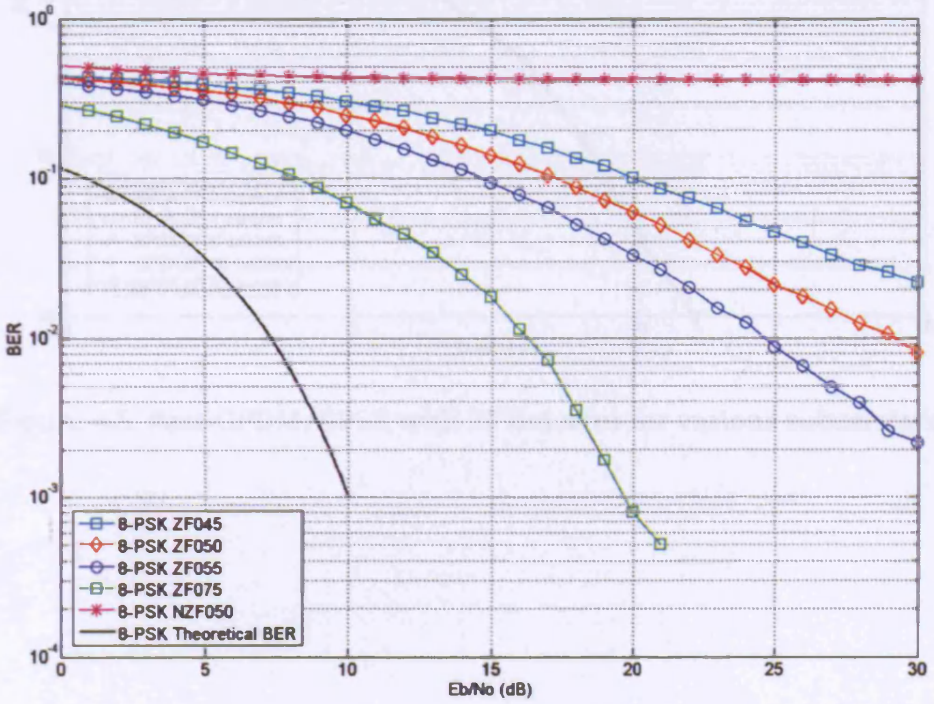

Figure 4.4. 8-PSK variable spacing FDM with ZF detector with 4 subcarriers

Figure 4.5, Figure 4.6 and Figure 4.7 show the BER performance of the Fast-OFDM system with various number of subcarrier in BPSK, QPSK and 8-PSK modulations, respectively. Observation of the figures reveals that increasing the number of subcarriers results in a degradation in BER performance of the system. This is due to the fact that increasing of the number of subcarriers leads to noise enhancement, as predicted by equation (4.22), as the coloured noise component is calculated as $\mathbf{n}_i\mathbf{R}^{-1}$, where $\mathbf{R}$ is the correlation matrix.

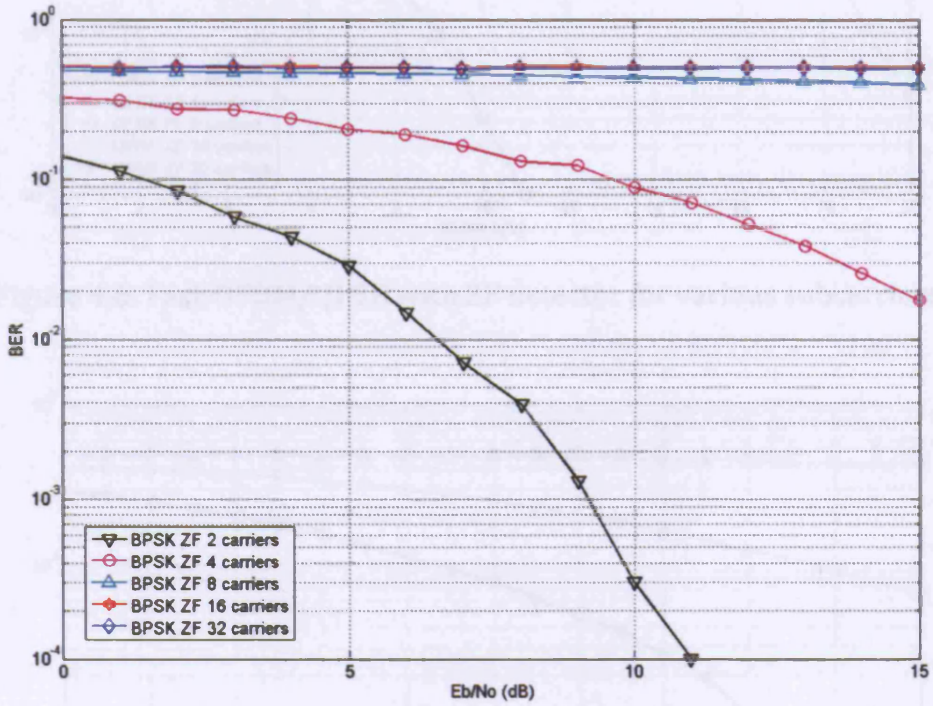

Figure 4.5. Fast-OFDM/BPSK with ZF detector for various subcarriers

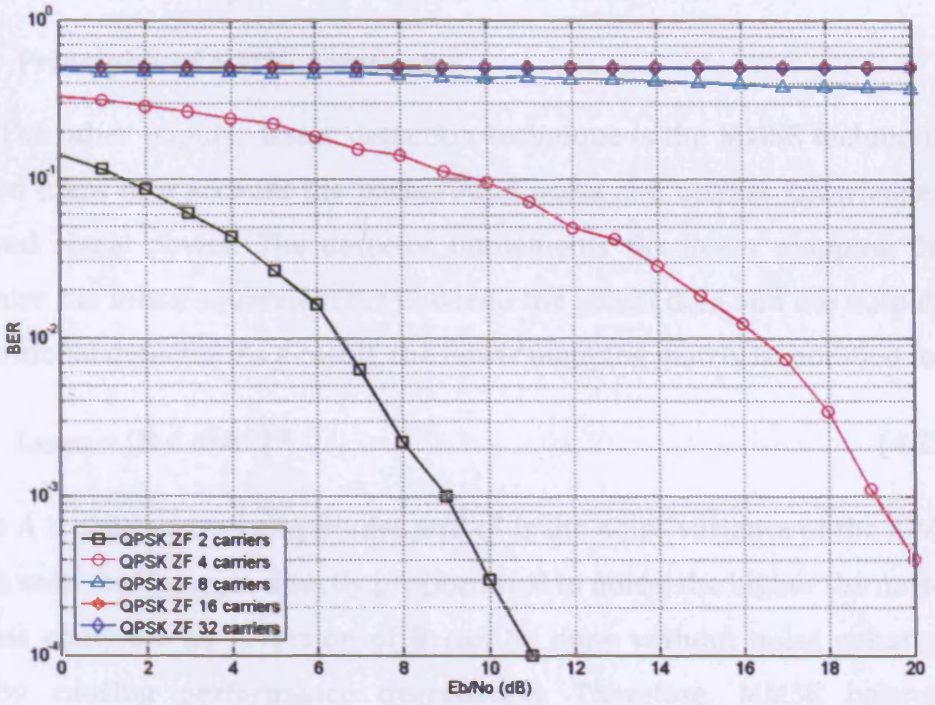

Figure 4.6. Fast-OFDM/QPSK with ZF detector for various subcarriers

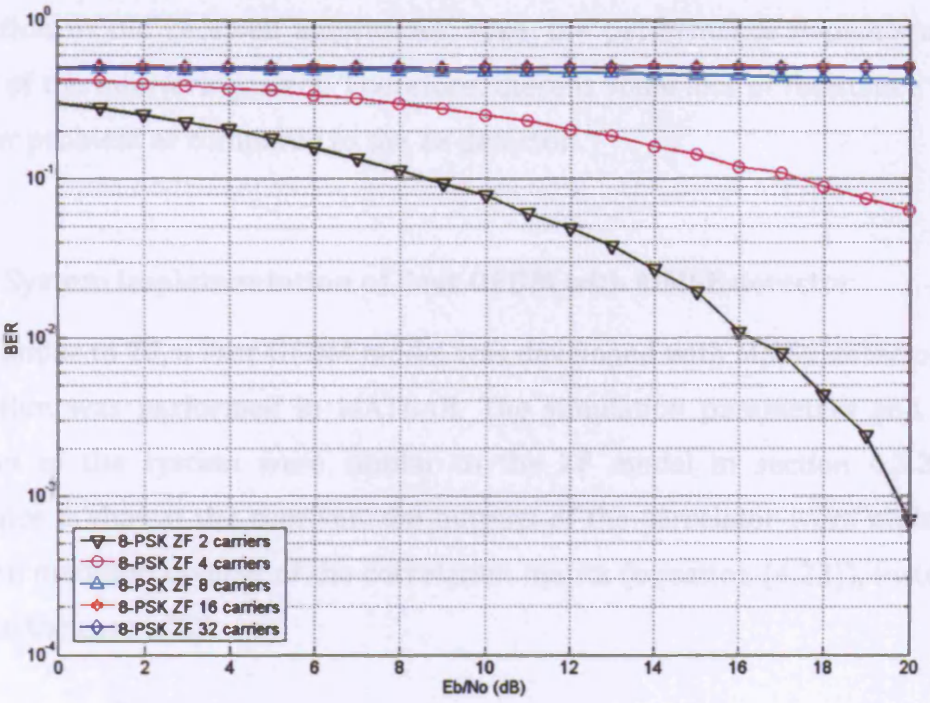

Figure 4.7. Fast-OFDM/8-PSK with ZF detector for various subcarriers

4.4 Fast-OFDM system with MMSE detector

4.4.1. Principles of MMSE detection

The other popular linear detection technique is the MMSE technique. This method takes into account the background noise and utilizes knowledge of the received signal power. The detector implements the linear mapping that can minimise the mean-squared error between the actual data and the output of the conventional detector. As a result, the linear mapping matrix is modified to:

$$\mathbf{L}_{MMSE} = [\mathbf{R} + \sigma^2\mathbf{A}^{-2}]^{-1} \quad (4.23)$$

where **A** is the received amplitudes and σ^2 is the noise variance of the AWGN. As can be seen that $\mathbf{L}_{MMSE}$ is directly proportional to noise; the higher the noise level, the less complete an inversion of **R** can be done without noise enhancement, thereby causing performance degradation. Therefore, MMSE balances ICI elimination against noise enhancement.

A key drawback of this detector is that, unlike ZF detector, it requires estimation of the received amplitudes. Also, the performance depends on the power of the interfering users. Therefore, there is some loss of resistance to the near-far problem as compared to the ZF detector.

4.4.2. System implementation of Fast-OFDM with MMSE detector

Similar to ZF, a Fast-OFDM model was developed with MMSE detector. The simulation was performed in MATLAB. The simulation parameters and block diagram of the system were similar to the ZF model in section 4.3.2. The difference is that at the receiver, the outputs of the correlator were multiplied with the modified inverse of the correlation matrix (equation (4.23)), instead of $\mathbf{R}^{-1}$ as in the case of ZF.

4.4.3. Simulation results and discussion of Fast-OFDM with MMSE detector

The BER performance of the variable subcarrier spacing FDMs with MMSE detector in BPSK, QPSK and 8-PSK modulations are shown in Figure 4.8, Figure 4.9 and Figure 4.10, respectively. Observing all three figures reveals that the BER performance is close to the theoretical for large overlapping coefficients. In other words, the BER performance degrades with decreasing subcarrier spacing. This is due to the fact that the ICI increases as the subcarriers are placed closer. In all modulation schemes, the trend of the BER performance is similar to the case of ZF detector, except that the performance is improved due to the consideration in noise enhancement reduction in MMSE.

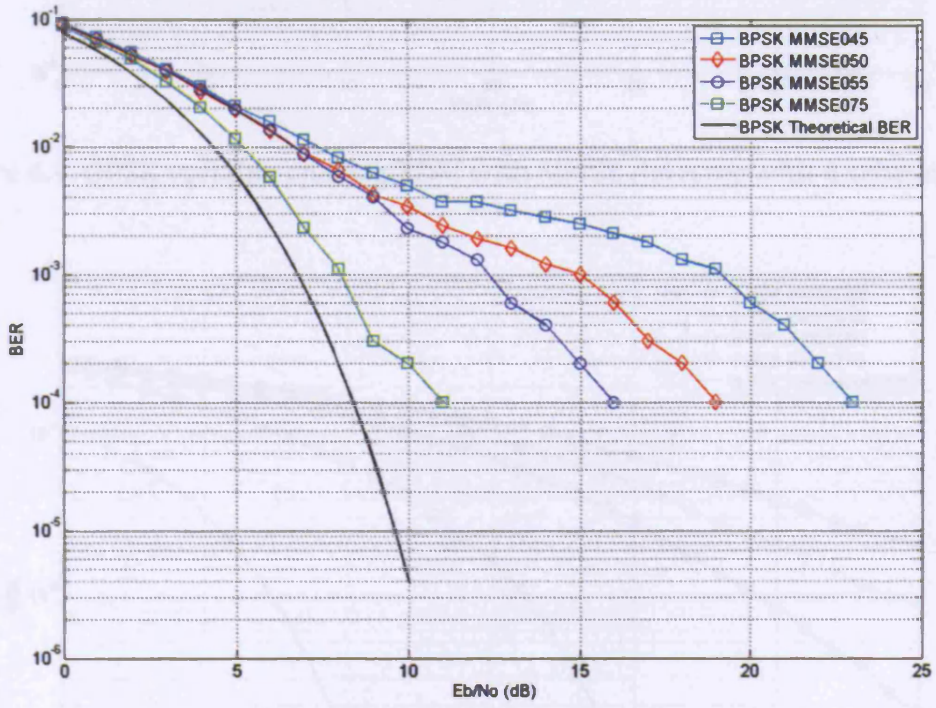

Figure 4.8. BPSK variable spacing FDM with MMSE detector with 4 subcarriers

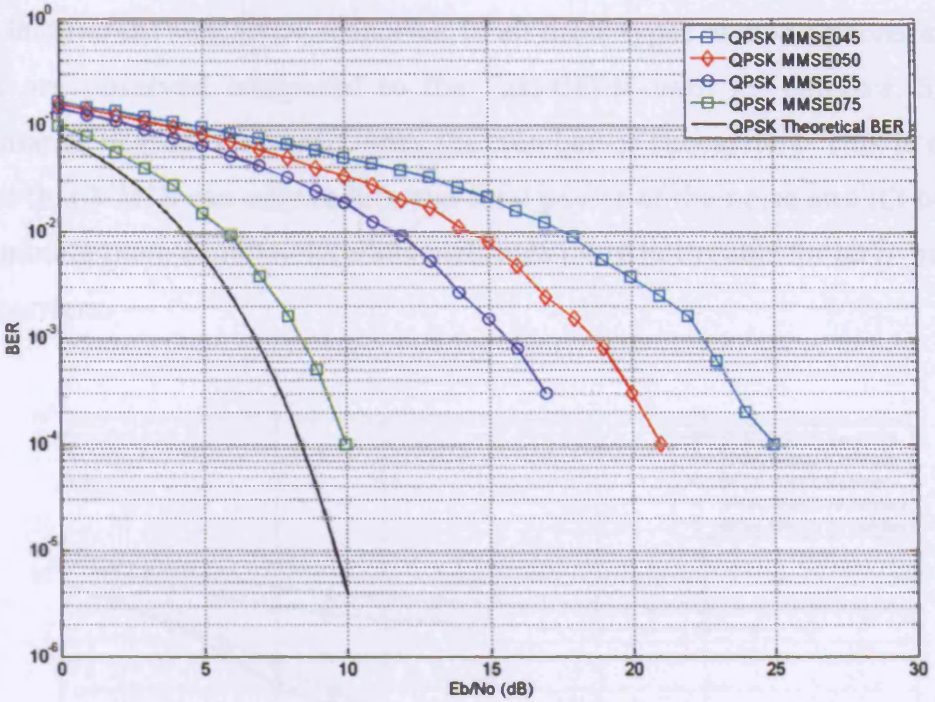

Figure 4.9. QPSK variable spacing FDM with MMSE detector with 4 subcarriers

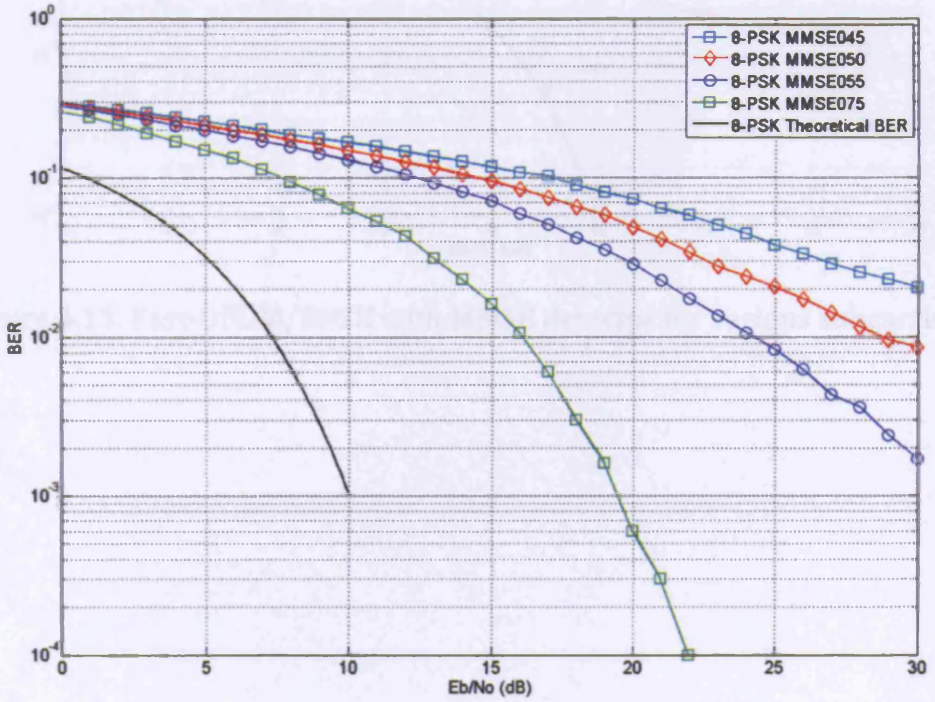

Figure 4.10. 8-PSK variable spacing FDM with MMSE detector with 4 subcarriers

Figure 4.11, Figure 4.12 and Figure 4.13 present the BER results for Fast-OFDM in different subcarrier scenarios. In all three types of modulations, similar results are observed compared to the Fast-OFDM with ZF detector. System performance degrades severely with the number of subcarriers. This is due to the fact that MMSE can only reduce the total power of the noise and ICI but can not eliminate them completely, which becomes more noticeable for large number of subcarriers.

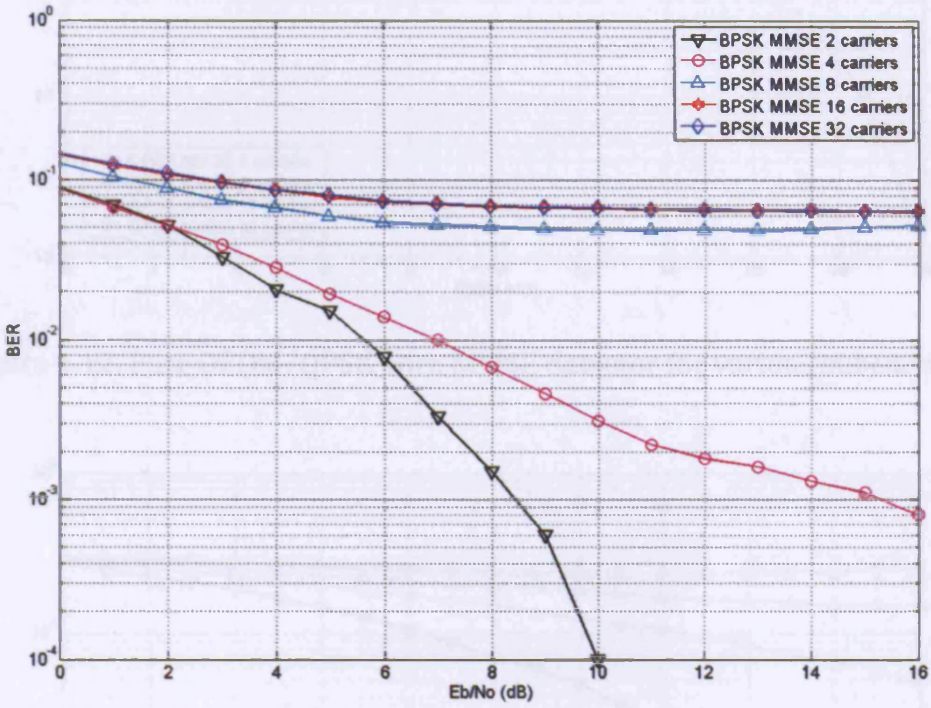

Figure 4.11. Fast-OFDM/BPSK with MMSE detector for various subcarriers

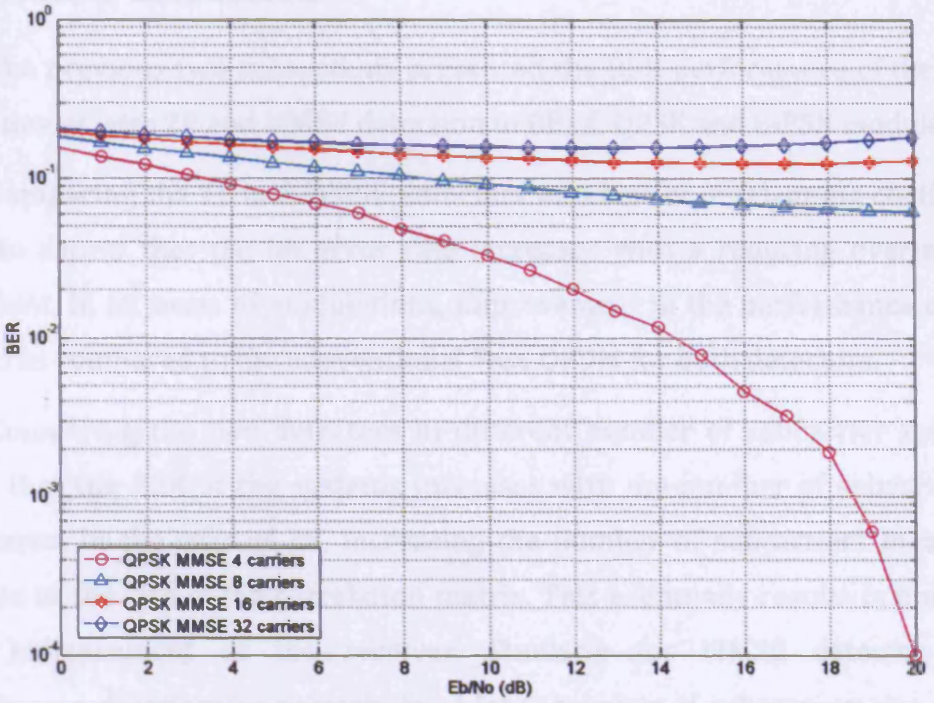

Figure 4.12. Fast-OFDM/QPSK with MMSE detector for various subcarriers

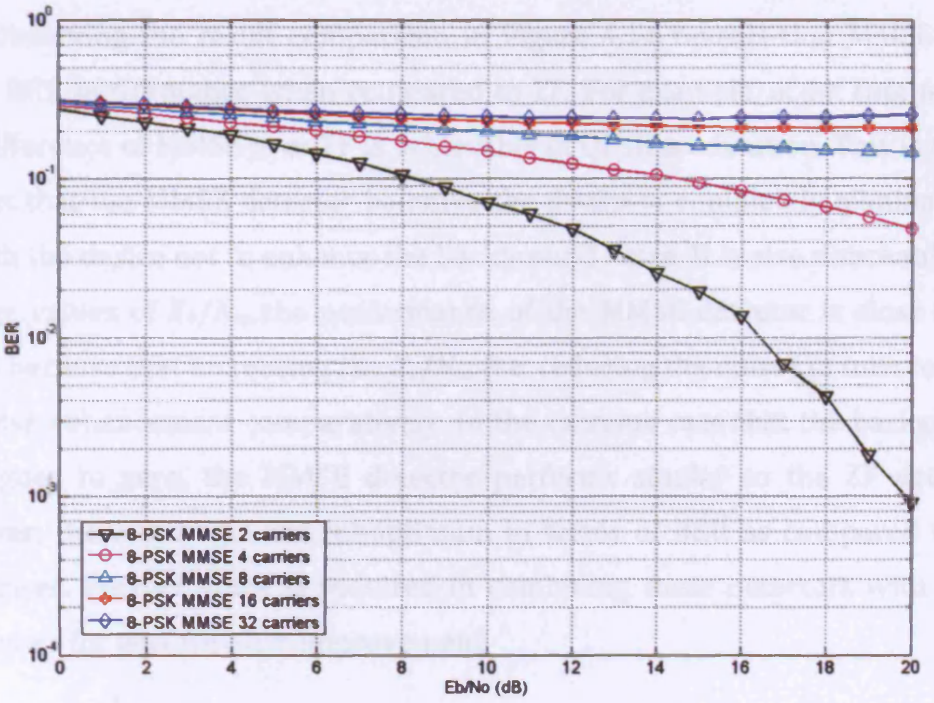

Figure 4.13. Fast-OFDM/8-PSK with MMSE detector for various subcarriers

4.5 Results discussion

The previous two subsections presented the BER performance of the Fast-OFDM model with ZF and MMSE detection in BPSK, QPSK and 8-PSK modulations.

Comparing the ZF and MMSE detectors in different overlapping coefficient scenario shows that the bit error rate increases with a reducing overlapping coefficient. In all cases of modulations, improvement in the performance can be noticed as compared to the conventional Fast-OFDM for both detectors.

Comparing the two detectors in different number of subcarrier scenario shows that the BER of the systems increases with the number of subcarrier in both cases. In the case of ZF, increasing the number of subcarriers means an increase in the size of the correlation matrix. This eventually results in enlarged noise enhancement at the receiver. Similarly for MMSE detector, BER performance deteriorates severely for a large number of subcarriers due to the fact that the total power of the noise cannot be eliminated completely in MMSE, though the noise enhancement is taken into consideration.

Observing the result comparison in Figure 4.14 reveals that MMSE gives better BER performance when compared to ZF. For example, at bit rate of 10^{-2}, 2dB difference of MMSE over ZF is achievable in QPSK modulation. This is due to the fact that the MMSE detector balances the desire to completely eliminate the ICI with the desire not to enhance the background noise. It is also noticeable that at large values of E_b/N_o, the performance of the MMSE detector is close to ZF. This is because that increasing the E_b/N_o, (i.e. reducing the noise) in turn reduces the noise enhancement comparatively. In the extreme case that the background noise goes to zero, the MMSE detector performs similar to the ZF detector. However, these systems are suboptimum in terms of BER as compared to the ideal cases. Further work is required in combining these detectors with other techniques for performance improvement.

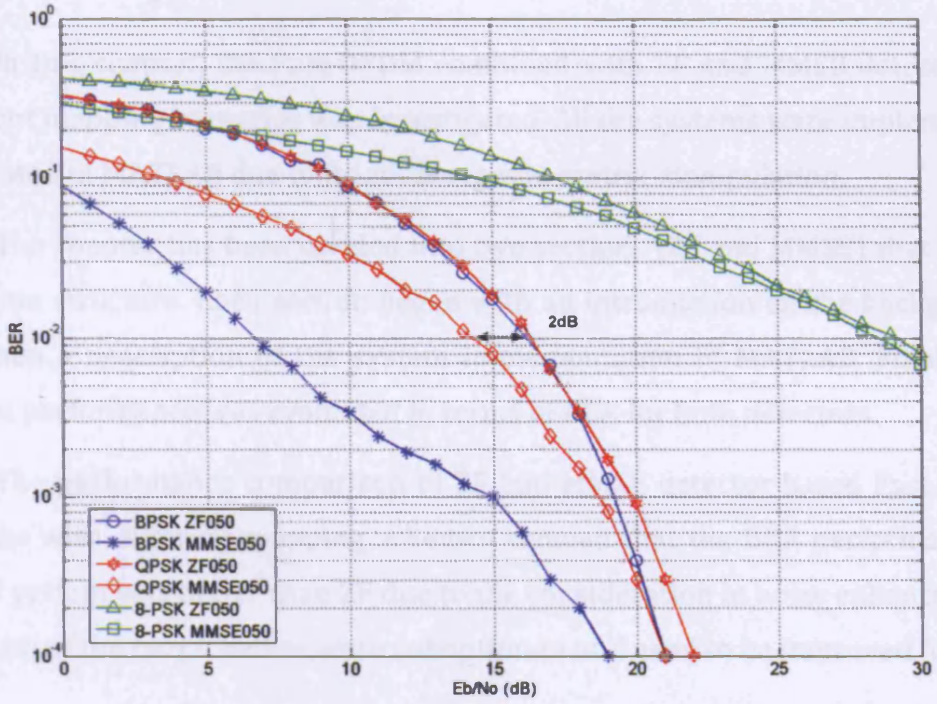

Figure 4.14. Fast-OFDM with MMSE detector for BPSK, QPSK and 8-PSK

In summary, both the ZF and MMSE detectors allow sub-optimum operation of higher order modulation schemes with Fast-OFDM and other FDM schemes. For BPSK, schemes show performance degradation when compared to the simple correlation detector of section 2.7.5 (Figure 2.57). The complexity of the MMSE makes its use impractical for a large number of carriers, whilst the ZF is more practical. The degraded operations of both schemes, however, makes their use limited and either other detection schemes may be investigated for a large number of carriers or the use of forward error correcting code [90] should be considered. Alternative detection schemes are now the subject of further research at UCL [91].

4.6 Summary

In this chapter, the Fast-OFDM combined with ZF and MMSE detectors in different mapping scenarios was investigated. All the systems were implemented and tested in MATLAB due to its advantages in matrix manipulation.

The chapter has been divided into two sections (ZF and MMSE) that follow the same structure. Each section began with an introduction on the background and then a description of the system implementation in MATLAB. Finally the system performance was evaluated in terms of BER for both detectors

The performance comparison of ZF and MMSE detector based Fast-OFDM systems with different mapping schemes showed that the BER performance of MMSE system was better than ZF due to the consideration in noise enhancement. Yet, both of the two schemes were suboptimum and need to be improved further.

Chapter 5 Conclusions and future work

This chapter summarises the research work carried out in the thesis, and reviews the main research findings. It is concluded by suggestions for future work.

5.1 Concluding remarks on the thesis

Performance issues related to the Fast-OFDM system have been addressed in this thesis. Comparative studies of the system relative to conventional OFDM and overlapping multi-carrier CDMA systems combined with different mapping schemes have been carried out by modelling and simulation of various architectures in the presence of AWGN. Applying linear detection techniques in Fast-OFDM with complex modulation schemes has also been studied. Throughout the thesis, a small number of carriers was employed (up to 32) so that the behaviour of these systems can be carefully observed.

In Chapter 2, an overview of the wireless communications and multi-carrier modulations was presented and OFDM and Fast-OFDM were introduced. The chapter outlined the principal concepts of OFDM, whereby the two structures of OFDM models (namely oscillator-based and FFT-based OFDM) were discussed. The fundamental elements of OFDM such as guard interval, cyclic prefix, coding, interleaving, channel estimation, pilot symbols, nonlinearity effects and synchronisation issues were discussed.

The principal idea and the limitations of Fast-OFDM were also addressed. The performance of the two systems was studied in terms of BER performance, spectral efficiency, peak-to-average-power ratio (PAPR), nonlinear performance and adjacent channel interference (ACI) analysis.

Investigation of the performance of the two systems showed that Fast-OFDM has the clear advantage in bandwidth efficiency over conventional OFDM for a large number of subcarriers. The BER performance of Fast-OFDM was comparable to OFDM in the case of BPSK and deteriorated severely when complex modulation schemes (QPSK and 16-QAM) were applied. Investigation of the effects of ICI on the BER performance of the frequency spacing varying OFDM systems indicated that the orthogonality among subcarriers remained at the points where frequency spacing were $0.5i/T_s$ (i=1,2,...) and i/T_s (i=1,2...) for BPSK and QPSK, respectively. Further decreasing the subcarrier spacing (as compared to Fast-OFDM) resulted in exponential BER performance degradation due to ICI. Analyzing the ACI effects of the two systems revealed that OFDM has higher ACI resistance as compared to Fast-OFDM. However, the difference is not significant for a large number of subcarriers and small ACI distortions. It is also interesting to note that OFDM systems outperforms Fast-OFDM in the presences of nonlinear distortions, though Fast-OFDM has better CCDF due to the fact that less peaks happen in Fast-OFDM compared to OFDM.

In Chapter 3, the conceptual issues of multi-carrier CDMA systems and the overlapping multi-carrier systems were investigated. The fundamentals of CDMA were presented. A summary of the multi-carrier CDMA schemes proposed in literature with various adaptations of each scheme were detailed. Finally, the idea of overlapping multi-carrier CDMA systems was addressed. The performance of the systems compared to OFDM and Fast-OFDM has been studied in terms of BER performance, spectral efficiency, PAPR and ACI analysis.

Investigation in the effects of ICI on the BER performance of the overlapping multi-carrier CDMA systems revealed that increasing the code

length did not affect the BER performance. Both of the systems were comparable to frequency spacing varying FDM systems. In the special cases of overlapping - MT-CDMA, MC-DS-CDMA, OFDM and Fast-OFDM - system performance are close to theoretical results when BPSK mapping scheme was applied in the presence of AWGN and ICI. In the case of QPSK, as expected, the bit error rate of fast systems (Fast-OFDM, Fast MC-DS-CDMA and Fast MT-CDMA) increased significantly whereas others were still close to the theoretical QPSK BER results. Studying the performance of the systems in terms of PAPR and ACI showed that the fast multi-carrier CDMA systems is advantageous in bandwidth efficiency but exhibits high BER with complex modulations and worse ACI performance compared to conventional schemes.

Applying two different linear detection techniques, namely ZF and MMSE, in Fast-OFDM combined with single dimensional and complex modulation schemes was studied in Chapter 4. The background knowledge of each type of detection was outlined. The performance in terms of BER was also discussed.

Comparing the two detectors in the scenarios of different overlapping coefficient and different number of subcarriers showed that decreasing the subcarrier spacing and increasing the number of subcarriers degraded the BER performance. In terms of BER results, MMSE, although computationally complex, provided slightly better performance than ZF due to the consideration in noise enhancement reduction. The conclusion of these studies is that Fast-OFDM (and other non-orthogonal FDM schemes) can be used in communication systems and detectors may be designed for them. However, optimal detection is not possible and computational complexity may be prohibitive when the number of carriers becomes large. Unless these detection issues are resolved, the use of Fast-OFDM remains limited.

5.2 Future work

Based on the experience and knowledge acquired during the research, areas of research that are worthy of future investigations can be suggested. These are:

- Performance assessment of Fast-OFDM and OFDM in multipath fading channels. This study would further help understand the properties of Fast-OFDM and its suitability for wireless systems.

- Performance comparison of multi-tone CDMA and Fast-OFDMA in fading channels. Multi-tone CDMA is different from MC-DS-CDMA in the closer subcarrier spacing for improved bandwidth efficiency [5;65], similarly for Fast-OFDMA compared to OFDMA. Substantial research, e.g. [75;92;93], has been done to evaluate the performance of multicarrier schemes in the presence of multipath fading. In [94], the performance of OFDMA and MC-DS-CDMA systems in severely fading channel is also investigated. The results show that when multiuser and high data rates are required, OFDMA is appealing. If though narrowband interference suppression is required, employing the MC-DS modulation would give better performance. Therefore, this study can be further extended to both multi-tone CDMA and fast-OFDMA in fading channels.

- Performance evaluation of M-QAM modulated Fast-OFDM with other advanced detection techniques, such as MMSE-ML [91] and Lattice reduction aided ZF detection [95]. Such studies, although in their early stages, are expected to lead to practical systems with a large number of carriers and reasonable computational complexity.

It is hoped that the work presented in this thesis and the future work proposed may act as one of the small building bricks in this vast and ever expanding structure of wireless systems.

Reference

[1] F. Xiong, "M-ary amplitude shift keying OFDM system," *IEEE Transactions on Communications*, vol. 51, no. 10, pp. 1638-1642, 2003.

[2] M. R. D. Rodrigues and I. Darwazeh, "Fast OFDM: A proposal for doubling the data rate of OFDM schemes," *Proceedings of the International Conference on Telecommunications*, vol. 3, pp. 484-487, 2002.

[3] D. Karampatsis, "Modelling and performances assessment of OFDM and fast-OFDM wireless communication." PhD thesis in University College London, 2004.

[4] S. Hara and R. Prasad, "DS-CDMA, MC-CDMA and MT-CDMA for mobile multi-media communications," in *IEEE 46th Vehicular Technology Conference, 'Mobile Technology for the Human Race'*, vol. 2, 1996, pp. 1106-1110.

[5] S. Hara and R. Prasad, "Overview of multicarrier CDMA," *IEEE Communications Magazine*, vol. 35, no. 12, pp. 126-133, 1997.

[6] L. Hanzo, L.-L. Yang, E.-L. Kuan, and K. Yen, *Single- and multi-carrier DS-CDMA multi-user detection space-time spreading, synchronisation and standards*. Chichester, England: John Wiley & Sons, 2003.

[7] D. Karampatsis, M. Rodrigues, and I. Darwazeh, "Performance comparison of OFDM and FOFDM communication systems in typical GSM multipath environments," 7th World Multiconference on Systemics, Cybernetics, and Informatic (SCI 2003), Orlando, USA, 2003.

[8] L. Hanzo and T. Keller, *OFDM and MC-CDMA a Primer*. Chichester: John Wiley & Sons, 2006.

[9] J. A. C. Bingham, "Multicarrier modulation for data transmission: an idea whose time has come," *IEEE Communications Magazine*, vol. 28, no. 5, pp. 5-14, 1990.

[10] S. J. Vaughan-Nichols, "OFDM: back to the wireless future," *Computer*, vol. 35, no. 12, pp. 19-21, 2002.

[11] A. J. Paulraj, D. A. Gore, R. U. Nabar, and H. Bolcskei, "An overview of MIMO communications - a key to gigabit wireless," *Proceedings of the IEEE*, vol. 92, no. 2, pp. 198-218, 2004.

[12] J. Schiller, *Mobile Communications*, 2nd ed. Boston: Addison Wesley, 2008.

[13] "GSM World statistics, GSM Association," 2007, http://www.gsmworld.com/news/statistics/index.shtml, (Accessed on September, 2008).

[14] "GSM/3G Market Update, 31 July, 2008," http://www.gsacom.com/gsm_3g/market_update.php4#GSM_3G_Market_Update (Accessed on September, 2008).

[15] J. L. Pinto, D. Karampatsis, and I. Darwazeh, "GSM Evolution towards 3rd Generation from 2.5 Generation," International Symposium on Telecommunications: 2001, pp. 239-243.

[16] "Special Issue on IMT-2000: Standards Efforts of the ITU," *IEEE Personal Communications*, vol. 4, pp. 8-40, 1997.

[17] B. Beheshti, "Study of the technology migration path of the cellular wireless industry from 3G to 3.5G and beyond," *Long Island Systems, Applications and Technology, 2005. IEEE Conference*, pp. 15-28, 2005.

[18] H. Holma, *HSDPA/HSUPA for UMTS: High Speed Radio Access for Mobile Communications*, 2nd ed John Wiley & Sons, 2002.

[19] K. Young Kyun and R. Prasad, *4G roadmap and emerging communication technologies* Artech House, 2006.

[20] W. Mohr, "Mobile Communications Beyond 3G in the Global Context," 2002, Siemens mobile, http://www.cu.ipv6tf.org/pdf/werner_mohr.pdf (Accessed on September, 2008).

[21] K. R. Santhi, V. K. Srivastava, G. SenthilKumaran, and A. Butare, "Goals of true broad band's wireless next wave (4G-5G)," *IEEE 58th Vehicular Technology Conference (VTC)*, vol. 4, pp. 2317-2321, 2003.

[22] L. Hanzo, W. Webb, and T. Keller, *Single- and multi-carrier quadrature amplitude modulation : principles and applications for personal communications*, 2nd ed Chichester : John Wiley & Sons, 2000.

[23] R. W. Chang, "Orthogonal Frequency Division Multiplexing," *U. S. Patent 3,488,445, Filed November 14*, 1970.

[24] B. Saltzberg, "Performance of an Efficient Parallel Data Transmission System," *IEEE Transactions on Communications*, vol. 15, no. 6, pp. 805-811, 1967.

[25] ETSI, "Digital audio broadcasting (DAB); DAB to mobile, portable and fixed receivers," European Telecommunications Standard, ETS 300-401,Feb.1995.

[26] ETSI, "Digital video broadcasting (DVB); Framing structure, channel coding, and modulation for digital terrestrial television," European Telecommunications Standard, ETSI EN 300-744,Mar.1997.

[27] ETSI, "Broadband radio access networks (BRAN); HIPERLAN type 2; Physical (PHY) layer," European Telecommunications Standard, TS 101-475,2000.

[28] IEEE Standard 802.16 Working Group, "IEEE Standard for Local and Metropolitan Area Networks part 16: Air Interface for Fixed Broadband Wireless Access Systems," IEEE,2004.

[29] B. G. Evans and K. Baughan, "Visions of 4G," *Electronics & Communication Engineering Journal*, vol. 12, no. 6, pp. 293-303, 2000.

[30] J. Ha, S. H. Kim, and K. Dae-Sik, "A phased approach to 4G mobile network system," in *10th International Conference on Telecommunications (ICT)*, vol. 2: 2003, pp. 1318-1322.

[31] S. Weinstein and P. Ebert, "Data Transmission by Frequency-Division Multiplexing Using the Discrete Fourier Transform," *IEEE Transactions on Communications*, vol. 19, no. 5, pp. 628-634, 1971.

[32] R. Nee and R. Prasad, *OFDM for Wireless Multimedia Communications.* Norwood: MA:Artech House, 2000.

[33] L. Junsong and M. Kavehrad, "OFDM-CDMA systems with nonlinear power amplifier," in *IEEE, Wireless Communications and Networking Conference (WCNC)*, 1999, pp. 1167-1171.

[34] R. Morrison, L. J. Cimini, Jr., and S. K. Wilson, "On the use of a cyclic extension in OFDM," in *IEEE, Vehicular Technology Conference (VTC)* vol. 2, 2001, pp. 664-668.

[35] A. R. S. Bahai and B. R. Saltzberg, *Multi-carrier Digital Communications: Theory and Applications of OFDM.* New York: Kluwer Academic/Plenum Publishers, 1999.

[36] J. G. Proakis, *Digital Communications*, 3rd ed. New York: McGraw-Hill, 1995.

[37] C. van den Bos, M. H. L. Kouwenhoven, and W. A. Serdijn, "The influence of non-linear distortion on OFDM bit error rate," in *IEEE International Conference on Communications (ICC)* vol. 2, 2000, pp. 1125-1129.

[38] A. Saleh, "Frequency-Independent and Frequency-Dependent Nonlinear Models of TWT Amplifiers," *IEEE Transactions on Communications*, vol. 29, no. 11, pp. 1715-1720, 1981.

[39] A. Papoulis, *Probability Radom Variables and Stochastic Process*, 2nd ed. Singapore: McGraw Hill, 1985.

[40] P. Banelli and S. Cacopardi, "Theoretical analysis and performance of OFDM signals in nonlinear AWGN channels," *IEEE Transactions on Communications*, vol. 48, no. 3, pp. 430-441, 2000.

[41] P. Banelli, G. Baruffa, and S. Cacopardi, "Effects of HPA nonlinearity on frequency multiplexed OFDM signals," *IEEE Transactions on Broadcasting*, vol. 47, no. 2, pp. 123-136, 2001.

[42] P. Banelli, "Theoretical analysis and performance of OFDM signals in nonlinear fading channels," *IEEE Transactions on Wireless Communications,* vol. 2, no. 2, pp. 284-293, 2003.

[43] C. van den Bos, M. H. L. Ksuwenhoven, and W. A. Serdijn, "Effect of smooth nonlinear distortion on OFDM symbol error rate," *IEEE Transactions on Communications,* vol. 49, no. 9, pp. 1510-1514, 2001.

[44] E. Costa, M. Midrio, and S. Pupolin, "Impact of amplifier nonlinearities on OFDM transmission system performance," *IEEE Communications Letters,* vol. 3, no. 2, pp. 37-39, 1999.

[45] X. D. Li and L. J. Cimini, Jr., "Effects of clipping and filtering on the performance of OFDM," in *IEEE 47th Vehicular Technology Conference,* vol.3, 1997, pp. 1634-1638.

[46] T. May and H. Rohling, "Reducing the peak-to-average power ratio in OFDM radio transmission systems," in *IEEE 48th Vehicular Technology Conference (VTC),* vol. 3, 1998, pp. 2474-2478.

[47] J. A. Davis and J. Jedwab, "Peak-to-mean power control in OFDM, Golay complementary sequences, and Reed-Muller codes," *IEEE Transactions on Information Theory,* vol. 45, no. 7, pp. 2397-2417, 1999.

[48] C. Tellambura, "Improved phase factor computation for the PAR reduction of an OFDM signal using PTS," *Communications Letters, IEEE,* vol. 5, no. 4, pp. 135-137, 2001.

[49] R. Kumar, D. Taggart, C. Chen, and N. Wagner, "Simulation and modeling of amplifier nonlinearities with 16-QAM modulated waveforms in wireless communication systems," in *IEEE 60th Vehicular Technology Conference (VTC),* vol. 6, 2004, pp. 4212-4216.

[50] T. Pollet and M. Moeneclaey, "Synchronizability of OFDM signals," in *IEEE Global Telecommunications Conference (GLOBECOM),* vol.3, 1995, pp. 2054-2058.

[51] T. Pollet, "BER sensitivity of OFDM systems to carrier frequency offset and Wiener phase noise," *IEEE transactions on communications,* vol. 43, no. 2, p. 191, 1995.

[52] H. Steendam and M. Moeneclaey, "Sensitivity of Multicarrier Systems to Synchronization Errors," in *International Symposium on Signals, Systems and Electronics ISSSE'01* Tokyo: 2001, pp. 66-69.

[53] O. Jung-Yeol and L. Myoung-Seob, "The bandwidth efficiency increasing method of multi-carrier CDMA and its performance evaluation in comparison with DS-CDMA with RAKE receivers," *IEEE 49th Vehicular Technology Conference,* vol. 1, pp. 561-565, 1999.

[54] M. C. Jeruchim, P. Balaban, and K. Shanmugan, *Simulation of Communication Systems: Modeling, Methodology and Techniques,* 2nd ed Springer, London, 2000.

[55] A. Goldsmith, *Wireless Communications,* Cambridge University Press, 2005.

[56] J. L. Pinto, "Studies of Predetection Filters and Error Vector Magnitude in GSM and EDGE Mobile Communication Systems," *PhD thesis in University of Manchester Institute of Science and Technology (UMIST),* Nov.2001.

[57] J. L. Pinto and I. Darwazeh, "Simulation of adjacent channel interference between GSM and EDGE mobile communication systems," *Proceeding of the International Conference on Telecommunications,* pp. 474-478, 2003.

[58] V. M. DaSilva and E. S. Sousa, "Performance of orthogonal CDMA codes for quasi-synchronous communication systems," in *ICUPC 93', IEEE* Ottawa, Canada: 1993, pp. 995-999.

[59] K. Fazel and L. Papke, "On the performance of convolutionally-coded CDMA/OFDM for mobile communications system," *PIMRC, 1993 IEEE,* pp. 468-472, Sept.1993.

[60] L. Vandendorpe, "Multitone spread spectrum multiple access communications system in a multipath Rician fading channel," *IEEE Transactions on Vehicular Technology,* vol. 44, no. 2, pp. 327-337, 1995.

[61] N. Yee, Linnartz J.P., and G. Fettweis, "Multi-carrier CDMA in indoor wireless radio network," in *PIMRC, 1993 IEEE* 1993, pp. 109-113.

[62] A. Chouly, A. Brajal, and S. Jourdan, "Orthogonal multicarrier techniques applied to direct sequence spread spectrum CDMA systems," *Global Telecommunications Conference, 1993, including a Communications Theory Mini-Conference. Technical Program Conference Record, IEEE in Houston. GLOBECOM '93., IEEE,* pp. 1723-1728, 1993.

[63] S. Kondo and L. Milstein, "On the use of multicarrier direct sequence spread spectrum systems," in *IEEE Military Communications Conference Conference record.'Communications on the Move',* vol. 1, 1993, pp. 52-56.

[64] N. Hathi, M. Rodrigues, I. Darwazeh, and J. O'Reilly, "Performance assessment of MC-CDMA and MC-DS-CDMA in the presence of high power amplifier non-linearities," in *IEEE 55th Vehicular Technology Conference* vol.3, 2002, pp. 1467-1471.

[65] R. Prasad and S. Hara, "An overview of multi-carrier CDMA," *IEEE 4th International Symposium on Spread Spectrum Techniques and Applications Proceedings,* vol. 1, pp. 107-114, 1996.

[66] F. Fllersick, "A conversation with Claude Shannon," *Communications Magazine, IEEE,* vol. 22, no. 5, pp. 123-126, 1984.

[67] G. R. Cooper and R. W. Nettleton, "A spread spectrum technique for high capacity mobile communications," in *27th IEEE Vehicular Technology Conference,* vol.27, 1977, pp. 98-103.

[68] J. S. Lee, "Overview of the technical basis of Qualcomm's CDMA cellular telephone system design: a view of North American TIA/EIA IS-95," in *Singapore ICCS '94.Conference Proceedings,* vol.2, 1994, pp. 353-358.

[69] T. Ojapera and R. Prasad, in *Wideband CDMA for third generation mobile communications* Artech House, 1998.

[70] M. R. Karim, in *W-CDMA and CDMA-2000 for 3G mobile networks* McGraw-Hill, 2002.

[71] C. Qingxin, E. S. Sousa, and S. Pasupathy, "Multicarrier CDMA with adaptive frequency hopping for mobile radio systems," *IEEE Journal on Selected Areas in Communications,* vol. 14, no. 9, pp. 1852-1858, 1996.

[72] L. L. Yang and L. Hanzo, "Slow frequency-hopping multicarrier DS-CDMA," International Symposium on Wireless Personal Multimedia Communications (WPMC'99), Amsterdam, The Netherlands: 1999, pp. 224-229.

[73] H. K. Yun, S. Iickho, Y. Seokho, and R. P. So, "A multicarrier CDMA system with adaptive subchannel allocation for forward links," *IEEE Transaction on Vehicular Technology,* vol. 48, no. 5, pp. 1428-1436, 1999.

[74] S. Hara and R. Prasad, "Design and performance of multicarrier CDMA system in frequency-selective Rayleigh fading channels," *IEEE Transaction on Vehicular Technology,* vol. 48, no. 5, pp. 1584-1595, 1999.

[75] E. A. Sourour and M. Nakagawa, "Performance of orthogonal multicarrier CDMA in a multipath fading channel," *IEEE Transactions on Communications,* vol. 44, no. 3, pp. 356-367, 1996.

[76] Q. M. Rahman and A. B. Sesay, "Performance evaluation of non-coherent multi-tone CDMA system," *2000 Canadian Coference on Electrical and Computer Engineering,* vol. 1, pp. 245-249, 2000.

[77] Q. M. Rahman and A. B. Sesay, "Performance analysis of MT-CDMA system with diversity combining," *Military Communications Conference, 2001. MILCOM 2001. Communications for Network-Centric Operations: Creating the Information Force. IEEE,* vol. 2, pp. 1360-1364, 2001.

[78] Q. M. Rahman and A. B. Sesay, "Noncoherent MT-CDMA system with post-detection diversity combining," *Canadian Journa of Electrical and Computer Engineering,* vol. 28, no. 2, pp. 81-88, 2003.

[79] D. W. Matolak, V. Deepak, and F. A. Alder, "Performance of multitone and multicarrier DS-SS in the presence of imperfect phase synchronization," in *MILCOM 2002.Proceedings,* vol.2, 2002, pp. 1002-1006.

[80] A. R. Enayati, P. Azmi, and E. Jedari, "Low-Rate Channel Coding Scheme for Replica MT-CDMA Communication System," *IEEE International Conference on Communications (ICC),* vol. 11, pp. 4936-4940, 2006.

[81] D. L. Schilling and R. L. Pickholtz, "Improved PCN efficiency through the use of spectral overlay," in *IEEE International Conference on Communications(ICC), Conference record, SUPERCOMM/ICC '92, Discovering a New World of Communications,* 1992, pp. 243-244.

[82] F. Behbehani and H. Hashemi, "On spectral efficiency of CDMA mobile radio systems," in *IEEE International Conference on Communications (ICC), SUPERCOMM/ICC '94, Conference Record, Serving Humanity Through Communications,* 1994, pp. 505-509.

[83] H. H. Jin and W. K. Sang, "Optimal spectral overlay of DS/CDMA communication systems," in *4th IEEE International Conference on Universal Personal Communications,* 1995, pp. 625-629.

[84] H. H. Jin and W. K. Sang, "Capacity of DS/CDMA communication systems with optimum spectral overlap," *Communications Letters, IEEE,* vol. 2, no. 11, pp. 298-300, 1998.

[85] L. L. Yang and L. Hanzo, "Overlapping M-ary frequency shift keying spread-spectrum multiple-access systems using random signal sequences," *IEEE Transactions on Vehicular Technology,* vol. 48, no. 6, pp. 1984-1995, 1999.

[86] I. Sen and D. W. Matolak, "Reduced-complexity bandwidth efficient multitone direct sequence spread spectrum," *IEEE Sarnoff Symposium on Advances in Wired and Wireless Communication,* pp. 131-134, 2004.

[87] I. Sen, "Bandwidth efficient reduced complexity MT-DS-SS via reduced subcarrier frequency spacing." Master thesis, Ohio University, 2004.

[88] S. Moshavi, "Multi-user detection for DS-CDMA communications," *Communications Magazine, IEEE,* vol. 34, no. 10, pp. 124-136, 1996.

[89] Z. Xie, R. T. Short, and C. K. Rushforth, "A family of suboptimum detectors for coherent multiuser communications," *IEEE Journal on Selected Areas in Communications,* vol. 8, no. 4, pp. 683-690, 1990.

[90] K. Sathananathan and C. Tellambura, "Forward error correction codes to reduce intercarrier interference in OFDM," in *The 2001 IEEE International Symposium on Circuits and Systems,* vol.4, 2001, pp. 566-569.

[91] I. Kanaras, A. Chorti, M. Rodrigues, and I. Darwazeh, "A Combined MMSE-ML Detection for a Spectrally Efficient non Orthogoanl FDM Signal," Fifth International Conference on Broadband Communications, Networks and Systems, London, UK: 2008.

[92] L. L. Yang and L. Hanzo, "Performance of generalized multicarrier DS-CDMA over Nakagami-m fading channels," *IEEE Transactions on Communications,* vol. 50, no. 6, pp. 956-966, 2002.

[93] S. Kondo and B. Milstein, "Performance of multicarrier DS CDMA systems," *IEEE Transactions on Communications,* vol. 44, no. 2, pp. 238-246, 1996.

[94] D. W. Matolak, S. Indranil, and X. Wenhui, "Multicarrier multiuser modulation performance in severely fading channels," *Joint IST Workshop on Mobile Future and the Symposium on Trends in Communications. Sympo (TIC),* pp. 88-91, 2006.

[95] Y. Huan and G. W. Wornell, "Lattice-reduction-aided detectors for MIMO communication systems," in *IEEE Global Telecommunications Conference (GLOBECOM)*, vol.1, 2002, pp. 424-428.

Appendix A Simulation models in ADS

A.1 OFDM/Fast-OFDM model

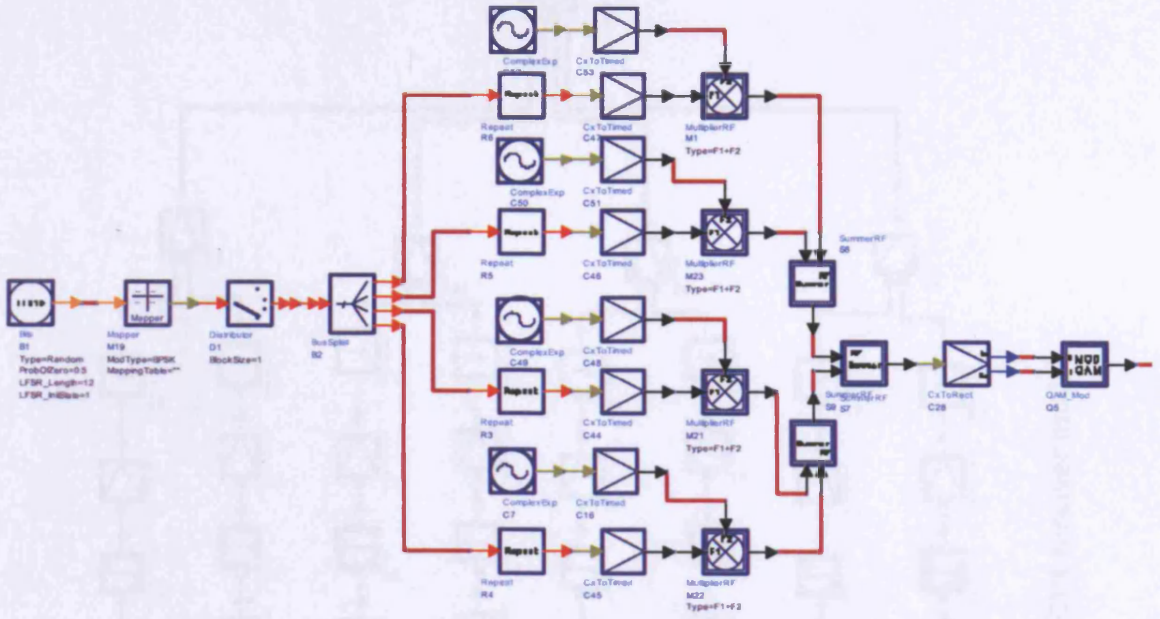

Figure A.1. BPSK-OFDM/Fast-OFDM transmitter model

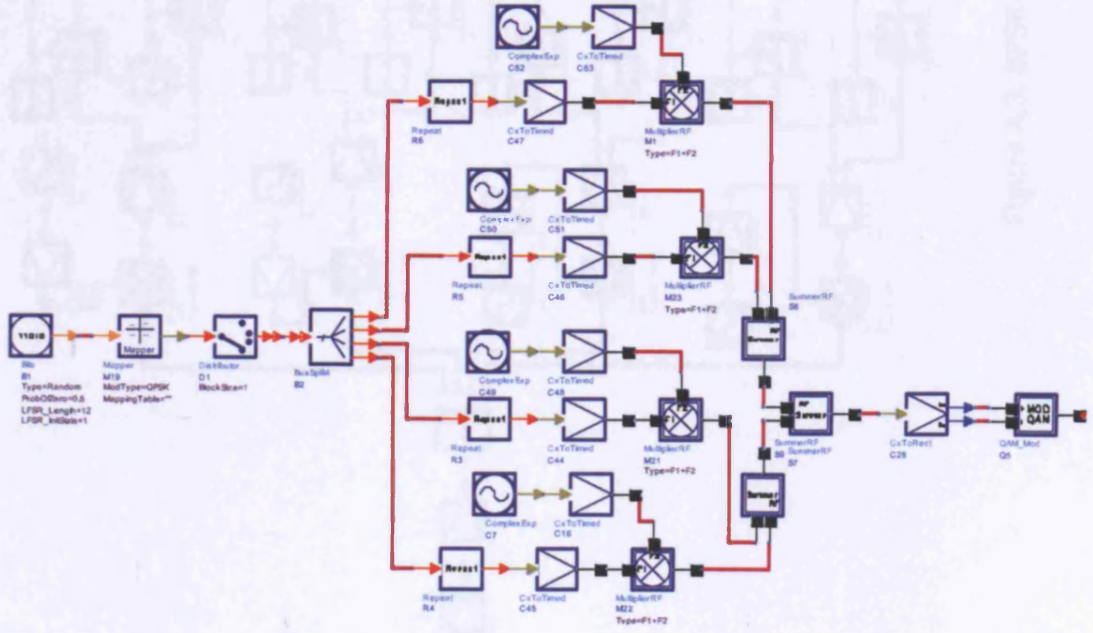

Figure A.2. QPSK-OFDM/Fast-OFDM transmitter model

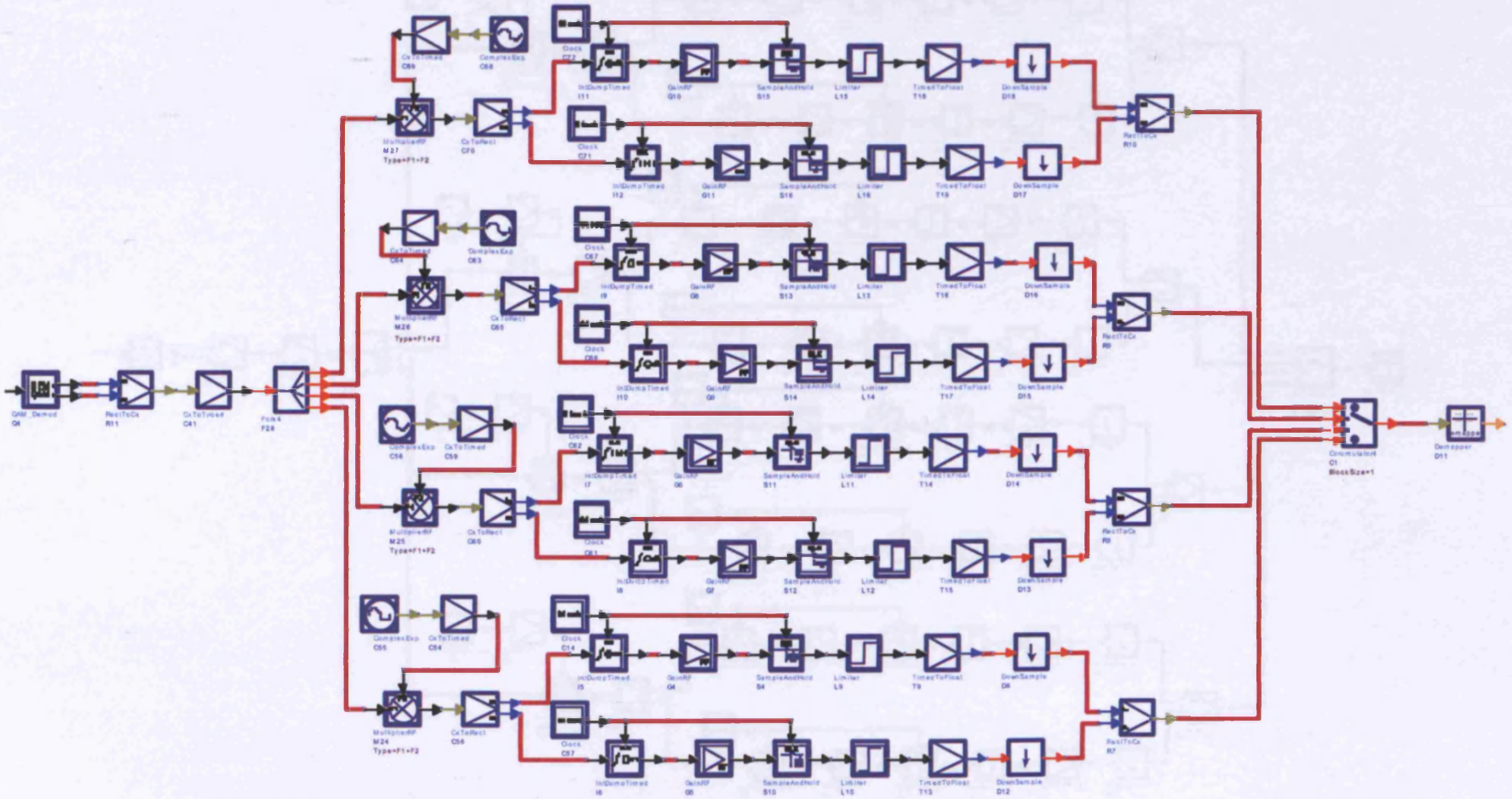

Figure A.3. BPSK-OFDM/Fast-OFDM receiver model

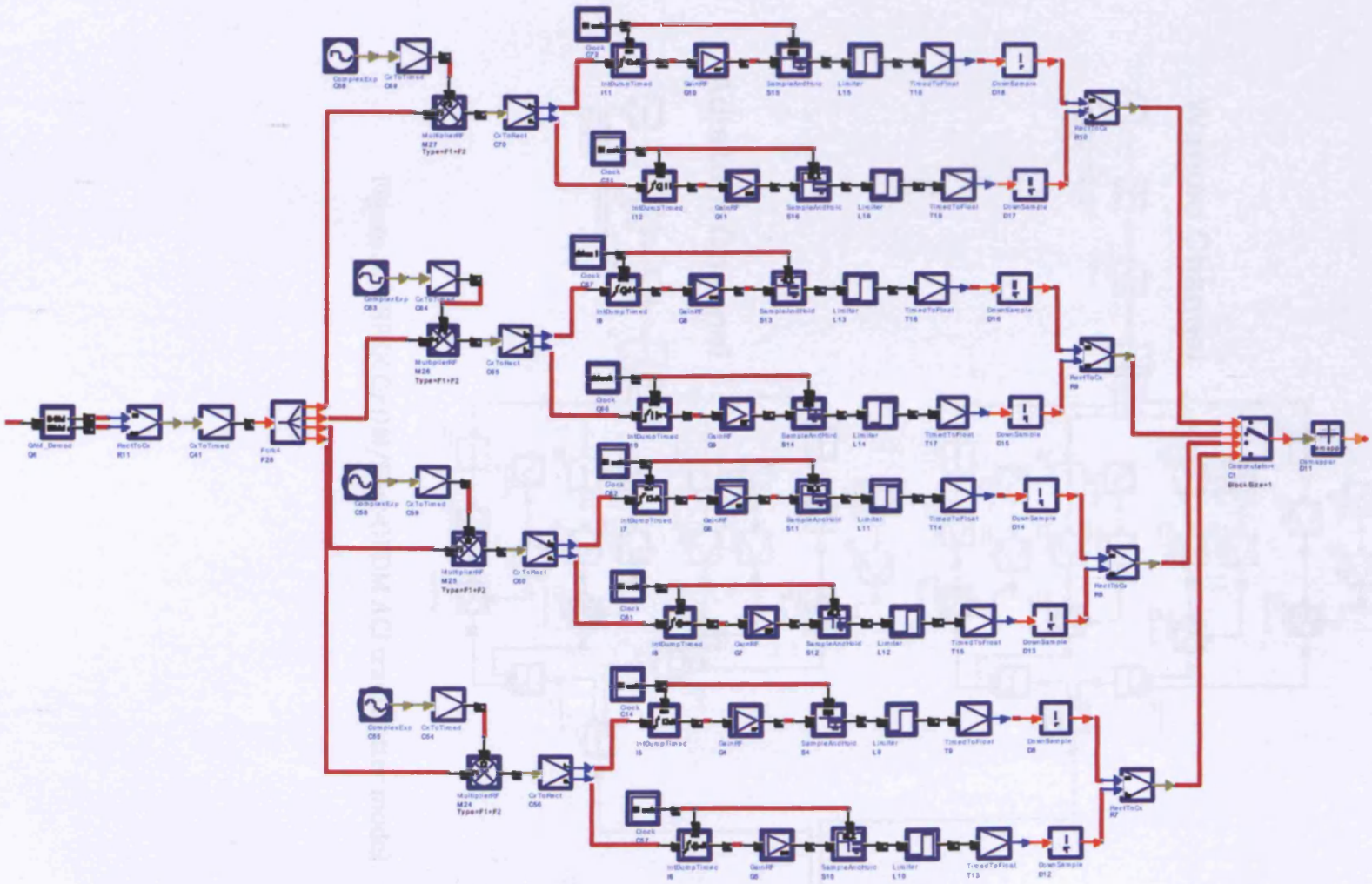

Figure A.4. QPSK-OFDM/Fast-OFDM receiver model

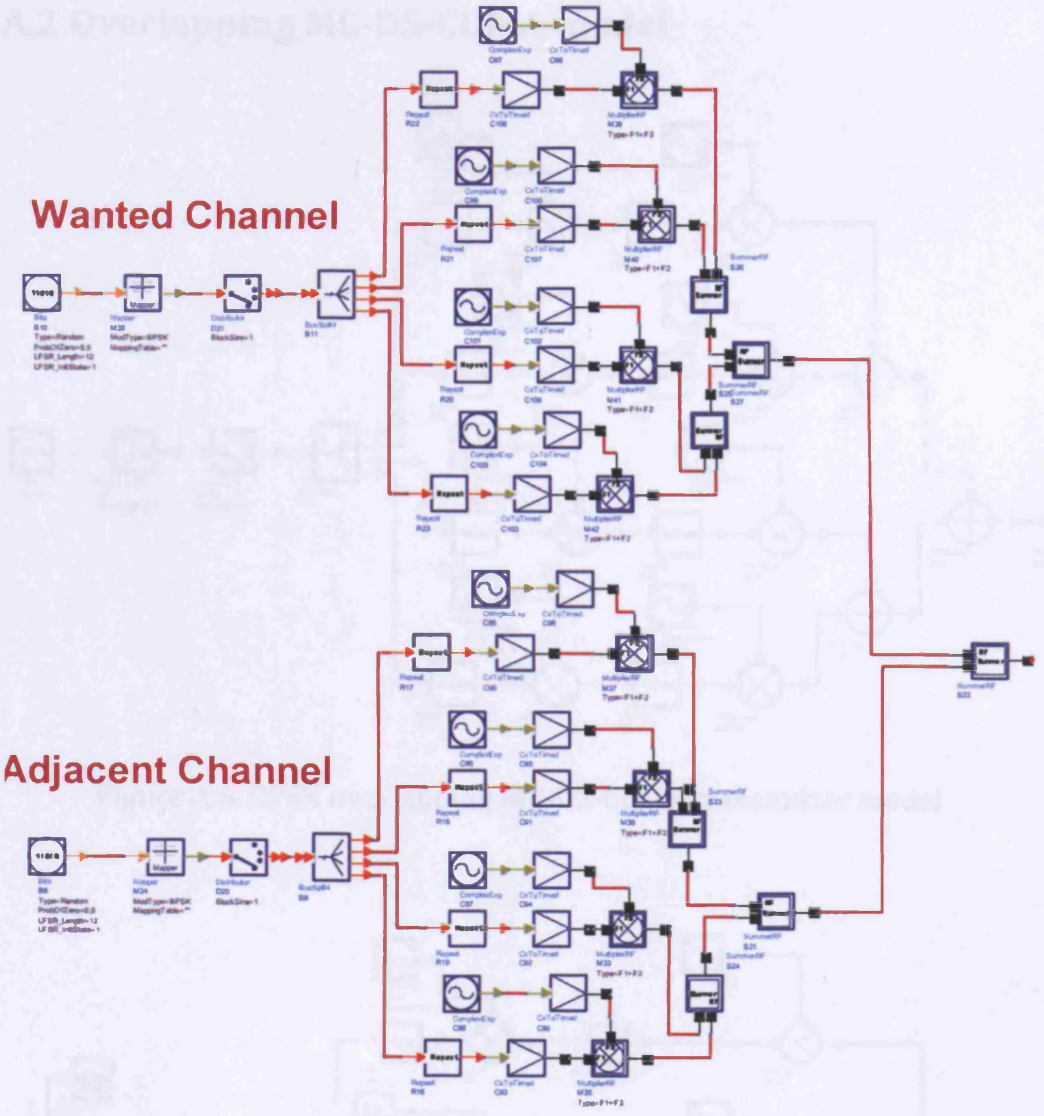

Figure A.5. BPSK OFDM/Fast-OFDM ACI transmitter model

A.2 Overlapping MC-DS-CDMA model

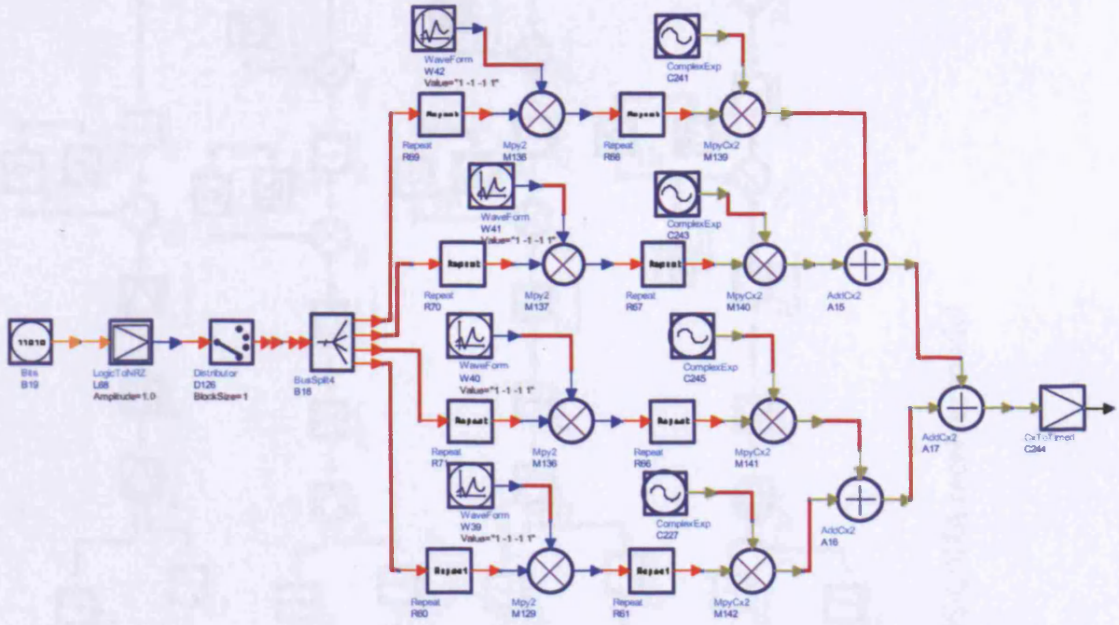

Figure A.6. BPSK overlapping MC-DS-CDMA transmitter model

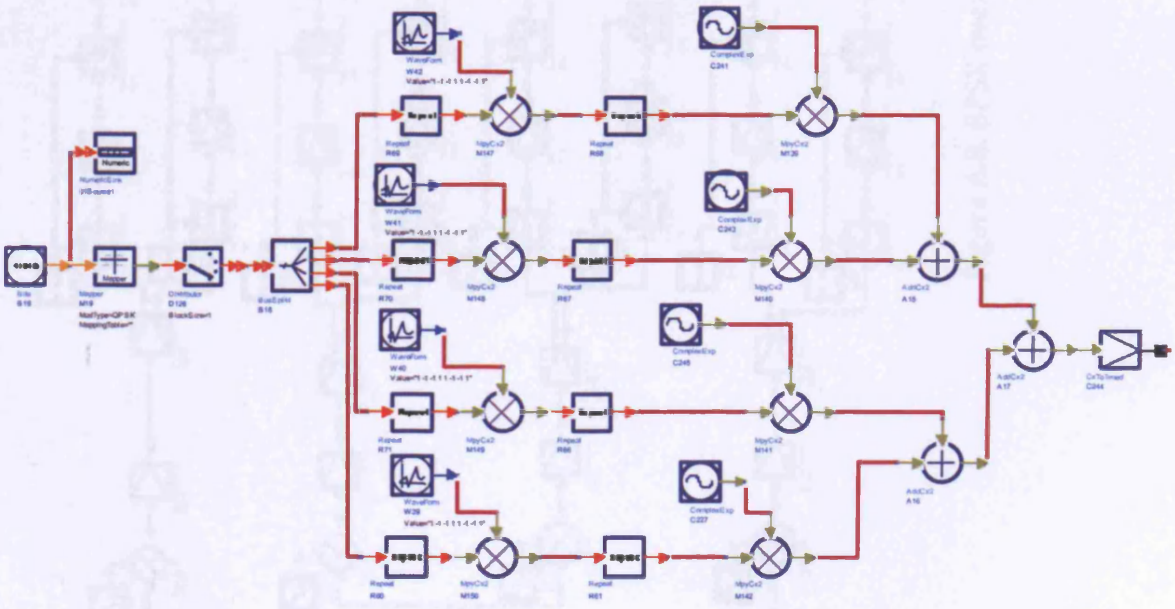

Figure A.7. QPSK overlapping MC-DS-CDMA transmitter model

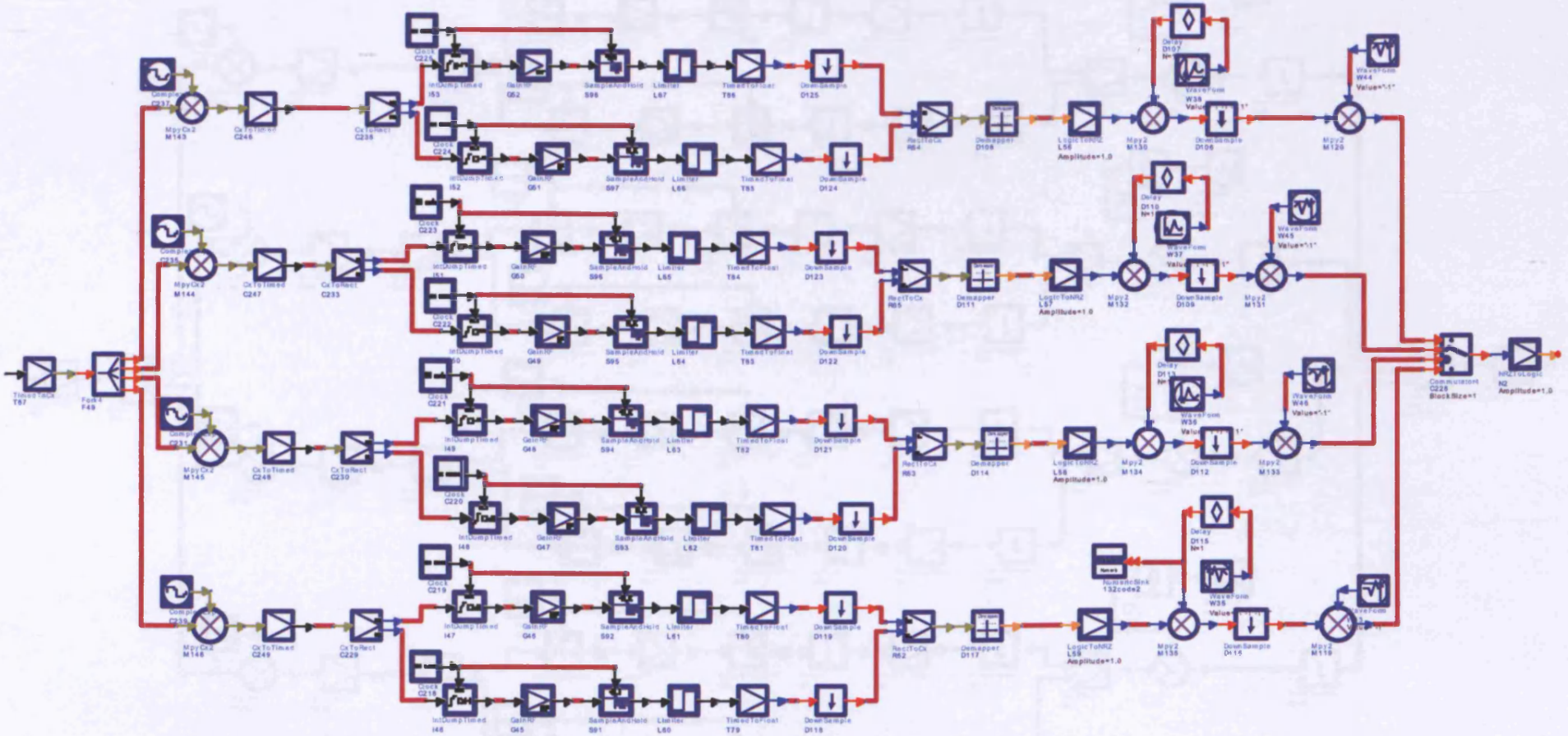

Figure A.8. BPSK overlapping MC-DS-CDMA receiver model

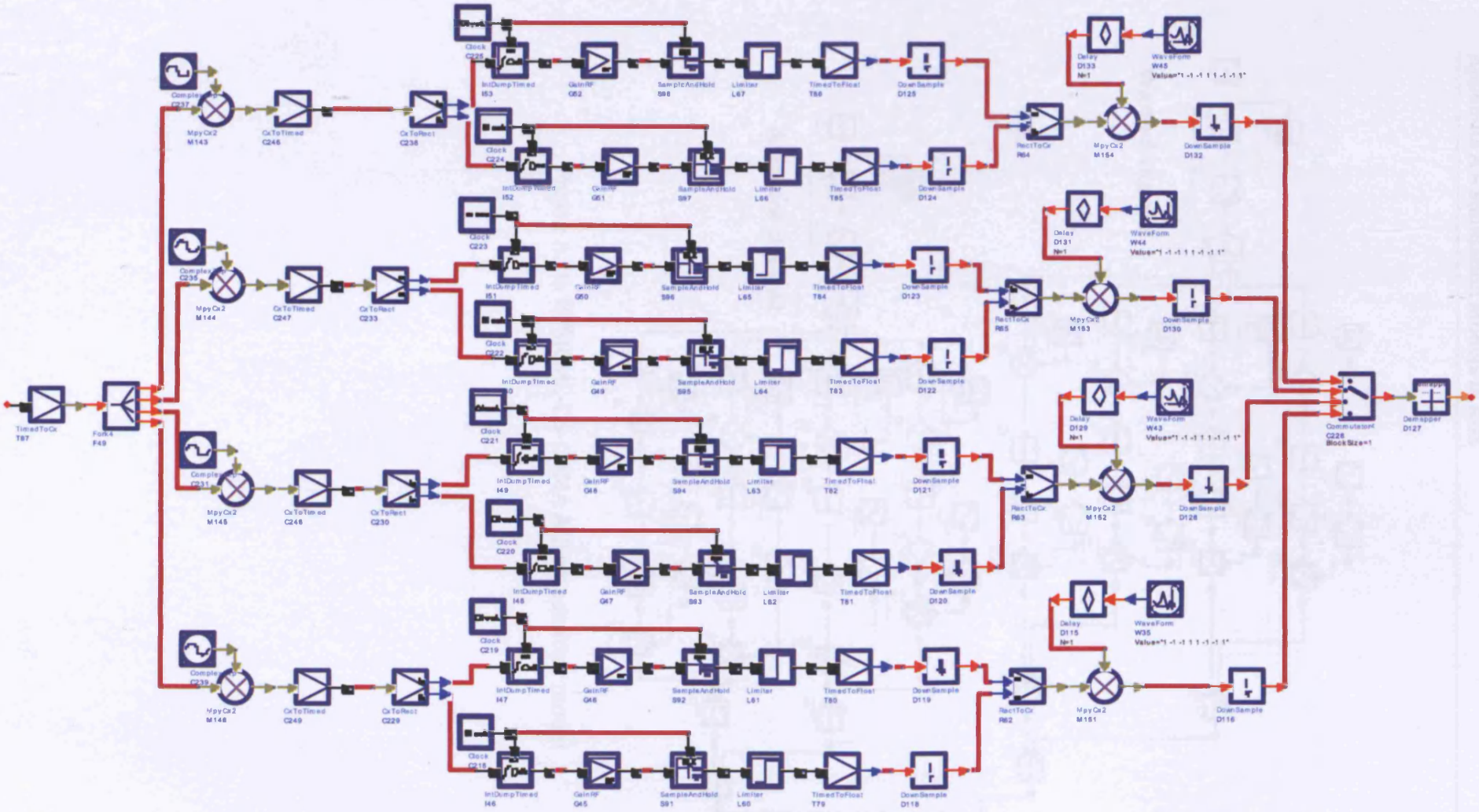

Figure A.9. QPSK overlapping MC-DS-CDMA receiver model

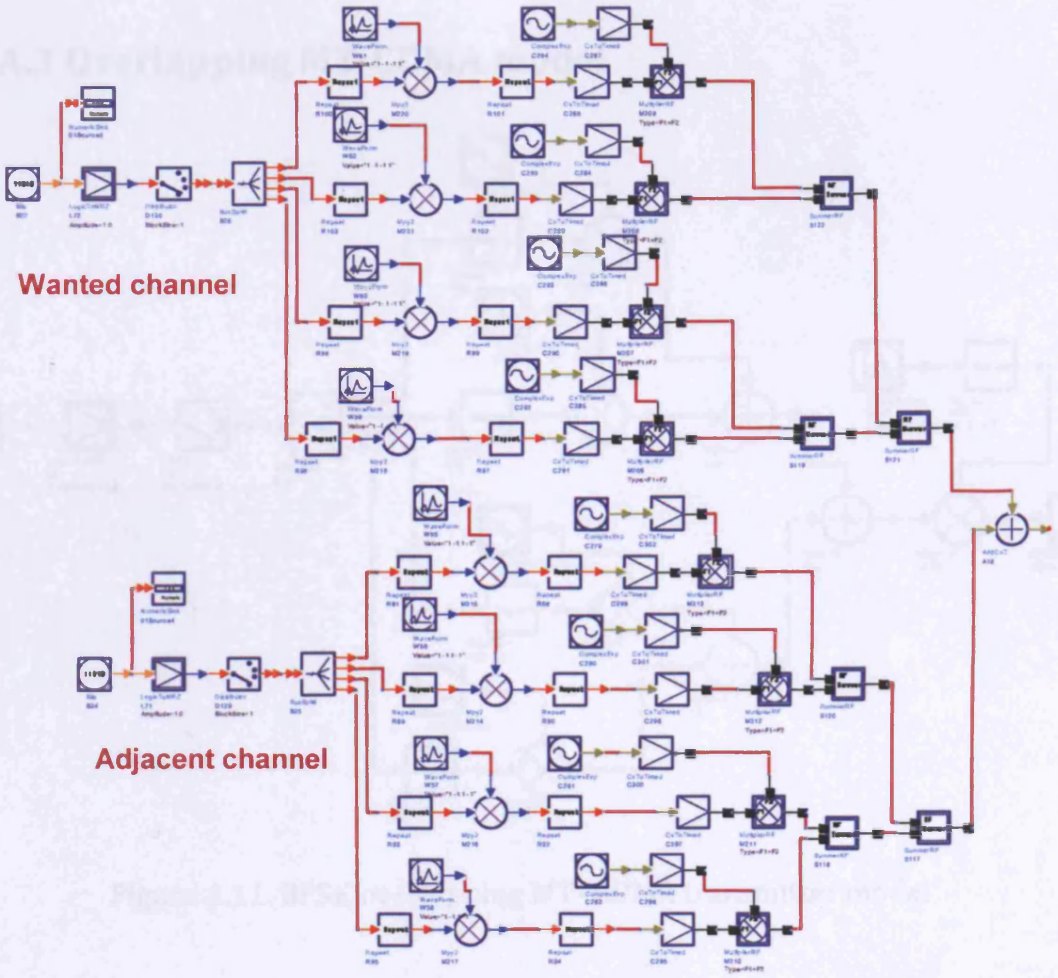

Figure A.10. BPSK MC-DS-CDMA ACI transmitter model

A.3 Overlapping MT-CDMA model

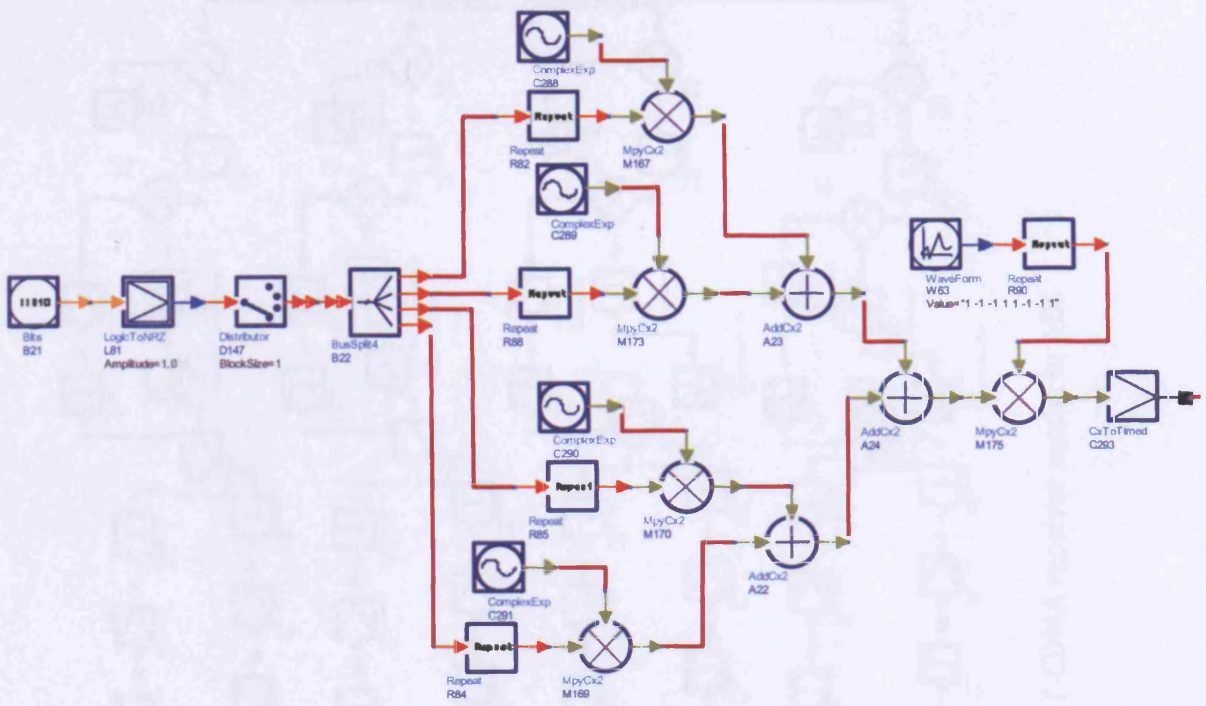

Figure A.11. BPSK overlapping MT- CDMA transmitter model

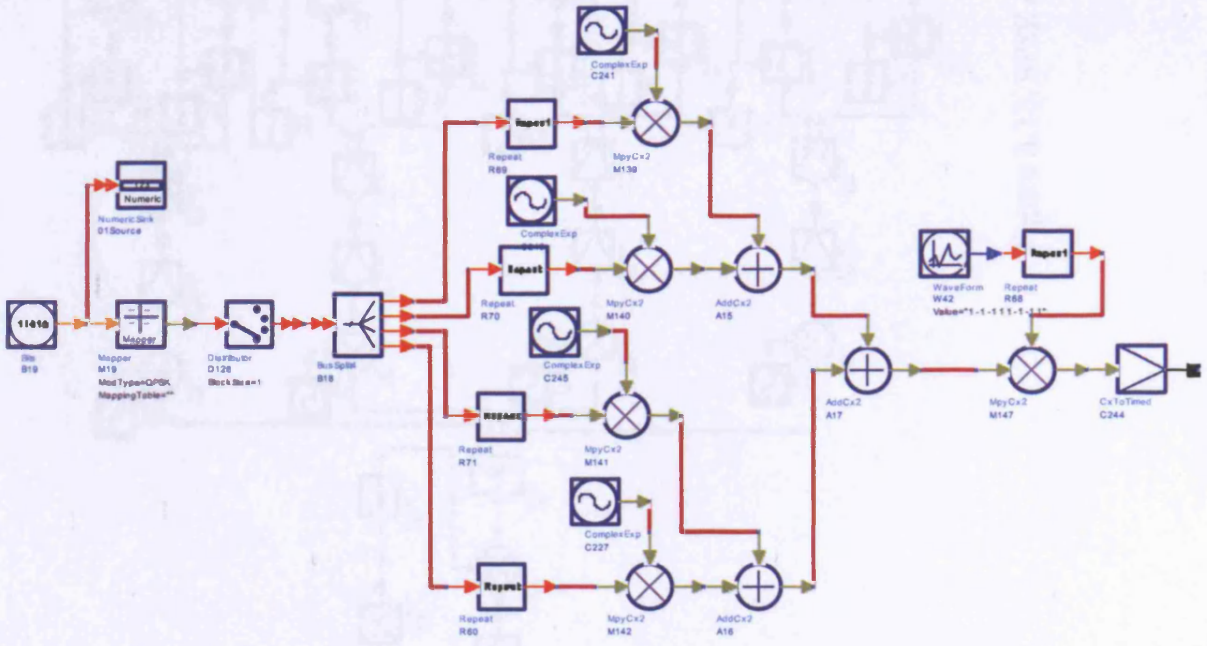

Figure A.12. QPSK overlapping MT- CDMA transmitter model

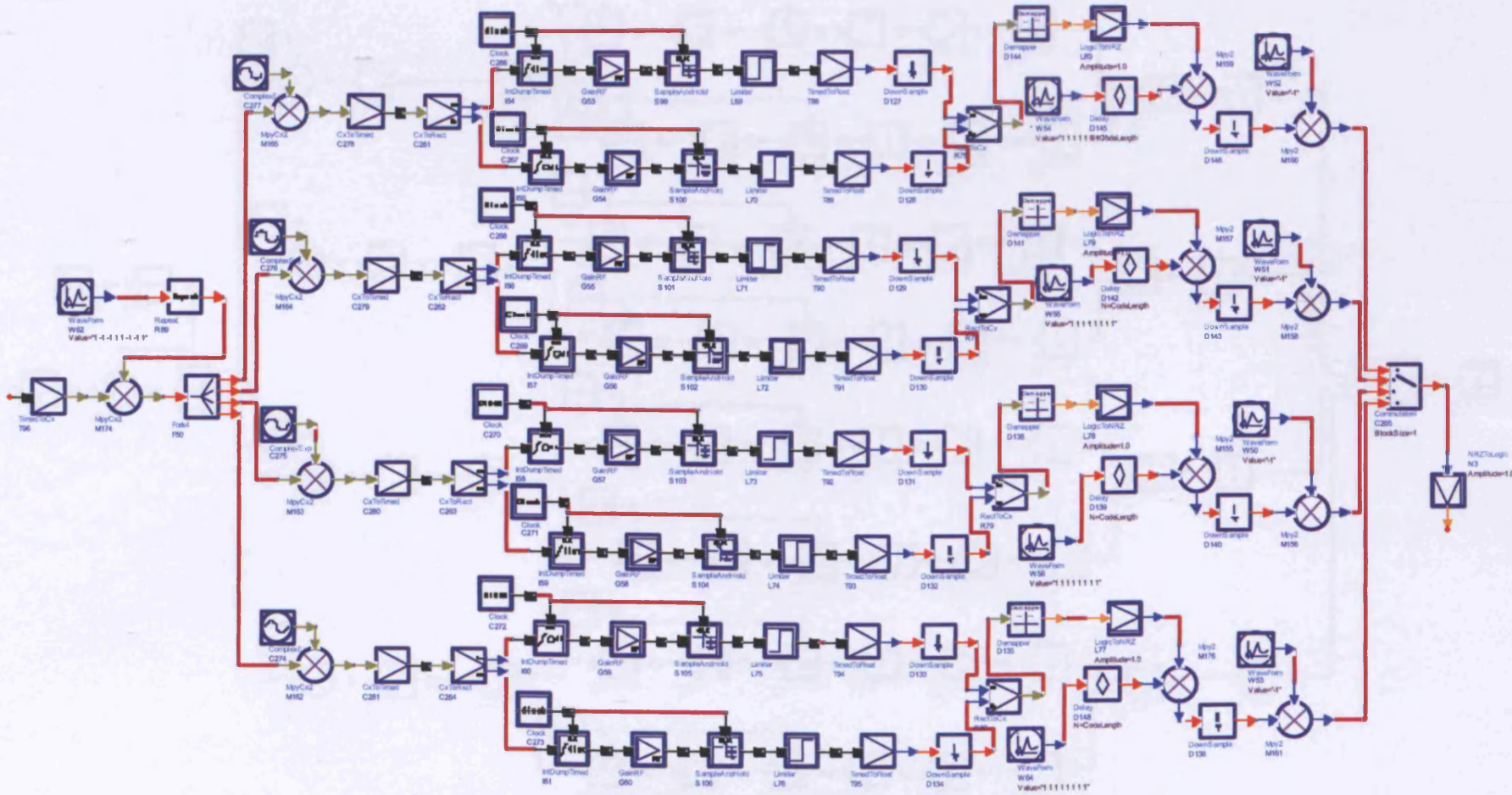

Figure A.13. BPSK overlapping MT-CDMA receiver model in ADS

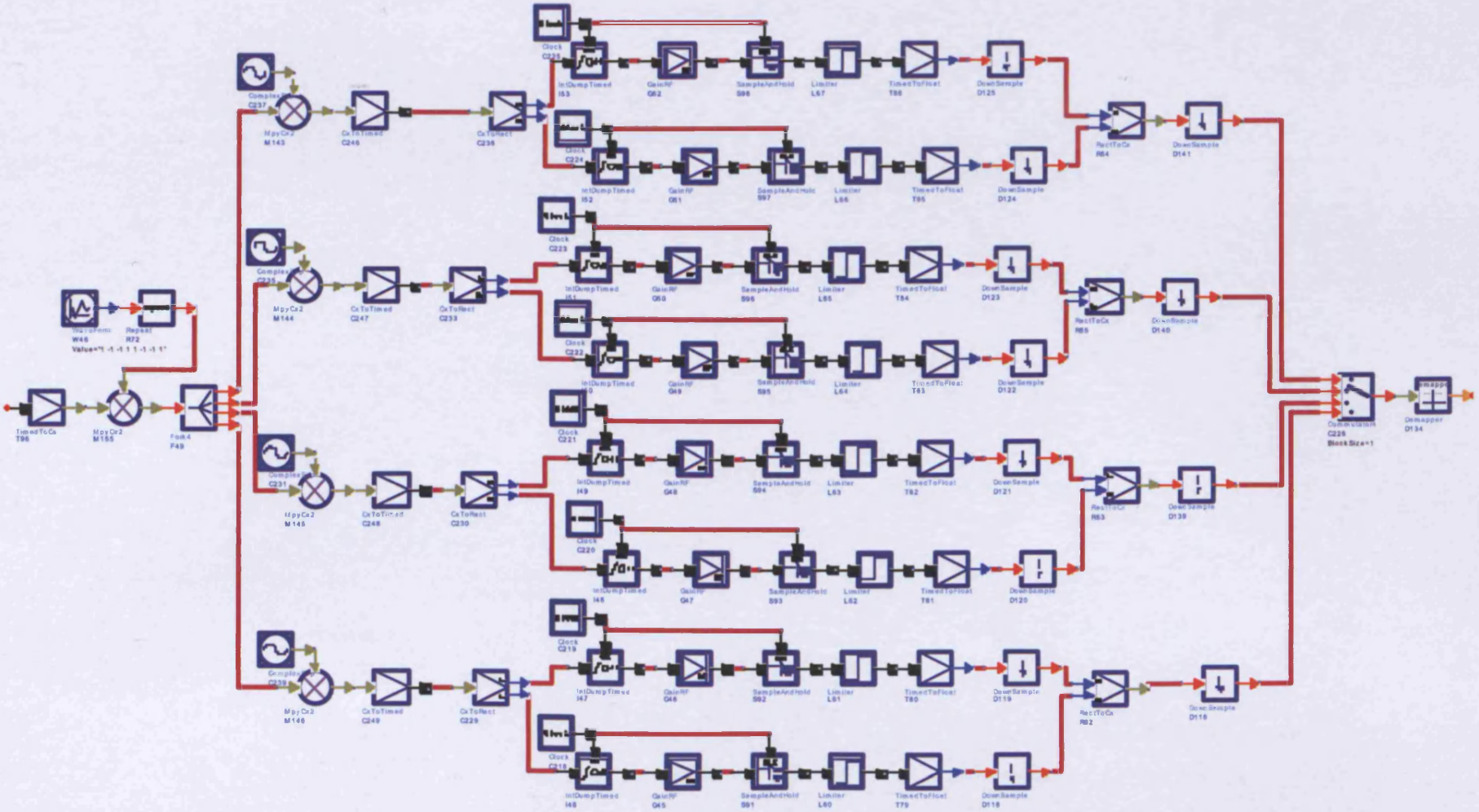

Figure A.14. QPSK overlapping MT-CDMA receiver model in ADS